Performance of calcium sulfoaluminate cement-based mixtures used for permafrost regions

by

Guangping Huang

A thesis submitted in partial fulfillment of the requirements for the degree of

Doctor of Philosophy

in

Mining Engineering

Department of Civil and Environmental Engineering
University of Alberta

Abstract

Canada has approximately 50% of land mass covered with permafrost. With the increasing of mining and construction activities in permafrost regions, cement-based mixtures (e.g., concrete, shotcrete, backfill, and grout) are expected to be increasingly used in these regions. However, cold temperature (< 5 ºC) causes the slow strength development of cement-based mixtures, which is unfavorable since it decreases construction efficiency, increases costs, and raises safety issues. In addition, early-age frost damage may happen if cement-based mixtures could not gain sufficient strength (compressive strength 3.5 MPa) before getting frozen. Once early-age frost damage happens, the strength of cement-based mixtures cannot be ensured to reach an adequate value even if it is re-cured at normal temperatures (e.g., 20 °C), which is also unsafe.

In response these issues, this Ph.D. program aims to develop calcium sulfoaluminate (CSA) cement-based mixtures for permafrost region applications. Experiments were conducted to investigate the hydration reaction, strength development, resistance to early-age frost damage, and thermal properties (e.g., thermal conductivity, diffusivity, and heat capacity). A numerical model was developed to predict the temperature profiles in hardening CSA cement-based mixtures.

The results show that the hydration reaction and the strength development of CSA-based mortar were much faster than Portland cement-based mortar at cold temperatures (< 5 °C). For example, CSA cement-based mortar cured at -10 °C achieved a UCS of 15.5 MPa at 1 day, while OPC-based mortars almost have no strength developed at 28 days. CSA cement-based mixtures also showed high resistance to early-age frost damage owing to the fast strength development. After re-curing, CSA cement-based mortar that had exposed to -10 °C reached 117.8% of the UCS of

the same mixtures directly cured at 23 °C, while the data for OPC-based mortars with and without antifreeze admixture (calcium nitrate) were 56.0% and 45.1%, respectively. In addition, the thermal conductivity of 28-day CSA cement-based mortars reduced from 0.97 W/m·K to 0.57 W/m·K, 0.29 W/m·K, and 0.13 W/m·K when 30%, 60%, and 100% volume of aggregates were replaced with expanded perlite. These CSA cement-based thermo-insulting mortars are expected to not only provide mechanical support, but also work as thermal insulation materials for mitigating the heat exchange among permafrost, cement-based mixtures, and air. At last, the developed numerical model was validated by comparing the modeled temperature profiles with experimentally measured temperature profiles in hardening CSA cement samples. After validation, the influence of curing temperature, curing modes (e.g., curing in permafrost or curing in cold air), and sample sizes on the temperature profiles of hardening CSA cement mixtures was investigated and compared with that on an OPC-based mixture. The results suggest that samples should be cured in cold soil or sand when investigating the performance of cement-based mixtures used in permafrost regions since the different curing modes caused a large influence on the temperature profiles of hardening cement-based mixtures. The temperature gradient in CSA-based sample was more significant than that in OPC-based sample. Precautions are needed to control the thermal cracks when CSA cement-based mixtures are used in cold temperatures, even if the structure size is small (e.g., Ø300×600mm).

Overall, this thesis developed CSA cement mixtures that can achieve fast strength development and have high resistance to early-age frost damage for permafrost region applications. The findings provide a new solution to accelerate strength development and prevent early-age frost damage when cement-based mixtures are applied in permafrost regions.

Preface

This thesis is an original work by Guangping Huang, which developed calcium sulfoaluminate cement-based mixtures for potential applications in permafrost regions in Canada's North. This thesis is based on five journal papers that are published or submitted for consideration for publication.

Chapter 2 of this thesis has been accepted as **G. Huang**, R. Gupta, W. V. Liu, Effects of sodium gluconate on hydration reaction, setting, workability, and strength development of calcium sulfoaluminate cement mixtures, *Journal of Sustainable Cement-based Materials.* ©Taylor & Francis. (2021).

Chapter 3 of this thesis has been published as **G. Huang**, D. Pudasainee, R. Gupta, W. V. Liu, Hydration reaction and strength development of calcium sulfoaluminate cement-based mortar cured at cold temperatures, *Construction and Building Materials.* © Elsevier. 224 (2019) 493–503.

Chapter 4 has been published as **G. Huang**, D. Pudasainee, R. Gupta, W.V. Liu, The performance of calcium sulfoaluminate cement for preventing early-age frost damage, *Construction and Building Materials*. © Elsevier. 254 (2020) 119322.

Chapter 5 has been published as **G. Huang**, D. Pudasainee, R. Gupta, W.V. Liu, Thermal properties of calcium sulfoaluminate cement-based mortars incorporated with expanded perlite cured at cold temperatures. *Construction and Building Materials*. © Elsevier. 274 (2021) 122082.

Chapter 6 has been submitted for peer review as **G. Huang**, Y. Guo, E. Bescher, R. Gupta, W.V. Liu, Numerical modeling of temperature profiles in hardening calcium sulfoaluminate cement-

based mortars for permafrost region applications. *Construction and building materials.* © Elsevier. (With Editor)

In this thesis, my work includes conceptualization, experiment design, data collection, numerical modeling, data analysis, writing, review, and editing. Dr. Wei Victor Liu was my academic supervisor, who contributed to conceptualization, supervision, resources, review, and editing. Dr. Rajender Gupta was my academic co-supervisor, who was involved in supervision, resources, review, editing. In Chapters 3, 4, and 5, Dr. Deepak Pudasainee assisted in data collection, review, and editing. In Chapter 6, Dr. Eric Bescher helped conduct isothermal calorimetry tests to determine the heat generation rate of cement hydration, and Yunting Guo contributed to improving the numerical model.

DEDICATION

This thesis is dedicated to my wife Yuping Zhou,

my daughter Meirui Huang, and my son Siwei Huang.

I love you all dearly.

Acknowledgement

First and foremost, I would like to express my sincere gratitude to my supervisors, Dr. Wei Victor Liu and Dr. Rajender Gupta for their invaluable supervision and continuous support during my Ph.D. program. I am so lucky to have such great supervisors who are smart, enthusiastic, and patient. They always provide me constructive comments and insightful discussions promptly when I need their help. Their immense knowledge, plentiful experience, and passion to academic research always inspire me to be a better researcher.

My appreciation goes to Rizaldy Mariano, Rebecca Funk, and Ni Yang, Jim Skwarok, technicians at the University of Alberta, for their training and help in my experimental work. I would like to express my gratitude to Nick de Ocampo from CTS Cement Manufacturing Cooperation for his coordination in cement donation and to Dr. Bescher Éric Pascal, vice president, Technology, CTS Cement Manufacturing Cooperation, a professor at the University of California Los Angeles for his help in isothermal calorimetry.

I would like to thank my colleagues Dr. Linping Wu, Dr. Deepak Pudasainee, Dr. Xincheng Hu, Dr. Yuanyuan Pu, Yuting Guo, Shaosen Ma, Chengkai Fan, Hau Yu, and my former roommates Wenyuan Huang and Muziyuan Gao for their kind help and support on my study and daily life. I appreciate my former colleague Dr. Lin Liao, who encouraged me to go overseas to pursue my Ph.D. degree and provided my valuable suggestions for scholarship application. I am also grateful to my friends for the wonderful time we had together.

I would like to acknowledge the Chinese Scholarship Council (CSC) for providing me with the living cost during my Ph.D. study and the Natural Sciences and Engineering Research Council of Canada (NSERC) for the financial support to my research.

Lastly, I would like to express my sincere gratitude to my wife Yuping Zhou for her understanding, tremendous support, encouragement, and love. She takes care of our little babies and makes our home full of love. I also extremely appreciate my parents Tongquan Huang and Guiying Yu for their unwavering support and unconditional love.

Table of contents

List of tables

List of figures

List of abbreviations

a/c	Aggregate to cement ratio
AFm	Monosulfate
AFt	Ettringite
AH_3	Aluminium hydroxide
Al_2O_3	Aluminium oxide
ASTM	American Society for Testing and Materials
C_2S	Calcium silicate, belite
C_2ASH_8	Strätlingite
C_3A	Tricalcium aluminate
C_4AF	Tetracalcium aluminoferrite, brownmillerite
$C_4A_3\bar{S}$	Tetracalcium trialuminate sulfate, ye'elimite
$C\bar{S}$	Calcium sulfate
CaO	Calcium oxide
CH	Calcium hydroxide
CN	Calcium nitrate
CSA	Calcium sulfoaluminate
C-S-H	Calcium silicate hydrate

DTG	Derivative of thermogravimetric
Fe_2O_3	Ferric oxide
IEA	International Energy Agency
MgO	Magnesium oxide
MIP	Mercury intrusion porosimetry
OPC	Ordinary Portland cement
PC	Portland cement
QXRD	Quantitative X-ray diffraction
RMSE	Root mean square error
SEM	Scanning electron microscopy
SiO_2	Silicon dioxide
SO_3	Sulfur trioxide
SSD	Saturated surface dry
TG	Thermogravimetric
TGA	Thermogravimetric analysis
TPS	Transient plane source
UCS	Unconfined compressive strength

UPV	Ultrasonic pulse velocity
w/c	Water to cement ratio

List of nomenclatures

Nomenclatures

m_0	The initial mass of the powder used for a TGA test (g)
m_i	The residual mass at different temperatures during a TGA test (g)
w_l	Weight loss (%)
w_r	Residual weight (%)
$\Delta\bar{T}$	Average temperature increase (K)
P_0	Heating power (W)
r	Radius of sensor (mm)
k	Thermal conductivity (W/mK)
α_t	Thermal diffusivity (mm^2/s)
t_t	Measurement time (s)
I_0	Modified Bessel function
τ_t	Dimensionless time
m	Number of concentric rings on the sensor
C_p	Specific heat capacity (J/kgK)
ρ	Density (kg/m^3)

D	Diameter of cement mortar (mm)
L	Length of cement mortar (mm)
A_V	Reference heat generation rate (W/g)
$\alpha(t)$	Hydration degree
α_{max}	The maximum hydration degree
$C_{p,f}$	Heat capacity at frozen state (J/kg/K)
$C_{p,u}$	Heat capacity at unfrozen state (J/kg/K)
C_p	Heat capacity (J/kg/K)
E_A	Activation energy (J/mol)
h_{eff}	Heat transfer coefficient (W/m^2/K).
$H(t)$	Cumulative hydration heat (J/g)
Hu	Total heat that can be released when all cement is reacted (J/g)
k	Thermal conductivity (W/m/K)
k_f	Thermal conductivity at frozen state (W/m/K)
k_u	Thermal conductivity at unfrozen state(W/m/K)
$L_{f\rightarrow u}$	Latent heat (kJ/kg)
q	Heat generation rate (W/g)

q_h	Heat flux between cement mortar and surrounding air (W)
R	Universal gas constant, 8.314 J / mol·K
t	Time (hour)
T	Temperature (K)
T_a	Air temperature (K)
T_{Curing}	Curing temperature (°C)
T_m	Temperature of the surface of cement mortar (K)
T_r	Reference temperature (K)
t_e	Equivalent age (hour)
θ_u	Fraction of frozen phase
θ_f	Fraction of unfrozen phase
β	Hydration shape factor
τ	Hydration time parameter (h)
δ	Thickness of the sand layer (mm)

Chapter 1. Introduction

1.1. Research background

Canada has the second largest coverage of permafrost in the world (Gruber, 2012; Ran et al., 2012). Approximately 50% of Canada's land mass is covered with permafrost (Gruber, 2012). With the increase of mining and construction activities in permafrost, cement-based mixtures (e.g., concrete, shotcrete, grout, and backfill) are expected to be widely used in these regions. For example, a large amount of concrete is required for building and infrastructure construction; shotcrete, backfill, and grout are essential materials for rock support in the mining industry. However, the application of cement-based mixtures in permafrost regions is challenging since cold weather poses severe issues to the setting and strength development of cement-based mixtures (Keen, 1993).

When placed in permafrost regions, fresh cement-based mixtures tend to dissipate heat to surroundings, resulting in a cold temperature (< 5 ºC). At cold temperatures, the hydration reaction rate between cement and water is very slow, which delays the gelation and densification of cement hydration products, ultimately resulting in slow strength development (ACI, 2010; Ioannidou et al., 2016). The slow strength development is unfavorable since it decreases construction efficiency, increases costs, reduces profits, and raises safety issues. For example, in the mining industry, the slow strength development of shotcrete at cold temperatures not only postpone re-entry, delay production, but also increase the potential for accidents caused by the failure of the weak structures.

In addition, early-age frost damage may happen if cement-based mixtures could not gain sufficient strength (compressive strength 3.5 MPa) before getting frozen. Early-age frost damage

is an irreversible deterioration of the properties of cement-based mixtures (e.g., compressive strength) caused by the freezing of the hardening cement-based mixtures (ACI, 2010; Bernhardt, 1956; Choi et al., 2017; Yi et al., 2011). After early-age frost damage, strength of cement-based structures cannot be ensured to reach an adequate value even if it is re-cured at normal temperatures (e.g., 20 °C) (ACI, 2010). This irreversible deterioration can be explained in two ways: (1) cracks caused by the volume expansion of ice lenses in hardening cement-based mixtures; (2) cavities formed in cement-based mixtures after the thawing of the ice lenses (Liu et al., 2014a; Powers, 1956; Yi et al., 2011). At a sub-zero temperature, water in fresh cement-based mixtures gets frozen and forms ice lenses (Rosenqvist et al., 2016). During the forming of ice lenses, the phase changing process from water to ice lead to a volume expansion by 9%, which induces internal tensile stress in cement-based mixtures. This tensile stress results in cracks in hardening cement-based mixtures if sufficient strength has not been developed (Corr et al., 2003). Once the temperature increased to above the melting point, the ice lenses melt and leave many cavities in cement-based mixtures (Monteiro, 2006). The cracks and cavities cannot be repaired even if recurring the cement-based mixtures at a normal temperature. As a result, an irreversible deterioration occurs. The cement-based mixtures that suffered from early-age frost damage cannot reach the designed strength. It is unsafe since insufficient support may increase the potential of accidents.

To address these problems, ACI 306 (ACI, 2010) suggests not to place cement-based mixtures when the environmental temperature is lower than 5 °C or special precautions should be taken to accelerate the strength development if cement-based mixtures are needed to be placed at cold temperatures. According to the literature, measures to accelerate the strength development of cement-based mixtures at cold temperatures include but are not limited to (1) increasing the

placing temperature by heating aggregates and water (ACI, 2010; Kumar et al., 2014; Zhu, 2013); (2) adding a larger portion of cement content or using cement that has high hydration heat and high early-age strength (Biggar et al., 1993; Nmai, 1998); (3) applying insulation form or covering the fresh paste with insulation materials to reduce the heat loss (Kosmatka et al., 2011; Won et al., 2016); (4) providing external heating sources, such as a stove, steam, infrared heater, and heating forms (Choi et al., 2017; Guo et al., 2014; Lee et al., 2012); and (5) adding accelerator or antifreeze admixtures to speed up the hydration reaction and prevent the fresh cement-based mixtures from freezing (Demirboğa et al., 2014; Karagöl et al., 2013; Karagol et al., 2015; Polat, 2016; Ryou and Lee, 2012, 2013). In permafrost regions, engineers usually use a combination of various measures to accelerate strength development. For example, when constructing at Diavik mine that is located at a permafrost region, engineers increased the cement content from 400 kg/m^3 to 585 kg/m^3, added calcium chloride as an antifreeze admixture, used steam and hot air to heat aggregates and rock substate, and forced hot air to accelerate the strength development of cement-based mixtures. However, these methods can arise new problems: (1) addition of calcium chloride can result in the corrosion of reinforcements (Dodson, 2013), which has been prohibited in many countries; (2) hot air can induce the thawing of permafrost, which causes instability and increases the risks of rock collapse and ground subsidence (Guo et al., 2011a; Khokholov and Kurilko, 2004; Li et al., 2017).

A new solution to accelerate strength development is using CSA cement, which has the features of rapid set and fast strength development (Juenger et al., 2011; Telesca et al., 2014; Yu et al., 2018). It was reported to achieve a UCS of 25 MPa within one hour (Ballou, 2013). The feature of fast strength development indicates that CSA cement has great potential to be applied in permafrost regions. Using CSA cement in permafrost regions could contribute significantly to

the mining and construction industries. First, it may solve the engineering problems related to slow strength development at cold temperatures and ensure safety. Second, it is possible to develop sufficient strength to resist the early-age frost damage before getting frozen, ensure the long-term quality of cement-based structures. Third, it can help to improve the efficiency of construction since delays caused by cold temperatures can be avoided. Moreover, substituting CSA cement for Portland cement can reduce CO_2 emissions from cement manufacturing. Despite its significance, the performance of CSA cement used in permafrost regions has never been reported in the literature. Therefore, it is of great interest to develop CSA cement-based mixtures for permafrost region applications and evaluate their performance at permafrost environments.

1.2. Literature review

Currently, many studies (ACI, 2010; Biggar et al., 1993; Choi et al., 2017; Karagöl et al., 2013; Korhonen and Cortez, 1991; Liu et al., 2018a; Yi et al., 2011) have been conducted to understand the behavior of cement-based mixtures used at cold temperatures and to accelerate the strength development and prevent early-age frost damage when cement-based mixtures are used in cold temperatures. According to the literature, the strength development rate is mainly controlled by the curing temperature, admixtures, and cement type (ACI, 2010; Karagöl et al., 2013; Korhonen and Cortez, 1991; Yi et al., 2011). Therefore, the most widely used measures to accelerate the setting and strength development are increasing curing temperature, adding admixtures, or using high early-age strength cement. Accelerating the strength development can also prevent early-age frost damage. This is because the hardening cement-based mixtures can develop resistance to the early-age frost damage after gaining sufficient strength (Yi et al., 2011). The other measure to prevent fresh cement-based mixtures from early-age frost damage is depressing the freezing point of pore solution by antifreeze admixtures (Karagöl et al., 2013). In

a word, the main factors affecting strength development and early-age frost damage are the curing temperature, admixtures, and cement type. Relevant literature relating to each of the main factors is reviewed below.

1.2.1. Influence of curing temperature

The hydration reaction rate between cement and water can be described with the Arrhenius equation (Martinelli et al., 2013), as shown in Equation (1-1).

$$\alpha = A_V e^{-\frac{E_A}{RT}} \quad (1\text{-}1)$$

Where R is the universal gas constant, 8.314 J/mol·K; A_V is a relevance rate, [%/h], E_A is activation energy, [J/mol]; T is the curing temperature, [K].

With the drop of curing temperature, the hydration reaction rate decreases exponentially. Therefore, in cold temperatures, it is essential to take some measures to increase the curing temperature. From literature, measures to increase the curing temperature include but are not limited to: (1) increasing the placing temperature (ACI, 2010; Kumar et al., 2014; Zhu, 2013); (2) covering with insulation materials (Kosmatka et al., 2011; Won et al., 2016); (3) providing external heating sources (Choi et al., 2017; Guo et al., 2014; Lee et al., 2012); and (4) increasing cement content or using cement that has high hydration heat (Biggar et al., 1993; Nmai, 1998).

1.2.1.1. Increasing placing temperature

In cold temperatures, ACI 306R-10 standard (ACI, 2010) recommended minimum placing temperatures for different concrete dimensions and ambient temperatures. Generally, industry increases the placing temperature by heating the raw materials, such as water, cement, and aggregate. The most practical and effective method is heating water. This is because the specific heat capacity of water is almost five times as much as the other raw materials; the temperature of water is easy to control while the aggregates and cement are difficult to be heated uniformly

(Kosmatka et al., 2011). Heating aggregates is also required if there are some ice, snow or frozen lumps attached on the aggregates (ACI, 2010).

1.2.1.2. Insulation materials

To accelerate the strength development and prevent frost damage, the temperature in the cement-based mixtures should be maintain at the placing temperature for a recommended time after placement (ACI, 2010). Covering the insulation materials at the surface can reduce the heat loss from the fresh cement-based mixtures to the surroundings due to their low heat conductivities. The commonly used insulation materials include straw, sawdust, insulating blanket, batt, polystyrene foam sheets, urethane foam, and polyethyene board (ACI, 2010; Lee et al., 2012; Zhang et al., 2011). For high-rise structures, insulation materials can be integrated with the formworks (Won et al., 2016).

1.2.1.3. External heating sources

Another method for keeping the fresh cement-based mixtures warm is providing external heating sources such as stove, steam, hydronic system, infrared heater, and electric heating wires. In recent years, several innovative heating curing methods were proposed for accelerating the strength development of cement-based mixtures and prevent early-age frost damage. For example, Choi et al. (2017) developed a heating form that utilized the heat released from the exothermic reaction between lime and water to prevent fresh concrete from early-age frost damage. Liu et al. (2018a, 2018b) used carbon nanofiber and graphene nanoplatelets to improve the electrical conductivity of cement-based mixtures, then applied alternating voltage on fresh cement-based mixtures to generate heat for accelerating the strength development at low temperatures. In addition, radio-wave was used to heat the fresh concrete in Höhlig's research

(2015). It indicated that this method can significantly accelerate the hydration reaction and hydration heat generation (Höhlig et al., 2015).

1.2.1.4. Hydration heat

As mentioned, the hydration between cement and water is an exothermic reaction. The heat release from the hydration reaction can work as a heating source. Using additional cement or the high hydration heat cement (e.g., type III and high alumina cement) can increase the heat released from hydration (Bernhardt, 1956; Biggar et al., 1993; Nmai, 1998). Generating more hydration heat is able to increase the temperature in the fresh cement-based mixtures. Therefore, increasing cement content or using high hydration heat cement is a choice for applying cement-based mixtures in cold temperatures.

1.2.2. Influence of admixtures

To protect cement-based mixtures in cold temperatures, the common approach is to keep the cement-based mixtures warm by the measures mentioned above. Another approach is to use chemical admixtures (e.g., accelerators and antifreeze admixtures) to accelerate the strength development or depress the freezing point of the fresh cement-based mixtures.

1.2.2.1. Accelerator

The commonly used accelerators are two categories: alkaline accelerators (e.g., alkali aluminates, alkali metal hydroxides, alkali silicates); alkali-free accelerators (e.g., calcium chloride, calcium nitrate, calcium nitrite, aluminum sulfate and organic accelerators) (Cheung et al., 2011; Maltese et al., 2007; Salvador et al., 2016; Thomas et al., 2009). These chemical admixtures accelerate the hydration reaction, setting and strength development of cement-based mixtures. The acceleration mechanisms are complexed. Usually, the acceleration effect is based on more than one of the following mechanisms: (1) targeting on aluminate and accelerating

ettringite formation; (2) accelerating calcium hydroxide nucleation and disruption of barrier layers; (3) accelerating C-S-H nucleation; (4) accelerating C-S-H growth by increasing the permeability of hydration products (Cheung et al., 2011).

At cold temperatures, accelerator can be used to improve the early-age strength and prevent early-age frost damage (Kim et al., 2016; Ryou and Lee, 2012, 2013). As mentioned before, the fresh cement-based mixtures can develop resistance to early-age frost damage after gaining sufficient strength.

The choice of accelerator should be very careful since some accelerators may arise new problems. For example, the accelerated setting lead to a rapid loss in workability (Ryou and Lee, 2012); Chloride compounds result in the corrosion of reinforcements (Dodson, 2013); alkaline accelerators are dangerous for worker and also reduce the durability of the cement-based mixtures if the aggregates are reactive (Won et al., 2012); excessive use of organic accelerator (e.g. triethanolamine) retards the hydration reaction or results in flash setting (Cheung et al., 2011).

1.2.2.2. Antifreeze admixture

Although accelerators are able to improve the early-age strength, some of them cannot prevent the fresh cement-based mixtures from freezing. Once fresh cement-based mixtures get frozen, the hydration reaction will stop since no liquid water is available (Çullu and Arslan, 2013). To protect against freezing, antifreeze admixtures can be added to fresh cement-based mixtures. Antifreeze admixtures protect the fresh cement-based mixtures by depressing the freezing point of pore solution and enabling the hydration reaction to continue at cold temperatures. According to literature, several chemicals have been used as antifreeze admixtures, such as calcium chloride, calcium nitrate, calcium nitrite, sodium chloride, sodium nitrite, urea, potash,

hydroxyethyl amine, and polyhydroxy amine (Çullu and Arslan, 2013; Karagöl et al., 2013; Karagol et al., 2015; Korhonen and Cortez, 1991; Polat, 2016). However, the usage of antifreeze admixture may lead to some side effects. For example, some of the antifreeze admixtures are excellent accelerators, which may reduce the workability of the fresh cement-based mixtures (Ryou and Lee, 2013); chloride compounds corrode the reinforcements (Dodson, 2013); urea retards the setting (Karagol et al., 2015).

1.2.3. Influence of cement type

The cement type is another factor that affects the setting, strength development and early-age frost damage of cement-based mixtures used in cold temperatures. Cements such as Type III, Ciment Fondu, and calcium sulfoaluminate (CSA), having high early age strength and high hydration heat, are believed to have the potential for construction projects in cold regions (e.g., permafrost regions) (Biggar et al., 1993; Glasser and Zhang, 2001; Winnefeld and Barlag, 2009a; Yi et al., 2011). Previous researchers investigated the use of Type III cement and Ciment Fondu. Nmai (1998) suggested that Type III cement can be used in cold temperatures to accelerate the concrete setting. Biggar et al. (1993) reported that a high content Ciment Fondu-based grout could harden without freezing when cured in permafrost at a temperature of -10 °C.

One new solution is CSA cement, which has the features of rapid set, fast strength development, and high hydration heat (Juenger et al., 2011; Telesca et al., 2014; Yu et al., 2018). For example, it was reported to achieve a UCS of 25 MPa in 1 hour (Ballou, 2013), which is much faster than Type III and Ciment Fondu. The features of rapid set and fast strength development indicate that CSA cement has a great potential to be applied in permafrost regions. Substituting CSA cement for OPC may help solve the engineering problems related with slow strength development and early-age frost damage.

Despite its great potential, no research has been conducted to evaluate the performance of CSA cement used in permafrost regions. There are some research gaps regarding the performance of CSA cement-based mixtures used in permafrost regions:

(1) no study has been conducted to understand the hydration reaction and strength development of CSA cement-based mixtures cured at permafrost environments.

(2) the performance of CSA cement-based mixtures for preventing early-age frost damage is unknown.

(3) the thermal properties of CSA cement-based mixtures have never been reported in the literature.

(4) there is no numerical model developed for predicting the temperature profiles of hardening CSA cement-based mixtures used in permafrost regions.

To fill these research gaps, a systematic study should be conducted to develop CSA cement-based mixtures for permafrost region applications and evaluate their performance at permafrost environments.

1.3. Research objectives

The overall objective this Ph.D. program is to develop calcium sulfoaluminate (CSA) cement-based mixtures for permafrost region applications and to evaluate their performance. To achieve this overall objective, five sub-objectives are proposed as follows:

(1) To understand the hydration reaction of CSA cement at various temperatures;

(2) To investigate the strength development of CSA cement-based mixtures at cold temperatures;

(3) To evaluate the performance of CSA cement-based mixtures for preventing early-age frost damage;

(4) To determine the thermal properties of CSA cement-based mixtures cured at cold temperatures; and

(5) To develop a numerical model for predicting the temperature profile in CSA cement-based mixtures cured at permafrost environments.

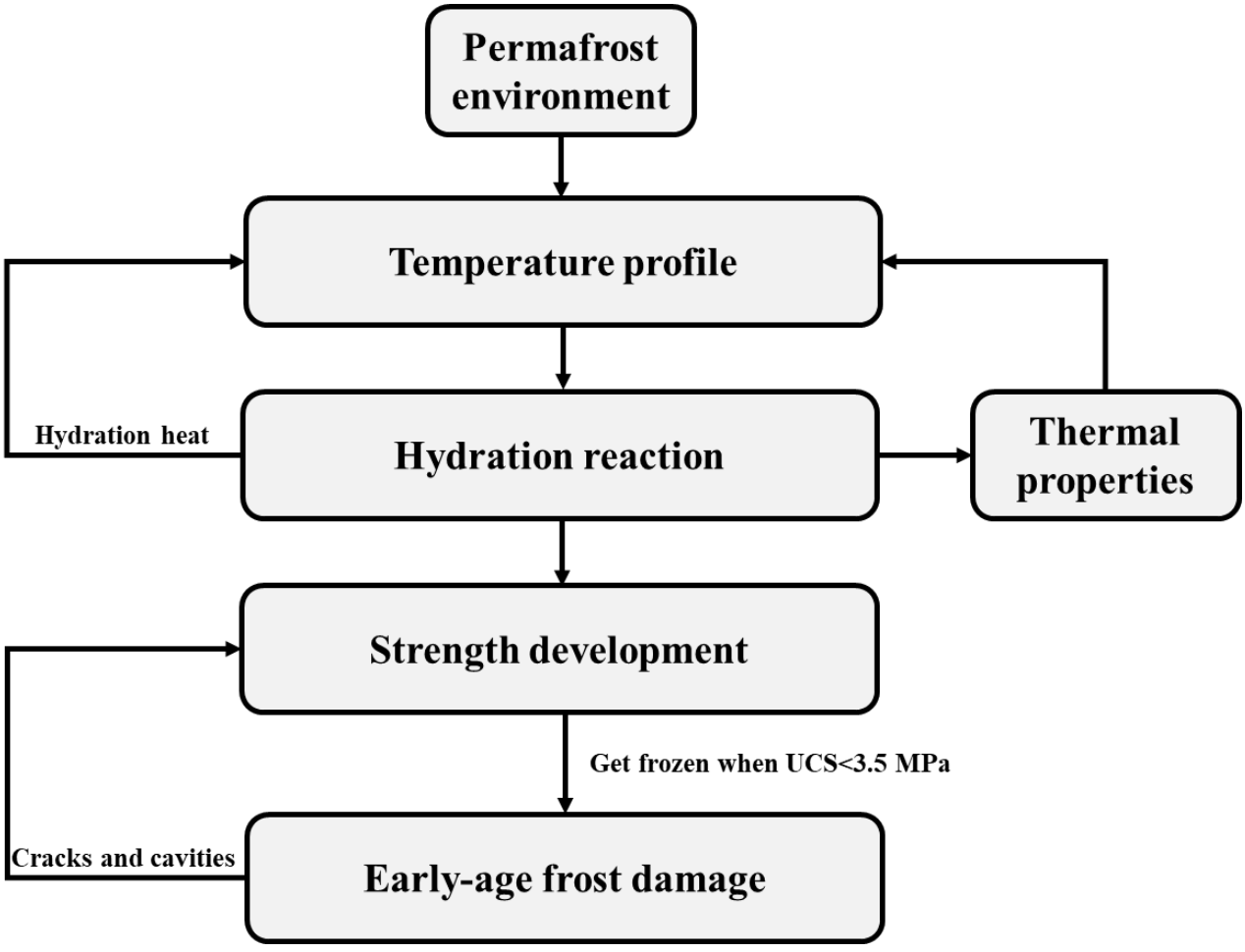

Figure 1.1 A flow chart showing the connection between these objectives.

The connection between these sub-objectives is presented in Figure 1.1. As shown in Figure 1.1, permafrost environments will cause a decrease in the temperature of fresh cement-based mixtures when they are placed in permafrost regions. With the decrease of temperature in fresh cement-based mixtures, the hydration reaction rate between cement and water will be decelerated, consequently the strength development will be slowed down (Choi et al., 2017; Liu et al., 2017; Yi et al., 2011). If the temperature in fresh cement-based mixtures decreases to freezing point before gaining sufficient strength (compressive strength 3.5 MPa), early-age frost damage will happen; as a result, the strength of cement-based mixtures cannot reach the designed value (ACI, 2010; Liu et al., 2018b; Yi et al., 2011). Figure 1.1 shows that the temperature profile in fresh cement-based mixtures is a critical factor affecting the strength development and early-age frost damage. The temperature profile in fresh cement-based mixtures is not only influenced by permafrost environment but also affected by thermal properties (i.e., thermal conductivity, thermal diffusivity, and heat capacity) of cement-based mixtures. For example, the thermal conductivity of cement-based mixtures determines the ability to conduct heat between the cement-based mixtures and the surroundings (Holman, 2001; Mydin, 2016), consequently affecting the temperature profiles in the cement-based mixtures. Additionally, cement hydration is an exothermic reaction (Kim, 2010; Livesey et al., 1991), the heat generated from cement hydration can increase the temperature or slow down the decreasing rate of the temperature in cement-based mixtures.

In summary, the hydration reaction, thermal properties, and temperature profile of hardening cement-based mixtures have direct or indirect connections with the strength development and early-age frost damage of cement-based mixtures cured in permafrost environment. To develop CSA cement-based mixtures for permafrost region applications, a comprehensive study should

be conducted to understand the hydration reaction, to evaluate the strength development and resistance to early-age frost damage, to determine the thermal properties, and to predict the temperature profiles of hardening CSA cement-based mixtures.

1.4. Thesis statement and thesis outline

Thesis statement: Calcium sulfoaluminate (CSA) cement-based mixtures can achieve fast hydration reaction, rapid strength development, and have high resistance to early-age frost damage at cold temperatures; CSA cement can be substituted for Portland cement to solve the problem of slow strength development and early-age frost damage when used in permafrost regions.

As shown in Figure 1.2, this thesis includes seven chapters, presenting in a paper-based format. The summary of each chapter is listed as follows.

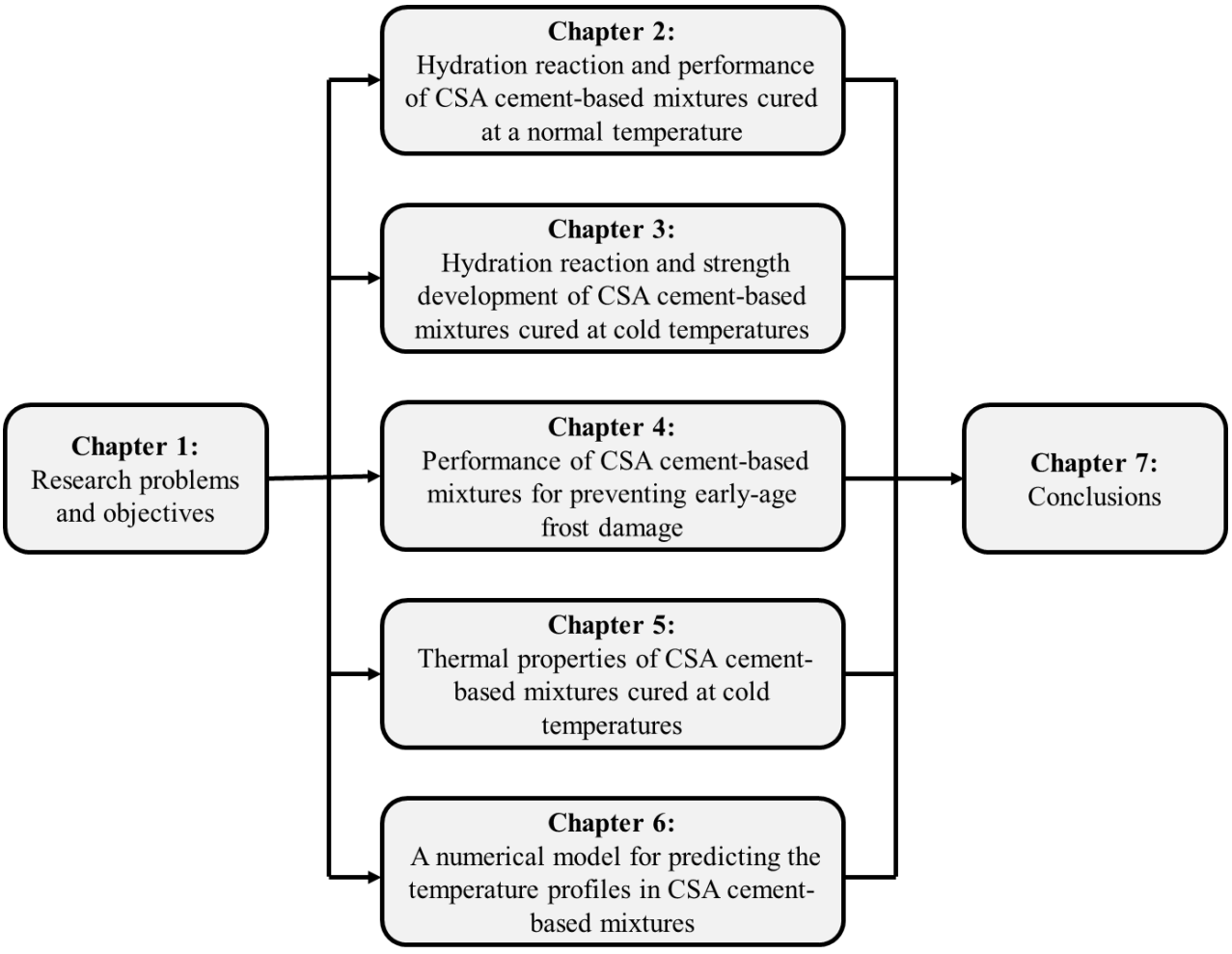

Figure 1.2 A flow chart showing the outline of this thesis.

Chapter 1 introduces the background of this research, points out the research problems, and objectives. When cement-based mixtures are placed in permafrost regions, their strength development is very slow, which decreases construction efficiency and may cause safety issues. In addition, early-age frost damage may happen if cement-based mixtures cannot gain sufficient strength (compressive strength 3.5 MPa) before getting frozen. There is a demand to develop innovative cement-based mixtures for permafrost region applications. CSA cement has the potential to solve the problems of slow strength development and early-age frost damage when used in permafrost regions; however, the performance of CSA cement-based mixtures has not been investigated. To fill this gap, this study aims to develop CSA cement-based mixtures for permafrost region applications, then evaluate and understand their performance.

Chapter 2 aims to understand the hydration reaction and performance of CSA cement-based mortar cured at a normal temperature (23 °C). Since the setting of CSA cement is fast at a normal temperature, sodium gluconate (SG) was added as a setting retarder. In this chapter, quantitative X-ray diffraction (QXRD), thermogravimetric analysis (TGA), and scanning electron microscopy (SEM) were performed to understand the effects of different dosage of SG on the hydration and microstructure of CSA cement mixtures. The influence of different dosage of SG on the setting, workability, and strength development of CSA cement-based mixtures was investigated. The results showed that the hydration, setting, strength development of CSA cement is very fast at a normal temperature (23 °C); Low dosages (≤0.5%) of SG effectively extended the setting time and improved the workability of CSA cement pastes without slowing down strength development. Instead, low dosages of SG increased the unconfined compressive strength (UCS) of CSA cement mortars at all ages (from 2 hours to 90 days) due to the reduction

in void content, fast diminishment of the retarding effect at early ages, and acceleration on belite hydration at later ages.

Chapter 3 investigated the hydration reaction and strength development of CSA cement-based mortar cured at cold temperatures (i.e., 5 °C, 0 °C, -5 °C and -10 °C). In this study, both CSA cement-based and ordinary Portland cement (OPC)-based mortar samples were cured in wet sands at temperatures of 5 °C, 0 °C, -5 °C and -10 °C. During the investigation, the temperature profiles in both sands and the centers of mortar samples were recorded. In addition, TGA and UCS tests were conducted on the samples at 1, 3, 7 and 28 days. The results showed that the hydration reaction and strength development of CSA cement was very fast even cured in frozen sands with temperatures at -5 °C and -10 °C.

Chapter 4 aims to explore the possibility of using CSA cement to prevent early-age frost damage. CSA-based and OPC-based mortars with and without calcium nitrate were exposed to -10 °C for 3 days, then re-cured at 23 °C until 28 days. Another group of mortars were directly cured at 23 °C as references. TGA and UCS tests were conducted at various ages; mercury intrusion porosimetry (MIP), and SEM were performed at 28 days. The results show that re-cured OPC-based mortars only achieved about half of the UCS of their references at 28 days, confirming a severe early-age frost damage. However, re-cured CSA Mix achieved 117% of the UCS of its reference, showing high resistance to early-age frost damage.

Chapter 5 determined the thermal properties of CSA cement-based mixtures. In this chapter, expanded perlite was incorporated into CSA cement-based mortars to develop a novel construction and building material that has low thermal conductivity for applications in permafrost regions. CSA cement mortars were cured at 23 °C and cold temperatures (i.e., 0 °C and -10 °C), and experiments were conducted for thermal properties (i.e., thermal conductivity,

thermal diffusivity, and heat capacity), UCS, density, ultrasonic pulse velocity (UPV), and TGA. The results showed that incorporating expanded perlite can significantly affect the thermal properties of CSA cement-based mortars. For example, thermal conductivity decreased exponentially from 0.97 ± 0.01 to 0.13 ± 0.002 W/mK when the aggregate replacement ratio increased from 0% to 100%. These CSA cement-based mixtures incorporated with expanded perlite can be used for mitigating the heat exchange among permafrost, cement-based mixtures, and air when used for rock support in permafrost regions or reducing the heat loss to outdoor environment when used as building materials.

Chapter 6 developed a numerical model for understanding the temperature profiles in CSA cement-based mixtures used in permafrost regions. Isothermal calorimetry and the Arrhenius equation were used to determine the heat generation rate of CSA cement. The modeling of temperature profiles in CSA cement-based mixtures was implemented COMSOL, the developed numerical model was validated with experimental results. After validation, the model was employed to investigate the influence of curing temperatures, curing modes (e.g., curing in air and curing in sand), and sample sizes on the temperature profiles in OPC-based and CSA-based mixtures. The results indicate that the temperature profiles in CSA-based samples were significantly affected by curing temperatures, curing modes, and sample sizes. In addition, the temperature in CSA-based sample was notably higher than that in OPC-based samples with the same size at curing conditions.

Chapter 7 summarized the primary conclusions, contributions, limitations of this thesis. Recommendations for future research are also discussed.

Chapter 2. Hydration reaction and performance of calcium sulfoaluminate cement mixtures with the addition of sodium gluconate

This chapter has been accepted as **G. Huang**, R. Gupta, W. V. Liu, Effects of sodium gluconate on hydration reaction, setting, workability, and strength development of calcium sulfoaluminate cement mixtures, *Journal of sustainable cement-based materials.*

Nomenclatures

ACI	American Concrete Institute
AFm	Monosulfate
AFt	Ettringite
AH_3	Aluminium hydroxide
ASTM	American Society for Testing and Materials
C_2ASH_8	Strätlingite
C_2S	Calcium silicate, belite
C_3A	Tricalcium aluminate
C_4AF	Tetracalcium aluminoferrite, brownmillerite
$C_4A\bar{S}H_{12}$	Monosulfate, AFm
$C_4A_3\bar{S}$	Tetracalcium trialuminate sulfate, ye'elimite
$C_6A\bar{S}_3H_{32}$	Etringite, AFt
$C\bar{S}$	Calcium sulfate
CH	Calcium hydroxide
CSA	Calcium sulfoaluminate
C-S-H	Calcium silicate hydrate

OPC	Ordinary Portland cement
PC	Portland cement
SSD	Saturated surface dry
SEM	Scanning electron microscopy
TGA	Thermogravimetric analysis
UCS	Unconfined compressive strength (MPa)
QXRD	Quantitative X-ray diffraction

2.1. Introduction

Calcium sulfoaluminate (CSA) cement is an eco-friendly building material that has been regarded as a cleaner alternative to Portland cement (PC) for reducing CO_2 emissions associated with the cement industry (Juenger et al., 2011). According to the life cycle assessment by Hanein et al. (2018), manufacturing CSA cement generates about 25% to 35% fewer CO_2 emissions than producing the same amount of PC. The reduced CO_2 emissions are primarily attributed to a lower calcination temperature (about 1250 °C, being 200 °C lower than that for PC) and a lower limestone proportion in feedstock (Hanein et al., 2018). Moreover, CSA cement can be produced with industrial wastes (Beretka et al., 1993; Ren et al., 2017; Rungchet et al., 2016). Ren et al. (2017) reported that using industrial wastes (e.g., red mud, flue gas desulfurization gypsum, aluminum slug, and carbide slag) to produce CSA cement could further reduce CO_2 emissions by about 40% when compared with the conventional method.

In addition to having low CO_2 emissions, CSA cement mixtures have high early-age strength and comparable long-term strength compared to PC mixtures. Generally, the main mineralogical compositions in CSA cement include belite, ye'elimite, and calcium sulfate (e.g., gypsum, bassanite, or anhydrite) (García-Maté et al., 2015; García-Maté et al., 2016; Winnefeld and Lothenbach, 2010). Once it encounters water, ye'elimite reacts quickly with calcium sulfate and water to generate ettringite (AFt or $C_6A\bar{S}_3H_{32}$) and alumina hydroxide (AH_3), or it hydrates rapidly to form monosulfate (AFm or $C_4A\bar{S}H_{12}$) and AH_3 when calcium sulfate is not available, as shown in Equations (2-1) and (2-2) (García-Maté et al., 2015; Tang et al., 2015; Telesca et al., 2014). The rapid hydration reaction of ye'elimite allows fast strength development at very early ages. For example, our previous studies (Huang et al., 2020a, 2020b) showed that CSA cement mortar gained a UCS of 17.0 MPa at 1 hour, which was 4.2 MPa higher than the 1-day UCS of

ordinary Portland cement (OPC) mortar with the same mixture proportion. At later ages, belite reacts with alumina hydroxide to form strätlingite (C_2ASH_8) following Equation (2-3) (Winnefeld and Lothenbach, 2010; Winnefeld et al., 2017). Strätlingite is unstable in the presence of belite since it can react with belite to form amorphous C-S-H and siliceous-hydrogarnet (Morin et al., 2017; Wang, 2010). The hydration of belite contributes to the strength development of CSA cement mixtures at later ages, ensuring a high long-term strength (Bescher and Kim, 2019; Rungchet et al., 2017). Winnefeld and Barlag (2009b) reported that the compressive strength of CSA cement mortars could reach up to 100 MPa after 28 days.

$$C_4A_3\bar{S} + 2C\bar{S}H_x + (38 - 2x)H \rightarrow C_6A\bar{S}_3H_{32} + 2AH_3 \quad (2\text{-}1)$$

$$C_4A_3\bar{S} + 18H \rightarrow C_4A\bar{S}H_{12} + 2AH_3 \quad (2\text{-}2)$$

$$C_2S + AH_3 + 5H \rightarrow C_2ASH_8 \quad (2\text{-}3)$$

Despite its low CO_2 emissions and great mechanical performance, CSA cement so far is still limited to small-scale repairing (Burris and Kurtis, 2018; Guan et al., 2017). Large-scale applications are restricted since the setting time of CSA cement mixtures is excessively short (e.g., 5 minutes (Burris and Kurtis, 2018; Huang et al., 2020b)). The fast setting (or short setting time) causes rapid loss of workability and restricts the available time for transportation and placement, further impeding the widespread applications of CSA cement (Burris and Kurtis, 2018). Therefore, adding admixtures to extend the setting time is critical for spreading the applications of CSA cement and helping reduce CO_2 emissions.

From the literature, citric acid is primarily recommended for extending the setting of CSA cement mixtures since a couple of studies have been done to understand its influence on the hydration reaction, setting, and strength development, which can provide guidance for achieving desired properties in a mixture design (Burris and Kurtis, 2018; Gwon et al., 2018; Hu et al.,

2017; Nguyen et al., 2019; Roswurm, 2018). However, citric acid may reduce the workability of CSA cement mixtures (Zhang et al., 2016). For example, Zhang et al. (2016) reported that adding 0.15% of citric acid reduced the flow diameter of CSA cement paste with the addition of 1.75% of aminosulfonic acid-based superplasticizer from 210 mm to about 150 mm at 5 minutes. The drop of workability is unfavourable since sufficient workability is the key to proper placing and compacting of cement mixtures.

In addition to citric acid, sodium gluconate ($HOCH_2[CH(OH)]_4COONa$), the sodium salt of gluconic acid, has also shown an effective retarding effect on the hydration and setting of CSA cement mixtures, and it improves the workability of CSA cement mixtures (Li et al., 2018; Zajac et al., 2016; Zhang et al., 2016). For example, Zhang et al. (2016) found that 0.15% of sodium gluconate extended the initial setting time of a CSA cement paste with a 1.25% dosage of polycarboxylate acid-based superplasticizer from 25 minutes to 70 minutes and increased the flow diameter of the pastes from 170 mm to about 270 mm at 15 minutes. A similar improvement in workability was also reported in the study from Li et al. (2018), in which 0.09% of sodium gluconate expanded the flow diameter of CSA cement pastes from 170 mm to 235 mm at 15 minutes under 40 °C. These studies indicate that sodium gluconate has the potential to be used as a retarder for CSA cement mixtures without compromising their workability. However, until now, there has been no research investigated the influence of different dosages of sodium gluconate on the hydration reaction, setting time, workability, early-age strength, and long-term strength of CSA cement mixtures. A comprehensive study should be conducted to understand the influence of sodium gluconate dosages on the hydration reaction, setting time, workability, and strength development since it can help guide future CSA mixture design to achieve desired

properties, ultimately spreading the application of eco-friendly CSA cement and reducing CO_2 emissions associated with cement production.

To this end, the objective of this study is to investigate the influence of different sodium gluconate dosages on the hydration reaction, setting time, workability, and strength development of CSA cement mixtures. X-ray diffraction (XRD) and thermogravimetric analysis (TGA) were performed to investigate the influence of sodium gluconate dosages on the hydration of CSA cement pastes. Scanning electron microscopy (SEM) was conducted to observe the influence of sodium gluconate dosages on the morphology of the hydration products and the microstructure of CSA cement pastes.

2.2. Materials and Methods

2.2.1. Materials

The raw materials used in this study included CSA cement (its composition is presented in Table 2.1, water, fine aggregate, and sodium gluconate. The particle size distribution of CSA cement, which is shown in Figure 2.1(a), was measured in an ethyl alcohol suspension using a Matersizer 3000 laser particle size diffraction analyzer (Malvern Instruments, UK). The fine aggregate had an oven-dry bulk density of 1668 kg/m^3. Its particle size distribution was within the American Concrete Institute (ACI) aggregate grading No.1 limits, as shown in Figure 2.1(b) (ACI, 2009b). Anhydrous sodium gluconate (98% purity) was used as a retarder for CSA cement. Sodium gluconate was dissolved in water before being mixed with cement and fine aggregates.

Table 2.1The oxide and mineralogical compositions of CSA cement.

Mineralogical compositions	Weight%	Oxide compositions	Weight%
Ye'elimite ($C_4A_3\bar{S}$)	26.3	SiO_2	15.4
Belite (C_2S)	48.8	Al_2O_3	14.7
Anhydrite ($C\bar{S}$)	12.8	Fe_2O_3	1.7
Bassanite ($C\bar{S}H_{0.5}$)	3.7	CaO	49.5
Brownmillerite (C_4AF)	1.8	MgO	1.4
Calcite (Cc)	3.4	K_2O	0.7
Quartz (S)	1.3	SO_3	13.8
Periclase (M)	1.0	LOI@950°C	2.0
Dolomite (CMc_2)	0.9		

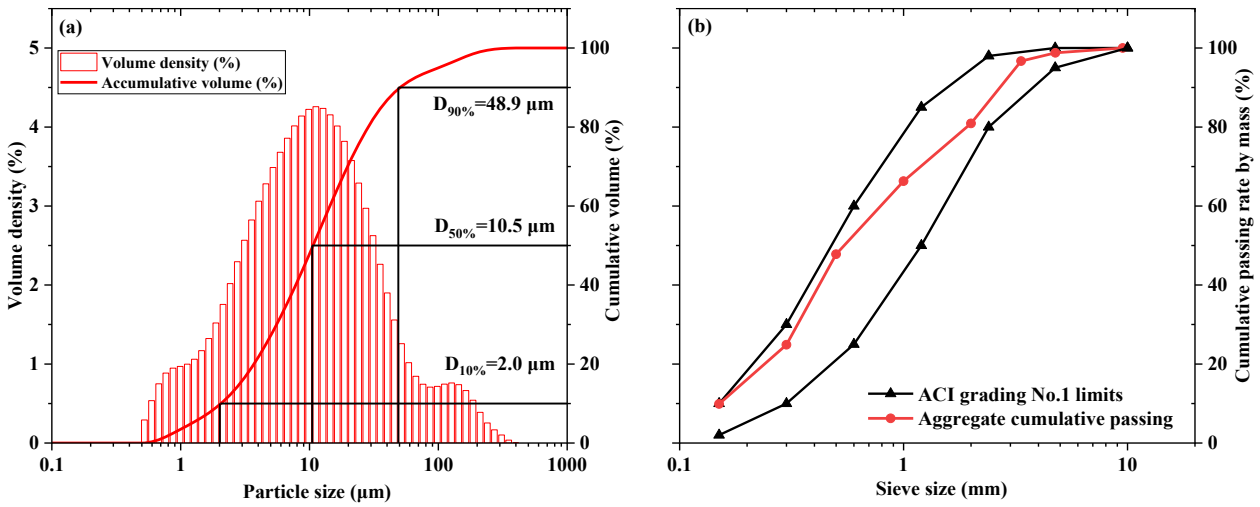

Figure 2.1The particle size distribution of (a) CSA cement and (b) fine aggregates.

2.2.2. Mixture proportions and methods

CSA cement pastes and mortars with different sodium gluconate dosages were prepared and tested following the mixture proportions and experimental design shown in Table 2.2. All the CSA cement pastes and mortars for tests that were conducted at specific ages were cured in a moisture room with a humidity of about 100% and a temperature of 23 ± 2 °C.

Table 2.2. Mixture proportions and experimental design.

Mixture	w/c ratio	a/c ratio	Sodium gluconate dosage (% of cement mass)	Tests	Testing ages
Cement paste	0.3	0	0%, 0.25%, 0.5%, 1%, 2%, and 3%	Setting time	-
				Flow diameter	-
	0.5	0	0%, 0.25%, 0.5%, 1%, and 2%	TGA	30 min, 2 hours, 6 hours, 1 day, 28 days, and 90 days
			0%, 0.5%, and 2%	XRD	2 hours and 90 days
				SEM	90 days
Cement mortar	0.5	3.125	0%, 0.25%, 0.5%, 1%, and 2%	Density and void content	28 days
				UCS	2 hours, 6 hours, 1 day, 7 days, 28 days, and 90 days

To understand the influence of sodium gluconate dosage on the setting and workability of CSA cement pastes, paste samples with water to cement (w/c) ratios of 0.3 (normal consistency status) were prepared for measuring the initial setting time, final setting time, and flow diameter as per

the ASTM standards C191-13 (ASTM International, 2013a) and C1437-15 (ASTM Interantional, 2015).

TGA and XRD analyses were conducted on the hydrated CSA cement pastes with a w/c ratio of 0.5 for investigating the effects of the sodium gluconate dosage on the hydration reaction of CSA cement. After being cured for specific ages (i.e., 30 min, 2 hours, 6 hours, 1 day, 28 days, and 90 days), CSA pastes were crushed into small particles (< 2 mm), immersed in acetone for 24 hours, and dried in a vacuum oven at 40 °C for 24 hours to stop CSA cement hydration following the same method used in our previous studies (Huang et al., 2019, 2020a, 2020b). Following the drying, the particles were further ground to pass through a 63-μm sieve, and then the powder (< 63 μm) was collected and stored in a desiccator before TGA and XRD tests. TGA tests were conducted with a Leco TGA 701 (Leco Corporation, USA) on hydration-stopped powder samples with various sodium gluconate dosages (i.e., 0%, 0.25%, 0.5%, 1%, and 2%) and different ages (i.e., 30 min, 2 hours, 6 hours, 1 day, 28 days, and 90 days). For each sample, 1.2 ± 0.05 g of hydration-stopped powder was heated from 20 °C to 500 °C at a rate of 5 °C/minute under a nitrogen atmosphere.

Before XRD analysis, ~2.000g hydration stopped powder sample was added with ~0.400g of NIST 676a alumina (corundum) powder which was an internal standard for quantify the total content of amorphous phases. After well-mixed, the sample was ground in a McCrone micronizing mill under 100% ethanol for 2 minutes. The grounded powder was air-dried, then analyzed using an Ultima IV X-ray diffractometer (Rigaku Corporation, Japan) with CoKα radiation (λ = 1.78899 Å). The X-ray diffractometer was operated at 38 kV and 38 mA, and scans were performed in a 2θ-range of 5º - 80º at a step size of 0.02º and a scan speed of 1.2º /minute. The crystalline phases in each sample were identified by interpreting the obtained XRD

patterns using the 2020 International Centre for Diffraction Data Database PDF 4+ and the 2020-1 Inorganic Crystal Structure Database. Quantitative analysis was performed with Rietveld refinement method using a free software GSAS II (Toby and Von Dreele, 2013).

SEM analysis was performed with a Zeiss Sigma 300 VP-FESEM (Zeiss group, Germany) to observe the microstructure and morphology of CSA cement pastes with different sodium gluconate dosages. After being cured for 90 days, CSA cement pastes with a w/c ratio of 0.5 were fractured into small pieces, then hydration-stopped and dried following the method described above. After that, the samples were coated with gold and then observed with a backscatter electron detector at a magnification of 400 times and with a secondary electron detector at a magnification of 10,000 times.

CSA cement mortars were prepared for investigating the influence of the sodium gluconate dosage on the physical and mechanical properties (i.e., density, void content, and UCS). CSA cement mortars were mixed with a w/c ratio of 0.5 and an aggregate-to-cement (a/c) ratio of 3.125, modified from ACI 506.5 (ACI, 2009b). Fine aggregates were weighed at a saturated surface dry (SSD) condition that had a water content of 2.1%. Then, the mortars were cast into cylindrical molds with dimensions of Ø50×100 mm and demolded at 24 hours except for those used for UCS tests at 2 hours and 6 hours (which were demolded before the UCS tests). The density and void content were measured at 28 days guided by the ASTM C642 Standard (ASTM International, 2013b), while the UCS tests were performed at 2 hours, 6 hours, 1 day, 28 days, and 90 days following the ASTM C39 Standard (ASTM International, 2018).

2.3. Results and discussion

2.3.1. Setting time

Figure 2.2 shows the influence of sodium gluconate dosages on the setting time of CSA cement pastes. As shown in Figure 2.2, CSA cement paste without sodium gluconate set rapidly, and its initial and final setting times were 5 minutes and 11 minutes, respectively. The addition of sodium gluconate retarded the setting of CSA cement pastes, and the retarding effect was enhanced with the increase of the dosage when it was lower than 2% of the cement mass. For example, the initial setting time was extended effectively from 5 minutes to 17 minutes, 31 minutes, 38 minutes, and 48 minutes when the sodium gluconate dosage increased from 0% to 0.25%, 0.5%, 1%, and 2%, respectively. When the sodium gluconate dosage was further increased from 2% to 3%, the setting time did not keep extending. Instead, the initial and final setting time was shortened by 4 minutes and 45 minutes. Compared with the setting of Portland cement, the setting of CSA cement pastes with the addition of sodium gluconate was still very fast since ASTM standard C150/C150M-19 (ASTM International, 2019) specified that the initial setting time of Portland cement should be no less than 45 minutes. Only the CSA cement paste with a 2% sodium gluconate addition met the minimum requirement for the initial setting. Compared with the retarding effect of citric acid (the most popular retarder for CSA cement (Burris and Kurtis, 2018; Hu et al., 2017; Nguyen et al., 2019; Zhang et al., 2016)), the retarding effect of sodium gluconate seemed less effective. Burris and Kutis (2018) investigated the retarding effect of citric acid on two types of CSA cement (CSA1 and CSA2). For CSA1, its initial setting time was extended from 5 minutes to 121 minutes when the citric dosage was increased from 0% to 3%, and the initial setting time for CSA2 was retarded from 21 minutes to 125 minutes as the citric dosage increased from 0% to 1%.

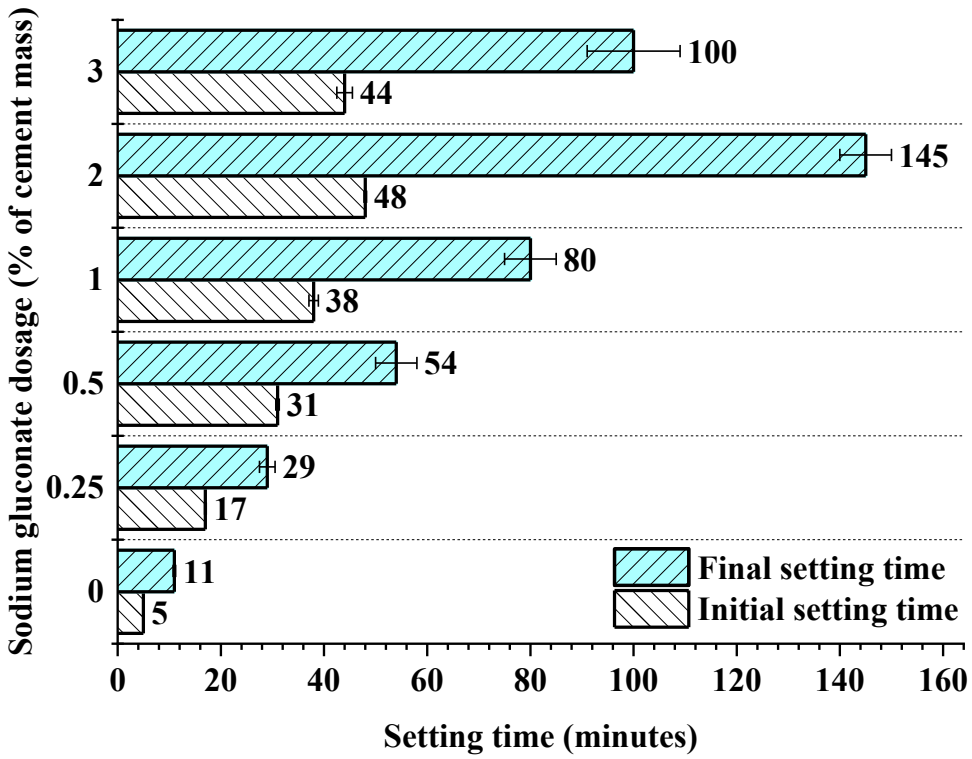

Figure 2.2 The influence of the sodium gluconate dosage on the setting of CSA cement pastes.

2.3.2. Workability

As shown in Figure 2.3, flow diameter was determined in order to investigate the influence of sodium gluconate dosages on the workability of CSA cement pastes. CSA cement paste without sodium gluconate had very low workability with a flow diameter of only 116 mm. The low workability was mainly caused by the fast hydration reaction of ye'elimite. As shown in Equation (2-1), one mole of ye'elimite consumes 38 moles of water to form ettringite when calcium sulfate is available. Due to the fast consumption of water, less free water was available among CSA cement particles, consequently leading to low workability. Meanwhile, the formation of ettringite caused the rapid loss of workability due to the bonding between ettringite crystals and unreacted cement particles (Huang et al., 2020b; Yu et al., 2019).

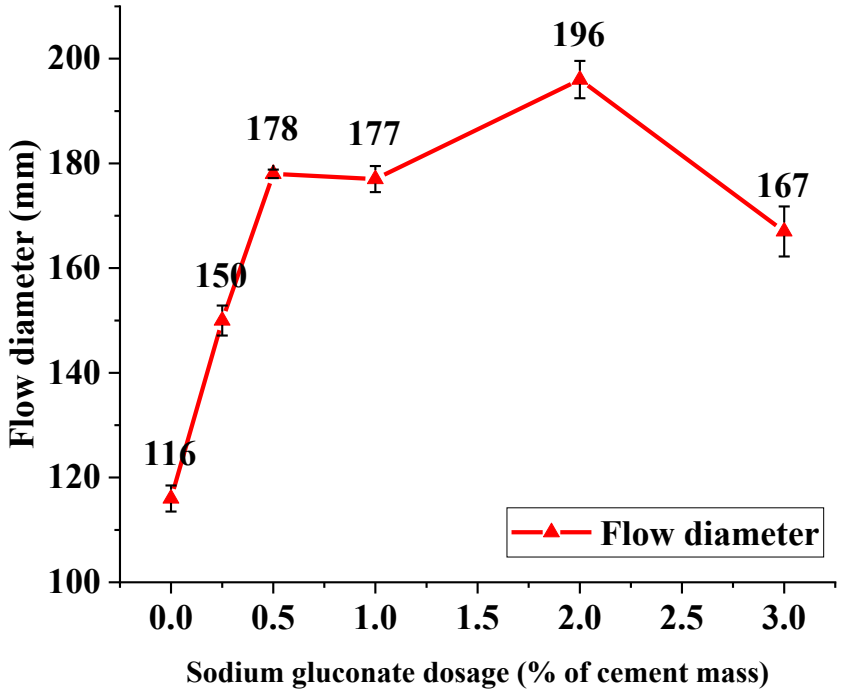

Figure 2.3 The influence of sodium gluconate dosages on the workability of CSA cement pastes.

The addition of sodium gluconate enlarged the flow diameter of CSA cement pastes, and the flow diameter increased with the increase of sodium gluconate dosage when the sodium gluconate dosage was lower than 2%. With the sodium gluconate dosage increase from 0% to 2%, the flow diameter of CSA cement pastes kept increasing from 116 mm to 196 mm, indicating that the workability improved with the increase of sodium gluconate dosage. There are three reasons for the improvement in workability. First, the addition of sodium gluconate retarded the hydration of CSA cement, and the retarding effect was enhanced with the increase in sodium gluconate dosage (the evidence is shown in Figure 2.4 and Figure 2.5). As a result, less water was consumed, and more free water was available among the cement particles, promising higher workability. Second, fewer ettringite crystals were formed with the increase of sodium gluconate dosage, as shown in Figure 2.5, mitigating the loss of workability. In addition, sodium

gluconate is known as a water reducer that can adsorb on cement particles during mixing and apply electrostatic and steric forces to overcome the Van der Waals attractive force among cement particles (Cheung et al., 2011; Lesage et al., 2015; Perez, 2007). In this way, it reduces the agglomeration of cement particles and liberates entrapped water, ultimately improving the workability of cement pastes (Cheung et al., 2011; Lesage et al., 2015; Perez, 2007). It is of note that the flow diameter of CSA cement paste was reduced from 196 mm to 167 mm when the sodium gluconate dosage was increased from 2% to 3%. Therefore, overdose should be avoided when sodium gluconate is added as a retarder for CSA cement since overdose not only reduces the retarding and plasticizing effects but also increases the costs on this admixture.

Compared with other retarders (e.g., citric acid (Ke and Zhang, 2020) and borax (Li et al., 2018)), sodium gluconate shows better performance regarding its influence on workability. For example, Ke and Zhang (2020) concluded that using citric acid as a retarder for CSA cement requires a higher dosage of superplasticizer to maintain its workability. Li et al. (2018) reported that the flow diameter of CSA cement paste was decreased from 225 mm to 108 mm when the borax dosage increased from 0% to 0.5%, showing that borax degrades the workability of CSA cement pastes. In contrast to citric acid and borax, sodium gluconate effectively improved the workability of CSA cement pastes.

2.3.3. Density and void content

Table 2.3 presents the void content and oven-dry bulk density of CSA cement mortars with different sodium gluconate dosages at 28 days. As shown in Table 2.3, the addition of sodium gluconate reduced the void content and increased the oven-dry bulk density of the CSA cement mortars. When the sodium gluconate dosage increased from 0% to 0.5%, a remarkable decrease from 27.0 vol% to 21.7 vol% could be observed in the void content of CSA cement mortars.

However, the rate of decrease slowed down when the sodium gluconate dosage was further increased from 0.5% to 2%, causing a slight reduction (~1.3 vol%) in the void content of CSA cement mortars. The decrease in the void content was caused by the improved workability with the addition of sodium gluconate, which helped the cement paste to fill in voids and facilitated air to escape from cement mortars. A similar decrease was reported in our previous study (Huang et al., 2020b), in which the void content of CSA cement mortars decreased when molasses was used as a retarder of CSA cement mixtures. The decrease in the void content resulted in a denser structure in CSA cement mortars. The oven-dry bulk density of CSA cement mortars rose from 1885 kg/m^3 to 1975 kg/m^3 as the sodium gluconate dosage increased from 0% to 0.5%, and then it almost became constant when the sodium gluconate dosage was further increased to 2%.

Table 2.3. Void content and oven-dry bulk density at 28 days.

Sodium gluconate dosage	Void content (vol%)	Oven-dry bulk density (kg/m^3)
0%	27.0±1.4	1885±13
0.25%	25.5±0.1	1941±4
0.5%	21.7±1.2	1975±2
1%	21.2±0.4	1971±3
2%	20.4±0.2	1971±5

2.3.4. Thermogravimetric analysis

TGA analysis was performed to understand the influence of sodium gluconate dosage on the hydration of CSA cement pastes, and its results were plotted as thermogravimetric (TG) curves and derivative thermogravimetric (DTG) curves. The TG and DTG curves in Figure 2.4 display

the residual weight and the derivative weight loss of the hydration-stopped samples during the TGA tests.

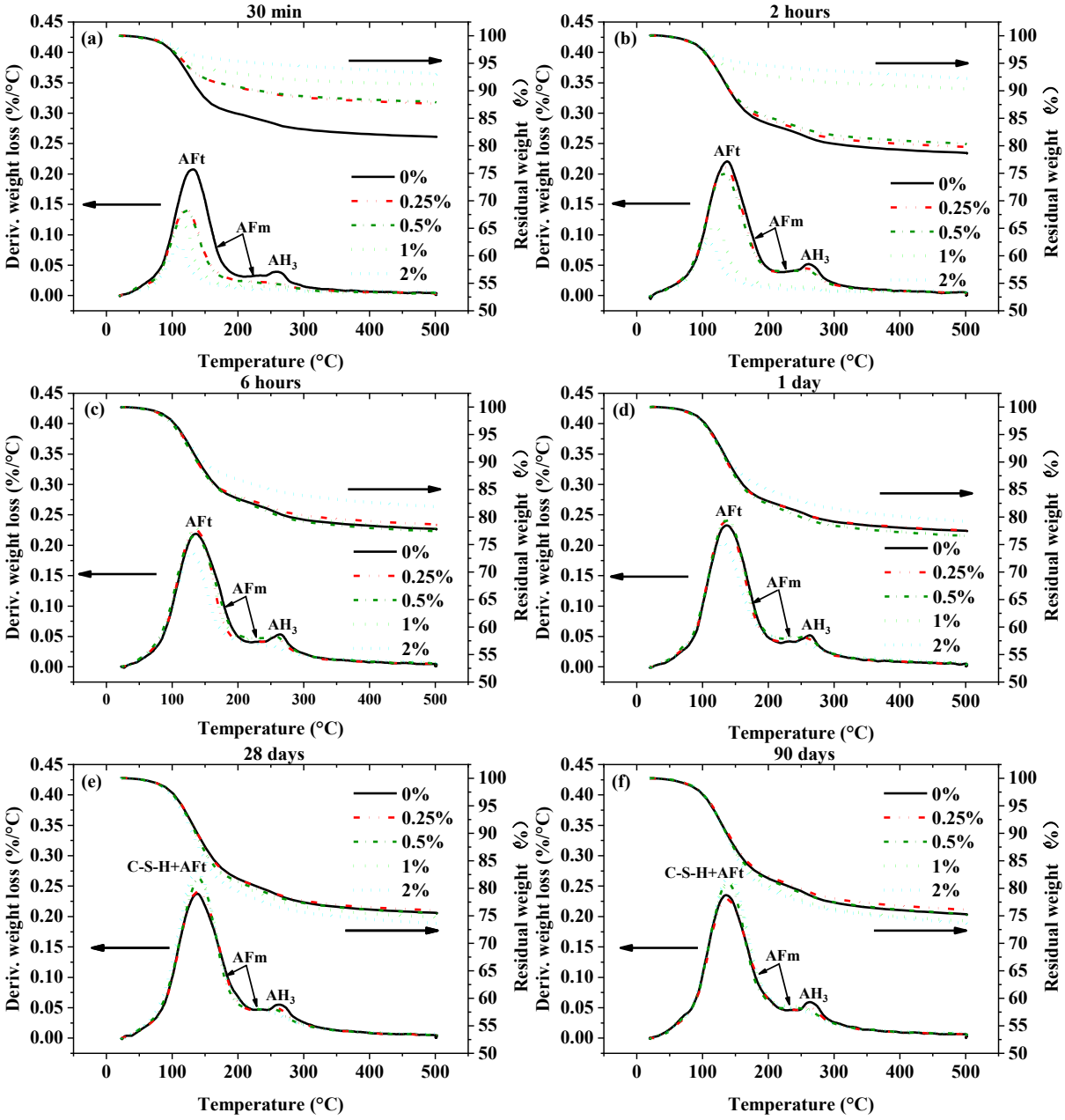

Figure 2.4 The TG and DTG plots of CSA cement samples after being hydrated for (a) 30 minutes; (b) 2 hours; (c) 6 hours; (d) 1 day; (e) 28 days; and (f) 90 days.

Figure 2.4 shows that the sodium gluconate dosage significantly affected the residual weight in TG curves and the peak intensities in DTG curves at early ages (e.g., 30 mins), indicating a strong influence on CSA cement hydration. As shown in Figure 2.4(a), there is an intensive peak for AFt in the DTG curve of the 30-minute sample without sodium gluconate, and the residual weight of this sample was low (81.5%). These peaks confirmed that the hydration reaction in the CSA cement paste without sodium gluconate was very fast, and a large amount of AFt had formed within 30 minutes. The fast formation of AFt explained why the CSA cement paste without sodium gluconate could set rapidly. When the sodium gluconate dosage was increased from 0% to 0.25%, 0.5%, 1.0%, and 2.0%, the residual weight went up from 81.5% to 87.5%, 87.8%, 91.0%, and 92.9%, respectively. Moreover, the peaks for AFt in the DTG curves were less intensive with the increase of sodium gluconate dosage. These peaks indicated that the addition of sodium gluconate retarded the hydration reaction of ye'elimite, and the retarding effect was enhanced with the increase of the sodium gluconate dosage. Consequently, the setting time was extended with the increase of the sodium gluconate dosage from 0% to 2%.

With aging, the retarding effect of sodium gluconate on ye'elimite was gradually diminished, and the hydration of ye'elimite accelerated at different ages depending on the sodium gluconate dosage. For example, the residual weights for the 2-hour samples with sodium gluconate dosages of 0.25% and 0.5% were only slightly (1.1% and 1.6%) higher than the residual weight for the sample without sodium gluconate, as shown in Figure 2.4(b). This means that the retarding effect of sodium gluconate was almost diminished within 2 hours at a low dosage (≤0.5%). Similar deminishment of the retarding effect was also observed by Zajac et al. (2016) who found that the concentration of sodium gluconate reduced 90% within one hour since gluconate ion can react with the hydration products (e.g., calcium aluminate (Smith et al., 2012)) of CSA cement. At

higher dosages (1% and 2%), the diminishment of retarding effect happened later, the hydration of ye'elimite accelerated at 2 hours to 6 hours. As a result, the difference in the residual weight of samples with different sodium gluconate dosages noticeably reduced within 6 hours. At 28 days and 90 days, the residual weight of samples with different sodium gluconate dosages were very close to each other.

It is worth mentioning that the small peak at around 260 °C accounts for the dehydration of AH_3. The signals for AH_3 in samples with the addition of sodium gluconate were less intensive when compared with the sample without sodium gluconate, indicating that sodium gluconate impeded the formation of AH_3. This coincides with the findings from Rossiter et al. (1998; 1996) that sodium gluconate blocks the formation of AH_3 by poisoning AH_3 precipitation.

2.3.5. Quantitative X-ray diffraction

2.3.5.1. Qualitative analysis

Figure 2.5 and Figure 2.6 show the comparison between observed XRD profiles and calculated XRD profiles by Rietveld refinement for 2-hour and 90-day samples. As shown in Figure 2.5, the main crystalline phases in CSA cement pastes after being cured for 2 hours, mainly including ettringite, anhydrite, ye'elimite, calcium carbonate. Crystalline alumina hydroxide (gibbsite) was not detected since alumina hydroxide can exist in an amorphous form. This coincides with Winnefeld and Lothenbach's study (2010), in which crystalline gibbsite was not identified by XRD but instead detected by TGA.

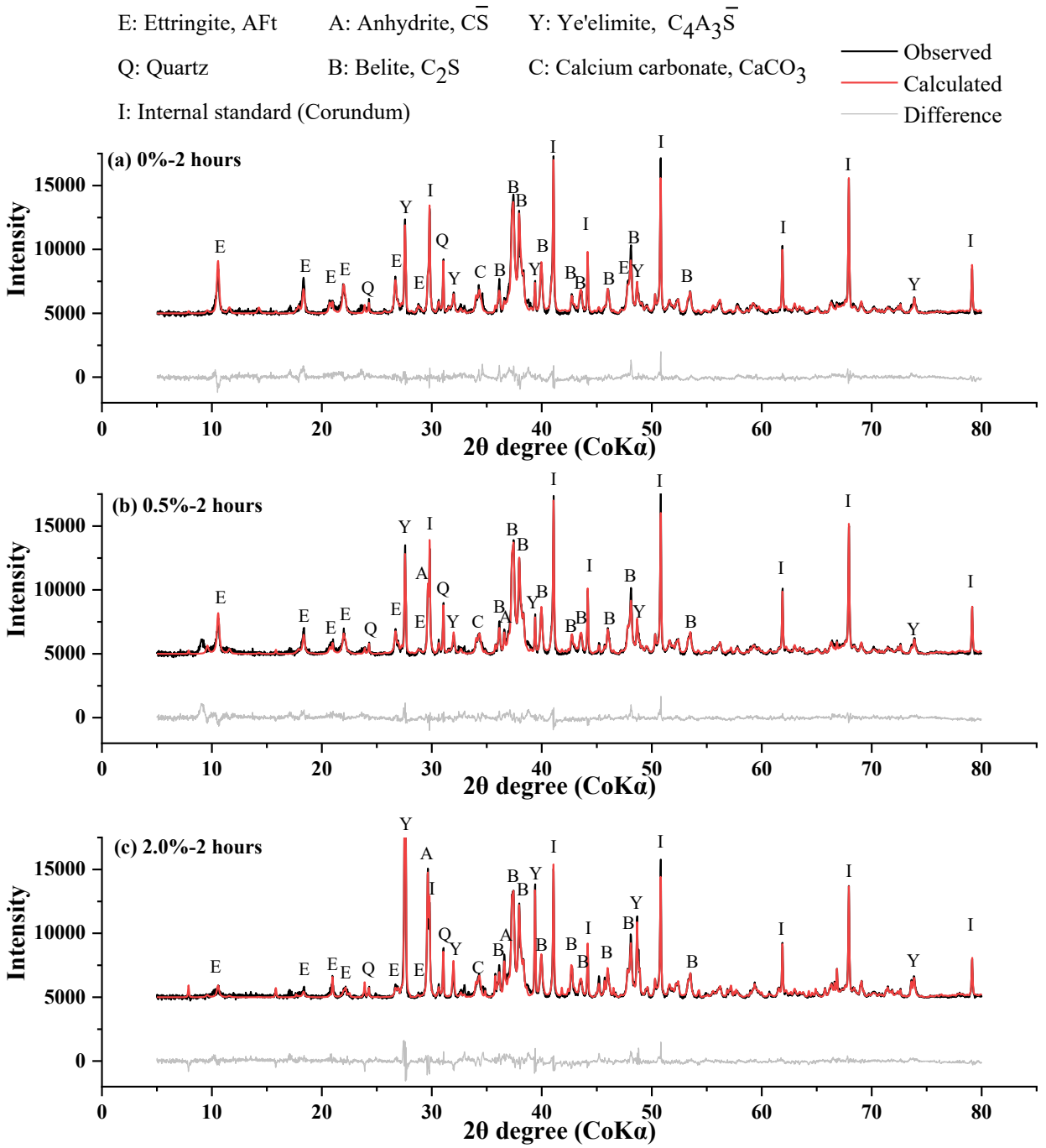

Figure 2.5 Rietveld refinement for CSA cement paste samples after being cured for 2 hours: (a) with 0% of sodium gluconate; (b) with 0.5% of sodium gluconate; (c) with 2% of sodium gluconate.

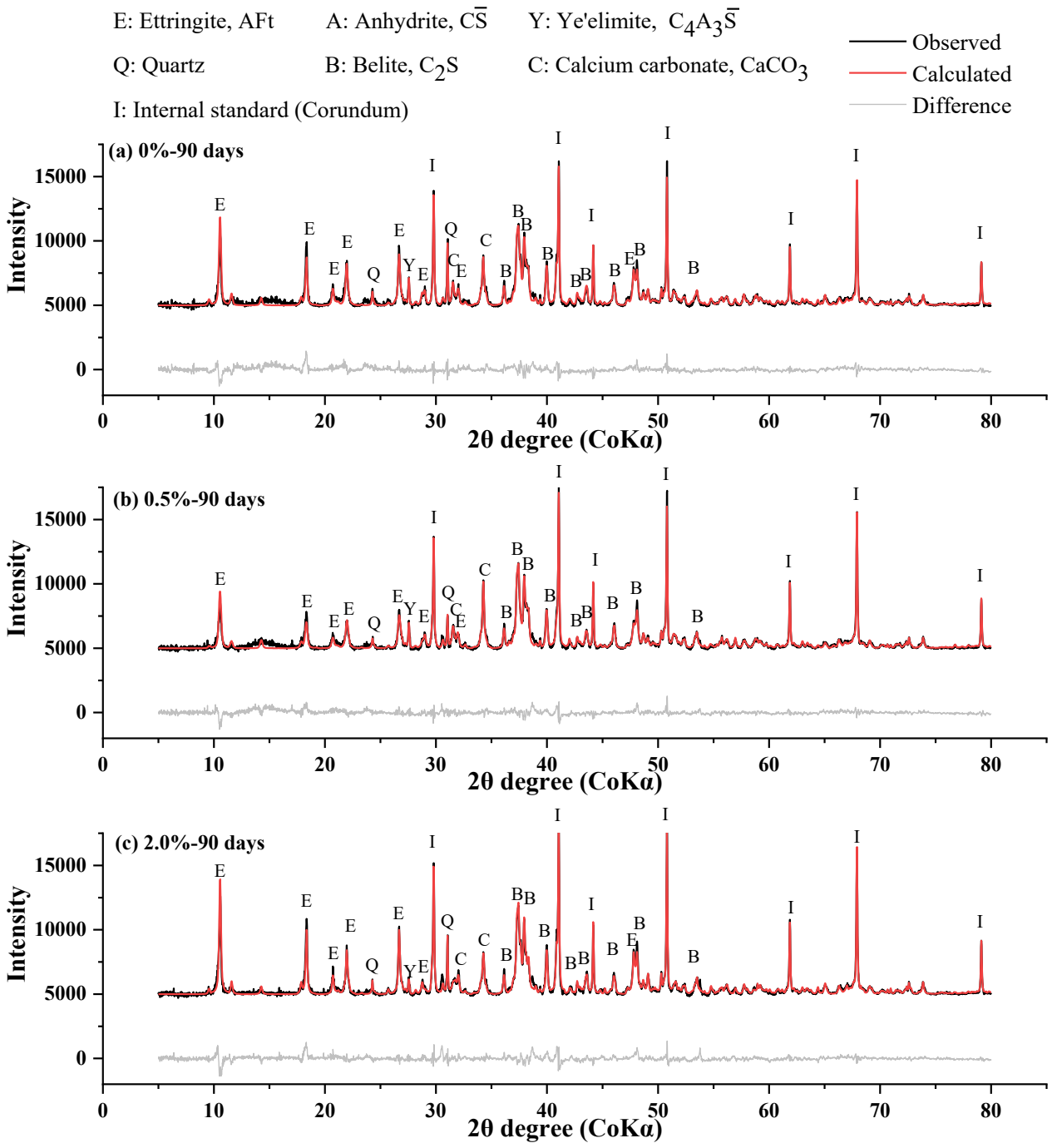

Figure 2.6 Rietveld refinement for CSA cement paste samples after being cured for 90 days: (a) with 0% of sodium gluconate; (b) with 0.5% of sodium gluconate; (c) with 2% of sodium gluconate.

Figure 2.6 depicts the influence of the sodium gluconate dosage on the phase content in CSA cement pastes at a later age (90 days). The XRD patterns show that the crystalline phases in the CSA cement pastes at 90 days included ettringite, calcium carbonate, unreacted belite, and trace amounts of ye'elimite regardless of the sodium gluconate dosage. This shows that the types of hydration products were not affected by the addition of sodium gluconate. In all the CSA cement pastes, most of the ye'elimite had reacted at 90 days. However, the obvious peaks for belite were observed in all the CSA cement pastes at 90 days because the hydration reaction of belite is very slow (Glasser and Zhang, 2001; Peterson et al., 2005; Trauchessec et al., 2015). In CSA cement, the hydration of belite can be further impeded by a lack of water since the hydration of ye'elimite is fast and consumes large amounts of water at early ages (Trauchessec et al., 2015). In general, the belite in CSA cement is believed to react with alumina hydroxide to form strätlingite (C_2ASH_8) (Winnefeld and Lothenbach, 2010; Winnefeld et al., 2017). However, no peak for strätlingite was observed in the XRD patterns, as shown in Figure 2.6. According to the literature, the formation of strätlingite usually occurs at a high w/c ratio (e.g., 0.8) (Jeong et al., 2018; Li et al., 2019), and strätlingite is unstable in the presence of belite since it can react with belite to form amorphous C-S-H and siliceous-hydrogarnet (Morin et al., 2017; Wang, 2010). In this study, the w/c ratio of CSA cement pastes for XRD tests was 0.5, and there was a large amount of unreacted belite in these cement pastes until 90 days, which explained the absence of strätlingite.

2.3.5.2. Quantitative analysis

Although the types of crystalline hydration products were not affected by the addition of sodium gluconate, the amounts of hydration products were changed with the addition of sodium gluconate. Figure 2.7 presents the phase content in CSA pastes after being cured for 2 hours and

90 days. At 2 hours, only 6.1% of ye'elimite was left in the CSA cement paste without sodium gluconate, and the content of ettringite and the total content of amorphous phases (inlduding AFm, AH_3, and C-S-H) reached 12.3% and 35.5%, respectively. With the addition of 0.5% of sodium gluconate, the consumption of ye'elimite within 2 hours was even slightly higher than that of the sample without sodium gluconate. This coincides with the finding from TGA analysis that the retarding effect of a low dosage (≤0.5%) of sodium gluconate was diminished within 2 hours. However, the content of ettringite was 2.7% less than that of the sample without sodium gluconate, and 1.1% more anhydrite was left at 2 hours. This indicates that a low dosage of sodium gluconate changed the hydration mechanism of ye'elimite—less ye'elimite reacted with anhydrite to form ettringite when a low dosage of sodium gluconate was added, instead, more ye'elimite hydrated to form amorphous phases (e.g., AFm). In addition, a low dosage of sodium gluconate slightly retarded the hydration of belite. At a sodium gluconate dosage of 2%, the ye'elimite and belite content was as high as 19.9% and 45.6% at 2 hours, and the content of ettringite and total amorphous phase was 3.3% and 14.2%, respectively. The content of unreacted ye'elimite and belite was significantly higher than that of the sample without sodium gluconate, indicating that a high dosage of sodium gluconate remarkably retarded the hydration of ye'elimite and belite. The influence of a high dosage of sodium gluconate on ye'elimite coincides with the finding by Zajac et al. (2016) that 2% of sodium gluconate strongly slowed the dissolution of ye'elimite and belite at early ages, as a result, it inhibited the generation of hydration products (e.g., ettringite and C-S-H).

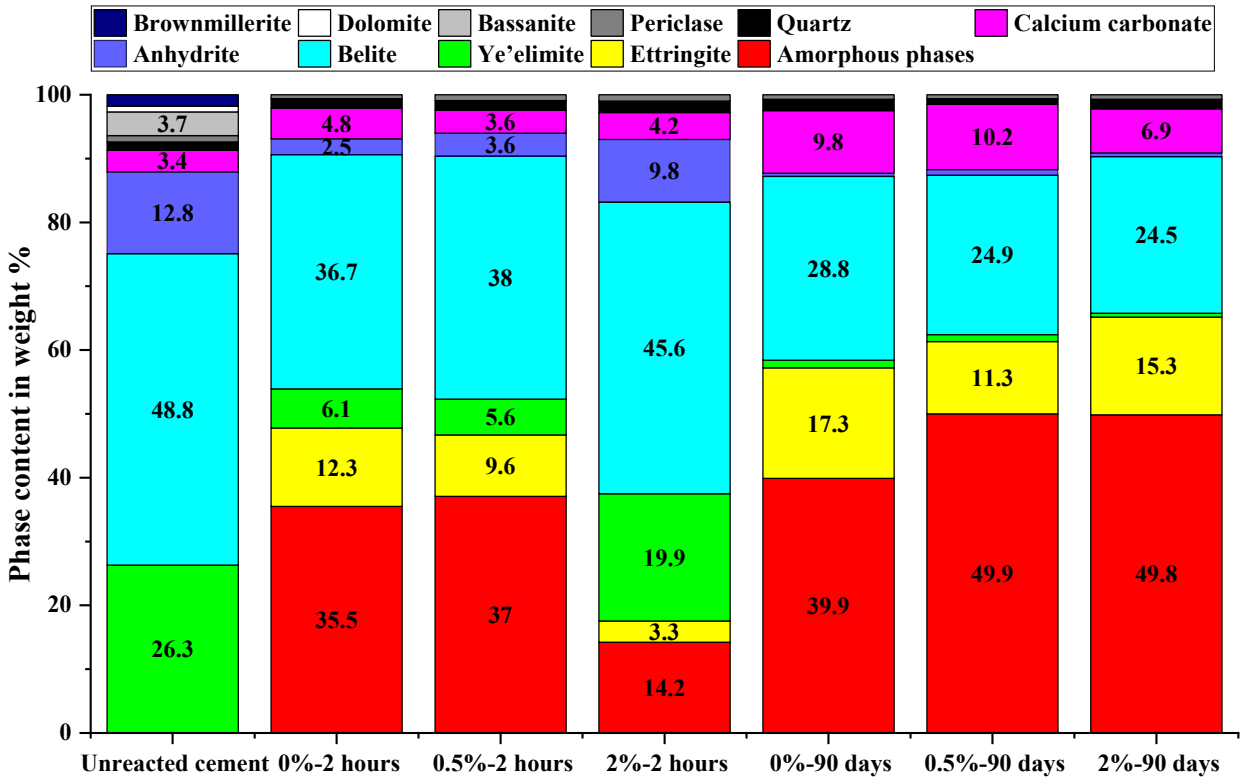

Figure 2.7 The phase content in CSA cement paste samples with different dosages of sodium gluconate calculated from Rietveld refinement.

At 90 days, the influence of sodium gluconate on the phase content in CSA cement pastes can still be observed. As shown in Figure 2.7, the addition of sodium gluconate caused a lower content (2%-6%) of ettringite in the CSA cement paste samples when similar amount of ye'elimite was consumed; whereas, the content of total amorphous phases in samples with sodium gluconate was 10% higher than that in sample without sodium gluconate. It means that the formation of amorphous phases (e.g., AFm) was favoured with the addition of sodium gluconate, while the formation of ettringite was inhibited. Lv et al. (2020) also reported that sodium gluconate can inhibit the formation of ettringite in OPC pastes when it was added at a dosage higher than 0.06%. Moreover, sodium gluconate had a slight influence on the hydration of belite at later ages. The content of unreacted belite in 90-day samples reduced from 28.8% to

24.9% and 24.5% when sodium gluconate dosage was increased from 0% to 0.5% and 2%. The decrease in the content of unreacted belite indicates the addition of sodium gluconate slightly promote the hydration of belite at later ages (e.g., 90 days).

It is worth mentioning that calcium carbonate was detected in both 2-hour and 90-day samples. This is because 3.4% of calcium carbonate (calcite) exsited in the unreacted CSA cement. Another reason is the carbonization of hydration products (e.g., C-S-H and AFt), which can happen during the curing, treatment, and storage of samples (Chen et al., 2017; Deboucha et al., 2017; Ramadan et al., 2020; Wang et al., 2020a; Wu et al., 2021). In order to mitigate carbonization during sample treatment and storage, crushed cement paste samples were dried in vacuum oven, then sealed in plastic bags and stored in a desiccator over silica gel and quicklime to reduce the contact with CO_2 in air. In the 2-hour samples, the calcium carbonate content is in a range of 3.6% - 4.2%, which is slightly (0.2%-1.2%) higher than the original calcium carbonate content in the unreacted CSA cement. This slightly increase indicates that the treatment and storage of samples did not cause severe carbonization of hydration products. However, the calcium carbonate content in 90-day samples was in a range of 6.9%-10.2%. The remark increase (3.5%-6.8%) in calcium carbonate content should be mainly caused by the carbonization of hydration products during the curing stage. The carbonization of cement hydration products at curing stage can be mitigated by many methods (e.g., sealing samples in plastic bags) in a laboratory. However, it may not be prohibited when cement-based mixtures are used for construction.

2.3.6. Scanning electron microscopy

Figure 2.8 depicts the influence of sodium gluconate dosages on the microstructures and morphology of CSA cement pastes hydrated for 90 days. At a magnification of 400 times, the

SEM images show that cracks can be observed in all CSA cement pastes regardless of the sodium gluconate dosages since various reasons can cause cracks (e.g., thermal stress (Riding, 2007) and dry shrinkage (Bentz and Jensen, 2004)). The microstructures of CSA cement pastes with a 0.5% sodium gluconate addition had no significant difference compared with those without sodium gluconate. However, the addition of 2% sodium gluconate caused a looser microstructure in the CSA cement paste compared with the other two samples. This was caused by the influence of a high dosage of sodium gluconate on the hydration of CSA cement.

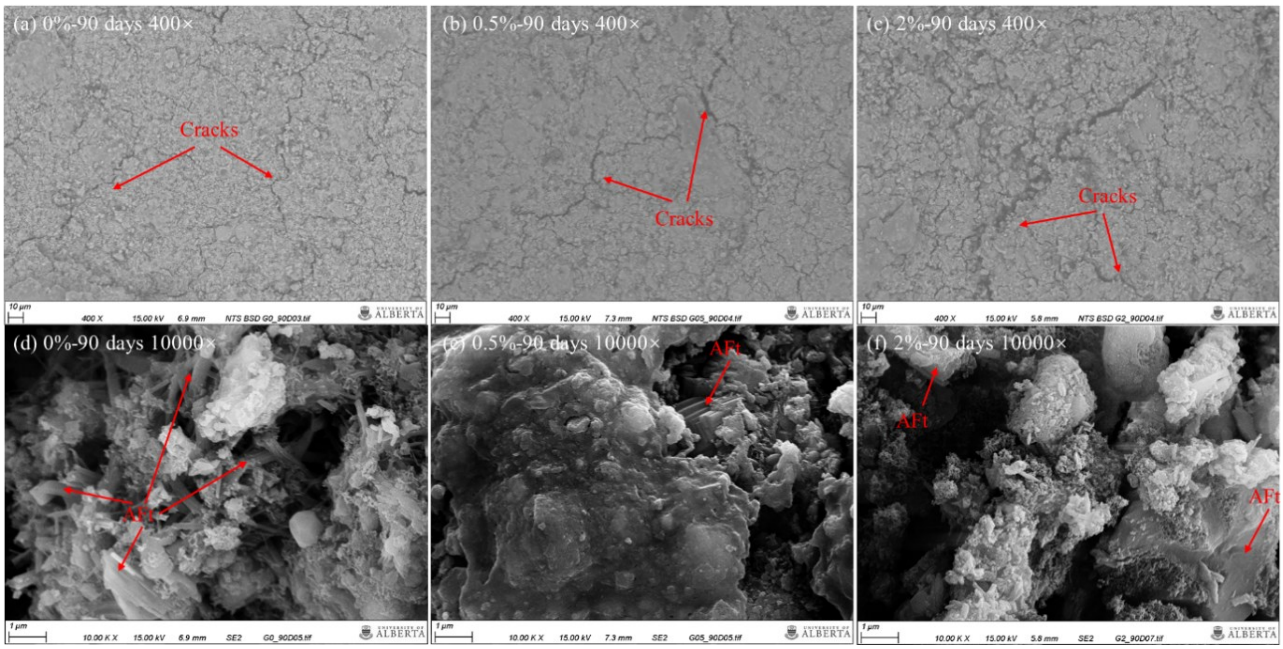

Figure 2.8 SEM images of 90-day CSA cement pastes with different sodium gluconate dosages observed at different magnifications: (a) 0% magnified 400 times; (b) 0.5% magnified 400 times; (c) 2% magnified 400 times; (d) 0% magnified 10000 times; (e) 0.5% magnified 10000 times; and (f) 2% magnified 10000 times.

The addition of sodium gluconate not only affected the microstructure but also had a significant influence on the morphology of hydration products. As shown in Figure 2.8(d), many rod-shaped ettringite crystals were distributed randomly in the CSA cement paste without sodium gluconate.

With the addition of 0.5% sodium gluconate, more amorphous hydration products can be observed in the CSA cement paste with 0.5% sodium gluconate, which coincided with the QXRD results presented in Figure 2.7. In addition, ettringite crystals tended to bond parallelly with each other, forming rods with a large size. At a sodium gluconate dosage of 2%, the formed ettringite was presented as large rods or bulks. A similar phenomenon was observed in the study of Zajac et al. (2016), in which ettringite was shown as "elongated tablets" with cross-sections larger than 1 μm instead of small rods when 2% of sodium gluconate was added. In addition, Zhang et al. (2017) also found the addition of sodium gluconate changed the morphology of ettringite; in their study, the size of ettringite was increased when sodium gluconate was added into a Portland cement-calcium aluminate cement-anhydrite binder at a dosage of 0.12% and 0.24%.

2.3.7. Unconfined compressive strength

Figure 2.9 presents the UCS of CSA cement mortars with different sodium gluconate dosages at various ages (e.g., 2 hours, 6 hours, 1 day, 7 days, 28 days, and 90 days). CSA cement mortar without sodium gluconate developed a UCS of 17.5 MPa at 2 hours, which was 4.7 MPa higher than the 1-day UCS of OPC-based mortar with the same mixture proportion and curing condition reported in our previous study (Huang et al., 2020a). The high early-age strength was attributed to the fast hydration of ye'elimite and formation of ettringite. With the increase in age, the UCS of the CSA cement mortar without sodium gluconate kept increasing and reached 73.8% and 98.8% of the 28-day UCS (33.2 MPa) at 1 day and 7 days, respectively. From 28 days to 90 days, the UCS of CSA cement mortars without sodium gluconate experienced a noticeable increase, from 33.2 MPa to 41 MPa. This was mainly attributable to the hydration of belite since

the belite usually reacts at later ages and contributes to long-term strength (Bescher and Kim, 2019; Rungchet et al., 2017).

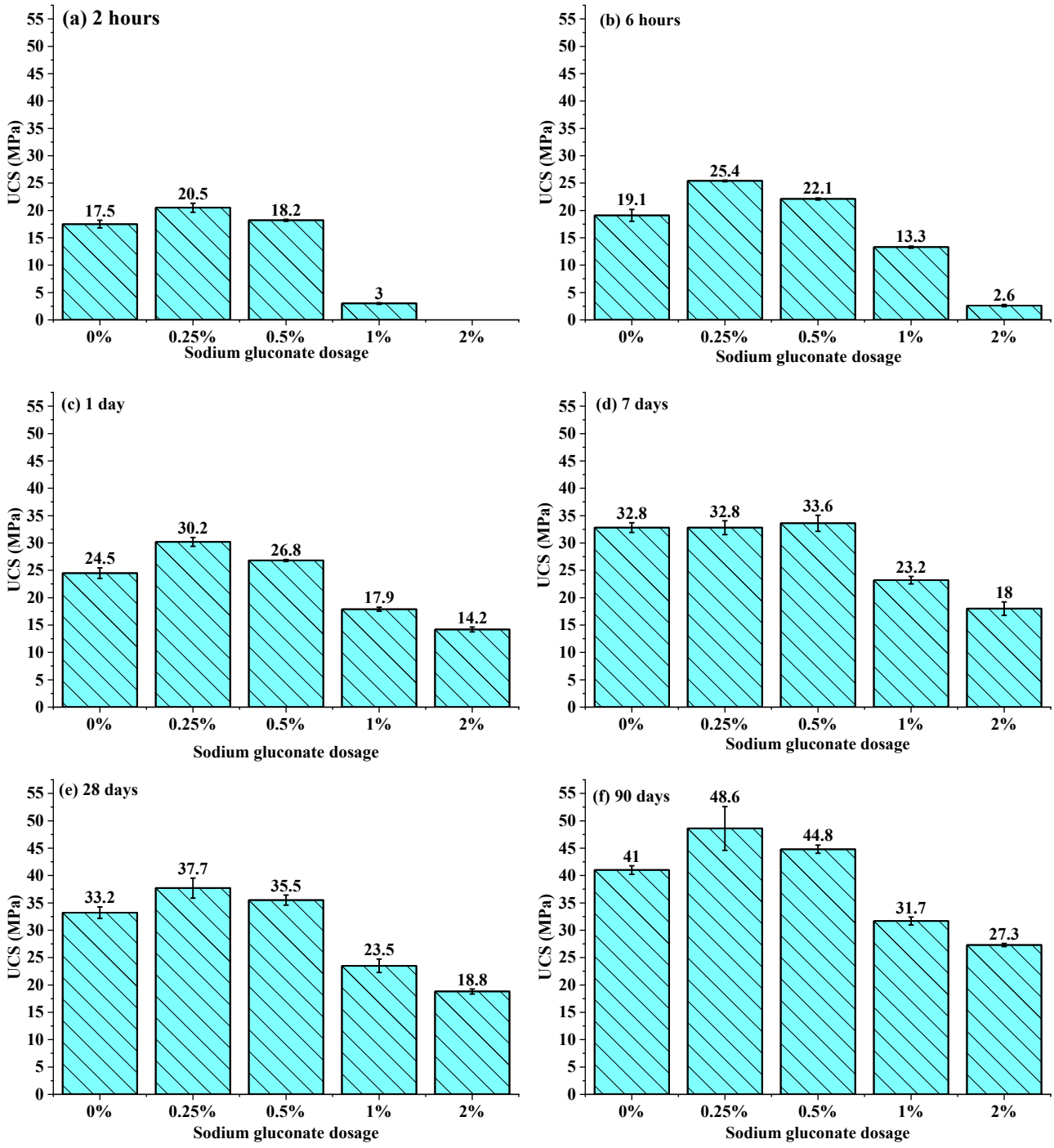

Figure 2.9 The influence of sodium gluconate dosages on the UCS of CSA cement mortars at: (a) 2 hours; (b) 6 hours; (c) 1 day; (d) 7 days; (e) 28 days; and (f) 90 days.

The addition of sodium gluconate affected the strength development of CSA cement mortars, and different dosages had very different influences. At a low dosage (≤ 0.5%), the addition of sodium gluconate, despite retarding the setting of CSA cement pastes, enhanced the UCS of CSA cement mortars at all ages from 2 hours to 90 days. At 2 hours, the UCS of CSA cement mortars with 0.25% and 0.5% of sodium gluconate was 20.5 MPa and 18.2 MPa, respectively, being 3 MPa and 0.7 MPa higher than the UCS of the mortar without sodium gluconate. This is because the retarding effect of sodium gluconate was diminished, and the hydration of ye'elimite was accelerated in the period from 30 minutes to 2 hours when sodium gluconate was added at dosages of 0.25% and 0.5%. In addition, 0.25% and 0.5% of sodium gluconate effectively reduced the void content in the CSA cement mortars, as shown in Table 2.3, forming denser structures and promising a higher UCS. At 90 days, the UCS of CSA cement mortars with 0.25% and 0.5% of sodium gluconate was 7.6 MPa and 3.8 MPa higher, respectively, than the UCS (41 MPa) of CSA cement mortar without sodium gluconate. The higher UCS at 90 days was because a low dosage (≤ 0.5%) of sodium gluconate promote the hydration reaction of belite and the formation of amorphous phases, as discussed before.

In contrast to a low dosage, a high dosage (≥1%) of sodium gluconate addition had a negative effect on both early-age strength and long-term strength. For example, the CSA cement mortar with 1% of sodium gluconate only gained a UCS of 3 MPa at 2 hours; meanwhile, no strength was developed at a sodium gluconate dosage of 2%. At 90 days, the UCS of CSA cement mortars with 1% and 2% of sodium gluconate was 9.3 MPa and 13.7 MPa lower, respectively, than that without a sodium gluconate addition. The low strength at early ages was mainly caused

by the strong retarding effect of a high dosage of sodium gluconate on the hydration of ye'elimite. Less AFt was formed at early ages, as shown in Figure 2.4 and Figure 2.7, which consequently caused low strength. At later ages, although a high dosage of sodium gluconate reduced the void content and promoted the formation of amorphous phase, the UCS of CSA cement mortars with a high dosage of sodium gluconate was significantly lower than that without sodium gluconate. This is because a looser microstructure was formed in the CSA cement pastes with high sodium gluconate dosages. In addition, the change in morphology of ettringite may also explain why CSA cement mortars with a high dosage of sodium gluconate had a lower UCS.

The low dosage and high dosage of sodium gluconate had very different effects on the strength development of the CSA cement mortars. The difference in UCS caused by sodium gluconate dosages can be as high as about 20 MPa at both early ages (e.g., 2 hours) and later ages (e.g., 90 days). Therefore, caution is essential when sodium gluconate is used as a retarder for CSA cement, and overdose must be avoided since it not only retards early-age strength development but also significantly compromises long-term strength.

2.4. Conclusion

This study investigated the influence of sodium gluconate dosages on the hydration reaction, setting, workability, and strength development of CSA cement mixtures for providing guidance to CSA cement mixture design. The main conclusions are enumerated as follows:

(1) At a normal temperature (23 °C), the hydration of CSA cement is very fast. In anhydrous CSA cement, the ye'elimite and anhydrite contents were 26.3% and 12.8%, respectively. After hydrated for 2 hours, the unreacted contents of ye'elimite and anhydrite decreased

to 6.1% and 2.5%, respectively, indicating that most of the ye'elimite and anhydrite were reacted within 2 hours.

(2) Sodium gluconate effectively extended the setting time and improved the workability of CSA cement pastes. With the sodium gluconate dosage increased from 0% to 0.5% and 2%, the initial setting time extended from 5 minutes to 31 minutes and 48 minutes, respectively. Meanwhile, the flow diameter expanded from 116 mm to 178 mm and 196 mm. However, an overdose (e.g., 3%) shortened the setting time to 44 minutes and reduced the flow diameter to 167 mm compared with the CSA cement paste with 2% of sodium gluconate.

(3) At early ages, sodium gluconate retarded the hydration of ye'elimite and impeded the formation of ettringite. However, the retarding effect diminished, and the hydration of ye'elimite was accelerated at different ages depending on the sodium gluconate dosage. For example, the retarding effect of sodium gluconate dosages of 0.5%, 1.0%, and 2.0% disappeared within 2 hours, within 6 hours, and after 1 day, respectively. At 90 days, more amorphous phases were detected in CSA cement pastes with a sodium gluconate addition since sodium gluconate facilitated the formation of amorphous phases (e.g., AFm) but impeded the growth of ettringite at later ages.

(4) The addition of sodium gluconate modified the morphology of ettringite and the microstructure of CSA cement pastes, which caused ettringite crystals to bond parallelly with each other, forming bunches of rods or ettringite bulks. Moreover, a high dosage of sodium gluconate (e.g., 2%) resulted in loose microstructures in CSA cement pastes.

(5) A low dosage (≤0.5%) of sodium gluconate increased the unconfined compressive strength (UCS) of CSA cement mortars throughout the ages from 2 hours to 90 days due

to the lower void content, fast diminishment of the retarding effect at early ages, and acceleration on belite hydration at later ages. However, a high dosage (≥1%) significantly degraded the UCS of CSA cement mortars throughout the ages due to the strong retarding effect on ye'elimite hydration at early ages and influence on the microstructure of CSA cement pastes.

(6) Caution should be taken when selecting the dosage since different sodium gluconate dosages have significantly different effects on the hydration and performance of CSA cement mixtures.

Chapter 3. Hydration reaction and strength development of calcium sulfoaluminate cement-based mortar cured at cold temperatures

This chapter has been published as **G. Huang**, D. Pudasainee, R. Gupta, W. Victor Liu, Hydration reaction and strength development of calcium sulfoaluminate cement-based mortar cured at cold temperatures, *Construction and Building Materials.* © Elsevier. 224 (2019) 493–503.

3.1. Introduction

Canada has the second largest coverage of permafrost in the world (Gruber, 2012; Ran et al., 2012). Approximately 50% of Canada's land mass is covered with permafrost (Gruber, 2012). When used in a permafrost region, fresh cement-based mixtures (e.g., concrete, shotcrete, grout, and backfill) tend to dissipate heat to surrounding environment, resulting in a cold temperature (< 5 °C) in the fresh cement-based mixtures. At cold temperatures, the setting and strength development of cement-based mixtures are very slow due to the slow hydration reaction between cement and water (ACI, 2010). The slow setting and strength development not only extend the construction time, but also increase the potential for accidents caused by the failure of the weak structures. Therefore, during the placing and curing period, special precautions are required to accelerate the hydration reaction and the strength development of cement-based mixtures constructed in cold temperatures (Karagöl et al., 2013).

According to literature, measures to accelerate the strength development of cement-based mixtures at cold temperatures include but are not limited to (1) increasing the placing temperature by heating aggregates and water (ACI, 2010; Kumar et al., 2014; Zhu, 2013); (2) adding a larger portion of cement content or using cement that has high hydration heat and high early-age strength (Biggar et al., 1993; Nmai, 1998); (3) applying insulation form or covering the fresh paste with insulation materials to reduce the heat loss (Kosmatka et al., 2011; Won et al., 2016); (4) providing external heating sources, such as a stove, steam, infrared heater, and heating forms (Choi et al., 2017; Guo et al., 2014; Lee et al., 2012); and (5) adding accelerator or antifreeze admixtures to speed up the hydration reaction and prevent the fresh cement-based mixtures from freezing (Demirboğa et al., 2014; Karagöl et al., 2013; Karagol et al., 2015; Polat, 2016; Ryou and Lee, 2012, 2013).

Among these measures, cement such as Type III, Ciment Fondu, and calcium sulfoaluminate (CSA), all of which have high hydration heat and high early age strength, have the potential for use in construction projects in permafrost (Biggar et al., 1993; Glasser and Zhang, 2001; Winnefeld and Barlag, 2009a; Yi et al., 2011). Previous researchers investigated the use of Type III cement and Ciment Fondu. Nmai (Nmai, 1998) suggested that Type III cement can be used in cold temperatures to accelerate the concrete setting. Biggar et al. (1993) reported that a high content Ciment Fondu-based grout could harden without freezing when cured in permafrost at a temperature of -10 °C. However, there is very little in the literature about the performance of CSA cement-based mixtures cured at cold temperatures, especially at freezing temperatures (i.e., the application in a permafrost region).

Typically, the main components in CSA cement include 30-70 wt% of ye'elimite ($C_4A_3\bar{S}$), 10-25% of calcium sulfate ($C\bar{S}$, including anhydrite, gypsum or hemihydrate), and other constituents such as calcium aluminate (CA) and belite (C_2S) (Winnefeld et al., 2017) (abbreviated symbols used to present the components of cement or hydration products are presented here: $C = CaO, \bar{S} = SO_3, A = Al_2O_3, H = H_2O, S = SiO_2$). The hydration kinetics of CSA cement are primarily controlled by the types and the amount of calcium sulfate (García-Maté et al., 2015; Winnefeld et al., 2017). When enough calcium sulfate is dissolved in the pore solution, the main hydration products are ettringite ($C_6A\bar{S}_3H_{32}$ or AFt) and aluminium hydroxide (AH_3), as shown in Equation (3-1) (Winnefeld and Lothenbach, 2010). As the depletion of calcium sulfate or the dissolving rate of calcium sulfate is slower than its consumption rate, monosulfoaluminate ($C_4A\bar{S}H_{12}$ or AFm) and aluminium hydroxide are formed according to Equation (3-2) (Tang et al., 2015). The transformation can occur between AFt and AFm at certain conditions—see Equations (3-3) and (3-4) (Tang et al., 2015). AFt transforms to AFm when Ca^{2+} and $SO_4{}^{2-}$ are

not sufficient in the pore solution or at a high temperature, while AFm turns to AFt when newly-dissolved Ca^{2+} and $SO_4{}^{2-}$ are available during the hydration of CSA cement (Tang et al., 2015; Xu et al., 2017). Belite slowly reacts with water, forming calcium hydroxide (CH) and calcium silicate hydrate (C-S-H) gel as shown in Equation (3-5)(Cuesta et al., 2018; Glasser and Zhang, 2001). The presence of CH can accelerate the formation of AFt as shown in Equations (3-6) and (3-7) (Li et al., 2018).

$$C_4A_3\bar{S} + 2C\bar{S} + 38H \rightarrow C_6A\bar{S}_3H_{32} + 2AH_3 \quad (3\text{-}1)$$

$$C_4A_3\bar{S} + 18H \rightarrow C_4A\bar{S}H_{12} + 2AH_3 \quad (3\text{-}2)$$

$$C_4A\bar{S}H_{12} + 2C\bar{S} + 20H \rightarrow C_6A\bar{S}_3H_{32} \quad (3\text{-}3)$$

$$C_6A\bar{S}_3H_{32} \rightarrow C_4A\bar{S}H_{12} + 2C\bar{S} + 20H \quad (3\text{-}4)$$

$$C_2S + 4.2H \rightarrow C_{1.8}SH_4 + 0.2CH \quad (3\text{-}5)$$

$$C_4A_3\bar{S} + 8C\bar{S} + 6CH + 90H \rightarrow 3C_6A\bar{S}_3H_{32} \quad (3\text{-}6)$$

$$AH_3 + 3CH + 3C\bar{S} + 26H \rightarrow 3C_6A\bar{S}_3H_{32} \quad (3\text{-}7)$$

CSA cement has attracted much attention in the last few years, owing to its various advantages such as low carbon dioxide (CO_2) emission during manufacturing, rapid setting, fast strength development, and shrinkage compensation (Glasser and Zhang, 2001; Juenger et al., 2011; Yu et al., 2018). It is also reported that the heat generation rate during CSA cement hydration is noticeably higher than that released from Portland cement hydration (Bullard et al., 2011; Le Saoût et al., 2013; Winnefeld and Barlag, 2009a). Due to the various advantages, CSA cement may be suitable for the application at cold temperatures. There are great potential benefits to use CSA cement at cold temperatures. On the one hand, using CSA cement can solve the problem of slow strength development of cement-based mixtures used at cold temperatures. On the other hand, substituting CSA cement for traditional cement can reduce CO_2 emissions that result from

cement manufacturing. Despite these potential benefits, at present, research about CSA cement used at cold temperatures is scarce in literature.

To this end, the objective of this study is to investigate the hydration reaction and the strength development of CSA-based mortar cured at cold temperatures (e.g., in the permafrost region). The performance of CSA-based mortar was compared with OPC-based mortar cured at same conditions. Methods used in this research included temperature recording, thermogravimetric analysis (TGA), and unconfined compressive strength (UCS) measurements. This study has provided valuable insights into future projects involving cement-based mixtures at cold temperatures (e.g., in Canada's North and other permafrost regions).

3.2. Materials and methods

3.2.1. Materials

CSA cement, type OPC ordinary Portland cement, fine aggregates and tap water were used to make the mortar mixtures. The main oxide compositions of CSA cement and type OPC cement are shown in Table 3.1. The principle mineral constituents in the CSA cement include ye'elimite ($C_4A_3\bar{S}$), anhydrite ($C\bar{S}$) and belite (C_2S), proportioned 27.7%, 17.8%, and 45.0%, respectively. The fine aggregates were under the saturated surface dry (SSD) condition, with a water content of 1.52%. The bulk density of the fine aggregates was 1606.8 kg/m^3 under oven-dry conditions. Figure 3.1 shows the sieve analysis result of this fine aggregate, indicating that the grain size distribution was within the American Concrete Institute (ACI) No.1 grading limits (ACI, 2009b).

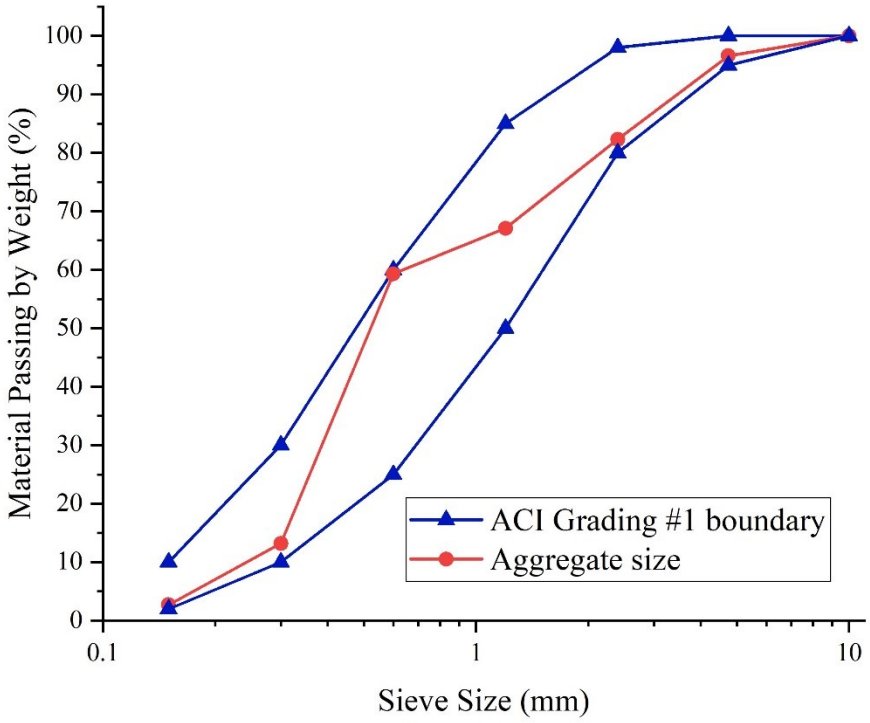

Figure 3.1 Particle size distribution of fine aggregates

Table 3.1 The main oxide compositions of CSA cement and type OPC cement (mass %)

Oxide compositions	SiO_2	Al_2O_3	Fe_2O_3	CaO	MgO	SO_3
CSA	15.4	14.7	1.7	49.5	1.4	13.8
OPC	19.9	3.8	3.5	62.2	4.6	2.9

3.2.2. Sample preparation

The mortar mixtures were mixed with a water-to-cement ratio (w/c) of 0.5 and a fine aggregate-to-cement ratio of 3.125, modified from ACI 506.5 (ACI, 2009b). They were mixed and cast in a laboratory, following the ASTM C192 (ASTM International, 2016b). Mortars were cast into

galvanized steel cylindrical molds with a diameter of 65 mm, height of 130 mm, and thickness of 0.4 mm. Compared with plastic molds, steel molds can reduce the thermal insulation effect caused by plastic molds. ACI 306R-10 (ACI, 2010) suggests that the minimum placing temperature is 18 °C for structure with a section size less than 300 mm when environmental temperature is between -1°C to -18 °C. In this study, the placing temperature of the fresh mortar was controlled to be 20 °C by storing the cement, aggregates and water at 20 °C and mixing the mortar at 20 °C (Kumar et al., 2014).

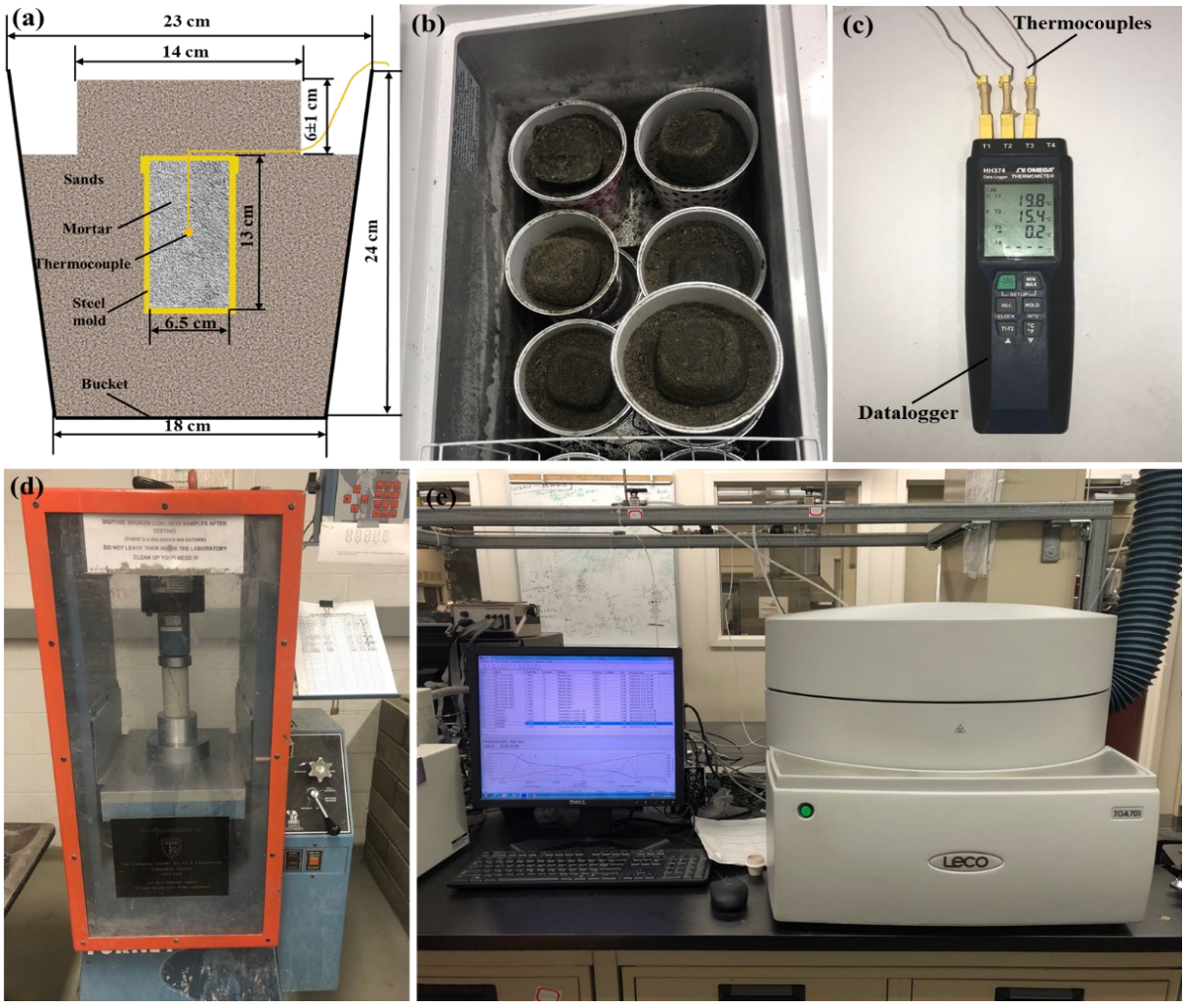

Figure 3.2 Experimental setup: (a) schematic of curing cement mortar in cold sands; (b) inside view of freezer; (c) temperature recording with thermocouples and data logger; (d) UCS tests; (e) TGA instrument

3.2.3. Curing condition

Usually, cementitious materials were cured in cold air (in a freezer or cold room) to investigate how cold temperatures influenced their strength development (Brusletto, 2018; Karagöl et al., 2013; Yi et al., 2011). However, this method may not be suitable to investigate how permafrost influences the strength development of cementitious materials. First, the thermal conductivity of air (about 0.025 W/m·K (Montgomery, 1947)) is much lower than that of permafrost, which is typically about 1.2-3.6 W/m·K at frozen conditions (Romanovsky and Osterkamp, 1997). Besides, the air temperature is easily to be disturbed, due to its low value of volumetric heat capacity (1.0 KJ/m^3·K) (Wu et al., 2007). In this research, a new curing condition was adopted as shown in

Figure 3.2 Experimental setup: (a) schematic of curing cement mortar in cold sands; (b) inside view of freezer; (c) temperature recording with thermocouples and data logger; (d) UCS tests; (e) TGA instrument(a) and (b), which is similar to the real curing condition within permafrost—solid-to-solid heat conduction. Water-saturated sands were placed in plastic buckets and put into the freezer to mimic the cold soil and rock in the permafrost region. After cast in galvanized steel molds and covered with steel lid, the samples were embedded in the sands immediately. It took 9 to 10 minutes to mix, cast and embed samples into sands. The temperatures in the sands were controlled to 5 °C, 0 °C, -5 °C and -10 °C, respectively. Another group of control samples were curing at methods room temperature (20 °C) in air as the reference.

3.2.4. Experiment

3.2.4.1. Temperature profiles with time

The temperature profiles with time reflect the hydration reaction status of the mortar because the cement hydration is an exothermic reaction (Livesey et al., 1991). Meanwhile, the temperature in the sample has a significant impact on the hydration reaction and strength development (Jones et al.; Martinelli et al., 2013). In this study, the temperature in the centers of mortar samples were recorded by the Type K thermocouples with an accuracy of ± 0.1% reading value and HH374 handheld data loggers as shown in

Figure 3.2(c).

After the mortar mixtures were cast in steel molds, thermocouples were inserted into the centers of the OPC-based and CSA-based mortars at each curing temperature, and then these mortars were put into the sands immediately. In addition, another thermocouple was buried in the sands to record the temperature in the sands at each curing temperature. All of the thermocouples were connected with the data logger that recorded the temperatures in the mortars and sands at two-minute intervals.

3.2.4.2. Thermogravimetric analysis

TGA can help to identify the types and amount of hydration products formed during the hydration reaction (Trauchessec et al., 2015). Hence, it was used in this study to characterize the hydration reaction degree of OPC-based and CSA-based samples cured at different temperatures at 1, 3, 7 and 28 days.

The samples for TGA tests were prepared according to the following procedures. First, the aged mortars, after being taken from the freezer, were crushed to small particles. The crushed particles

were washed with acetone and immersed in acetone for 48 hours to stop the hydration reaction between the cement and water (Liao et al., 2011; Trauchessec et al., 2015). Acetone was selected because it is miscible in water (Liu et al., 2005) and it is widely used to grab non-structural water from hydrating cement to stop the hydration reaction (Choi et al., 2017; García-Maté et al., 2016; Telesca et al., 2014). After the immersion, the particles were dried in a vacuum oven at 40 °C for 24 hours to remove the acetone and moisture (Li et al., 2018; Zhang et al., 2016). Following the drying, the particles were passed through a 2-mm sieve to remove the coarse aggregates. The rest of the particles were further crushed and passed through a 150-µm sieve to further remove the fine aggregates. At the end, the powder samples were sealed in plastic bags and stored in a desiccator to avoid the hydration reaction between the cement and moisture in the air (García-Maté et al., 2016).

TGA was carried out with a Leco TGA 701 (Leco Corporation, USA). This device has an accuracy of ± 0.02% when measuring the residue weight of a sample. The temperature in this TGA can be controlled with an accuracy of 2% of the set point (or ± 2 °C). The TGA test was performed on 1.2±0.05g powder in a temperature range from 20 °C to 980 °C at a heating rate of 10 °C per minute under nitrogen atmosphere (Tang et al., 2015).

3.2.4.3. Unconfined compressive strength

Compressive strength is one of the most important properties of cementitious materials; it generally has a close relationship with other properties of cementitious materials (Mehta and Monteiro, 2006). In this study, the UCS of the OPC-based and CSA-based mortars were tested at the age of 1, 3, 7 and 28 days guided by the ASTM C39 standard (ASTM International, 2011). The samples used for UCS test had a diameter of 65 mm and a height of 130 mm.

3.3. Results and discussion

3.3.1. Temperature profiles with time

Figure 3.3 presents the temperature profiles with time in the centers of OPC-based and CSA-based mortars cured in sands at cold temperatures (5 °C, 0 °C, -5 °C and -10 °C) and cured in air at 20 °C (as reference). After 48 hours, all temperatures in the samples remained the same with the air temperature or sands temperatures; therefore, only the temperature profiles in the first 48 hours are shown in Figure 3.3. Furthermore, a zoom-in figure is added to show the temperature differences at the first 6 hours.

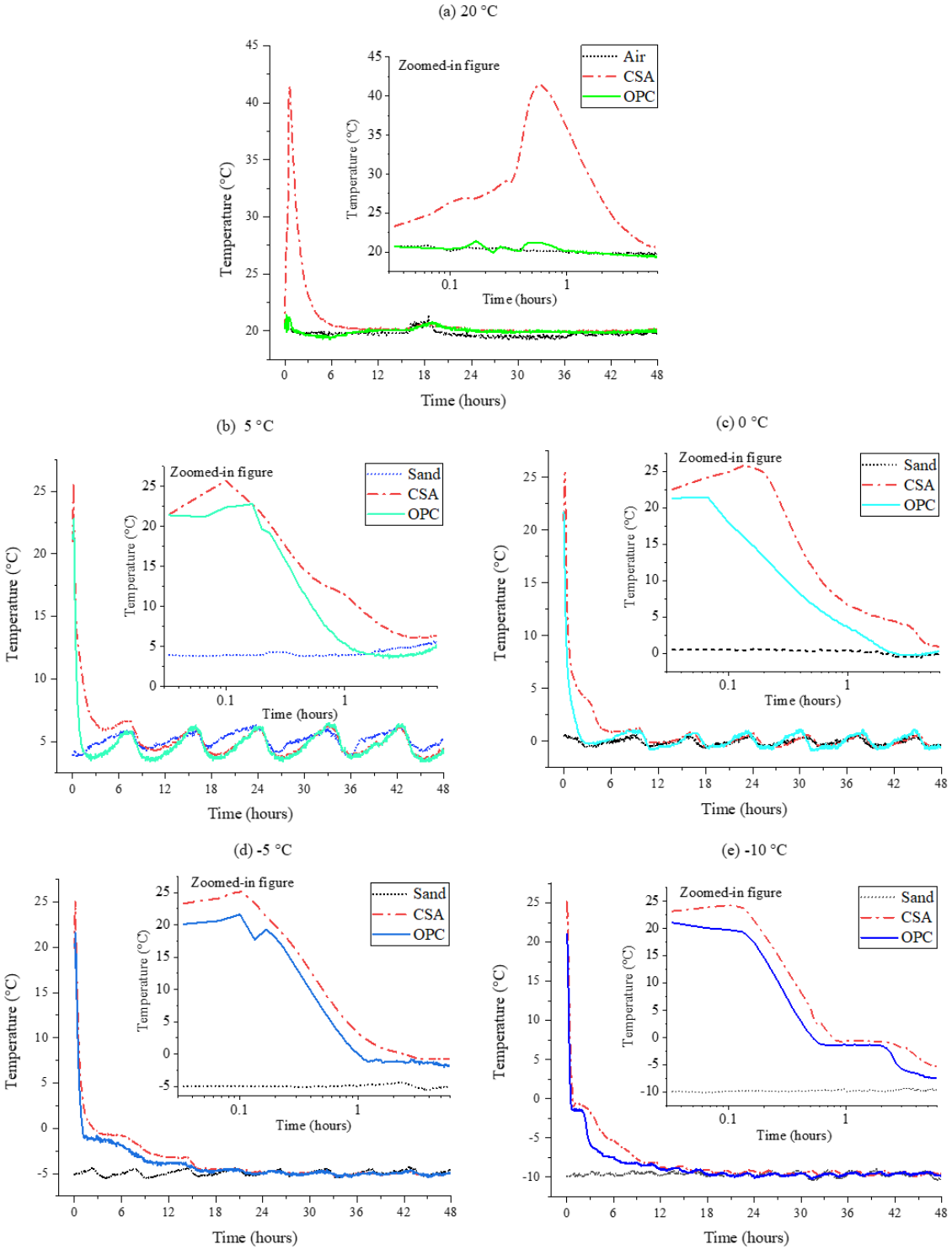

Figure 3.3 Temperature profiles with time in the centers of OPC-based and CSA-based mortars cured (a) in air at 20 °C; (b) in sand at 5 °C; (c) in sand at 0 °C; (d) in sand at -5 °C, and (e) in sand at -10 °C.

3.3.1.1. Temperature profiles with time in the mortars cured in air at 20 °C

Figure 3.3(a) shows the temperature profiles with time in the centers of OPC-based and CSA-based mortars cured in air at 20 °C. The actual recorded room temperature was 19.7 °C ± 0.7 °C except for a minor disturbance at about 18 hours when the temperature peaked at 21.4 °C. The temperature profile with time in the OPC-based mortar was consistent with the features of the four hydration stages of Portland cement, namely 1) the initial period, 2) induction period, 3) acceleration period, and 4) deceleration period (Bullard et al., 2011). The initial period occurred during the first 10 minutes. In this period, the temperature in the OPC-based mortar increased from 20.2 °C to 21.4 °C. This temperature rise was caused by the immediate release of heat when part of the OPC cement dissolved into water (Meredith et al., 1995). The induction period occurred from 10 minutes to ~6h. In this stage, the sample temperature declined to 19.4 °C, which was lower than the room temperature (20 °C). In this period, since the dissolution and hydration reaction were dormant (Damidot et al., 2007; Jennings and Pratt, 1979), much less heat was released, causing a decline in the sample temperature. The other reason for the temperature decline was the evaporation of water from the mortar. In the acceleration period, a slight increase from 19.4 °C to 20.7 °C was observed from 6h to 19h. This means that the hydration reaction sped up during the acceleration period—more hydration heat was released than in the induction period (Bullard, 2008). The deceleration period began after 19h. In this period, the temperature in the OPC-based mortar decreased to and remained consistent with the room temperature. The temperature decrease was caused by the slowdown in the hydration reaction (Bullard et al., 2011). In the deceleration period, the hydration reaction rate decreased with time since it was affected by the diffusion process and the availability of fine cement particles, water, and space (Bullard et al., 2011). Accordingly, less heat was generated, resulting in a decline in the sample temperature.

Compared with the OPC-based mortar, the temperature increase in the CSA-based mortar was more intensive in the first 6 hours cured in air at 20 °C. The temperature in the CSA-based mortar increased sharply and peaked at 41.4 °C at 35 minutes; then the sample temperature decreased exponentially to 20.4 °C at 6h. From 6h to 48h, the temperature was kept slightly (0.4 °C in average) higher than room temperature. The temperature profile in the CSA-based mortar reflects the high hydration heat and fast reaction characteristics of CSA cement. It was observed that most of the hydration heat of the CSA-based mortar was released in the first 6 hours, at an intensive hydration reaction.

3.3.1.2. Temperature profiles with time in the mortars cured in cold sands at 5 °C

Figure 3.3(b) shows the temperature profiles with time in the centers of OPC-based and CSA-based mortars cured in cold sands at 5 °C. The monitored sand temperature in the freezer varied from 3.8 °C to 6.5 °C with an average of 5.3 °C. The temperatures in the OPC-based and CSA-based mortars increased to 22.8 °C and 25.7 °C in 10 minutes, respectively. After that, the temperature in the OPC-based mortar fell steeply to 5 °C in 1 hour, and then it stayed the same as the sand temperature. Similarly, a sharp temperature drop from 25.7 °C to 5 °C was also observed in the CSA-based mortar, but the rate of decline was lower than that of the OPC-based mortar. It took 8.5 hours for the temperature in the CSA-based mortar to drop to 5 °C. This is 7.5 hours longer than that for the OPC-based mortar. Overall, in the first 14 hours, the temperature in the CSA-based mortar averaged ~1.6 °C higher than that in the OPC-based mortar. This can be attributed to the high hydration heat and fast reaction rate of the CSA cement.

3.3.1.3. Temperature profiles with time in the mortars cured in cold sands at 0 °C

Figure 3.3(c) presents the temperature profiles with time in the centers of OPC-based and CSA-based mortars cured in sands at 0 °C with respect to time. The actual temperature in the sands

was -0.1 °C ± 0.7 °C. The temperatures in the OPC-based and CSA-based mortars increased from 20 °C to 21.7 °C and 25.8 °C in the first 10 minutes. Then the temperatures in both the OPC-based and CSA-based mortars decreased sharply to 0 °C. However, the rate of decrease in the CSA-based mortar was lower than that in the OPC-based mortar. The temperature in the OPC-based mortar decreased to 0 °C at 2.5 hours and then varied with the fluctuation of the sand temperatures., It took about 10.5 hours for the CSA-based mortar to decrease to 0 °C, which shows that a larger amount of heat was released from the hydration reaction.

3.3.1.4. Temperature profiles in the mortars cured in frozen sands at -5 and -10 °C

Figure 3.3(d) and Figure 3.3(e) show the temperature profiles with time in the centers of the OPC-based and CSA-based mortars cured in frozen sands at -5 °C and -10 °C. The actual temperatures in the sands were -4.9 ±0.6 °C and -9.6 ±0.8 °C. The temperatures in the OPC-based and CSA-based mortars increased from 20 °C to 21 °C and 25 °C in the first 8 minutes. Once the mortar was embedded into the frozen sands, the temperatures in the OPC-based mortar decreased sharply to less than 0 °C in ~60 minutes and ~30 minutes, respectively. For the CSA-based mortar, it took ~140 minutes and ~50 minutes for the temperature to decrease to 0 °C when the samples were cured at -5 °C and -10 °C. After the sharp decrease, the temperatures in both the OPC-based and CSA-based mortar almost remained constant at around -1 °C for 2 to 4 hours, then decreased slowly to the sand temperatures. This is because latent heat was released during the phase change of the water, which mitigated the temperature decreasing in the mortars (Akyurt et al., 2002). It is worth mentioning that the temperatures in the CSA-based mortar were always higher than that in the OPC-based mortar before the temperatures in the mortars decreased to those in the sands. For example, the temperature in the CSA-based mortar averaged

2.1 °C higher than that of the OPC-based mortar in the first 12 hours when cured at -10 °C. This indicated that more heat was released from the hydration reaction of the CSA cement.

3.3.2. Hydration reaction

The results of the TGA test are expressed as weight loss (in %), residual weight (in %) and the first derivative of weight loss (in %/°C) (as shown in Figure 3.4 and Figure 3.5). The weight loss w_l and residual weight w_r is defined as Equations (3-8) and (3-9), in which m_0 [g] is the initial mass of the powder used for TGA test, and m_i [g] is the residual mass at different temperatures during the heating process. The total weight loss of each powder sample during the TGA test are summarized in Table 3.2 and Table 3.3.

$$w_l = \frac{m_0 - m_i}{m_0} \times 100\% \tag{3-8}$$

$$w_r = \frac{m_i}{m_0} \times 100\% \tag{3-9}$$

3.3.2.1. Thermogravimetric analysis of OPC-based samples

Figure 3.4 shows the thermogravimetric (TG) and derivative of thermogravimetric (DTG) curves of OPC-based samples cured at 20 °C, 5 °C, 0 °C, -5 °C and -10 °C. The TG curves present the residual weight (in %) of the samples during the heating process. The DTG curves show the intensity of the weight loss in the samples at temperatures ranging from 20 °C to 980 °C.

In each DTG curve, there are three peaks at around 110 °C, 500 °C, and 800 °C. The first peak accounts for the dehydration of ettringite (AFt) and C-S-H gel. The C-S-H gel dehydration occurred at a wide temperature range (from ~40 °C to ~550 °C) since C-S-H gel has variable Ca/Si ratios (Le Saoût et al., 2013), but the dehydration of C-S-H gel mainly happened at around 110 °C. The dehydration of calcium hydroxide happened between ~450 °C and ~550 °C, and it peaked at around 500 °C. At around 800 °C, the decarbonization of calcium carbonate also can

be observed. The calcium carbonate was formed since the carbonation of calcium hydroxide might be caused by the carbon dioxide in air (Glasser et al., 2008) and acetone (Zhang and Scherer, 2011). Besides, calcium carbonate also existed in raw materials—fine aggregates and cements. This was confirmed by the TGA tests conducted on the sands and un-hydrated cements.

Although the dehydration and decarbonation occurred in all the samples, the intensities differed depending on ages as shown in the DTG curves. In the first 7 days, the peak values of the DTG curves at 110 °C and 500 °C increased with the age at each curing temperature. This means that the dehydration and decarbonation intensities increased with age; the amount of C-S-H gel and calcium hydroxide increased with age. From 7 to 28 days, the peak values at 110 °C showed a decrease, while the derivative of weight loss at 28 days was obviously higher than that at 7 days in temperatures ranging from 200 °C to 450 °C. This indicates that part of the C-S-H gel had been transformed to more thermal stable structures that need a higher temperature for dehydration. These more thermal stable structures are believed to be C-S-H gel with a lower Ca/Si ratio, since the dehydration temperature of C-S-H gel increases with the decrease in the Ca/Si ratio (Giraudo et al., 2018).

In the TG curves, the final residual weight decreased with the curing age at each curing temperature. This means that the hydration degree had been increased, having formed more hydration products with the curing age. Note that the hydration reaction continued at cold temperatures. This might be explained by the influence of the initial placement temperature at 20 °C. Upon the initial placement, some hydration products were formed before the temperature was decreased to a cold temperature (< 5 °C). These resulting hydration products have acted as catalyst for the hydration reaction in the acceleration period since the hydration reaction is an autocatalytic chemical reaction (Bullard, 2008). At -5 °C and -10 °C, the hydration reaction still

continued slowly, which agreed with the findings of Francesca Ridi et al. (Ridi et al., 2009), who found that part of water confined in the small C-S-H gel pores does not freeze even at -42 °C. This liquid water can participate in the hydration reaction and enables the hydration reaction to continue slowly even at -5 °C and -10 °C.

Table 2 shows the total weight losses (in %) of OPC-based powder samples during the TGA test. A higher total weight loss means more hydration products dehydrated during the heating process, which indicates that more hydration products had formed during the curing stage. At the same age, the total weight loss decreased with the decline in the curing temperature since less hydration products were produced at lower temperatures. Especially, the hydration products of samples cured at -5 °C and -10 °C were much less than those cured at 0 °C, 5 °C, and 20 °C. In other words, the hydration reaction rate between cement and water decreased as the curing temperature decreased, which is consistent with the description of the Arrhenius equation (Martinelli et al., 2013; Riding et al., 2011).

3.3.2.2. Thermogravimetric analysis of CSA-based samples

Figure 3.5 shows the TG and DTG curves of CSA-based powder samples. In the DTG curves, there are two peaks and one shoulder. The first peak was at around 150 °C, reflecting the dehydration of AFt and C-S-H gel. The shoulder was at approximately 220 to 350 °C, reflecting the dehydration of monosulfoaluminate (AFm) and aluminum hydroxide (AH_3) (Telesca et al., 2014; Trauchessec et al., 2015). The second peak was at about 800 °C in each DTG curve, accounting for the decarbonation (Martín-Sedeño et al., 2010). The decarbonation is here due to the existence of carbonate in the raw materials (i.e., sands and CSA cements).

As shown in Table 3, for CSA-based samples, all the weight losses at 1, 3 and 7 days were close to each other, regardless the curing temperatures. All the weight losses on the 1, 3, and 7 days

approached an average of 19.7% ± 0.6%. This indicates that most of AFt was formed in the first day, even when samples were cured at cold temperatures, due to the fast reaction characteristic of CSA cement.

From the 7 days to the 28 days, an increase of the weight loss (~ 2% to 3%) could be found when the samples were cured at 20 °C, 5 °C, and 0 °C. This weight loss was caused by the dehydration of the C-S-H gel that was formed from the hydration reaction between belite and water. As mentioned before, belite is one of the main components of CSA cement. Belite is much less reactive than alite (Mehta and Monteiro, 2006) and ye'elimite (Martín-Sedeño et al., 2010); it reacts with water slowly (Glasser and Zhang, 2001). From the 7 days to the 28 days, belite kept hydrating and forming C-S-H gel when the samples were cured at 20 °C, 5 °C, and 0 °C. However, at -5 °C and -10 °C, the formed hydration products were almost the same at 7 days and 28 days. This indicates that the hydration reaction of belite nearly stopped at freezing temperatures.

Table 3.2 The total weight loss of OPC-based samples during the TGA tests

Age	Total weight loss (%)				
	20°C	5°C	0°C	-5°C	-10°C
1 day	13.7	10.1	9.2	8.0	7.7
3 days	16.0	11.3	10.6	9.4	9.5
7 days	17.7	15.6	14.1	10.2	9.8
28 days	18.7	17.4	15.0	10.7	10.1

Table 3.3 The total weight loss of CSA-based samples during the TGA tests

Age	Total weight loss (%)				
	20°C	5°C	0°C	-5°C	-10°C
1 day	20.2	19.0	20.0	19.3	20.5
3 days	20.1	19.2	19.6	18.9	19.3
7 days	20.2	18.7	20.4	20.2	20.3
28 days	22.5	21.0	23.6	20.4	19.9

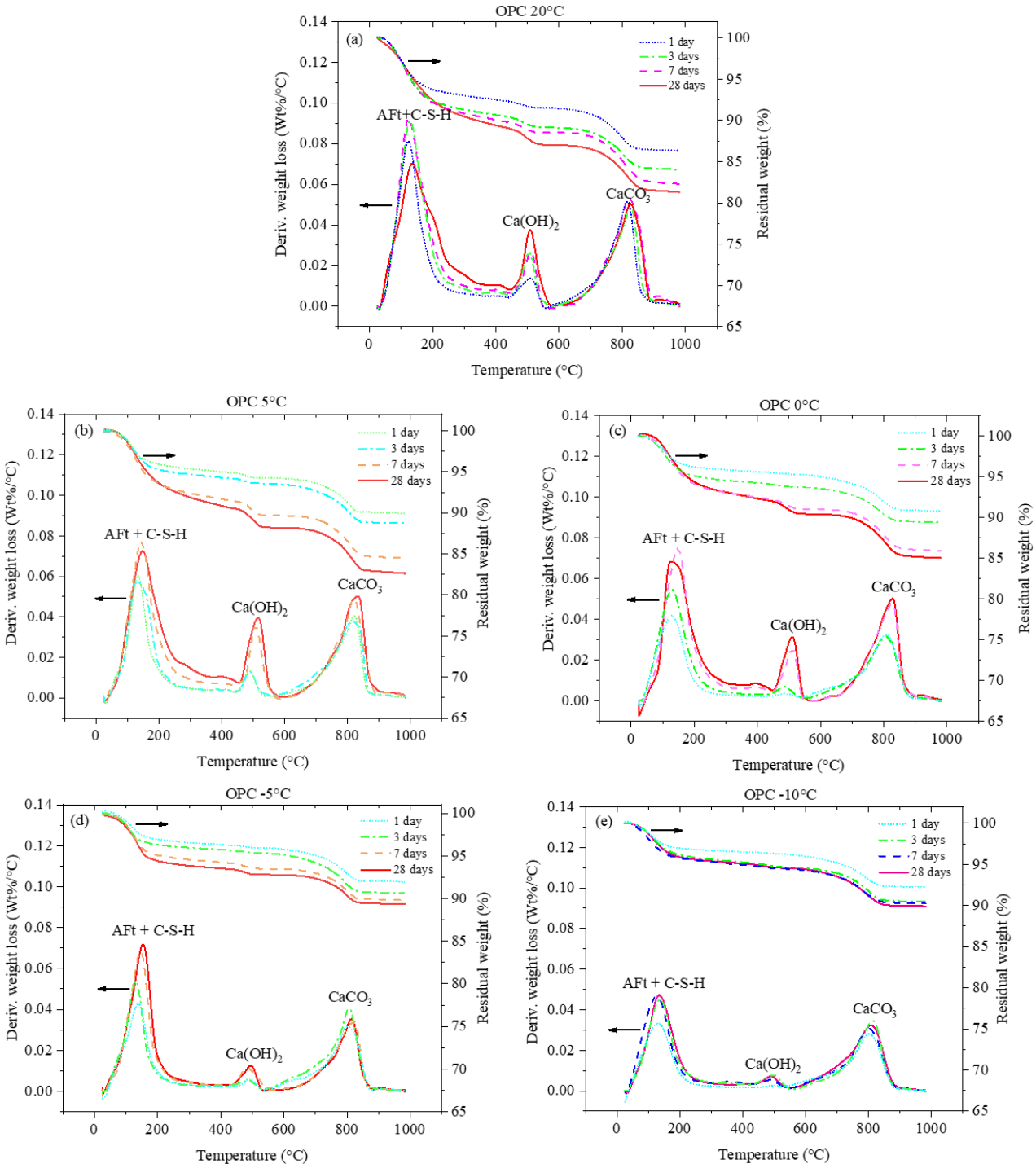

Figure 3.4 TG/DTG curves of OPC-based samples cured (a) in air at 20 °C; (b) in sand at 5 °C; (c) in sand at 0 °C; (d) in sand at -5 °C, and (e) in sand at -10 °C.

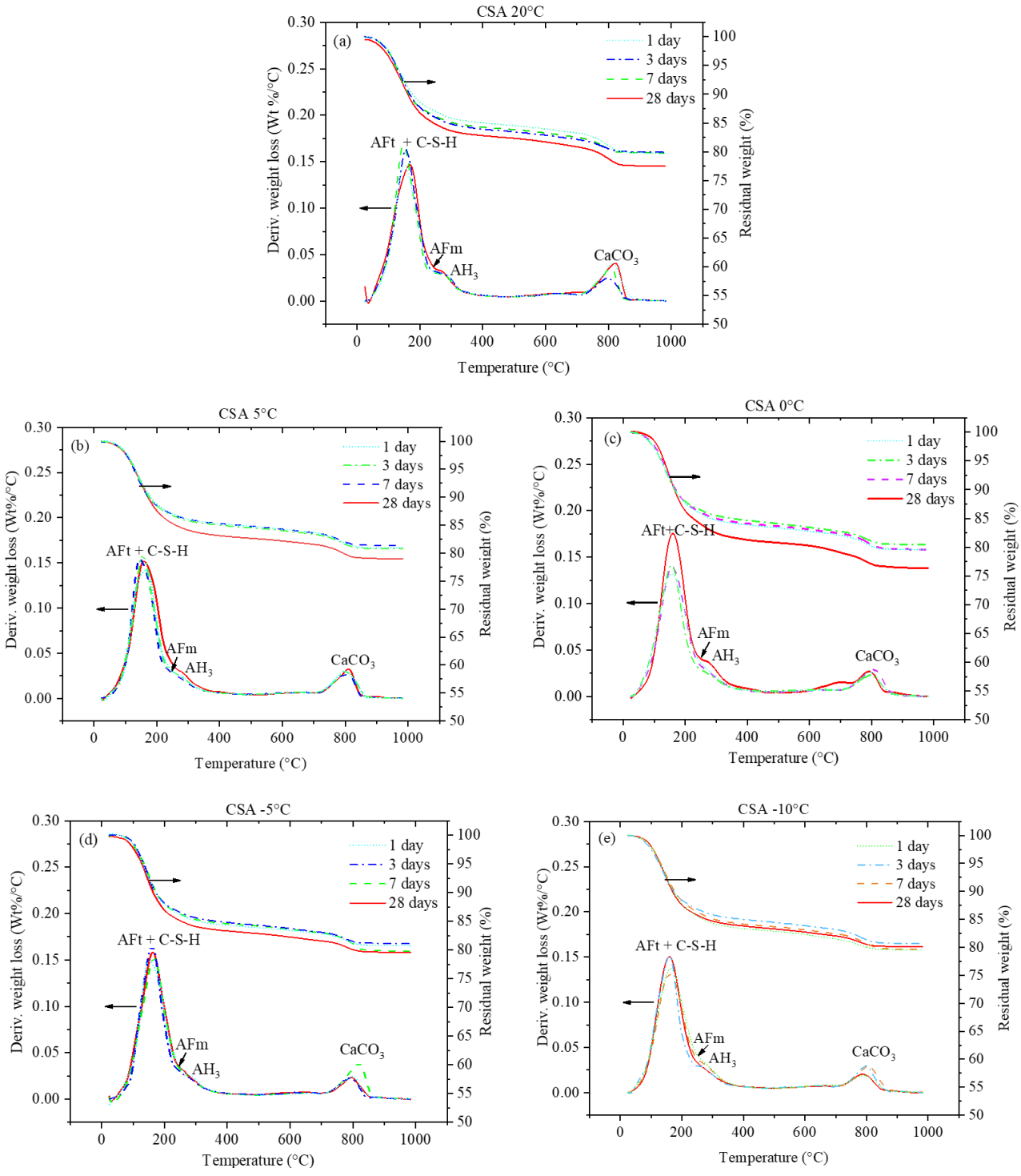

Figure 3.5 TG/DTG curves of CSA-based samples cured (a) in air at 20 °C; (b) in sand at 5 °C; (c) in sand at 0 °C; (d) in sand at -5 °C, and (e) in sand at -10 °C.

3.3.3. Unconfined compressive strength

Figure 3.6 shows the UCS of OPC-based and CSA-based mortars at 1, 3, 7, and 28 days cured in air at 20 °C and in sands at 5 °C, 0 °C, -5 °C and -10 °C. With the decrease of the curing temperature, a noticeable UCS decrease can be found in the OPC-based and CSA-based mortars at the same age. The curing age and cement type also dramatically affected the UCS of the samples. On the first day, the CSA-based mortar gained relatively high early-age strength, while the OPC-based mortar developed almost no strength. The only exception was the mortar cured at 20 °C. The strength development of the OPC-based mortar began after the first day and sped up after 3 days when the mortar was cured at 20 °C, 5 °C, and 0 °C. The UCS of the CSA-based mortar increased quickly in the first 3 days but slowed down after 3 days. Due to the fast strength development of the CSA-based mortar, the UCS of the CSA-based mortar was remarkably higher than that of the OPC-based mortar in the first 7 days. However, the UCS of the OPC-based mortar exceeded the UCS of the CSA-based mortar at the age of 28 days when cured at 20 °C, 5 °C, and 0 °C due to the acceleration of the strength development of the OPC-based mortar. When the curing temperature further went down to -5 °C and -10 °C, there was no strength developed for the OPC-based mortar until 28 days, whereas the UCS of the CSA kept increasing to 12.4 MPa and 5.8 MPa at 28 days.

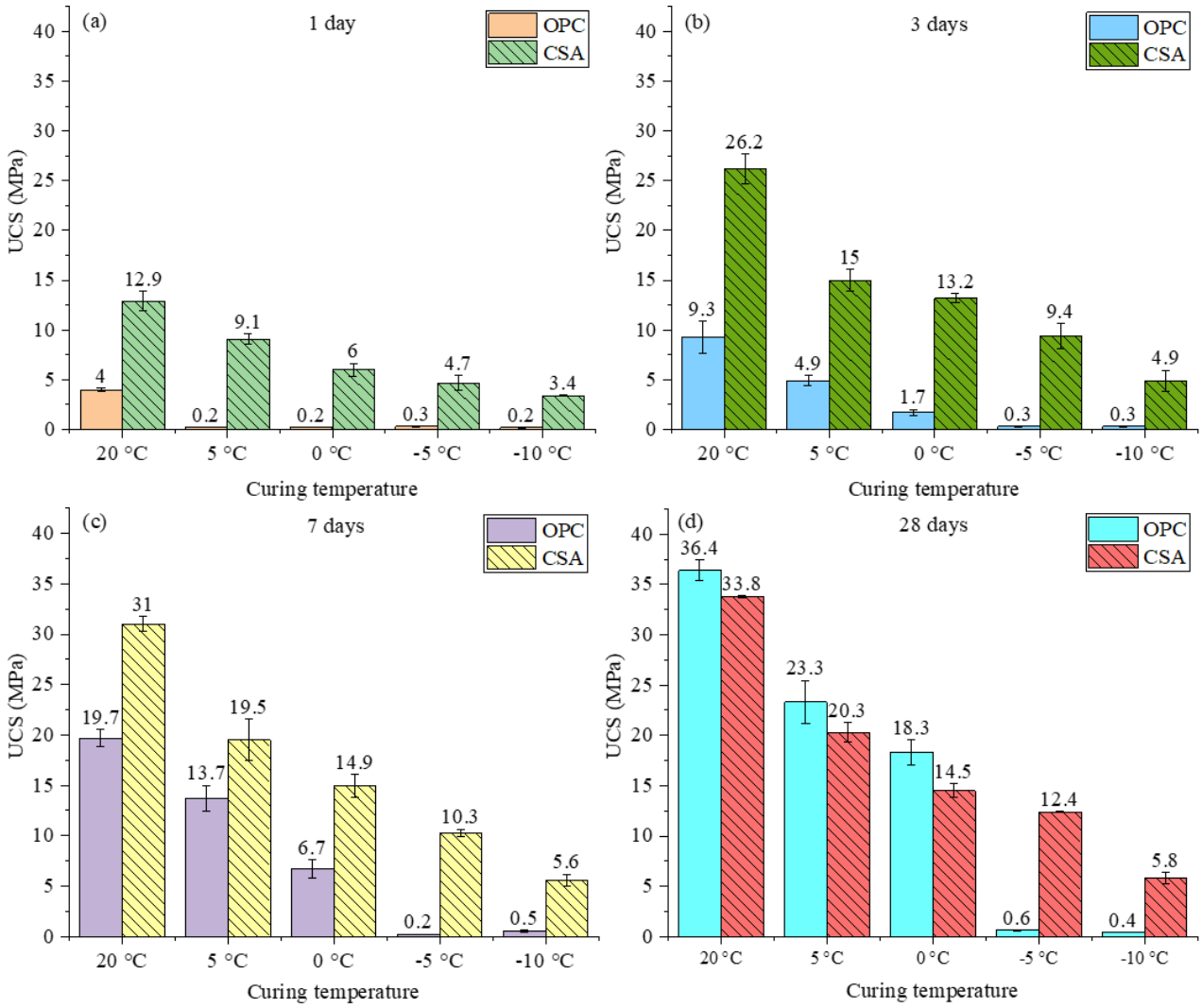

Figure 3.6 The UCS of OPC-based and CSA-based mortars at: (a) 1 day, (b) 3 days, (c) 7 days and (e) 28 days.

The strength development of CSA-based and OPC-based mortars can be partially explained by the TGA results. Regarding CSA-based mortars, the TGA results showed that most of the ettringite (AFt) was generated in the first day even at cold temperatures. As a result, CSA-based mortar can gain strength when cured at cold temperatures. However, it is interesting to note that although the amount of hydration products (e.g., AFt) formed on the first day was almost the same at different curing temperatures, the UCS decreased at lower temperatures. This is because

the strength of the cement-based mixtures is not simply affected by the amount of formed hydration products, but also affected by the other factors, including the densification degree of C-S-H gel (Ioannidou et al., 2016), crystallization degree of AFt (Tang et al., 2015), and the microstructures et al (Lothenbach et al., 2007; Mehta and Monteiro, 2006). Comprehensive investigation is needed in the future work. For OPC-based mortars, although part of C-S-H was formed on the first day due to the hydration reaction, almost no strength was developed. This confirms with Liu et al.'s work (2017) that even though C-S-H was formed, there was no strength developed at early age when samples were cured at low temperatures. According to Ioannidou et al. (Ioannidou et al., 2016), a repulsive force exists between the colloidal C-S-H nanoparticles when a low volume fraction C-S-H is formed at an early age. This repulsive force hinders the strength development of OPC-based mortars cured at low temperatures.

With the increase in curing time, the UCS of the OPC-based and CSA-based mortars increased except that the OPC-based mortar cured at -5 °C and -10 °C. For the OPC-based mortar, the hydration reaction continued with the age at 20 °C, 5 °C and 0 °C, leading to an accumulation of C-S-H gel. As a result, the UCS of the OPC-based mortar increased with the age. However, at -5 °C and -10 °C, the hydration reaction rate was very slow. As shown in Table 2, a low volume of C-S-H gel formed until 28 days, so hardly any strength was developed. For the CSA cement-based mortar, most of the ettringite was formed on the first day, and the amount of formed ettringite at the age of 1, 3, and 7 days was close to each other when cured at the same temperature. However, the UCS showed an increasing trend with the curing time. This also shows that the strength is not simply dominated by the amount of hydration products.

As expected, the CSA-based mortar achieved a remarkably higher UCS than the OPC-based mortar in the first 7 days when cured at the same temperature. However, at the 28 days, the UCS

of the OPC-based mortar exceeded the UCS of the CSA-based mortar at 20 °C, 5 °C and 0 °C. This is because the rapid hydration reaction of CSA cement ensured the high early-age strength. As shown in Figure 3.6, the UCS of the CSA-based mortar was mainly developed in the first 7 days. After that, the UCS gain of CSA-based mortar slowed down due to the decelerated hydration reaction. On the other hand, the hydration reaction between Type OPC cement and water continued after 7 days at the curing temperatures of 20 °C, 5 °C and 0 °C. As a result, the UCS kept increasing with the gelation and densification of C-S-H gel (Ioannidou et al., 2016). Ultimately, the UCS of the OPC-based mortar exceeded that of the CSA-based mortar when the mortars were cured at 20 °C, 5 °C and 0 °C.

3.4. Conclusion

In this study, calcium sulfoaluminate (CSA) cement and general used (OPC) Portland cement-based mortars were cast in steel molds and cured in wet sands at cold temperatures (i.e., 5 °C, 0 °C, -5 °C, and -10 °C) and cured in air at 20 °C (as a reference). The cold sands were used to mimic cold soils and rocks in a permafrost region (e.g., in Canada's North and other permafrost regions). The temperature profiles with time, hydration reaction, and strength development of CSA-based and OPC-based mortars were recorded and then analyzed. The main conclusions from this study are as follows:

(1) The temperature decreasing rate in CSA-based mortar was slower than that in OPC-based mortar when cured at cold temperatures (i.e., 5 °C, 0 °C, -5 °C, and -10 °C), due to the high hydration heat of CSA cement. The heat generation of CSA-based mortar was more intensive and faster than that of OPC-based mortar.

(2) The hydration reaction between CSA cement and water was fast regardless of cold curing temperatures.

(3) At 1 day, the OPC-based mortar developed no strength at cold temperatures (<5 °C) The CSA-based mortar achieved much faster strength development and gained a UCS of 9.1 MPa, 6 MPa, 4.7 MPa, and 3.4 MPa, respectively, when cured at 5 °C, 0 °C, -5 °C, and -10 °C due to the rapid hydration reaction of CSA cement.

(4) In the first 7 days, the UCS of the CSA-based mortar was remarkably higher than that of OPC-based mortar at each curing temperature. At 28 days, the UCS of the OPC-based mortar exceeded the UCS of the CSA-based mortar slightly when cured at 20°C, 5 °C and 0 °C.

(5) No strength was developed for the OPC-based mortar until 28 days when the mortar was cured in sands at -5 °C and -10 °C, whereas the CSA-based mortar achieved rapid strength development at those frozen temperatures.

Results showed that the hydration reaction and the strength development of CSA-based mortar were much faster than those for OPC-based mortars when used at cold temperatures (< 5 °C). Thus, CSA cement can be substituted for OPC cement to solve the problem of slow strength development when used in cold region (e.g., in a permafrost region).

Chapter 4. Performance of calcium sulfoaluminate cement for preventing early-age frost damage

Chapter 4 has been published as **G. Huang**, D. Pudasainee, R. Gupta, W.V. Liu, The performance of calcium sulfoaluminate cement for preventing early-age frost damage, *Construction and Building Materials*. © Elsevier. 254 (2020) 119322.

4.1. Introduction

Cold weather concreting has been a great challenge for the construction industry in cold regions, such as areas in Canada, northern China, Korea, and Russia (Choi et al., 2017; Liu et al., 2018a). When placed at frozen temperatures (i.e., -10 °C), fresh cement-based mixtures are vulnerable to early-age frost damage (ACI, 2010; Bernhardt, 1956). Early-age frost damage is an irreversible deterioration of the properties of cement-based mixtures (e.g., compressive strength) caused by the freezing of the hardening cement-based mixtures before sufficient strength (3.5 MPa) has been achieved (ACI, 2010; Bernhardt, 1956; Choi et al., 2017; Yi et al., 2011). After early-age frost damage, strength development cannot be ensured to reach an adequate value even if it is re-cured at normal temperatures (ACI, 2010).

The deterioration of cement-based mixtures that suffer from early-age frost damage can be presented as (1) cracks caused by tensile stress; and (2) cavities left in the cement-based mixtures (Liu et al., 2014a; Powers, 1956; Yi et al., 2011). First, under frozen temperatures (e.g., -10 °C), the water in fresh concrete freezes and forms ice lenses. During the formation and growth of ice lenses, the phase in which water turns to ice leads to a volume expansion of 9%, which induces internal tensile stress in hardening cement-based mixtures (Karagol et al., 2015). If sufficient strength has not been developed, this tensile stress will result in cracks in the hardening cement-based mixtures (Corr et al., 2003). Second, when the temperature increases to a value that is higher than the melting point of ice, the ice lenses melt and leave many cavities in the cement-based structure (Monteiro, 2006). These cracks and cavities in the structure profoundly influence the strength of the cement-based mixtures; they cannot be repaired even if the cement-based mixtures are re-cured under a normal curing temperature. Thus, this results in irreversible damage to the cement-based mixtures.

To prevent early-age frost damage, cement-based mixtures should gain sufficient strength before being frozen. The ACI 306R-10 (ACI, 2010) suggests that fresh cement-based mixtures must be protected from freezing until their compressive strength reaches at least 3.5 MPa, otherwise early-age frost damage may occur (ACI, 2010). From the literature, factors having a significant influence on early-age frost damage include onset time of freezing, antifreeze admixtures or accelerators, and cement type (Barna et al., 2011; Yi et al., 2011). Accordingly, there are three categories of measures for alleviating early-age frost damage on cement-based mixtures: (1) postponing the onset time of freezing (Choi et al., 2017; Guo et al., 2014; Kosmatka et al., 2011; Kumar et al., 2014; Lee et al., 2012; Won et al., 2016; Yi et al., 2011; Zhu, 2013); (2) adding antifreeze admixtures or accelerators (Korhonen and Cortez, 1991); and (3) using or adding cement having high early-age strength (Qin et al., 2018; Yi et al., 2011).

First, postponing the onset time of freezing can enable cement-based mixtures to gain enough strength to resist early-age frost damage (Yi et al., 2011). At present, the methods for postponing the onset time of freezing include, but are not limited to: (1) increasing the placing temperature (ACI, 2010; Kumar et al., 2014; Zhu, 2013); (2) covering with insulation materials (Kosmatka et al., 2011; Won et al., 2016); and (3) using heating devices such as a stove, steam, and infrared heater (Choi et al., 2017; Guo et al., 2014; Lee et al., 2012). Merely increasing the placing temperature or covering with insulation materials may be ineffective to postpone the onset of freezing. For example, research from Choi et al. (2017) increased the placing temperature of an OPC-based mortar to 10 °C and covered it with insulation materials. However, this mortar froze within 24 hours and only gained a compressive strength of 1.5 MPa at 3 days, which failed to reach the minimum compressive strength (3.5 MPa) for preventing early-age frost damage. Applying external heating sources can control the temperature of hardening cement-based

mixtures until they gain sufficient strength, but these methods are associated with issues such as high consumption of fuel or electricity, risk of fire or electrical shock, air pollution, and low construction efficiency (Guo et al., 2014; Liu et al., 2018b).

Second, adding admixtures, including antifreeze admixtures and accelerators, is another way to prevent early-age frost damage. Antifreeze admixtures can mitigate early frost damage by depressing the freezing point of water (Barna et al., 2011; Korhonen and Cortez, 1991; Nmai, 1998). At present, various antifreeze admixtures have been used to protect cement-based mixtures from early-age frost damage when exposed to freezing temperatures, such as calcium chloride, calcium nitrate, ammonium hydroxide, potassium carbonate, urea, sodium nitrite, sodium nitrate, sodium chloride, sodium sulfate, weak electrolytes and organic compounds, or a combination of these chemicals (Karagol et al., 2015; Korhonen and Cortez, 1991). Accelerators can speed up strength development and enable fresh cement-based mixtures to gain sufficient strength to resist early-age frost damage. Accelerators used in cold temperatures include calcium chloride, calcium nitrate, potassium carbonate, and others. Among these chemical admixtures, calcium nitrate is a good accelerator and antifreeze admixture for OPC cement. Calcium nitrate not only can accelerate the hydration of alite (C_3S) and belite (C_2S) (Kičaitė et al., 2017), but also can depress the freezing point of fresh concrete mixtures (Karagöl et al., 2013). It has been well-documented that calcium nitrate can mitigate early-age frost damage on OPC-based concrete even at -10 °C (Karagöl et al., 2013; Karagol et al., 2015; Korhonen and Cortez, 1991).

The third method is the use of cement with high early-age strength (e.g., Type III cement) to resist early-age frost damage. Compared with ordinary Portland cement (OPC), cement with high early-age strength can achieve faster strength development and may gain sufficient strength (3.5 MPa) to resist early age frost damage before freezing. Yi et al. (2011) found that Type III

cement-based concrete was less vulnerable to early-age frost damage compared with OPC-based concrete. Similar to Type III cement, CSA cement has high early-age strength (Juenger et al., 2011; Telesca et al., 2014; Yu et al., 2018). CSA cement mainly consists of ye'elimite ($C_4A_3\bar{S}$), belite (C_2S), calcium aluminate (CA), and calcium sulfate (Winnefeld et al., 2017) (Nomenclature: $\mathrm{C} = \mathrm{CaO}, \bar{S} = \mathrm{SO_3}, \mathrm{A} = Al_2O_3, \mathrm{H} = H_2\mathrm{O}, \mathrm{S} = \mathrm{SiO_2}$). $C_4A_3\bar{S}$ can react quickly to form ettringite (AFt), aluminum hydroxide (AH_3), and monosulfoaluminate (AFm), enabling fast strength development (García-Maté et al., 2015; Telesca et al., 2014). Our previous study (Huang et al., 2019) investigated the hydration reaction and strength development of CSA cement-based mortar cured at cold temperatures (i.e., 5 °C, 0 °C, -5 °C, and -10 °C). The results revealed that CSA cement-based mortar can achieve rapid strength development at cold temperatures without heat curing, due to the fast hydration reaction. CSA cement has the potential to prevent early-age frost damage since it may develop sufficient strength before freezing.

Using CSA cement to prevent early-age frost damage could contribute significantly to the engineering community in cold regions. First, it may avoid the deterioration of cement-based mixtures used at frozen temperatures and ensure the quality of the cement-based structure. Second, at cold temperatures, some contractors would like to shut down construction sites to prevent early-age frost damage on OPC-based concrete structures, but this method reduces construction efficiency. Using CSA cement to prevent early-age frost damage can help improve construction efficiency since CSA cement can achieve fast strength development even at cold temperatures and shutdown of construction sites can be avoided. Moreover, when OPC is used in cold temperatures, external heating sources usually are required, which leads to some problems, such as high energy consumption, air pollution, risk of fire and electrical shock; these problems

can be avoided when CSA cement is used since external heating sources are not required. Despite its significance, no research has been conducted to explore the possibility of using CSA cement to prevent early-age frost damage.

To this end, the main objective of this study is to evaluate early-age frost damage on CSA cement-based mortars cured at frozen temperatures (i.e., -10 °C) and to explore the possibility of using CSA cement to prevent early-age frost damage. The performance of CSA cement-based mortars was compared with that of OPC-based mortars with and without calcium nitrate. Methods used in this research included thermogravimetric analysis (TGA), ultrasonic pulse velocity (UPV), mercury intrusion porosimetry (MIP), scanning electron microscopy (SEM), and unconfined compressive strength (UCS) tests. This study has provided a new solution for preventing early-age frost damage when cement-based mixtures are used in cold regions (e.g., in Canada's North).

4.2. Materials and methods

4.2.1. Materials

The materials used to prepare mortar samples include OPC, CSA cement, tap water, fine aggregate, and calcium nitrate tetrahydrate ($Ca(NO_3)_2 \cdot 4H_2O$). The oxide compositions and mineralogical compositions of OPC and CSA cements are shown in Table 4.1 and Table 4.2, respectively. The particle size distributions of OPC and CSA cement are presented in Figure 4.1. The fine aggregates had a bulk density of 1607 kg/m^3 at oven-dry conditions. As shown in Figure 4.2, the particle size distribution of the fine aggregates was located in the American Concrete Institute (ACI) No.1 grading zone (ACI, 2009b). Calcium nitrate was added as an antifreeze admixture; its composition and chemical properties are given in Table 4.3.

Table 4.1 The oxide compositions of OPC and CSA cement (mass %)

Oxide compositions	SiO_2	Al_2O_3	Fe_2O_3	CaO	MgO	SO_3
OPC	19.9	3.8	3.5	62.2	4.6	2.9
CSA	15.4	14.7	1.7	49.5	1.4	13.8

Table 4.2 The mineralogical compositions of the OPC and CSA cement (mass%)

Compositions	$C_4A_3\bar{S}$	C_3S	C_2S	$C\bar{S}$	$C\bar{S}_{0.5}$	C_3A	C_4AF	Cc
OPC	-	62.7	9.9	-	-	4.1	10.8	-
CSA	26.3	-	48.8	12.8	3.7	-	1.8	3.4

Table 4.3 Chemical composition and properties of calcium nitrate tetrahydrate

Chemical compositions or properties	Values
Percent Purity	99% to 103%
Chloride (Cl)	≤0.005%
Sulfate (SO_4)	≤0.002%
Potassium (K)	≤0.005%
Sodium (Na)	≤0.01%
Magnesium (Mg)	≤0.05%
pH value	5 to 7

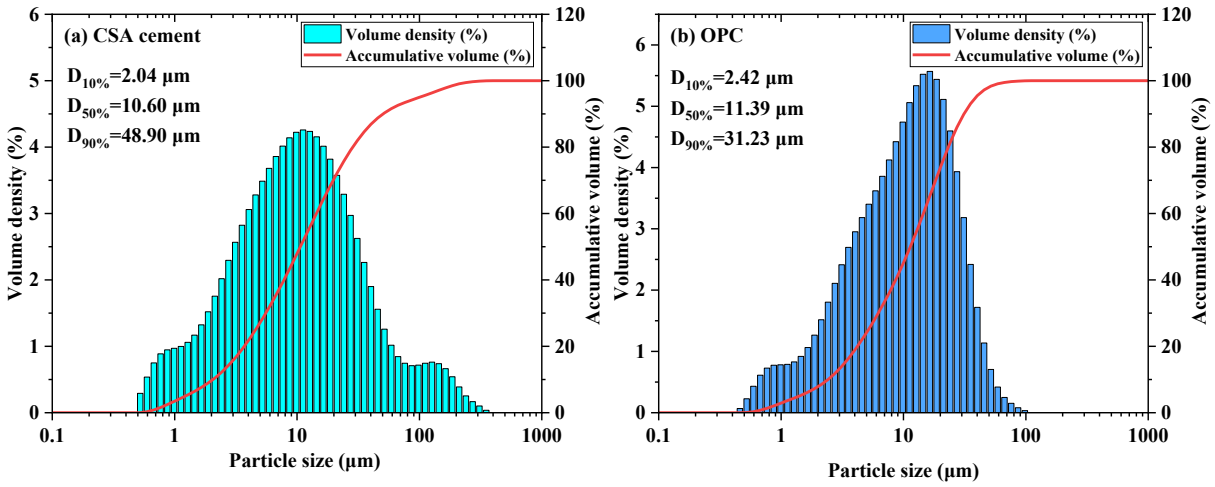

Figure 4.1 Particle size distribution: (a) CSA cement; (b) OPC.

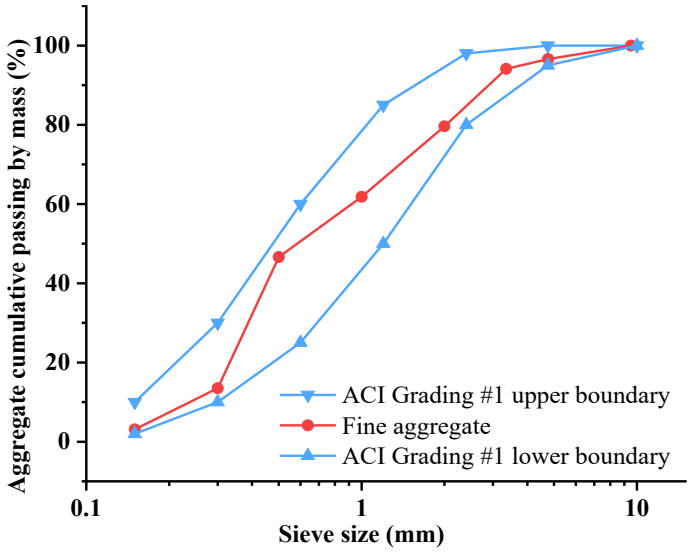

Figure 4.2 Particle size distribution of fine aggregates.

4.2.2. Sample preparation

As shown in Table 4.4, the water to cement (w/c) ratio and fine aggregates to cement (a/c) ratio were 0.5 and 3.125 respectively, according to the ACI 506.5 (ACI, 2009b). The fine aggregates were weighed and mixed with cement at a water saturated surface dry (SSD) condition (with a water content of 1.52%). To compare the performance of CSA cement mortar with OPC-based mortar (with and without calcium nitrate), four mixtures were prepared, including the OPC-based mortar without calcium nitrate (OPC Mix), the OPC-based mortar with calcium nitrate (OPC-CN Mix), the CSA cement-based mortar without calcium nitrate (CSA Mix), and the CSA cement-based mortar with calcium nitrate (CSA-CN Mix). Calcium nitrate was added at the dosage of 9% of cement mass, since this dosage showed good performance in Karagol's work (2015). The mortars were mixed in a laboratory. The ACI 306R suggests that the placing temperature should be higher than 18 °C when the size of the structure is less than 300 mm at a surrounding temperature between -1 °C to -18 °C (ACI, 2010). Hence, the placing temperature was controlled at 20 °C in this study. Note that the dissolving of calcium nitrate is endothermic. Before mixing

the mortar, the calcium nitrate solution was prepared and stored at 20 °C to avoid the endothermic influence of calcium nitrate on the placing temperature.

After mixing, the mortars were cast into cylindrical molds with a diameter of 75 mm and a height of 150 mm. After that, samples were transferred immediately to a freezer without any heat curing. The temperature in the freezer was set to -10 °C for following reasons. First, -10 °C is cold enough to freeze the hardening cement-based mixtures; thus, it was widely used as the temperature for investigating early-age frost damage (Choi et al., 2017; Provost-Smith et al., 2017; Yi et al., 2011). Second, Provost-Smith et al. (2017) demonstrated that further decreasing the curing temperature below -10 °C did not cause distinct differences when investigating the early-age frost damage on cement-based mixtures. The samples were then cured at -10 °C for 3 days, then re-cured in the moisture room at a temperature of 23 ± 2 °C and a humidity of 100%. Another group of samples were cured in the moisture room directly as the reference.

Table 4.4 Mixture design and curing condition.

Mixtures	Cement type	w/c ratio	a/c ratio	$Ca(NO_3)_2 \cdot 4H_2O$ (% of cement mass)	Curing condition
OPC Mix	OPC	0.5	3.125	0	N: cured at 23 °C F: cured at -10 °C R: re-cured at 23 °C after cured at -10 °C for 3 days
OPC-CN Mix	OPC	0.5	3.125	9	
CSA Mix	CSA	0.5	3.125	0	
CSA-CN Mix	CSA	0.5	3.125	9	

4.2.3. Methods

4.2.3.1. Density, absorption and voids

In this study, density, water absorption, and voids contents of the hardened mortar samples were measured following the ASTM C642 (ASTM International, 2013b). Two samples were tested for each mixture at 28 days.

4.2.3.2. Ultrasonic pulse velocity

The ultrasonic pulse velocity (UPV) method is a nondestructive method for evaluating the quality of a cement-based structure, which can reflect the internal cracks, cavities, defects, and deterioration (ASTM international, 2016c). In this study, the UPV method was employed to assess the cracks and cavities left in the cement mortars. At 28 days, 75 ×150 mm cylindrical samples were ground to ensure that the two ends were flat, then the UPV was determined per ASTM 597 (ASTM international, 2016c).

4.2.3.3. Thermogravimetric analysis

TGA tests were conducted to compare the amount of formed hydration products of different mixtures before and after re-curing. At 1day, 3 days, and 28 days, the cement mortars were crushed to small particles (<4 mm), and then treated with acetone. Acetone can grab non-structural water from hydrating cement to stop the hydration reaction (Choi et al., 2017; García-Maté et al., 2016; Telesca et al., 2014) since it is miscible with water (Liu et al., 2005). After being immersed for 24 hours, the particles were dried in a vacuum oven at 60 °C for 24 hours to remove the acetone and moisture. The oven-dry particles were passed through a 2-mm sieve to remove the coarse aggregate. Then the rest of the particles were crushed to pass through a 63-μm sieve to further remove the fine aggregates. To avoid contact with moisture in the air, the

hydration-stopped powder samples were sealed in plastic bags and stored in a desiccator (García-Maté et al., 2016).

Leco TGA 701 (Leco Corporation, USA) was employed for the TGA tests. The balance in this device can achieve an accuracy of ± 0.02%, and its heating system has an accuracy of 2% of set temperature (or ± 2 °C). The TGA tests were performed on 1.2 ± 0.05g hydration-stopped powder. The temperature was increased from 20 °C to 980 °C at a heating rate of 5 °C/min under nitrogen atmosphere.

The TGA results were expressed as residual weight (in %) and first derivative of weight loss against temperature (in %/°C) as defined in equations (4-1) and (4-2), respectively.

$$w_r = \frac{m_i}{m_0} \times 100\% \tag{4-1}$$

$$\Delta \mathrm{w}_l = \frac{(-\Delta m_i / m_0 \times 100\%)}{\Delta T_i} \tag{4-2}$$

Where, m_0 is the initial mass of hydration-stopped powder used for the TGA test, [g]; m_i [g] is the residual mass of the powder at time t_i [minute]; ΔT_i [°C] and Δm_i [g] are the temperature increase and the mass change during time period Δt_i [minute].

4.2.3.4. Pore structure and porosity

MIP method was adopted to assess the pore structure of the hardened cement mortars. At 28 days, two disks with a thickness of 2-3 mm were sawed from the middle of the cylindrical sample. Following that, the disks were fragmented manually to small pieces. The pieces that passed through an 8-mm sieve and retained on a 5-mm sieve were collected and treated with acetone to stop the hydration as mentioned before. Then these pieces were oven-dried at 60 °C for 24 hours.

After that, the MIP tests were performed on 3 ± 0.3 g of samples using a PoreMaster 33 mercury porosimeter (Quantachrome Instruments, USA). In the MIP tests, the mercury intrusion pressure went up to 227.5 MPa. The mercury used for the MIP tests had a density, surface tension, and contact angle of 13.5 g/cm^3, 480 dynes/cm, and 140°, respectively, at 20 °C and atmospheric pressure. These constants were used during the calculation of pore size distribution.

4.2.3.5. Scanning electron microscopy

SEM analyses were performed with FEI MLA 250 SEM (FEI company, USA) to observe the cracks and cavities. The SEM analyses were carried out with a secondary electrons detector since it is better for observing surface textures (i.e., cracks and cavities). Prior to SEM observation, samples hydrated for 28 days were cut, hydration-stopped, and dried in a vacuum oven following the same procedures for preparing MIP samples. Following the drying, the slices of samples were impregnated with epoxy, then polished down to 0.03 μm. Then gold was sputtered to the surface of the polished samples to generate a conductive layer.

4.2.3.6. Unconfined compressive strength

The UCS tests were performed on the cylindrical samples at 1, 3, 7, and 28 days, guided by the ASTM C39 standard (ASTM International, 2011).

4.3. Results and discussion

4.3.1. Density, absorption, and voids

Figure 4.3 presents the influence of curing conditions on the bulk density, apparent density, water absorption, and void content of OPC-based mortars (i.e., OPC Mix and OPC-CN Mix) and CSA-based mortars (i.e., CSA Mix and CSA-CN Mix) at 28 days.

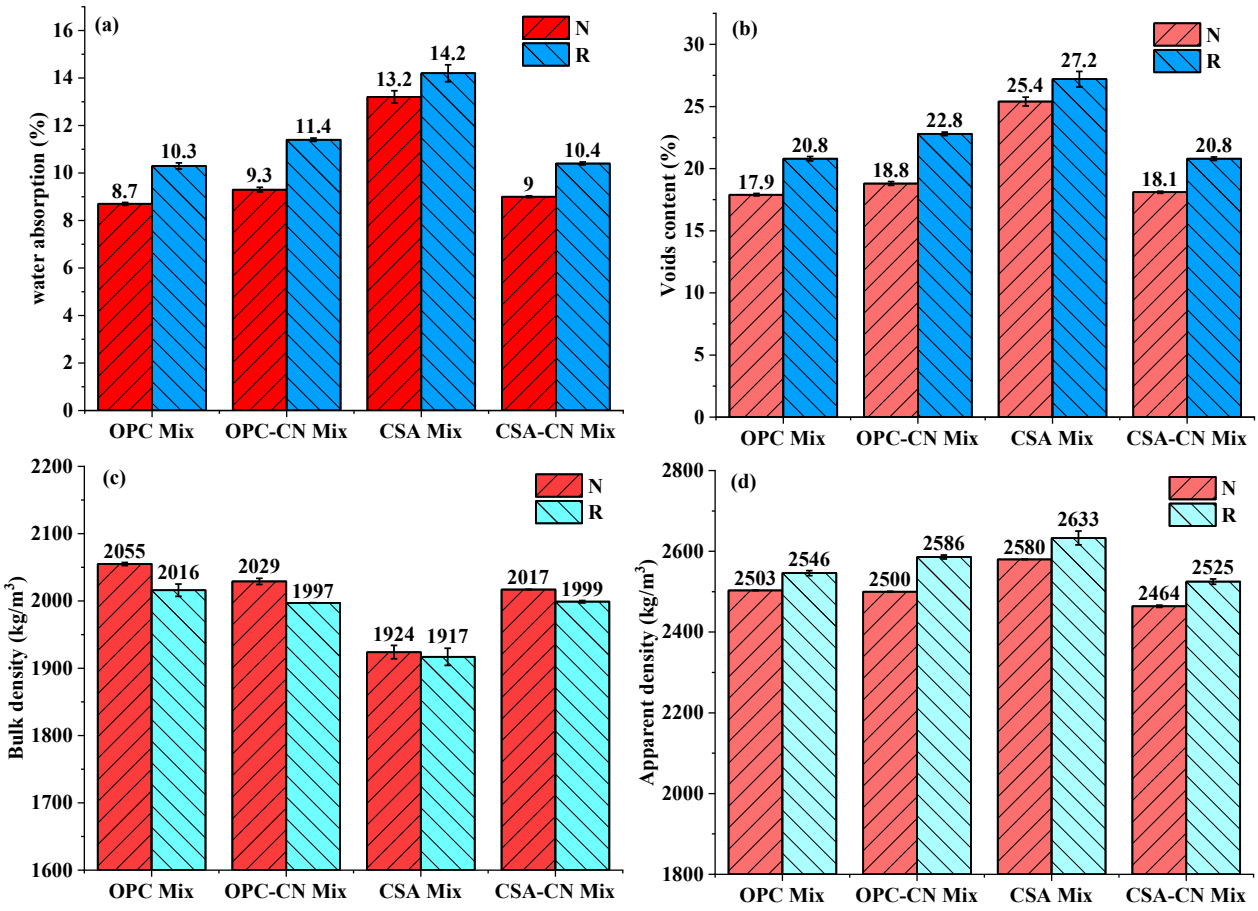

Figure 4.3 Density, water absorption, and voids content at 28 days. CN is the calcium nitrate added to the mixture as antifreeze admixture; N means that the samples were cured at 23 °C; R indicates that the samples were re-cured at 23 °C after being cured at -10 °C for 3 days.

All cement mortars exposed to -10 °C at early age had higher water absorption and voids content when compared with those cured at 23 °C. The increase in water absorption was between 1% and 1.8%; the increase in voids content varied from 2.1% to 4.0%. The change in the water absorption and voids content indicates that more permeable pores, voids, and cracks had formed in the cement mortars when the samples were exposed to -10 °C at the early age.

The changes of water absorption and voids content of CSA-based mortars were lower than those of OPC-based mortars, regardless of the addition of calcium nitrate. For example, the water absorption of CSA Mix-R and CSA-CN Mix-R was 1.0% and 1.4% higher than that of CSA Mix-N and CSA-CN Mix-N. With regard to OPC-based mortars, the water absorption of OPC Mix-R and OPC-CN Mix-R was 1.6% and 2.1% higher than OPC Mix-N and OPC-CN Mix-N.

Note that the addition of calcium nitrate did not decrease the water absorption and voids content in the OPC-based mortars exposed to -10 °C; instead, the water absorption and voids content of OPC-CN Mix-R was 1.1% and 2.0% higher than those of the OPC Mix-R. For CSA-based mortars, the addition of calcium nitrate noticeably decreased the water absorption and voids content regardless of the curing environments. For example, the water absorption and voids content of CSA-CN Mix-N were 4.2% and 7.3% lower than those of the CSA Mix-N.

The apparent densities of the mortars exposed to -10 °C were 43 kg/m^3 to 86 kg/m^3 higher than the mortars directly cured at 23 °C. According to ASTM C642 (ASTM International, 2013b), the increase in apparent densities means that fewer impermeable pores were formed in the cement mortars exposed to -10 °C. The influence of exposure to -10 °C on the sample's bulk density was opposite to that on the apparent density. The bulk densities of cement mortars exposed to -10 °C were lower than those mortars directly cured at 23 °C. The change in bulk density varied from 7 kg/m^3 to 39 kg/m^3 for different mixtures. For CSA-based mortars, the changes in bulk density were less than those of OPC-based mortars, and the CSA Mix especially had the lowest change in bulk density (7 kg/m^3). The difference trend between apparent density and bulk density indicated more permeable pores had formed in the mortars exposed to -10 °C. These permeable pores resulted in the decrease in the bulk density.

It can be concluded that exposure to -10 °C imposed less influence on the water absorption, void content, and density of CSA-based mortars when compared with that on OPC-based mortars. In particular, the CSA Mix had the lowest change.

4.3.2. Ultrasonic pulse velocity

The UPV values of the OPC-based and CSA-based mortars at 28 days were presented in

Figure 4.4. Exposing the samples to -10 °C at the early age resulted a lower UPV value, except for the CSA Mix. The UPV of CSA Mix-R was slightly (40 m/s) higher than CSA Mix-N. Exposing the samples to -10 °C had more significant effects on OPC-based mortars than on CSA-based mortars. A remarkable drop can be found in the UPV of OPC-based mortars exposed to -10 °C. The UPV of OPC Mix-R and OPC-CN Mix-R were 340 m/s and 285 m/s lower than the OPC Mix-N and OPC-CN Mix-N, respectively. The change of UPV can also be found for CSA-CN Mix exposed to -10 °C, but the change was less intensive: only 110 m/s lower than the same mixture cured at 23 °C. The addition of calcium nitrate increased the UPV for both OPC-based and CSA-based mortars when cured at 23 °C. For example, the UPV of CSA-CN Mix-N was 170 m/s higher than that of CSA Mix-N. However, the addition of calcium nitrate had only a very tiny effect on the UPV of OPC-based and CSA-based mortars exposed to -10 °C: the difference was within ± 20 m/s.

UPV technology can reflect the quantity of internal cracks, cavities, and defects (ASTM international, 2016c; Karagol et al., 2015). In this study, the UPV results indicate that exposing the samples to -10 °C increased the quantity of internal cracks, cavities, and defects in the cement mortars, except the CSA Mix. The OPC-based mortars were more susceptible to the frozen temperature than the CSA-based mortars. The addition of calcium nitrate did not

effectively reduce the internal cracks, cavities and defects in the OPC-based and CSA-based mortars exposed to -10 °C.

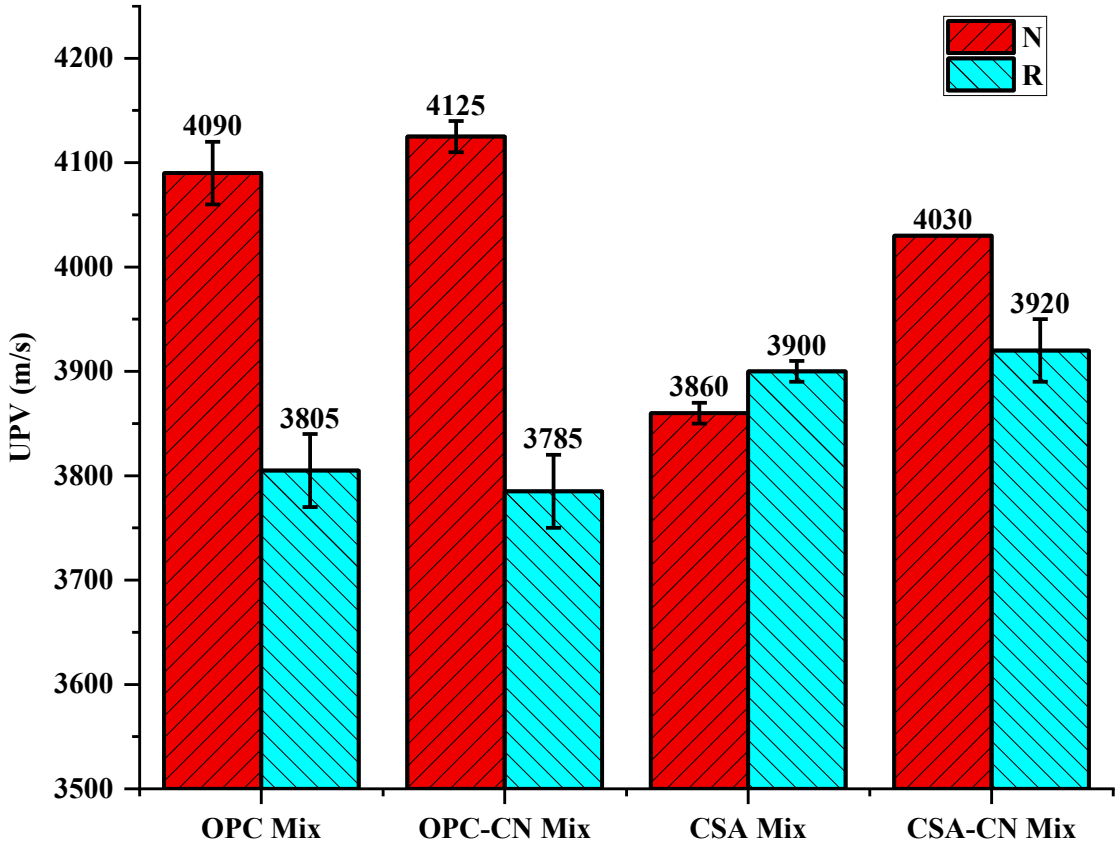

Figure 4.4 UPV values of OPC-based and CSA-based mortars at 28 days. CN is the calcium nitrate added to the mixture as antifreeze admixture; N means that the samples were cured at 23 °C; R indicates that the samples were re-cured at 23 °C after being cured at -10 °C for 3 days.

4.3.3. Thermogravimetric analysis

4.3.3.1. Thermogravimetric analysis on OPC-based samples

Figure 4.5(a) and Figure 4.5(b) show the TGA results of OPC-based mortars cured at different conditions. The signals in the derivative of thermogravimetric (DTG) curves allow us to identify

hydration products and reflect the intensity of the decomposition of different hydration products. The first signal at around 115 °C reveals the dehydration of the calcium silicate hydrate (C-S-H) gel and AFt. The C-S-H was the primary hydration product from OPC; AFt was formed due to the hydration of C_3A in the presence of calcium sulfate (Bullard et al., 2011). The dehydration of AFt mainly occurred at around 135 °C (Trauchessec et al., 2015), which overlapped with the signal for C-S-H gel. The second signal, between ~400 °C and ~500 °C, explains the decomposition of calcium hydroxide. The decarbonization of calcium carbonate can be observed at around 800 °C.

The thermogravimetric (TG) curves show the residual weight of the powder samples used for the TGA test. The lower residual weight means that more hydration products had been decomposed during the TGA test, which implies more hydration products had been formed during the curing period, indicating a higher hydration degree (Huang et al., 2019). As shown in Figure 4.5(a), the residual weight of the OPC Mix-F-3days was remarkably higher (11.6%) than that of the OPC Mix-N-3days. The huge difference in the residual weight indicates that the frozen temperature (i.e. -10 °C) dramatically slowed down the hydration reaction in the OPC Mix-F. After re-curing, the residual weight for the OPC Mix-R-28days was 79.3%, which was almost same as that for the OPC Mix-N-28days. The same residual weight means that the amount of formed hydration products in the OPC Mix-R was almost same as that in the OPC Mix-N at 28 days.

The influence of calcium nitrate on the hydration reaction of OPC-based mortars is presented in Figure 4.5(b). The addition of calcium nitrate accelerated the hydration of OPC-based mortars at both -10 °C and 23 °C. The residual weight of OPC-CN Mix-F-3days was 85.1% at the end of the TGA test. It was 6.3% lower than the residual weight of the OPC Mix-F-3days, indicating that more hydration products had been formed when calcium nitrate was added. However, the

residual weight for OPC-CN Mix-F-3days was still 8.5% higher than that of OPC-CN Mix-N-3days. This difference reveals that the hydration reaction of OPC-based mortar at -10 °C was still much slower than that cured at 23 °C, even if calcium nitrate was added as an antifreeze admixture and accelerator. After re-curing, the hydration in the OPC-CN Mix-R caught up with the OPC-CN Mix-N, reaching same degree of hydration.

4.3.3.2. Thermogravimetric analysis on CSA-based samples

Figure 4.5(c) and Figure 4.5(d) show that the TG and DTG curves of CSA-based mortars cured at different conditions. There are at least four signals in each DTG curve. The first signal, at around 135 °C, reflects the dehydration of AFt and C-S-H gel. The AFt is the hydration product of $C_4A_3\bar{S}$. When enough ${SO_4}^{2-}$ is available in the pore solution, $C_4A_3\bar{S}$ hydrates very fast, forming AFt and AH_3 (García-Maté et al., 2015; Winnefeld et al., 2017). The signal for the dehydration of AH_3 can be observed at around 260 °C. When ${SO_4}^{2-}$is not available in the pore solution, $C_4A_3\bar{S}$ reacts quickly to form AFm (Tang et al., 2015). The dehydration of AFm was detected at around 150 °C and 220 °C. The signal between 700 °C to 810 °C indicates the decomposition of calcium carbonate. Note that, for the CSA-CN Mix, a signal at around 480 °C can be observed, accounting for the dehydration of calcium hydroxide, whereas this peak does not show in the DTG curves for the CSA Mix. In the CSA Mix, the calcium hydroxide was consumed since it can participate in the hydration reaction of $C_4A_3\bar{S}$ (Li et al., 2018). In the CSA-CN Mix, more calcium hydroxide was formed, since calcium nitrate can accelerate the hydration of belite (Kičaitė et al., 2017). The formed calcium hydroxide did not run out by the hydration of $C_4A_3\bar{S}$.

The TG curves show that curing condition had negligible influence on the residual weight of CSA Mix; however, calcium nitrate addition posed large influence on the residual weight. For

the CSA Mix, the residual weight was about 81% at 1 day regardless the curing temperature. The similar residual weight at different temperatures indicates that the hydration of CSA cement was still fast even at -10 °C. This is consistent with our previous findings that the hydration reaction of CSA cement is very fast, even at frozen temperatures (i.e. -5 °C and -10 °C) (Huang et al., 2019). The residual weight for the CSA-CN Mix-F-1day was 85%, which was 6% higher than that of CSA-CN Mix-N-1day. The higher residual weight means that the hydration reaction in CSA-CN Mix-F was slower than that in CSA-CN Mix-N. The DTG curve for CSA-CN Mix-F-1day shows that there were fewer AFm and AH_3 formed, indicating that calcium nitrate retarded the hydration of ye'elimite in the first day when cured at -10 °C. This confirms with the statement of Kičaitė et al (2017) that both Ca^{2+} and NO_3^- can retard the hydration of aluminate. From 1 day to 3 days, the residual weight for CSA-CN Mix-F decreased 10%, which means that the hydration reaction in CSA-CN Mix-F sped up in this period. At 28 days, the residual weight for CSA-CN Mix-R and CSA-CN Mix-N had an average of 73.5% ± 0.8%, which was about 4% lower than that for the CSA Mix-R and CSA Mix-N. The lower residual weight means more hydration products dehydrated during the TGA tests, indicating that the CSA-CN Mix achieved a higher hydration degree at 28 days. The higher hydration degree was caused by calcium nitrate, which accelerated the hydration of belite (Kičaitė et al., 2017). It can be concluded that calcium nitrate can accelerate the hydration of belite but retard the hydration of ye'elimite.

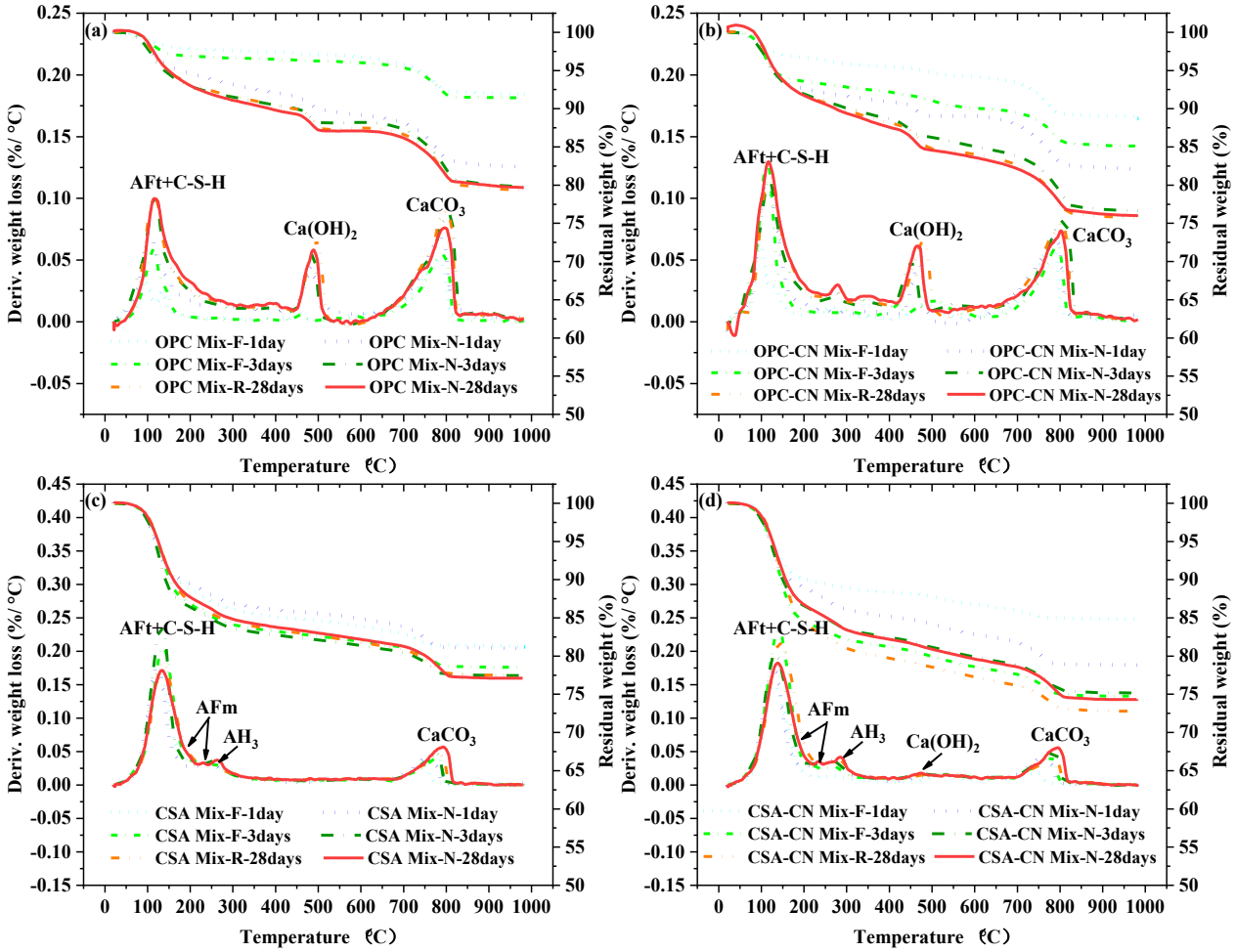

Figure 4.5 TG and DTG curves for hydrated: (a) OPC Mix; (b) OPC-CN Mix; (c) CSA Mix; and (d) CSA-CN Mix. CN is the calcium nitrate added to the mixture as antifreeze admixture; N means that the samples were cured at 23 °C; F indicates that the samples were cured at -10 °C; R means that the samples were re-cured at 23 °C after being cured at -10 °C for 3 days.

4.3.4. Pore structure and porosity

4.3.4.1. Pore structure and porosity in OPC-based mortars

Figure 4.6(a) shows the pore size distribution in the OPC-based mortar. The pore size distribution is expressed as a function of incremental mercury intrusion volume (dV/d(ln(D)) against pore diameter (D). In

Figure 4.6(a), the most obvious peak is located between 0.02 μm and 0.1 μm in each pore size distribution curve of the OPC-based mortars. For OPC Mix-R and OPC-CN Mix-R, the peak values were 0.025 cm^3/g and 0.037 cm^3/g, which were lower than those for OPC Mix-N (0.052 cm^3/g) and OPC-CN Mix-N (0.044 cm^3/g). This means that the OPC-based mortars exposed to -10 °C had generated fewer pores with a diameter smaller than 0.1 μm. However, OPC Mix-R and OPC-CN Mix-R had a higher volume of pores with a diameter larger than 0.1 μm. In particular, a second peak can be observed in the pore size distribution curves for OPC Mix-R and OPC-CN Mix-R, appearing at around 120 μm and 30 μm, respectively.

Exposing the fresh OPC-based mortars to -10 °C for 3 days resulted in a higher porosity, as shown in Table 5. The porosity of OPC Mix-R was 18.2%, being 3.2% higher than OPC Mix-N. The addition of calcium nitrate slightly decreased the porosity of OPC-based mortars exposed to -10 °C. The porosity of OPC-CN Mix-R was 0.8% lower than OPC Mix-R.

Figure 4.7(a) clearly shows that the increase in the porosity of OPC-based mortars exposed to -10 °C was mainly attributable to the increase in the accumulated volume of pores with a diameter larger than 0.1 μm. For OPC Mix-R and OPC-CN Mix-R, there were 0.046 cm^3/g and 0.042 cm^3/g of pores with a diameter larger than 0.1 μm, while the data for OPC Mix-N and OPC-CN Mix-N were 0.022 cm^3/g and 0.024 cm^3/g, respectively. This data indicates that more cracks and cavities had been generated in the OPC-based mortars exposed to -10 °C.

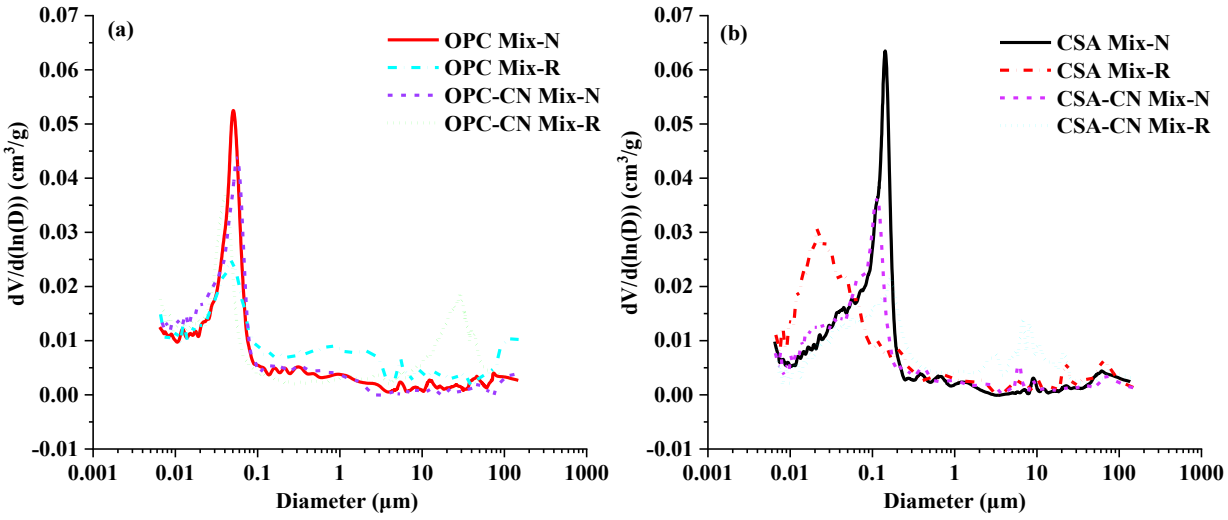

Figure 4.6 Pore size distribution in: (a) OPC-based mortars; (b) CSA-based mortars. CN is the calcium nitrate added to the mixture as antifreeze admixture; N means that the samples were cured at 23 °C; R indicates that the samples were re-cured at 23 °C after being cured at -10 °C for 3 days.

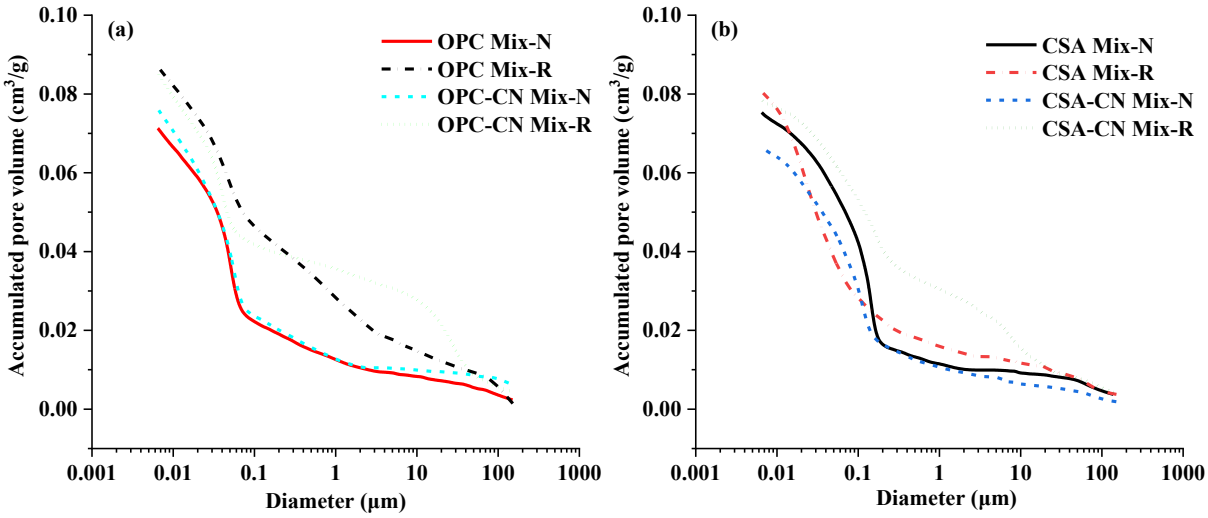

Figure 4.7 Accumulated pore volume in: (a) OPC-based mortars; (b) CSA-based mortars. CN is the calcium nitrate added to the mixture as antifreeze admixture; N means that the samples were cured at 23 °C; R indicates that the samples were re-cured at 23 °C after being cured at -10 °C for 3 days.

4.3.4.2. Pore structure and porosity in CSA-based mortars

Figure 4.6(b) presents the pore size distribution of CSA-based mortars. For CSA-based mortars, the maximum incremental mercury intrusion volume appears in the range from 0.1 μm to 0.2 μm, except for the CSA Mix-R. The incremental mercury intrusion volume for the CSA Mix-R peaks at 0.021 μm. This reveals that finer pore structure had formed in the CSA Mix-R. The addition of calcium nitrate decreased the maximum incremental mercury intrusion volume from 0.0635 cm^3/g to 0.035 cm^3/g when cured at 23 °C. However, several peaks were found in the diameter range between 2 μm and 30 μm in the CSA-CN Mix-R, indicating the addition of calcium nitrate generated more large pores in the CSA-based mortar exposed to -10 °C. This is because CSA-CN Mix cured at -10 °C only gained a strength of 1.6 MPa at 1 day (as shown in

Figure 4.12), which did not reach the minimum strength (3.5 MPa) for resisting the early-age frost damage suggested by ACI 306R-10 (ACI, 2010). Consequently, the CSA-CN Mix exposed to -10 °C suffered from early-age frost damage, more cracks had formed (The evidence is presented in Figure 4.11.) These cracks were identified as larger pores by the MIP test. It is worth mentioning that the addition of calcium nitrate reduced the porosity of CSA-based mortars at 23 °C. As shown in

Figure 4.6(b), the reduction in porosity is mainly attributed to the decrease in pores with a size between 0.1 μm and 0.2 μm. This decrease in porosity can be explained by pore-filling mechanism (Boumiz et al., 1996; Bullard et al., 2011) and TGA results. The TGA results in Figure 4.5(c) and Figure 4.5(d) showed that more hydration products had been formed in the CSA-CN Mix-N compared with that in the CSA Mix-N at 28 days. These hydration products precipitated and filled in the pores, generating a structure with lower porosity.

Table 4.5 shows that exposure to -10 °C increased the porosity of the CSA Mix and the CSA-CN Mix to different extents. The porosity of the CSA Mix-R was 16.5%, only 0.7% higher than that of the CSA Mix-N. This shows that exposing to -10 °C imposed minor effects on the CSA Mix. However, exposing to -10 °C had more intensive effects on the CSA-CN Mix. The porosity of the CSA-CN Mix-R was 1.8% higher than the CSA-CN Mix-N. The higher porosity of CSA-based mortars exposed to -10 °C was mainly attributed to the increase in the volume of pores larger than 0.2 μm, as presented in

Figure 4.7(b). In CSA Mix-R and CSA-CN Mix-R, the accumulated volumes were 0.023 cm^3/g and 0.041 cm^3/g for pores with a diameter larger than 0.2 μm, while the data was 0.016 cm^3/g for both CSA Mix-N and CSA-CN Mix-N.

Table 4.5 Porosity of OPC-based and CSA-based mortars

Sample ID	OPC Mix-N	OPC-CN Mix-N	CSA Mix-N	CSA-CN Mix-N
Porosity (%)	15.0	15.7	15.8	14.5
Sample ID	OPC Mix-R	OPC-CN Mix-R	CSA Mix-R	CSA-CN Mix-R
Porosity (%)	18.2	17.4	16.5	16.3

Note: CN is the calcium nitrate added to the mixture as antifreeze admixture; N means that the samples were cured at 23 °C; R indicates that the samples were re-cured at 23 °C after being cured at -10 °C for 3 days.

4.3.5. Scanning electron microscopy

SEM analyses were performed to observe cracks and cavities in the OPC-based and CSA-based mortars cured at different conditions. As shown in Figure 4.8-Figure 4.11, cracks can be observed in all samples. Cracks were observed in the mortars cured at 23 °C since cracks are

caused by a variety of reasons (e.g., dry shrinkage) (Bentz and Jensen, 2004; Bissonnette et al., 1999; Mehta and Monteiro, 2006; Sellevold and Bjøntegaard, 2006). It is noted that more cracks can be observed in OPC Mix-R, OPC-CN Mix-R, and CSA-CN Mix-R when compared with the same mixtures directly cured at 23 °C. These cracks were wider and connected to each other, forming meshes. Furthermore, more cavities were shown in the OPC Mix-R and the OPC-CN Mix-R. The higher volume of cracks and cavities coincides with the higher mercury intrusion volume and porosity in OPC Mix-R, OPC-CN Mix-R, and CSA-CN Mix-R measured by MIP tests. The large quantity of cracks and cavities indicates OPC Mix, OPC-CN Mix, and CSA-CN Mix failed to gain sufficient strength to resist the tensile stress during the formation of ice lens when exposed to -10 °C, consequently early-age frost damage occurred in these mixtures. For CSA Mix-R, the change in the quantity of cracks and cavities was marginal when compared with that in CSA Mix-N. This marginal change indicates that CSA Mix has high resistance to early-age frost damage.

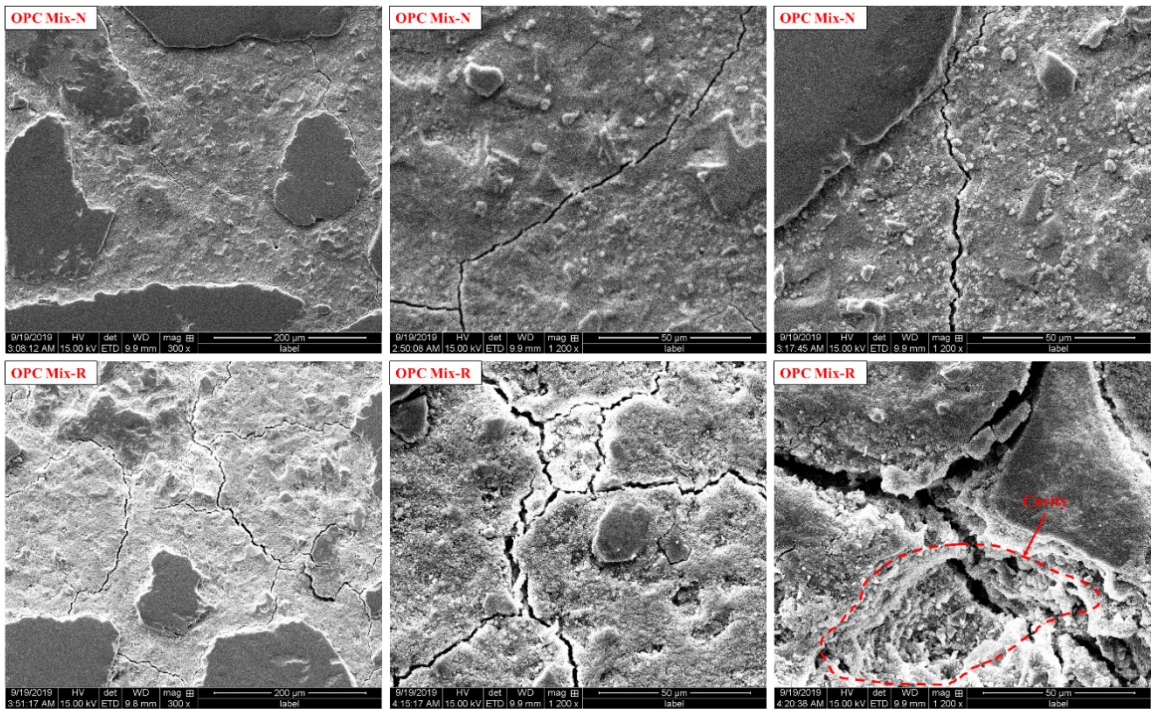

Figure 4.8 SEM images of OPC Mix for observing cracks and cavities. N means that the samples were cured at 23 °C; R indicates that the samples were re-cured at 23 °C after being cured at -10 °C for 3 days.

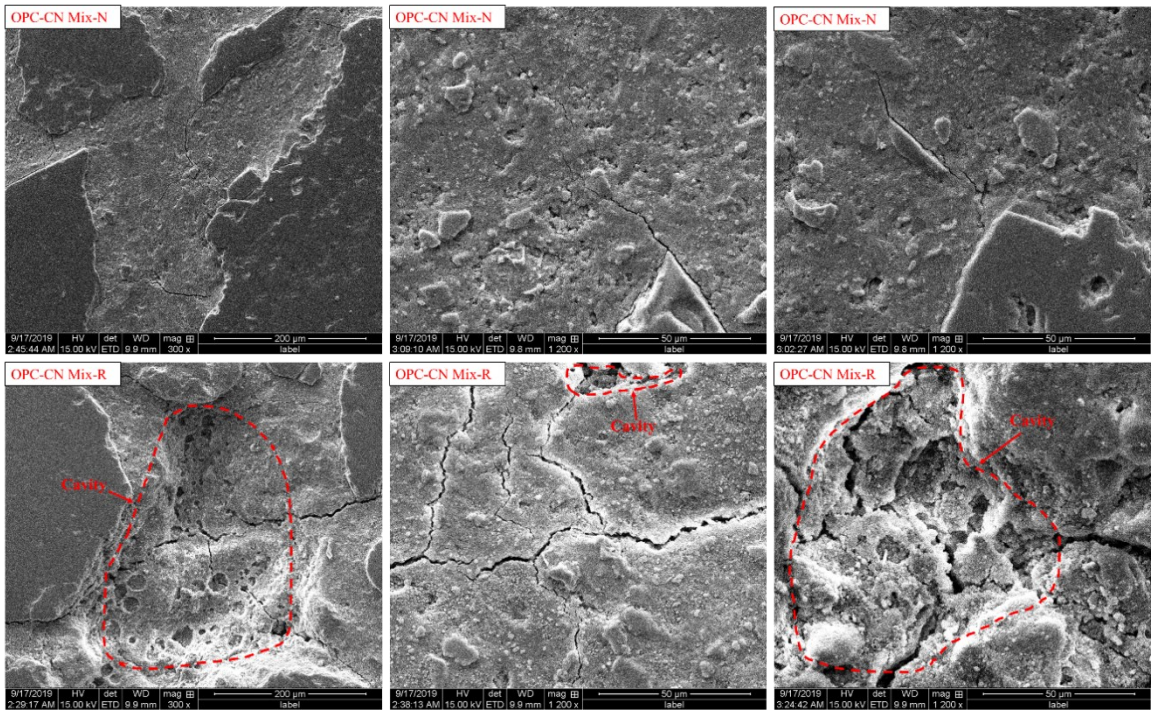

Figure 4.9 SEM images of OPC-CN Mix for observing cracks and cavities. CN is the calcium nitrate added to the mixture as antifreeze admixture; N means that the samples were cured at 23 °C; R indicates that the samples were re-cured at 23 °C after being cured at -10 °C for 3 days.

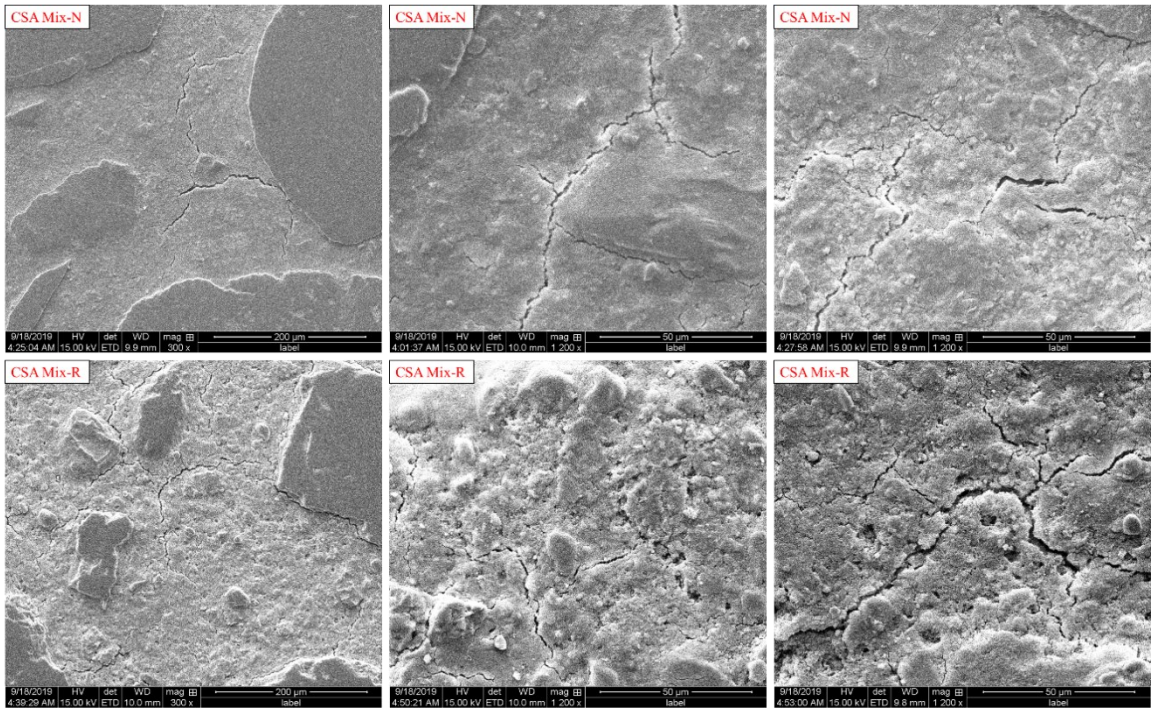

Figure 4.10 SEM images of CSA Mix for observing cracks and cavities. N means that the samples were cured at 23 °C; R indicates that the samples were re-cured at 23 °C after being cured at -10 °C for 3 days.

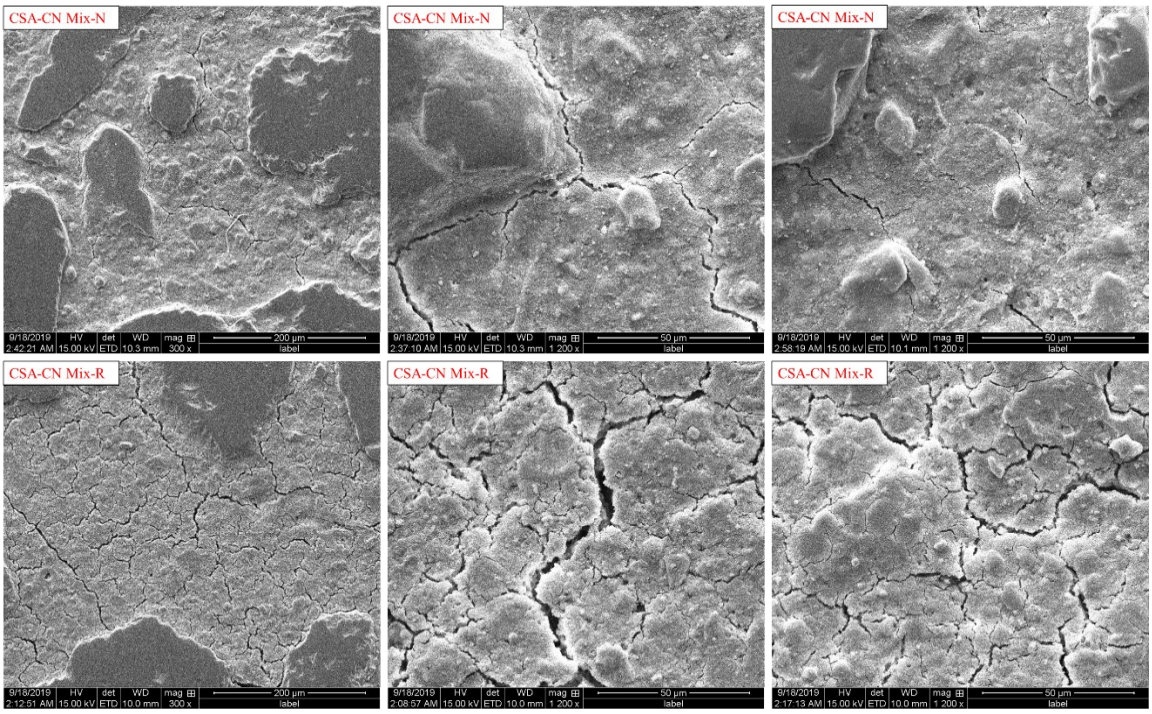

Figure 4.11 SEM images of CSA-CN Mix for observing cracks and cavities. CN is the calcium nitrate added to the mixture as antifreeze admixture; N means that the samples were cured at 23 °C; R indicates that the samples were re-cured at 23 °C after being cured at -10 °C for 3 days.

4.3.6. Unconfined compressive strength

Cementitious materials-based structures are usually designed to bear compressive stress (American Concrete Institute, 2005; Mehta and Monteiro, 2006). As mentioned, early-age frost damage degrades the compressive strength of cement-based mixtures. Therefore, the UCS of the OPC-based and CSA-based mortars was tested in this study. To present the effects of early-age frost damage on mechanical performance, the relative UCS was introduced as the ratio of the UCS of a re-cured sample compared with that of the same mixture directly cured at 23 °C.

The UCS of OPC-based and CSA-based mortars at different ages are depicted in

Figure 4.12. At 1 day, CSA-based mortars cured at 23 °C showed fast strength development. CSA Mix-N and CSA-CN Mix-N gained UCS of 25.8 MPa and 35.4 MPa at 1 day, which was two to three time of the UCS of OPC-based mortars. At -10 °C, the CSA Mix still achieved fast strength development. CSA Mix-F gained a UCS of 15.5 MPa at 1 day, while the UCS of the OPC Mix-F, OPC-CN Mix-F, and CSA-CN Mix-F were less than 2 MPa.

The difference in the UCS can be explained by the TGA results. The hydration in CSA Mix very fast and formed large amounts of hydration products at 1 day, even if cured at -10 °C. This enabled the CSA Mix to gain strength at a temperature as cold as -10 °C. The addition of calcium nitrate retarded the hydration of ye'elimite when cured -10 °C, consequently the UCS of CSA-CN Mix-F was very low at 1 day. For OPC-based mortars, the hydration reaction was much slower at -10 °C compared with those cured at 23 °C, and fewer hydration products were formed. As a result, the UCS of OPC-based mortars cured at -10 °C were low at 1 day.

From 1 day to 3 days, the UCS of OPC-based and CSA-based mortars cured at 23 °C kept increasing owing to the hydration reaction processing. However, the strength development of mortars cured at -10 °C nearly stopped, except for the CSA-CN Mix. The UCS of CSA-CN Mix-F increased ~10 MPa from 1 day to 3 days since the hydration reaction in this mixture sped up in this period. At 3 days, the CSA Mix-F and CSA-CN Mix-F achieved UCS of 16.2 MPa and 11.7 MPa, while the UCS of the OPC Mix-F and OPC-CN Mix-F were 1.4 MPa and 2.4 MPa. Both OPC Mix-F and OPC-CN Mix-F had not reached the minimum compressive strength for resisting the early-age frost damage required by ACI 306R (ACI, 2010).

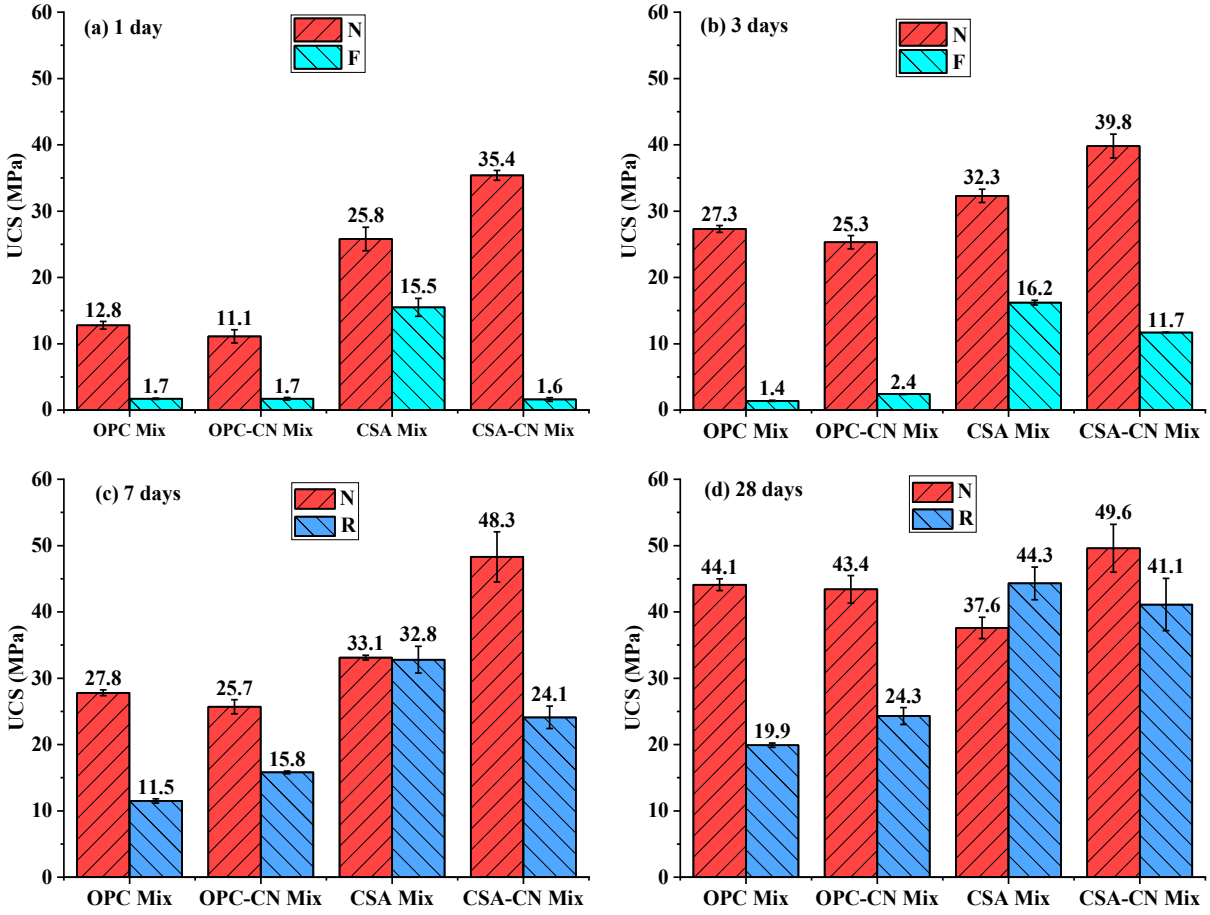

Figure 4.12 UCS of OPC-based and CSA-based mortars at: (a) 1 day; (b) 3 days; (c) 7 days; and (d) 28 days. CN is the calcium nitrate added to the mixture as antifreeze admixture; N means that the samples were cured at 23 °C; F indicates that the samples were cured at -10 °C; R means that the samples were re-cured at 23 °C after being cured at -10 °C for 3 days.

After 3 days, the mortars cured at -10 °C were re-cured in a moisture room with a temperature of 23 °C. During the re-curing, the strength development sped up. After being re-cured for 4 days (from 3 days to 7 days), the UCS of OPC Mix-R, OPC-CN Mix-R, CSA Mix-R, and CSA-CN Mix-R increased by 10.1 MPa, 13.4 MPa, 16.6 MPa, and 12.4 MPa, respectively. In the same period, the UCS of the mortars directly cured at 23 °C increased slightly (<1 MPa), except the CSA-CN Mix-N, which increased by 8.5 MPa, achieving a UCS of 48.3 MPa at 7 days.

From 7 days to 28 days, the UCS of all mortars further increased. However, the UCS of re-cured mortars failed to reach a similar or higher strength at 28 days compared with the mortars directly cured at 23 °C, except the CSA Mix-R. At 28 days, the OPC Mix-R and OPC-CN Mix-R had the UCS of 19.9 MPa and 24.3 MPa, which were much lower than those for the OPC Mix-N (44.1 MPa) and OPC-CN Mix-N (43.4 MPa). CSA Mix-R and CSA-CN Mix-R showed much better performance, achieving the UCS of 44.3 MPa and 41.1MPa at 28 days. The UCS of CSA Mix-R was even 6.7 MPa higher than CSA Mix-N. Note that the addition of calcium nitrate notably increased the 28-day UCS of CSA-based mortars cured at 23 °C, but it did not work for the CSA-based mortars exposed to -10 °C. At 28 days, the UCS of CSA-CN Mix-N was 49.6 MPa, which was 12 MPa higher than that of CSA Mix-N. However, the UCS of the CSA-CN Mix-R was 3.2 MPa lower than that of the CSA Mix-R at 28 days.

At 28 days, the TGA results show the formed hydration products in mortars exposed to -10 °C were nearly the same as the corresponding mixtures directly cured at 23 °C. However, the relative UCS of the OPC Mix and OPC-CN Mix were as low as 45.1% and 56.0%, respectively. This is because the OPC Mix and OPC-CN Mix exposed to -10 °C failed to gain sufficient strength before freezing to resist the early-age frost damage. In other words, the OPC Mix-R and OPC-CN Mix-R exposed to -10 °C experienced severe early-age frost damage. Lots of cracks and cavities were left in these OPC-based mortars, which were confirmed by the SEM images. Re-curing at 23 °C enabled the hydration reaction to continue but failed to repair these cracks and cavities. As a result, the relative UCS was very low even if the hydration degree had reached the same level. The results showed that OPC Mix has low resistance to the early-age frost damage, and the addition of calcium nitrate did not effectively improve the resistance of OPC-based mortars to early-age frost damage.

Compared with OPC-based mortars, CSA-based mortars showed better performance. The relative UCS of the CSA Mix and CSA-CN Mix reached 117.8% and 82.9 %, respectively, which were remarkably higher than those of the OPC Mix and OPC-CN Mix. The high relative UCS indicated that CSA-based mortars have high resistance to early-age frost damage, especially the CSA Mix. The feature of fast strength development enabled the CSA Mix cured at -10 °C to gain sufficient strength to resist early-age frost damage. At 28 days, the UCS of CSA Mix-R was 17.8% higher than CSA Mix-N. The explanation for the higher UCS lies in the pore size distribution and accumulated pore volume curves, as presented in

Figure 4.6(b) and

Figure 4.7(b). Exposing samples to -10 °C led to a finer pore structure in CSA Mix-R. It is well-known that the macropores (with a diameter larger than 0.05 μm) impose negative effects on the strength of the cement-based structure (Mehta and Monteiro, 2006). In CSA Mix-R, the accumulated volume of macropores was 0.038 cm^3/g, which was 0.018 cm^3/g lower than that of CSA Mix-N. The lower volume of macropores enabled the CSA Mix-R to achieve a higher UCS. The addition of calcium nitrate increased the UCS of CSA-based mortar cured at 23 °C, which was attributed to the increased amount of hydration products formed and the decrease in porosity. However, when exposed to -10 °C, CSA-CN Mix cured at -10 °C only gained a strength of 1.6 MPa at 1 day, which did not reach the minimum strength (3.5 MPa) for resisting the early-age frost damage suggested by ACI 306R-10 (ACI, 2010). Consequently, the CSA-CN Mix exposed to -10 °C suffered from early-age frost damage, more cracks had formed in the structure (The evidence is presented in Figure 4.11.) These cracks degraded the strength of CSA-CN Mix-R. As a result, the relative UCS of CSA-CN Mix was lower than the CSA Mix.

4.4. Conclusion

This study explored the possibility of using sulfoaluminate (CSA) to prevent early-age frost damage. Experimental investigations were conducted to compare the performance of CSA-based and ordinary Portland cement (OPC)-based mortars with and without calcium nitrate addition through thermogravimetric analysis (TGA), mercury intrusion porosimetry (MIP), scanning electron microscopy (SEM), and unconfined compressive strength (UCS), etc. The primary conclusions are enumerated as follows:

(1) TGA results indicate that hydration reaction in CSA-based mortar without calcium nitrate (CSA Mix) was much faster than that in OPC-based mortars at -10 °C. At 1 day, CSA Mix cured at -10 °C gained a UCS of 15.5 MPa, while OPC-based mortars did not reach the minimum strength (3.5 MPa) for resisting early-age frost damage.

(2) MIP results and SEM images shows that exposing to -10 °C noticeably increased the porosity, quantity of cracks, and cavities in OPC-based mortars, while almost had no negative influence on CSA Mix. Instead, a finer pore structure was observed in re-cured CSA Mix.

(3) At 28 days, re-cured OPC-based mortars only achieved about half of the UCS of their references (directly cured at 23 °C) even if they reached same hydration degree. However, re-cured CSA Mix achieved 117% of the UCS of its reference.

(4) Calcium nitrate retarded ye'elimite hydration. At 1 day, CSA-based mortar with calcium nitrate (CSA-CN Mix) only gained 1.6 MPa at -10 °C. At 28 days, the UCS of re-cured CSA-CN Mix was 82.9% of that of its reference since more cracks were formed.

(5) OPC-based mortars experienced severe early-age frost damage, while CSA-based mortars showed higher resistance to early-age frost damage. Calcium nitrate reduced the resistance of CSA-based mortar to early-age frost damage.

In summary, CSA cement can be used in cold weather to prevent early-age frost damage since it can achieve fast hydration and gain strength rapidly to resist the damage caused by freezing.

Chapter 5. Thermal properties of calcium sulfoaluminate cement-based mortars incorporated with expanded perlite cured at cold temperatures

Chapter 5 has been published as **G. Huang**, D. Pudasainee, R. Gupta, W.V. Liu, Thermal properties of calcium sulfoaluminate cement-based mortars incorporated with expanded perlite cured at cold temperatures. *Construction and Building Materials*. © Elsevier. 274 (2021) 122082.

Nomenclatures

AFm	Monosulfate
AFt	Ettringite
AH_3	Aluminium hydroxide
Al_2O_3	Aluminium oxide
ASTM	American Society for Testing and Materials
C_2S	Calcium silicate, belite
C_3A	Tricalcium aluminate
C_4AF	Tetracalcium aluminoferrite, brownmillerite
$C_4A_3\bar{S}$	Tetracalcium trialuminate sulfate, ye'elimite
$C\bar{S}$	Calcium sulfate
CaO	Calcium oxide
CSA	Calcium sulfoaluminate
C-S-H	Calcium silicate hydrate
Fe_2O_3	Ferric oxide
IEA	International Energy Agency
MgO	Magnesium oxide
PC	Portland cement

SiO_2	Silicon dioxide
SO_3	Sulfur trioxide
TGA	Thermogravimetric analysis
TPS	Transient plane source
UCS	Unconfined compressive strength (MPa)
UPV	Ultrasonic pulse velocity (m/s)
$\Delta\bar{T}$	Average temperature increase (K)
P_0	Heating power (W)
r	Radius of sensor (mm)
k	Thermal conductivity (W/mK)
α_t	Thermal diffusivity (mm^2/s)
t_t	Measurement time (s)
I_0	Modified Bessel function
τ_t	Dimensionless time
m	Number of concentric rings on the sensor
C_p	Specific heat capacity (J/kgK)
ρ	Density (kg/m^3)

5.1. Introduction

Energy consumption in buildings has shown an increasing trend in recent years. According to the International Energy Agency (IEA), energy consumed in buildings worldwide increased to 3060 million tonnes of oil equivalent (Mtoe) in 2018, resulting in direct carbon dioxide (CO_2) emissions of more than 3000 million tonnes (IEA, 2019). In cold regions (e.g., Canada), space heating to maintain thermal comfort in working or living spaces is a major share of energy consumption and emissions related to buildings (Asadi et al., 2018). Space heating represents about 56% of the total energy consumption in buildings in Canada (Natural Resources Canada, 2020). Energy consumption by space heating is significantly affected by the heat exchange intensity with the outdoor environment, especially the heat conduction through building materials (cement-based mixtures) (Asadi et al., 2018; Latha et al., 2015). Cement-based mixtures (e.g. concrete and mortar) are the most versatile building materials, accounting for about two-thirds of total building materials consumption (Oktay et al., 2015). Reducing thermal conductivity of cement-based mixtures is of great significance since low thermal conductivity can alleviate heat loss to the outdoor environment through heat conduction, and ultimately reduce energy consumption and CO_2 emissions related to buildings (Cuce et al., 2014; Jelle, 2011; Latha et al., 2015; Wu et al., 2015).

Incorporating expanded perlite is an excellent solution for reducing the thermal conductivity of cement-based mixtures (Karakoç and Demirboga, 2010; Liu et al., 2014b; Sengul et al., 2011). Expanded perlite is a lightweight, porous aggregate which is produced by heating perlite (an amorphous siliceous volcanic rock) to above 870 °C (Liu et al., 2014b; Sengul et al., 2011). Incorporating expanded perlite into cement-based mixtures can effectively reduce their thermal conductivity (Gandage et al., 2013; Karakoç and Demirboga, 2010; Liu et al., 2011; Liu et al.,

2014b; Sengul et al., 2011). For example, Liu et al. (2011) replaced normal aggregates with expanded perlite at volume ratios of 25%, 50%, 75%, and 100%, and the thermal conductivity reduced by 21.1%, 35.4%, 59.9%, and 79.3%, respectively. Similarly, Sengul (2011) reported that a reduction of 65% was observed in thermal conductivity when 80% of normal aggregates were replaced with expanded perlite. The noticeable reduction in thermal conductivity was mainly attributed to the large difference in the thermal conductivities of normal aggregates and expanded perlite. According to Khan (2002), the thermal conductivity of commonly used aggregates ranges from 1.16 to 8.58 W/mK, while the thermal conductivity of expanded perlite can be as low as 0.04 W/mK (Topçu and Işıkdağ, 2008).

In previous studies (Gandage et al., 2013; Karakoç and Demirboga, 2010; Liu et al., 2011; Liu et al., 2014b; Sengul et al., 2011), expanded perlite was mainly incorporated into Portland cement (PC)-based mixtures. However, it is challenging to apply PC-based mixtures in cold weather (< 5 °C) (Choi et al., 2017; Liu et al., 2018a), because the hydration and strength development of PC-based mixtures are very slow. Our previous study (Huang et al., 2019) showed that PC-based mortars cured at cold temperatures (< 5 °C) developed no strength in the first 24 hours; no strength was developed for 28 days when they were cured at -5 °C and -10 °C. Slow strength development prolongs construction time and reduces construction efficiency. In addition, early-age frost damage tends to occur if cement-based mixtures cannot gain sufficient compressive strength (3.5 MPa) before freezing (ACI, 2010). Cement-based structures that experienced early-age frost damage cannot reach the designed strength even if the curing temperature later increases to a normal temperature (e.g. 23 °C) (Huang et al., 2020a).

In contrast to PC, calcium sulfoaluminate (CSA) cement showed great performance when applied in cold weather (Huang et al., 2019, 2020a; Qin et al., 2018). Our previous study (Huang

et al., 2020a) indicated that CSA cement-based mortars cured at -10 °C achieved unconfined compressive strength (UCS) of 15.5 MPa within 1 day and showed high resistance to early-age frost damage, while severe early-age frost damage occurred in PC-based mortars. The fast strength development and high resistance to early-age frost damage were mainly attributable to special composites in CSA cement. Generally, CSA cement is composed of ye'elmite ($C_4A_3\bar{S}$), belite (C_2S), calcium sulfate (i.e. $C\bar{S}$, $C\bar{S}H_{0.5}$, *or* $C\bar{S}H_2$), calcium aluminoferrite (C_4AF), and calcium aluminate (i.e., $CA, C_3A, or\ C_{12}A_7$), etc. (Bullerjahn et al., 2019; Huang et al., 2020b; Jeong et al., 2018; Winnefeld et al., 2017) (cement oxides notation: $C = CaO, \bar{S} = SO_3, A = Al_2O_3, H = H_2O, S = SiO_2, F = Fe_2O_3$). With the presence of calcium sulfate, ye'elimite reacts rapidly with calcium sulfate and water to form ettringite (AFt) and aluminum hydroxide (AH_3); in the absence of calcium sulfate, ye'elimite reacts rapidly with water to form monosulfoaluminate (AFm) and aluminum hydroxide (Winnefeld and Lothenbach, 2010; Winnefeld et al., 2017). The fast hydration of ye'elimite enables CSA cement-based mixtures to gain sufficient strength rapidly to resist early-age frost damage even in cold weather.

Owing to the great performance of CSA cement, it would be sensible to incorporate expanded perlite with CSA cement-based mixtures for applications in cold regions, and four benefits can be expected. First, incorporating lightweight aggregate into CSA cement-based mixtures is expected to reduce thermal conductivity and alleviate heat conduction through the CSA cement-based building materials, thereby reducing energy consumption and CO_2 emissions in buildings. Second, CSA cement-based mixtures can achieve fast strength development at as cold as -10 °C, leading to a higher construction efficiency in cold weather. Third, CSA cement-based mixtures have high resistance to early-age frost damage (Huang et al., 2020a), resulting in fewer safety concerns and lower maintenance costs. Finally, the manufacturing of CSA cement is a cleaner

process that causes less energy consumption and fewer CO_2 emissions. According to the life cycle assessment by Hanein et al. (2018), manufacturing one tonne of CSA cement consumes 1×10^9 Joules less energy than that for PC and generates about 25% to 35% fewer CO_2 emissions. However, despite these four expected benefits, there is a lack of research on the thermal conductivity of CSA cement-based mixtures in previous literature, and CSA cement-based mixtures with low thermal conductivity have not been developed for cold region applications.

To this end, the objective of this study is to incorporate expanded perlite into CSA cement-based mortars to develop a novel building material that has low thermal conductivity for cold region applications. Experiments were conducted to measure the thermal conductivity, thermal diffusivity, heat capacity, oven-dry bulk density, ultrasonic pulse velocity (UPV), and UCS of CSA cement-based mortars incorporated with expanded perlite cured at various temperatures (i.e., 23 °C, 0°C and -10 °C). Following those experiments, the thermal conductivity, thermal diffusivity, heat capacity, and UCS were correlated with oven-dry bulk density and UPV values.

5.2. Materials and methods

5.2.1. Materials

Materials used in this study include CSA cement, fine aggregates, expanded perlite, and tap water. The main oxide and mineralogical compositions of CSA cement are presented in Table 5.1. The fine aggregates had a bulk density of 1668 kg/m^3 after being oven-dried for 24 hours at 105 °C, and a moisture content of 2.1wt% at a saturated surface dry (SSD) condition. The fine aggregate had a particle size distribution located in the American Concrete Institute (ACI) No.1 grading zone (ACI, 2009b). Expanded perlite had a bulk density of 123 kg/m^3 at an oven-dry condition and a water content of 150 wt% at an SSD condition.

Table 5.1 The main oxide and mineralogical compositions of CSA cement

Oxide compositions	Wt%	Mineralogical compositions	Wt%
SiO_2	15.4	Ye'elimite ($C_4A_3\bar{S}$)	26.3
Al_2O_3	14.7	Belite (C_2S)	48.8
Fe_2O_3	1.7	Anhydrite ($C\bar{S}$)	12.8
CaO	49.5	Bassanite ($C\bar{S}H_{0.5}$)	3.7
MgO	1.4	Calcite ($\mathit{C}c$)	3.4
SO_3	13.8	Calcium aluminoferrite (C_4AF)	1.8

5.2.2. Sample preparation

As shown in Table 5.2, four mixtures were prepared with different aggregate replacement ratios by expanded perlite. The reference mixture without expanded perlite had a water-to-cement (w/c) ratio of 0.5 and an aggregate-to-cement (a/c) ratio of 3.125 where fine aggregates were weighed at an SSD condition. In the other three mixtures, the cement content and w/c ratio were kept the same as the reference; fine aggregates were replaced with expanded perlite at different volumetric ratios, namely 30%, 60%, and 100%. It is of note that when keeping the same w/c ratio, the expanded perlite was pre-absorbed with 150 wt% of water to reach an SSD condition.

The four mixtures were mixed in a laboratory at 20 °C, since the ACI 306R (ACI, 2010) suggests that the placing temperature should be higher than 18 °C when samples are cast as a thin structure (thickness < 300mm) at -1°C to 18 °C. The fresh mixtures were then cast into cylindrical molds with a size of Ø75mm×150mm. After that, the samples were immediately put

into two freezers where the temperature was controlled at 0 °C and -10 °C (cold temperatures), respectively. Another group of samples were cured at 23 °C (room temperature).

Table 5.2 Mixture proportions of CSA cement mortar incorporated with expanded perlite.

Materials	Aggregate replacement ratio by expanded perlite (vol %)			
	0	30	60	100
Cement (kg/m^3)	520	520	520	520
Water (kg/m^3)	260	260	260	260
Fine aggregates (kg/m^3)	1625	1138	650	0
Expanded perlite (kg/m^3)	0	58	116	193
Pre-absorbed water by expanded perlite (kg/m^3)	0	87	174	289

5.2.3. Methods

5.2.3.1. Density and void content

At 28 days, the density and void content of the CSA cement-based mortars were measured following the ASTM standard C642 (ASTM International, 2013b).

5.2.3.2. Ultrasonic pulse velocity

The UPV method measures the velocity of ultrasonic pulses passing through cement-based mixtures, and this method is widely used to evaluate the quality of cement-based structures (ASTM international, 2016c). The UPV value not only has a close relationship with the mechanical performance (ASTM international, 2016c), but it also correlates with the thermal properties of cement-based mixtures (Liu et al., 2014b). The UPV values of samples with

different aggregate replacement ratios were determined as per ASTM 597 (ASTM international, 2016c) at 28 days. Before the UPV tests, cylindrical samples were ground to ensure their two ends were flat, and then they were oven-dried at 105 °C for 24 hours to remove the moisture content since it has a large influence on the UPV values (Güneyli et al., 2017; Lencis et al., 2013; Ohdaira and Masuzawa, 2000).

5.2.3.3. Thermogravimetric analysis

After being cured for 1 day (24 hours) and 28 days, the CSA-based samples were hydration-stopped following the procedures proposed in our previous study (Huang et al., 2020a). First, the samples were crushed and passed through a 4-mm sieve. The collected particles were immersed in acetone for 24 hours to stop hydration. In order to remove the acetone and moisture, the particles were filtered and dried in a vacuum oven at 40 °C for 24 hours. After that, a 2-mm sieve was used to remove coarse aggregates. Then the small particles (<2-mm) were further ground and passed through a 63-μm sieve to remove fine aggregates. Finally, the collected powder (<63-μm) was sealed in a plastic bag and stored in a desiccator.

TGA tests were carried out with a SDT Q600 (TA Instrument, USA) instrument under a nitrogen atmosphere. 60 ± 3 mg of hydration-stopped powder samples were heated from 20 °C to 500 °C at a rate of 10 °C/min.

5.2.3.4. Unconfined compressive strength

The UCS of CSA cement-based mortars with different expanded perlite contents was measured following the ASTM C39/C39M-18 standard [64] at 1 day, 3 days, 7 days, and 28 days.

5.2.3.5. Thermal properties measurement by transient plane source method

There are two categories of methods for determining the thermal properties of cement-based mixtures, namely steady-state methods and transient methods (Asadi et al., 2018; Li et al., 2016; Liu et al., 2014b). The most popular methods are steady-state methods (Mirzanamadi et al., 2018). However, they are time-consuming (2-3 hours per specimen) since they require the temperature gradient over a sample to be stable (Liu et al., 2014b). Compared with steady-state methods, transient methods are quicker for determining thermal properties (i.e., thermal conductivity, thermal diffusivity, and heat capacity). Transient methods can measure thermal properties within several minutes since they record temperature signals during a heating process, and a thermal steady state is unnecessary (Li et al., 2016; Liu et al., 2014b). Among transient methods, the transient plane source (TPS) method, developed by Gustaffson in the 1990s (Gustafsson, 1991), has been attracting increasing attention due to its wide testing range (e.g. thermal conductivity in the range from 0.005 to 1800 W/mK), high accuracy (within ±5%), and high speed (several minutes per sample).

Due to the various advantages of the TPS method, a hot disk TPS 500 instrument (Sweden) and a Capton sensor 5501 with a radius of 6.4 mm (as shown in Figure 5.1) were employed to measure the thermal properties of the CSA cement-based mortars in this study. The Kapton sensor consists of an electrically conductive double spiral etched onto a nickel foil with two thin layers of Kapton (insulation material) covering the surfaces of the nickel foil. During a TPS test, the Kapton sensor is sandwiched between two sample disks, acting as a heating source and a temperature sensor that records the temperature increase with time. As shown in Equation (5-1), the average temperature increase $\Delta\bar{T}$ [K] can be expressed as a function of heating power P_0 [W], radius of sensor r [mm], thermal conductivity k [W/mK], and a dimensionless specific time

function $D(\tau)$ (Gustafsson, 1991). $D(\tau)$ is expressed in Equation (5-2), where m is the number of concentric rings on the sensor, I_0 is the modified Bessel function, and τ_t is a function of thermal diffusivity α_t [mm^2/s], measurement time t_t [s], and radius of sensor r [mm] as shown in Equation (5-3) (Gustafsson, 1991; Liu et al., 2014b; Zhao et al., 2016). In these equations, thermal conductivity and diffusivity of the sample disks are unknown parameters, which can be obtained after a series of iteration by built-in software. Then volumetric heat capacity ρC_p [J/m^{3}K], defined as the product of specific heat capacity C_p [J/kg/K] and density ρ [kg/m^3], can be calculated with Equation (5-4) (Liu et al., 2014b).

$$\Delta\bar{T} = \frac{P_0 D(\tau_t)}{(\pi^{3/2} r k)} \tag{5-1}$$

$$D(\tau_t) = \frac{1}{m^2(m+1)^2}\int_0^{\tau_t}\frac{d\sigma}{\sigma^2} \times \sum_{i=1}^{m} i \sum_{j=1}^{m} k \exp\left(\frac{-(i^2+j^2)}{4m^2\sigma^2}\right) \times I_0\left(\frac{ij}{2m^2\sigma^2}\right) \tag{5-2}$$

$$\tau_t = \frac{\sqrt{\alpha_t t_t}}{r} \tag{5-3}$$

$$\rho C_p = k/\alpha_t \tag{5-4}$$

In this study, sample disks for the TPS tests were prepared and tested according to the following procedures. First, cylindrical samples were sawed into disks with a thickness of 15 ± 1 mm after being cured for 1 day, 3 days, 7 days, and 28 days. Then the sample disks were oven-dried at 105 °C for 24 hours to remove the moisture, as widely accepted in previous studies (Khan, 2002; Liu et al., 2011; Liu et al., 2014b; Real et al., 2016; Sengul et al., 2011; Uysal et al., 2004; Wu et al., 2015). The moisture content in the cement mortars should be removed since it can be very different (varied from 7.6% to 28% at different aggregate replacement ratios as reported by Liu et al. (2011)) and has a significant influence on the thermal properties (Asadi et al., 2018; Khan, 2002; Real et al., 2016). For example, thermal conductivity increases 6%-9% when the moisture

content increases 1% (ACI, 2009a; Asadi et al., 2018; Khan, 2002; Real et al., 2016). To understand the influence of expanded perlite contents and curing temperatures on the thermal properties, oven-drying was applied to eliminate the influence of different moisture contents. Three pairs of disks were prepared for each sample, and two measurements were conducted on each pair of sample disks.

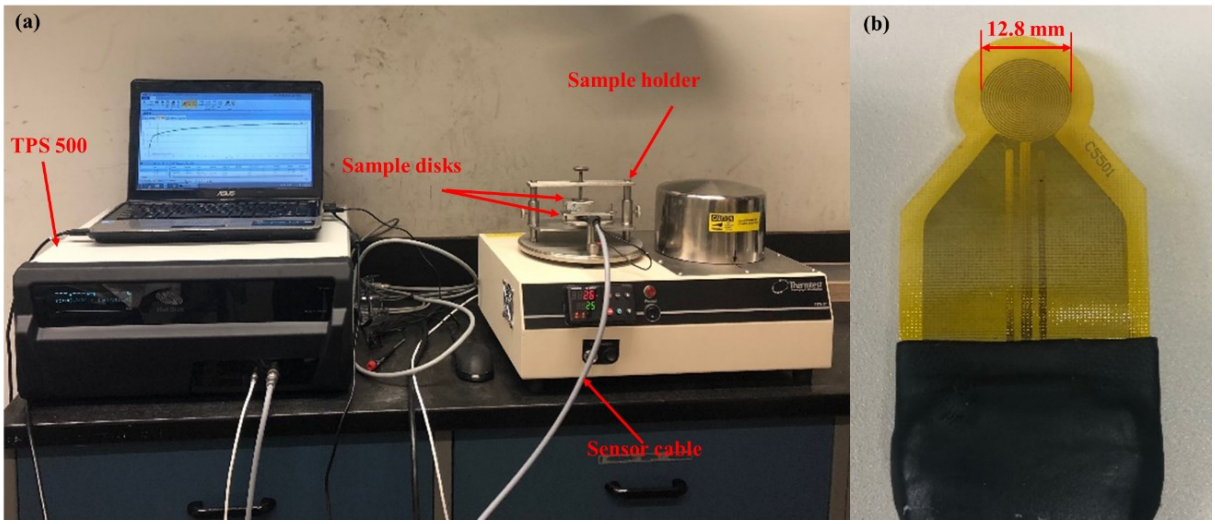

Figure 5.1 Thermal property test device: (a) TPS 500 instrument; (b) Capton sensor 5501

5.3. Results and discussion

5.3.1. Density and void content

Figure 5.2 presents the influence of the aggregate replacement ratio by expanded perlite and curing temperature on the void content and bulk density of CSA cement-based mortars. As shown in Figure 5.2(a), the average void content of CSA cement-based mortars cured at different temperatures increased from 25.9 ± 1.8 vol% to 31.8 ± 1.7 vol%, 40.0 ± 2.6 vol%, and 57.8 ± 2.4 vol%, respectively, when the aggregate replacement ratio increased from 0% to 30%, 60%, and 100%. This data showed that the aggegate replacement ratio had a notable influence on the void content of CSA cement-based mortars, which was mainly attributed to the high void volume in

the expanded perlite. However, cold curing temperatures had a minor influence on the void content of CSA cement-based mortars. This coincided with the results reported in our previous study (Huang et al., 2020a) that cold temperatures had a small influence on the porosity and void content of CSA cement-based mortars.

As shown in Figure 5.2(b), the aggregate replacement ratio significantly affected the oven-dry bulk density of CSA cement-based mortars, while the curing temperature had a negligible influence. The average oven-dry bulk densities of CSA-based mortars cured different temperatures decreased from 1904 ± 26 kg/m^3 to 1536 ± 36 kg/m^3, 1211 ± 22 kg/m^3, and 683 ± 20 kg/m^3, respectively, when aggregate replacement ratio increased from 0% to 30%, 60% and 100%. A similar decrease (with the increase of expanded perlite content) was also reported by Liu et al. (Liu et al., 2014b) and Sengul et al. (Sengul et al., 2011). In many cases, a lower density of cement-based building materials is favorable since it helps reduce the load on the foundation and building structures, ultimately make construction be easier and reduce costs (Lo et al., 2007).

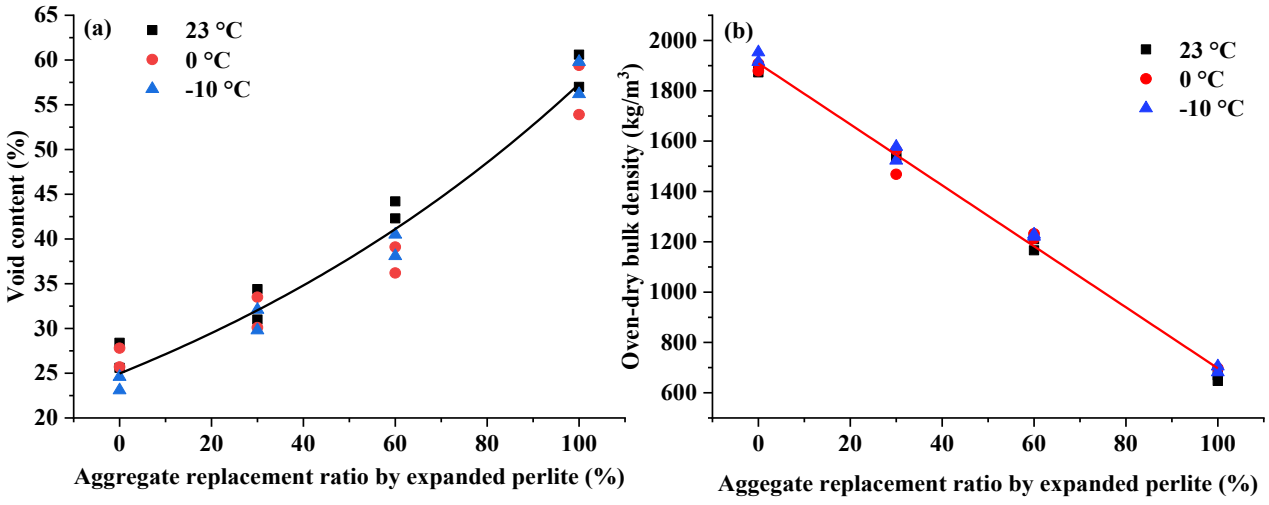

Figure 5.2 The void content and oven-dry bulk density of CSA cement-based mortars at 28 days

5.3.2. Ultrasonic pulse velocity

The UPV values of CSA cement-based mortars are presented in Figure 5.3. CSA cement-based mortars cured at 23 °C had a UPV value of 2400 ± 60 m/s, which decreased to 2140 ± 80 m/s, 1890 ± 90 m/s, and 1470 ± 310 m/s when the aggregate replacement ratio increased from 0% to 30%, 60%, and 100%, respectively. The decrease in UPV values was caused by an increase in the void content, since previous studies (Bogas et al., 2013; Ikpong, 1993) revealed that the velocity of an ultrasonic pulse wave passing through air voids is lower than that passing through solid materials. The same decreasing trend can be noted in the UPV values of CSA cement-based mortars cured at 0 °C and -10 °C. Previous studies (Jiang et al., 2020; Karagol et al., 2015; Xu et al., 2020; Zhang et al., 2009) showed that curing temperature is also an important factor affecting the UPV values of OPC cement-based mixtures since curing temperatures have a large influence on the rate of cement hydration and the pore volume. However, in current study, similar UPV values were observed in the samples cured at different temperatures. This because the hydration of CSA cement was fast even at cold temperatures (e.g. 0 °C and -10 °C) (Huang et al., 2019). Similar amount of hydration products was formed in the samples cured at different temperatures at 28 days, as illustrated by the TGA results shown in Fig. 4. In addition, cold curing temperatures only caused minor differences in void content of CSA cement-based mortars. As a result, the UPV values of samples cured at different temperatures were almost same.

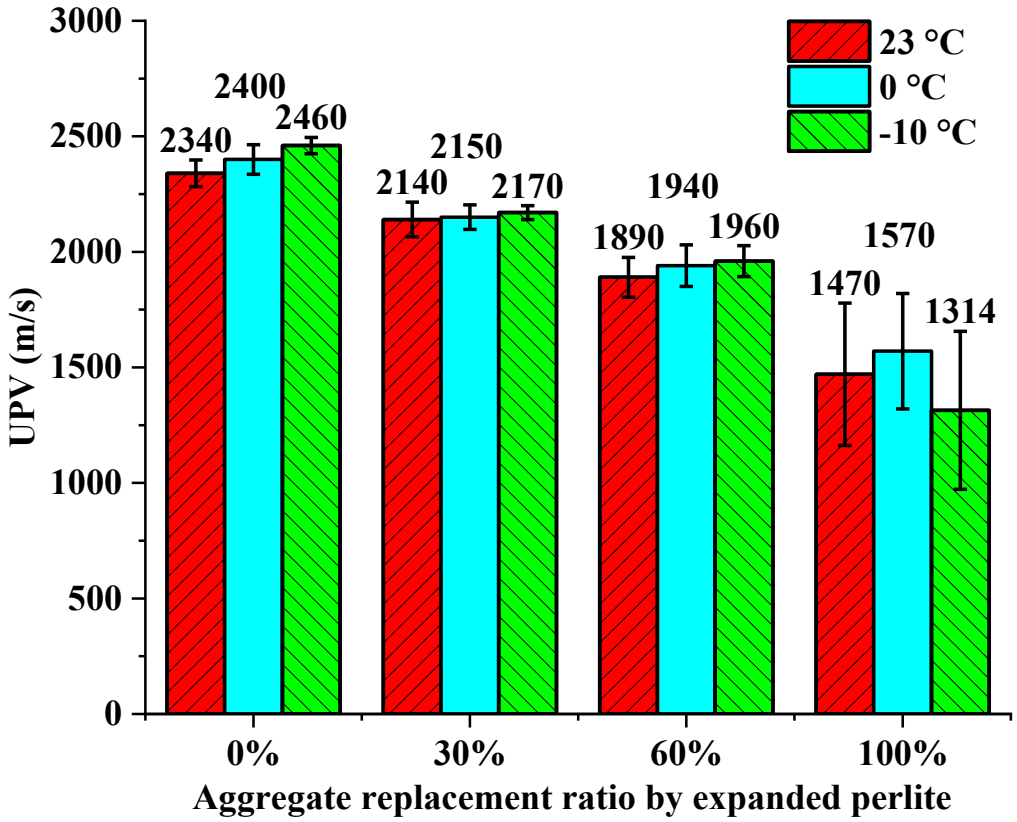

Figure 5.3 UPV values of CSA-based mortars at 28 days

5.3.3. Thermogravimetric analysis

During TGA tests, different hydration products of CSA cement decomposed at different temperatures. As shown in the derivative weight loss curves in Figure 5.4, the main peak at around 110 °C indicates the dehydration of AFt and calcium silicate hydrate (C-S-H). AH_3 decomposed at about 260 °C, while AFm dehydrated at about 150 °C and 220 °C. The signals in the derivative weight loss curves show that the peak for AFt and C-S-H was wider for the 28-day samples when compared with the 1-day samples, regardless of the curing temperatures and aggregate replacement ratios. In addition, the height of the peak for AH_3 was reduced from 1 day to 28 days. These changes indicated that the hydration product AH_3 participated in the later hydration reaction, and more C-S-H was formed from 1 day to 28 days. These findings are

confirmed by Morin et al. (2017), whose study found that AH_3 tends to react with belite generating strätlingite; however, strätlingite is not stable in the presence of belite and will further react with belite, forming silicelous hydrogarnet and C-S-H.

The residual weight curves in Figure 5.4 reflect the influence of curing temperatures, ages, and aggregate replacement ratios on the hydration of CSA cement. With the decomposition of hydration products, the structural water bonded in the hydration products was released and then evaporated; as a result, the residual weight reduced with the heating process. Lower residual weight indicates that more hydration products lost their structural water during the heating process, revealing a higher hydration degree. At 1 day, the residual weight at 600 °C for samples without aggregate replacement was 84.4 ± 0.4%, regardless of the curing temperature. Similar residual weights mean that the hydration of CSA cement was fast even at cold temperatures (e.g., -10 °C), which agreed with our previous study (Huang et al., 2020a). The residual weight at 600 °C for the 1-day samples decreased from 84.4% to 83.0 ± 0.2%, 82.1 ± 0.5%, and 81.4 ± 0.2% when the aggregate replacement ratio increased to 30%, 60%, and 100%, respectively. At 28 days, the residual weight at 600 °C for samples was 83.0 ± 0.6%, 81.0 ± 0.3%, 80.1 ± 0.1%, and 78.7 ± 0.6% at the aggregate replacement ratio of 0%, 30%, 60%, and 100%, respectively. This data reveals that residual weight decreased slightly with aging, which agreed with our previous findings (Huang et al., 2019) that the hydration reaction of CSA cement can continue even at -10 °C. These decreases were mainly attributed to the slow hydration of belite, which contributes to the strength development at later ages (Bescher and Kim, 2019; Kramar et al., 2019; Rungchet et al., 2017). In addition, these decreases were not obvious when compared with the changes in residual weight at early ages (e.g., 1 day). This is because the hydration products of belites have less structural water when compared with those of ye'elimite; consequently, less water was

evaporated during TGA tests. For example, one mole of C-S-H ($C_{1.8}\,SH_4$) only has about four moles of water, while one mole of AFt ($C_6A\bar{S}_3H_{32}$) bonds 32 moles of water (Huang et al., 2019). It is of note that the difference between the residual weights of 1-day and 28-day samples was more noticeable at higher aggregate replacement ratios (e.g., 100%). This difference suggests that the hydration degree increased with the increase of perlite content. This is because the pre-absorbed water in expanded perlite acted as a water source for internal curing and promoted cement hydration (Sengul et al., 2011). A similar conclusion was drawn by Lura et al (2004). They proposed using water-saturated pumice, a porous volcanic rock, to act as a water source for internal curing, which successfully enhanced cement hydration.

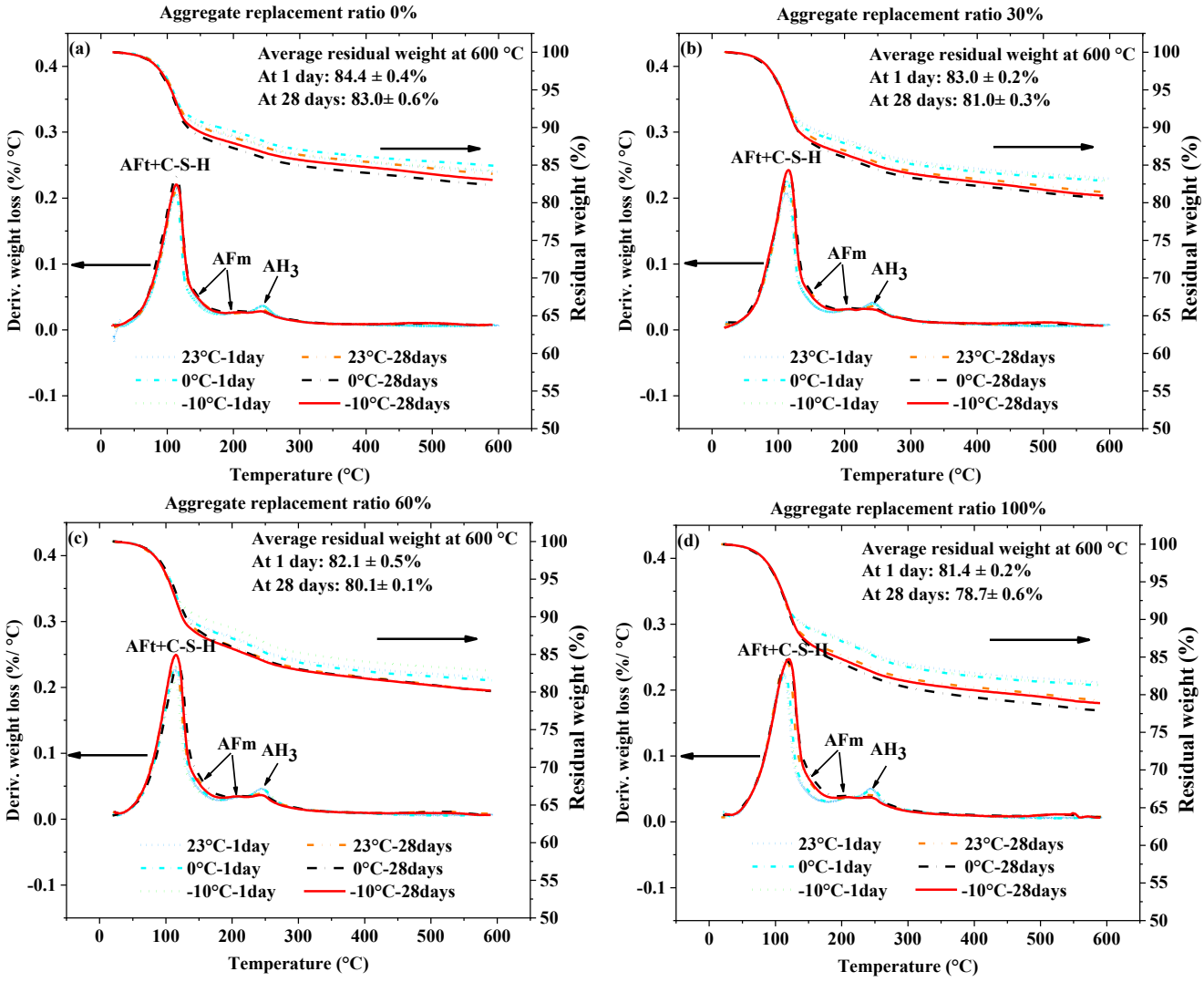

Figure 5.4 TGA results for CSA cement-based samples with different aggregate replacement ratios: (a) 0%; (b) 30%; (c) 60%; and (d) 100%.

5.3.4. Unconfined compressive strength

The UCS of CSA cement-based mortars are plotted, as shown in Figure 5.5. At 1 day, CSA-based samples without aggregate replacement gained UCS of 22.4 MPa, 19.2MPa, and 15.7 MPa when cured at 23 °C, 0 °C, and -10 °C, respectively. This data shows that the CSA cement-based mortars gained strength rapidly regardless of the curing temperatures. This statement can be

verified by comparing the UCS of CSA-based mortars with ordinary Portland cement (OPC)-based mortars. For example, our previous study (Huang et al., 2020a) showed OPC-based mortars cured at -10 °C had developed no strength at 28 days, while CSA-based mortars cured at -10 °C gained UCS of 15.7 MPa at 1 day even if the mixture proportion was the same with the exception of cement types. The fast strength development of CSA cement-based mortars was attributed to the rapid hydration reaction, as depicted in the TGA results in Figure 5.4. The comparison between CSA cement-based and OPC-based mortars highlights a significant advantage of CSA cement: it can achieve fast strength development at cold temperatures (even at -10 °C).

When incorporated with expanded perlite, the UCS of CSA cement-based mortars was significantly affected by the aggregate replacement ratio. For example, the 1-day UCS of CSA cement-based samples cured at 23 °C showed an exponential drop from 22.4 MPa to 4.8 MPa when the aggregate replacement ratio increased from 0% to 100%. This trend is also shown in the UCS of CSA-based mortars at different ages and curing temperatures. As depicted in Figure 5.2, incorporating expanded perlite remarkably increased the void content in CSA cement-based mortars. As a result, the UCS dropped with the increase of aggregate replacement ratio since the increased void content had a negative influence on the UCS (Mehta and Monteiro, 2006). Although the hydration reaction was enhanced at a higher aggregate replacement ratio, the UCS decreased. This trend runs counter to the study of Lura et al. (2004), where they found incorporating 4% or 8% of water-saturated porous pumice enhanced cement hydration and strength behavior. The opposite trend shown in the current study is because expanded perlite was added at very high volumes (i.e., 30%, 60%, and 100%), and the reduction in the UCS caused by

the porous structure of expanded perlite was more significant than the improvement resulting from enhanced hydration.

In addition to aggregate replacement ratio, curing temperature and age also affected the UCS of CSA cement-based mortars, as shown in Figure 5.5. From 1 day to 28 days, the UCS increased about 7.5-10.3 MPa, 2.2-5.3 MPa,1.8-2 MPa, and 0-0.9 MPa for the CSA cement-based mortars with 0%, 30%, 60%, and 100% of aggregate replacement ratio, respectively. The increase in the UCS was attributed to the improved degree of hydration, as discussed before. The UCS of CSA cement-based mortars decreased with a decrease in curing temperature. For example, the UCS of CSA based mortars without expanded perlite cured at -10 °C was 6.3 MPa and 8.0 MPa lower than that cured at 0 °C and 23 °C, respectively. However, the difference caused by curing temperature and age in the UCS was less obvious at higher volumes of expanded perlite incorporation (e.g., 60% and 100%). This shows that the UCS of CSA-based mortars was mainly affected by the aggregate replacement ratio at a higher volume of expanded perlite.

Note that all the CSA cement-based mortars reached the minimum UCS (~4.1 MPa) for non-load-bearing concrete units required by ASTM C129-17 (ASTM International, 2017). The CSA cement-based mortars with an aggregate replacement ratio of no more than 30% reached the minimum UCS (~13.1 MPa) for loadbearing concrete units required by ASTM C90-16a (ASTM International, 2016a) after being cured for 3 days, except for those with a 30% aggregate replacement ratio cured at -10 °C. Our previous study (Huang et al., 2020a) found that the CSA cement-based mortar exposed to -10 °C had a finer pore structure. After being re-cured at a warmer temperature (e.g., 23 °C), this mortar achieved higher strength than that directly cured at 23 °C. Therefore, it can be expected that the UCS of CSA cement-based mortar with 30%

aggregate cured at -10 °C will further increase to reach the minimum UCS requirement once the temperature rises.

The 28-day UCS of CSA cement-based mortars was correlated with oven-dry density and UPV values, as shown in Figure 5.6. The UCS of CSA-based mortars increased exponentially with the increase of oven-dry density and UPV values. This correlation was obtained since both oven-dry density and UPV values were closely related to the voids introduced by expanded perlite, and UCS exponentially decreased with the incorporation of expanded perlite, as shown in Figure 5.5. Previous studies also reported similar relationships such as a UCS-density correlation (Asadi et al., 2018; Liu et al., 2014b; Sengul et al., 2011) and a UCS-UPV correlation (Bogas et al., 2013; Wu et al., 2016) for OPC-based mixtures.

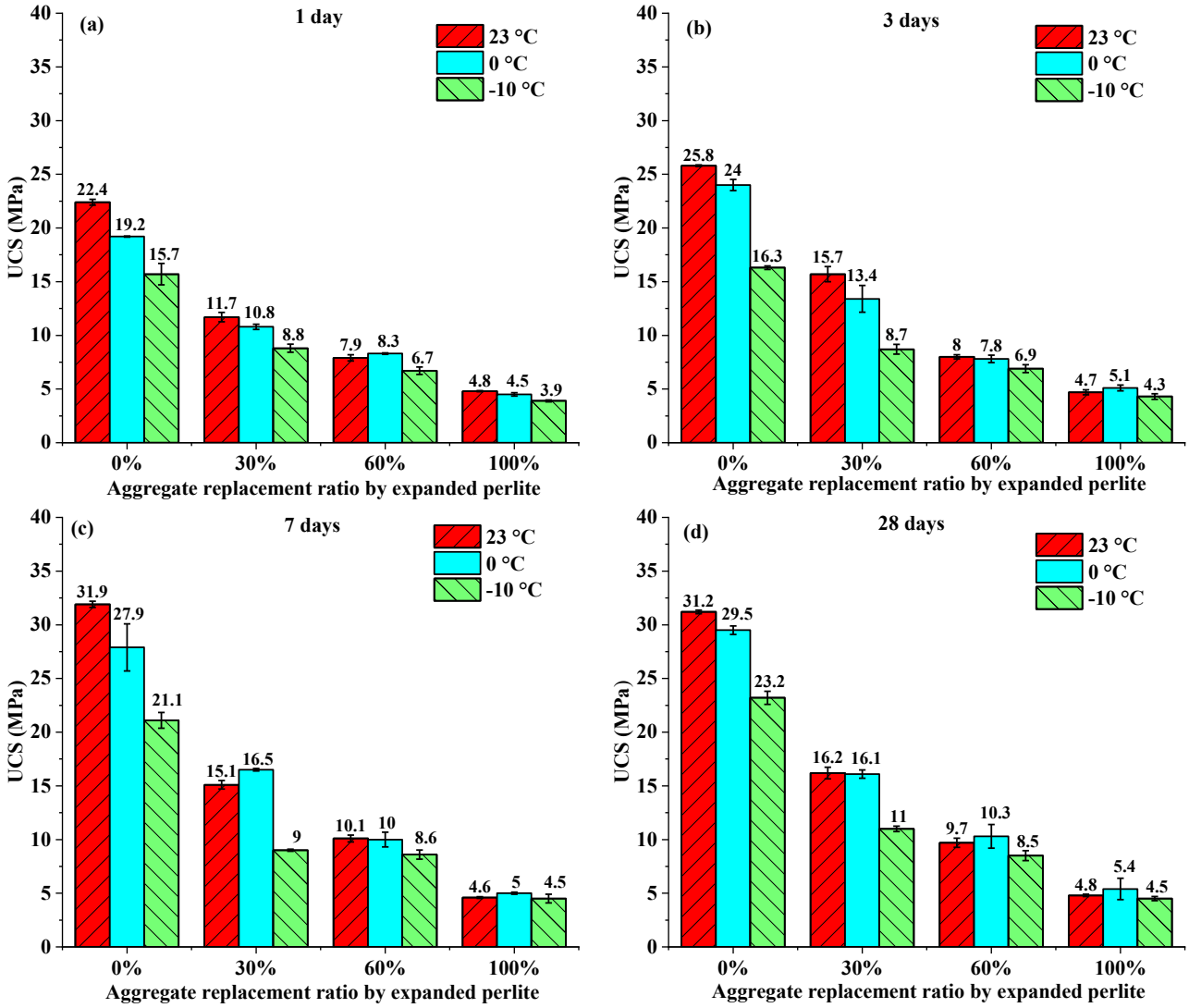

Figure 5.5 The UCS of CSA cement-based mortars at: (a) 1 day; (b) 3 days; (c) 7 days; and (d) 28 days.

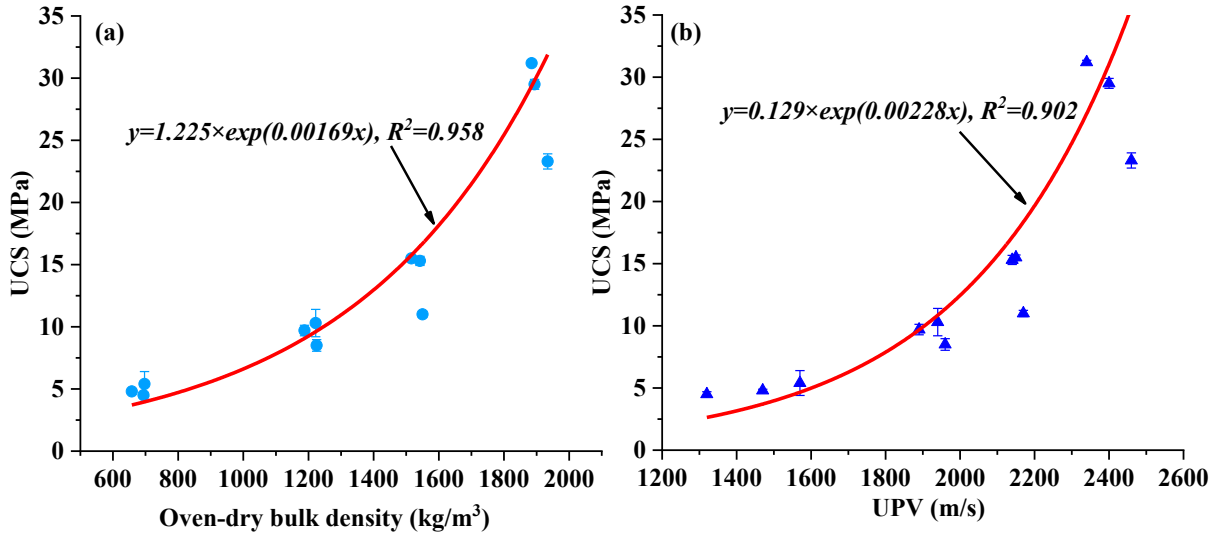

Figure 5.6 Correlation between (a) oven-dry bulk density and UCS; and (b) UPV and UCS

5.3.5. Thermal properties

5.3.5.1. Thermal conductivity

Thermal conductivity is a physical property describing the ability of a material to conduct heat from one side of a solid to the other (Holman, 2001). Figure 5.7 presents the influence of curing temperatures, ages, and aggregate replacement ratio on the thermal conductivity of CSA cement-based mortars. It shows that curing temperatures and ages had a negligible influence on the thermal conductivity of CSA cement-based mortars. For example, the CSA cement-based samples without aggregate replacement had an average thermal conductivity of 1.02 ± 0.06 W/mK even if they were cured at different temperatures for various ages. According to the literature, the thermal conductivity of OPC-based mixtures showed a decreasing trend when the curing temperature was increased to a high temperature (e.g., 60 °C) (Célestin and Fall, 2009; Kim et al., 2003). However, the effects of cold temperatures on thermal conductivity have rarely been reported. One study from Célestin and Fall (2009) reported that a negligible difference was found in the thermal conductivity of OPC-based mixtures cured at 2 °C and 20 °C, which

coincides with our findings. As for the influence of curing ages, Kim et al. (2003) reported that curing age had a negligible effect on the thermal conductivity of OPC-based concrete except for the period in the first 2 days. In the current study, CSA-based mortars reached a stable thermal conductivity after 1 day, even at a cold temperature, which was faster than OPC-based mixtures. This is because the hydration reaction of CSA cement was fast, regardless of the curing temperature.

As shown in Figure 5.7, the aggregate replacement ratio significantly affected the thermal conductivity of CSA cement-based mortars. When cured at 23 °C, the 28-day thermal conductivity of CSA cement-based mortars decreased exponentially from 0.97 ± 0.01 W/mK to 0.57 ± 0.02 W/mK, 0.29 ± 0.02 W/mK, and 0.13 ± 0.002 W/mK when the aggregate replacement ratio increased from 0% to 30%, 60%, and 100%. A similar trend was found for CSA-based mortars cured at different temperatures for different ages. This exponential reduction in thermal conductivity is attributed to the low thermal conductivity of porous expanded perlite. Topçu and Işıkdağ (2008) reported that expanded perlite had a thermal conductivity of ~0.04 W/mK, while normal aggregates have a thermal conductivity in the range of ~1.16 to 8.6 W/mK (Khan, 2002). The huge difference between the thermal conductivity of expanded perlite and normal aggregates resulted in the exponential decrease in the thermal conductivity of CSA-based mortars with the increase of aggregate replacement ratio. In practice, lower thermal conductivity is favorable for cement-based building materials since it alleviates the intensity of thermal conduction and reduces heat loss to the outdoor environment, ultimately mitigating energy consumption and CO_2 emissions related to space heating and cooling in buildings (Asadi et al., 2018; Latha et al., 2015).

It is worth mentioning that the thermal conductivity of CSA-based mortars without aggregate replacement was lower than OPC-based mortars, as presented in the literature. Liu et al. (2011)

employed the TPS method to determine the thermal conductivity of OPC-based mortars, which used the same cement content and cement-to-aggregate ratio with our current study. At oven-dry conditions, the 28-day thermal conductivity of their OPC-based mortar was 1.83 W/mK, which is 0.86 W/mK higher than that of CSA cement-based mortars (0.97 ± 0.01W/mK). This is because low workability at a fresh state (Huang et al., 2020b) and volume expansion (Glasser and Zhang, 2001; Juenger et al., 2011; Yu et al., 2018) during ettringite formation caused a low oven-dry bulk density (1885 kg/m^3) and a high void content (27.0%) in CSA cement-based mortars, whereas the data for OPC-based mortars was 2055 kg/m^3 and 17.9% (Huang et al., 2020a) since shrinkage usually occurs during the hydration of OPC cement (Bissonnette et al., 1999; Toledo et al., 2005). The higher air void content and lower density are attributed to the lower thermal conductivity of CSA-based mortars because the thermal conductivity of air is as low as 0.026 W/mK (Liu et al., 2014b), and the thermal conductivity of cement-based mixtures usually decreases with the decrease of density (Asadi et al., 2018; Liu et al., 2011; Sengul et al., 2011). In addition, the OPC-based mortar with an aggregate replacement ratio of 50% by expanded perlite had a thermal conductivity of 1.183 W/mK (Liu et al., 2011), still being about 22% higher than that of CSA-based mortar without expanded perlite.

As shown in Figure 5.8, thermal conductivity was correlated with oven-dry bulk density and UPV values, respectively. An exponential correlation with a correlation coefficient of 0.994 was presented between the thermal conductivity and oven-dry bulk density. Asadi et al. (2018) analyzed 185 experimental data for OPC-based mixtures from the literature and proposed Equation (5-5) to predict the thermal conductivity. As shown in Figure 5.8 (a), the obtained equation for CSA cement-based mortars is very similar to Equation (5-5) for OPC-based mixtures; however, the pre-exponential factor (0.0455) is lower than that (0.0625) in Equation

(5-5). Figure 5.8 (b) shows that thermal conductivity increased exponentially with the increase in UPV values. An exponential correlation between thermal conductivity and UPV value was also reported in previous studies (Karakoç and Demirboga, 2010; Liu et al., 2014b). The good thermal conductivity-density correlation and thermal conductivity-UPV correlation indicate that it is feasible to estimate the thermal conductivity of CSA cement-based mortars by densities or UPV values. It is worth mentioning that it is a non-destructive method using the UPV value to estimate the thermal conductivity.

$$\lambda = 0.0625e^{0.0015\rho} \ (R^2 = 0.87) \qquad (5\text{-}5)$$

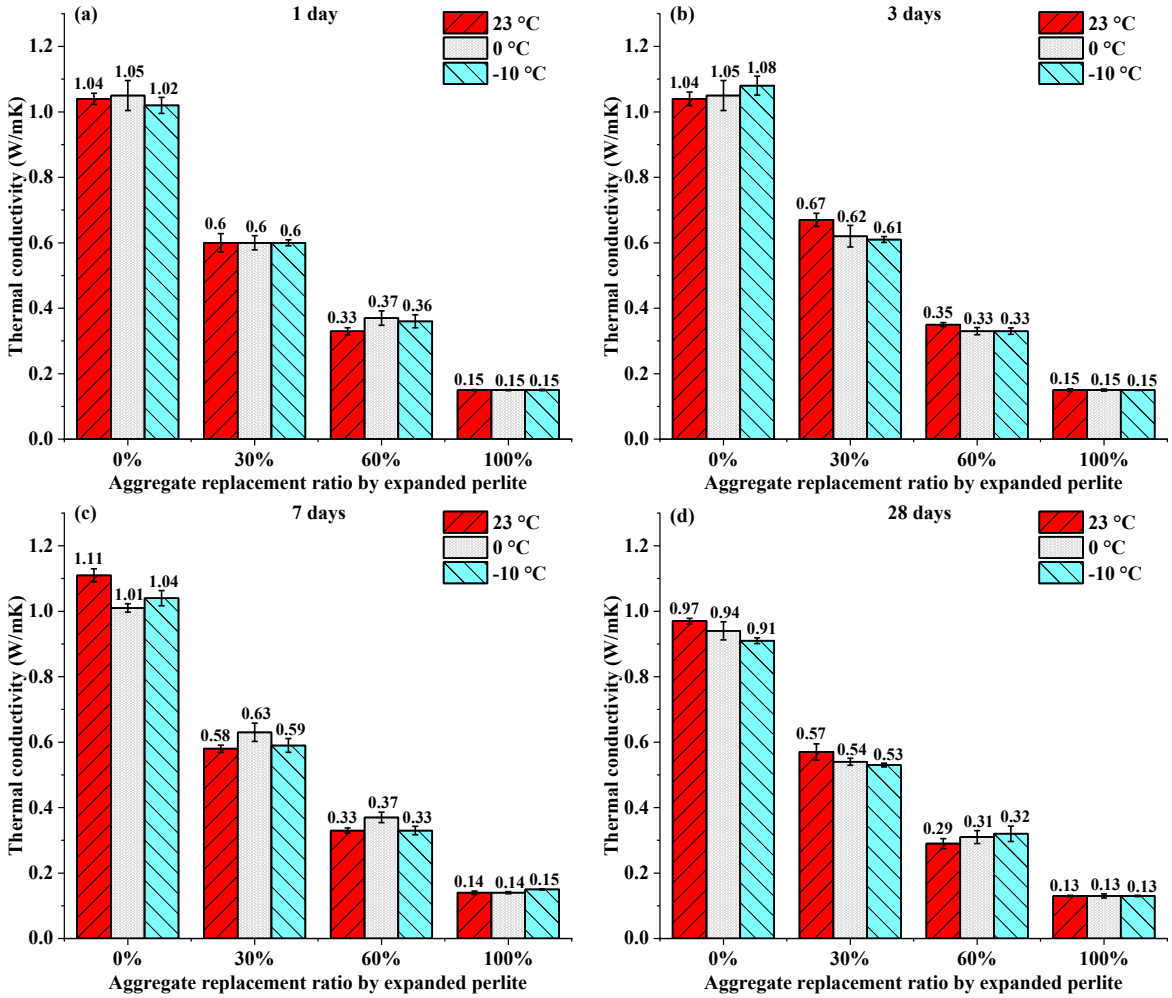

Figure 5.7 Thermal conductivity of CSA-based mortars at various ages: (a) 1 day; (b) 3 days; (c) 7 days; and (d) 28 days

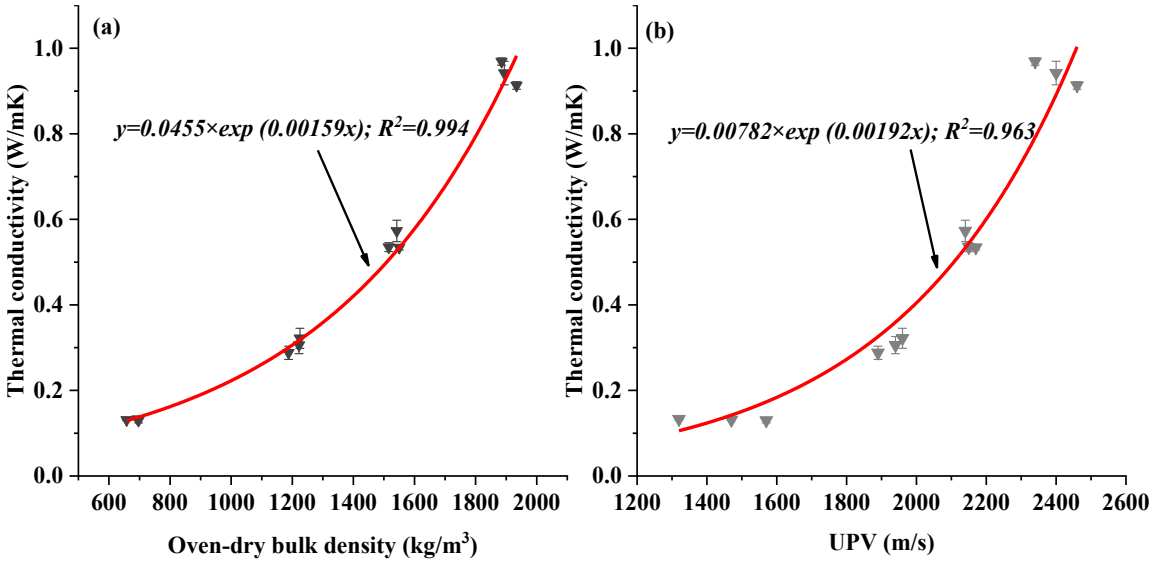

Figure 5.8 Correlation between (a) oven-dry bulk density and thermal conductivity; and (b) UPV and thermal conductivity

5.3.5.2. Thermal diffusivity

Thermal diffusivity is a physical property describing how fast a uniform temperature can be reached within a material, which is expressed by the thermal conductivity divided by density and specific heat capacity (Holman, 2001). Figure 5.9 shows the influence of curing temperatures, ages, and aggregate replacement ratio on the thermal diffusivity of CSA-based mortars. The curing temperature and ages caused little variation on the thermal diffusivity. However, the aggregate replacement ratio caused an exponential decrease in the thermal diffusivity of CSA cement-based mortars. For example, the 28-day thermal diffusivity of CSA-based mortars cured at 23 °C dropped from 0.70 mm^2/s to 0.55 ± 0.05 mm^2/s, 0.34 ± 0.07 mm^2/s, and 0.24 ± 0.01 mm^2/s as the aggregate replacement ratio increased from 0% to 30%, 60%, and 100%, respectively. A decreasing trend was also reported when OPC-based mixtures were incorporated with lightweight aggregates (Liu et al., 2011; Mydin, 2016; Oktay et al., 2015). Oktay et al. (2015) and Hassn et al. (2016) found thermal diffusivity decreased with the increase of pore and

void volume. In the current study, void content in the CSA cement-based mortars increased with the increase of aggregate replacement ratio; accordingly, the thermal diffusivity reduced with the increase of aggregate replacement ratio. According to the above-mentioned expression of thermal diffusivity, a lower thermal diffusivity means that the temperature difference between the indoor and outdoor surfaces of cement-based mixtures will take a longer time to reach a uniform value, indicating improved thermal insulation abilities.

It is of note that the 28-day thermal diffusivity of CSA cement-based mortars without perlite was ~0.3 mm^2/s lower than that of OPC-based mortars (1.0 mm^2/s) reported in the study of Liu et al. (2011), where they used same cement content and cement-to-aggregate ratio with our current study. The lower thermal diffusivity in CSA-based mortars can be explained by that CSA-based mortars had higher void contents than OPC-based mortars at the same mixture proportion, curing temperature, and age (Huang et al., 2020a).

As shown in Figure 5.10, the thermal diffusivity of CSA cement-based mortars exponentially decreased with the decrease of oven-dry bulk density or UPV value. A similar thermal diffusivity-density correlation (Liu et al., 2014b; Oktay et al., 2015) and thermal diffusivity-UPV correlation (Liu et al., 2014b) for OPC-based mixtures were also presented in previous studies.

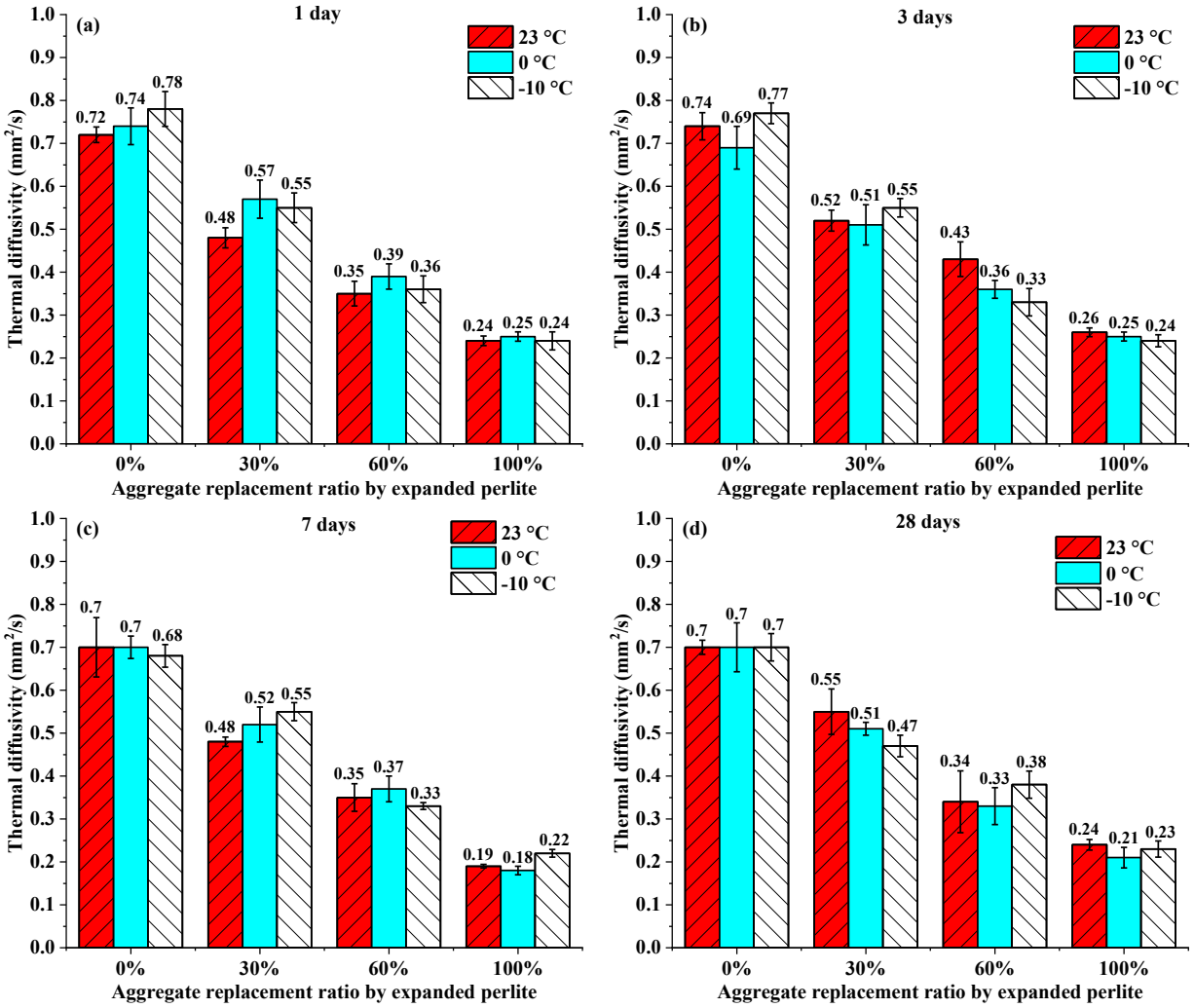

Figure 5.9 Thermal diffusivity of CSA-based mortars at various ages: (a) 1 day; (b) 3 days; (c) 7 days; and (d) 28 days

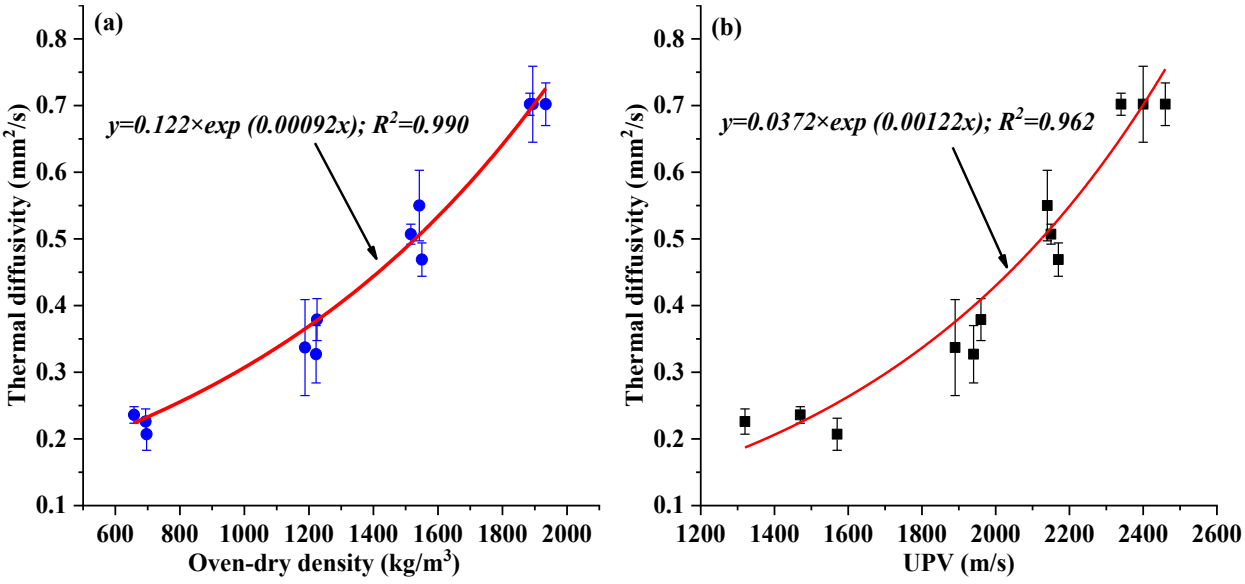

Figure 5.10 Correlation between (a) oven-dry bulk density and thermal diffusivity; and (b) UPV and thermal diffusivity

5.3.5.3. Volumetric heat capacity

Volumetric heat capacity is the heat required to generate a unit change in the temperature of a unit volume of a material. Figure 5.11 depicts the influence of curing temperatures, ages, and aggregate replacement ratio on the volumetric heat capacity of CSA cement-based mortars. It does not show a clear trend about how the curing temperatures and ages affect the volumetric heat capacity. This is because the CSA cement-based mortars were heterogeneous materials, of which volumetric heat capacity showed a large standard deviation (in the range between 2.4% to 11.8% with an average of 5.6%); the deviation in the volumetric heat capacity was larger than the difference caused by curing temperatures and ages.

The influence of aggregate on the volumetric heat capacity was more noticeable than that caused by curing temperatures and ages. As shown in Figure 5.11, a linear decrease in the volumetric heat capacity was observed with the increase of aggregate replacement ratio. At 23 °C, the 28-

day volumetric heat capacity of CSA cement-based mortars showed a reduction from 1.38 ± 0.04 MJ/m^3K to 1.04 ± 0.09 MJ/m^3K, 0.98 ± 0.05 MJ/m^3K, and 0.56 ± 0.02 MJ/m^3K with the aggregate replacement ratio increase from 0% to 30%, 60%, and 100%, respectively. A similar decrease was also observed in the volumetric heat capacity of the CSA cement-based mortars cured at other temperatures for different ages. It is worth mentioning that the volumetric heat capacity of CSA cement-based mortar without expanded perlite was about 0.46 MJ/m^3K lower than that (1.84 MJ/m^3K) of the OPC-based mortar reported in the study of Liu et al. (2011).

Figure 5.12 shows that the volumetric heat capacity of CSA-based mortars can be expressed as a function of oven-dry bulk density or UPV value. The volumetric heat capacity of CSA cement-based mortars increased linearly with the increase in oven-dry bulk density or UPV value. However, the correlation between volumetric heat capacity with density or UPV value has rarely been reported in the literature. The data reported by Oktay et al.(2015) showed a similar linear increase in volumetric heat capacity with the increase of bulk density after a conversion from specific heat capacity to volumetric heat capacity.

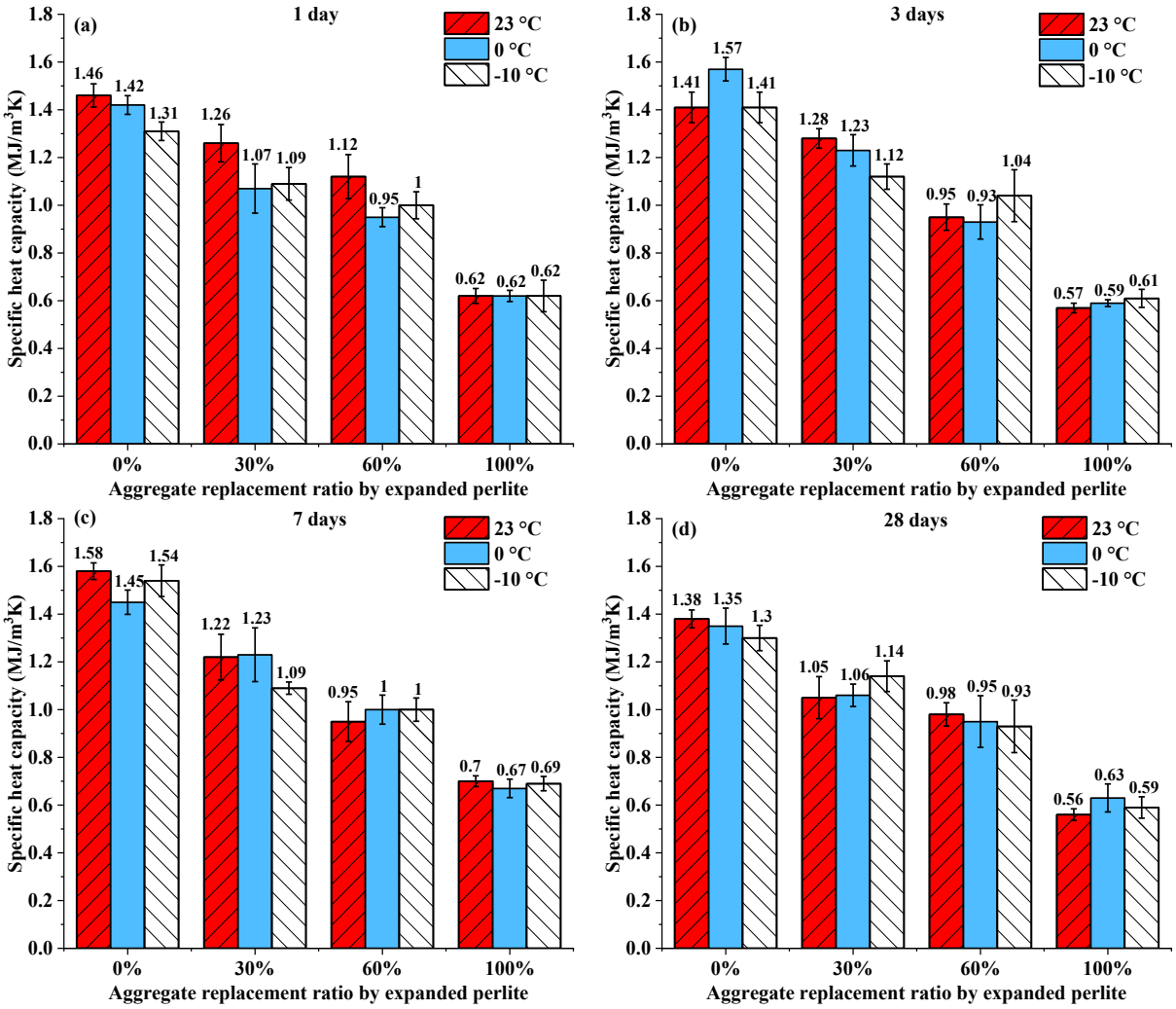

Figure 5.11 Specific heat capacity of CSA-based mortars at various ages: (a) 1 day; (b) 3 days; (c) 7 days; and (d) 28 days

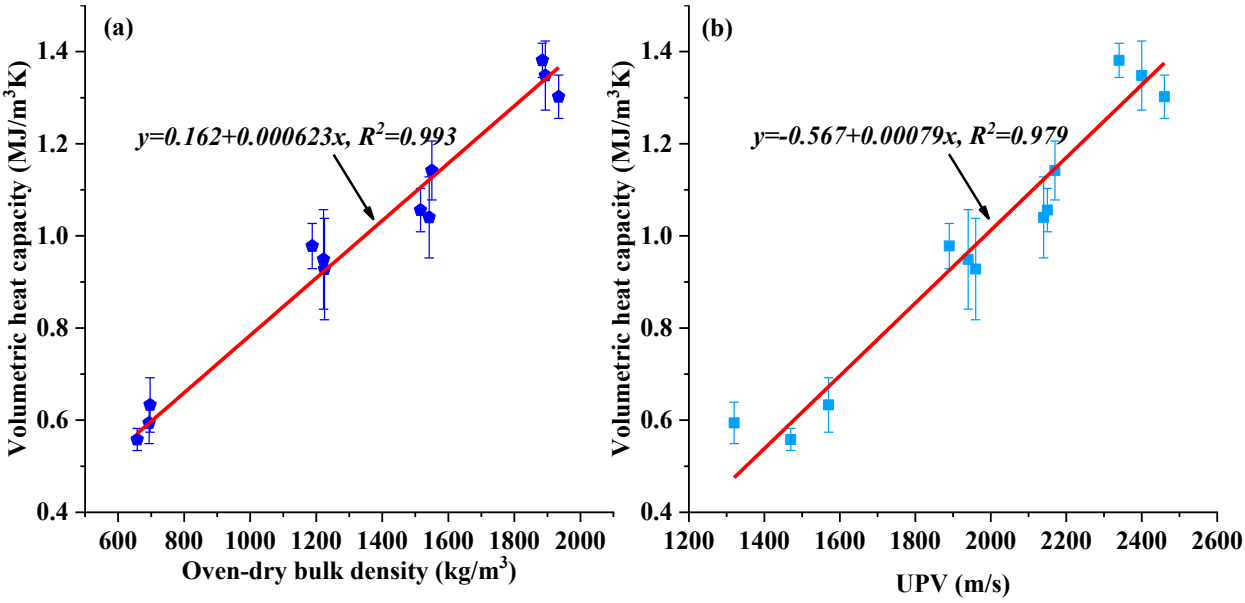

Figure 5.12 Correlation between: (a) oven-dry bulk density and volumetric heat capacity; and (b) UPV and volumetric heat capacity

5.4. Conclusion

This study developed an energy-efficient and environmentally-friendly building material by replacing normal aggregate with expanded perlite in calcium sulfoaluminate (CSA) cement-based mortars. Experiments were conducted to measure the thermal properties (thermal conductivity, thermal diffusivity, and heat capacity) and unconfined compressive strength (UCS) of CSA cement-based mortars with different aggregate replacement ratios. These thermal properties and UCS were then correlated with their oven-dry bulk density and ultrasonic pulse velocity (UPV). The main conclusions were enumerated as follows:

(1) CSA cement-based mortar gained strength rapidly, even at 0 °C and -10 °C. For example, CSA-based mortar without expanded perlite had a UCS of 15.7 MPa when cured at -10 °C. The UCS decreased exponentially with the increase of aggregate replacement ratio.

(2) The aggregate replacement ratio significantly affected the thermal properties of CSA-based mortars, while curing temperatures and ages had a negligible influence on the thermal properties.

(3) The 28-day thermal conductivity of CSA cement-based mortars cured at 23 °C decreased exponentially from 0.97 ± 0.01 W/mK, to 0.57 ± 0.02 W/mK, to 0.29 ± 0.02 W/mK, and to 0.13 ± 0.002 W/mK when the aggregate replacement ratio increased from 0% to 30%, 60%, and 100%. Similar exponential decrease (from 0.70 mm^2/s to 0.55 ± 0.05 mm^2/s, to 0.34 ± 0.07 mm^2/s, and to 0.24 ± 0.01 mm^2/s) was found in the thermal diffusivity of CSA cement-based mortars, while the volumetric heat capacity dropped linearly (from 1.38 ± 0.04 MJ/m^3K to 1.04 ± 0.09 MJ/m^3K, to 0.98 ± 0.05 MJ/m^3K, and to 0.56 ± 0.02 MJ/m^3K).

(4) Thermal properties and UCS showed a good correlation with oven-dry bulk density (or UPV value). Thermal conductivity, thermal diffusivity, and UCS decreased exponentially with the decrease of oven-dry bulk density (or UPV value), whereas volumetric heat capacity showed a linear decrease.

(5) The thermal conductivity of CSA cement-based mortars without expanded perlite was 47% lower than that of ordinary Portland cement-based mortar (1.83 W/mK) with a similar mixture design.

In summary, incorporating expanded perlite can effectively reduce the thermal conductivity of CSA-based mortars. These CSA cement-based mortars incorporated with expanded perlite have great potential for use as energy-efficient and environment-friendly building materials, especially in cold regions such as Canada's North.

Chapter 6. Numerical modeling of temperature profiles in hardening calcium sulfoaluminate cement-based mortars for permafrost region applications

This chapter has been submitted for peer review as **G. Huang**, Y. Guo, E. Bescher, R. Gupta, W.V. Liu, Numerical modeling of temperature profiles in hardening calcium sulfoaluminate cement-based mortars for permafrost region applications. *Construction and building materials.*

Nomenclature

CSA	Calcium sulfoaluminate
D	Diameter of cement mortar (mm)
L	Length of cement mortar (mm)
OPC	Ordinary Portland cement
RMSE	Root mean square error
UCS	Unconfined compressive strength (MPa)
A_V	Reference heat generation rate (W/g)
$\alpha(t)$	Hydration degree
α_{max}	The maximum hydration degree
$C_{p,f}$	Heat capacity at frozen state (J/kg/K)
$C_{p,u}$	Heat capacity at unfrozen state (J/kg/K)
C_p	Heat capacity (J/kg/K)
E_A	Activation energy (J/mol)
h_{eff}	Heat transfer coefficient (W/m^2/K).
$H(t)$	Cumulative hydration heat (J/g)
Hu	Total heat that can be released when all cement is reacted (J/g)

k	Thermal conductivity (W/m/K)
k_f	Thermal conductivity at frozen state (W/m/K)
k_u	Thermal conductivity at unfrozen state(W/m/K)
$L_{f\to u}$	Latent heat (kJ/kg)
q	Heat generation rate (W/g)
q_h	Heat flux between cement mortar and surrounding air (W)
R	Universal gas constant, 8.314 J / mol·K
t	Time (hour)
T	Temperature (K)
T_a	Air temperature (K)
T_{Curing}	Curing temperature (°C)
T_m	Temperature of the surface of cement mortar (K)
T_r	Reference temperature (K)
t_e	Equivalent age (hour)
θ_u	Fraction of frozen phase
θ_f	Fraction of unfrozen phase
β	Hydration shape factor

ρ	Density (kg/m^3)
τ	Hydration time parameter (h)
δ	Thickness of the sand layer (mm)

6.1. Introduction

Canada has about 50% of land mass covered with permafrost (Gruber, 2012). With the increasing of construction and mining activities in these permafrost regions, cement-based mixtures are expected to be increasingly used. When cement-based mixtures are applied in permafrost regions or frozen ground, unique challenges have arisen for construction. For example, when Portland cement-based mixtures are cast at cold temperatures (≤ 5 °C), their strength development is very slow. Huang et al. (2019) reported that Ordinary Portland cement (OPC)-based mortars had no strength gain after being cured at -5 °C for 28 days. To accelerate strength development, previous studies (Huang et al., 2019, 2020a) proposed to use calcium sulfoaluminate (CSA) cement to substitute for OPC when constructing in cold regions (e.g., Canada's North). The results showed that CSA cement-based mortar gained a unconfined compressive strength (UCS) of 15.5 MPa at 24 hours when cured at -10 °C (Huang et al., 2020a).

When cement-based mixtures are applied in permafrost regions, the temperature profile in hardening cement-based mixtures is of great significance, because the temperature profile has a close correlation with strength development and thermal cracks. It has been well-documented that the rate of strength development slows down at cold temperatures since cement hydration reaction rate decreases with the drop in temperature (ACI, 2010; Choi et al., 2017; Huang et al., 2019, 2020a; Liu et al., 2017). For example, Liu et al. reported (2017) that the 3-day compressive strength of an OPC-based mixture decreased from 22 MPa to 0 MPa when the curing temperature decreased from 20 °C to 0 °C. In massive cement-based structures, a high temperature might be observed in the center since cement hydration is an exothermic reaction, while the temperature at the surfaces usually is low due to the heat loss to cold surroundings. A large temperature difference between the center and surfaces can cause thermal cracks in

concrete structures (Harrison, 1981; Huang, 1999; Klemczak and Knoppik-Wróbel, 2011). In Klemczak and Knoppik-wróbel's study (2011), a temperature gradient of ~24 °C was observed between the center and top surface of an OPC-based massive concrete with a dimension of 10m×10m×3m cured at 20 °C, and this temperature difference caused thermal cracks on the top surface and in the edge area.

Due to the large influence of temperature on the strength development and thermal cracks, it is of great interest to predict the temperature profiles in hardening cement-based structures. From the literature, many methods have been developed to predict the temperature in hardening Portland cement-based structures, including but not limited to empirical graphical method (ACI, 2007), Schmidt method (ACI, 2007; Bobko et al., 2015; Riding et al., 2006), and numerical models (Azenha and Faria, 2008; Ballim, 2004; Ge, 2005; Ilc et al., 2009; Kim, 2010; Martinelli et al., 2013; Saeed et al., 2016; Tahersima and Tikalsky, 2017; Wang, 2013). Among these methods, numerical models are considered to be accurate and flexible (Bobko et al., 2015; Tahersima and Tikalsky, 2017). Generally, numerical models follow similar procedures: (1) to determine the heat generation rate of cement hydration with a calorimeter (e.g., adiabatic calorimeter (Ballim, 2004; Ilc et al., 2009; Martinelli et al., 2013), semi-adiabatic calorimeter (Xu et al., 2011), or isothermal calorimeter (Kim, 2010)); (2) to model the heat transfer in the cement-based structures and their surroundings with numerical methods (e.g., finite element method (Azenha and Faria, 2008; Ge, 2005; Kim, 2010; Tahersima and Tikalsky, 2017) or finite difference method (Ballim, 2004; Martinelli et al., 2013; Sun et al., 2018)). In addition, some commercial software was developed to provide a quick way for predicting the temperature profiles in hardening Portland cement-based structures. For example, the Federal Highway Administration of the United States developed a software suite for Portland cement-based concrete pavement

(Administration and McCullough, 1999; J.M. Ruiz and Rasmussen; Schindler et al., 2004). This software can estimate the heat generation rate according to cement types (six types of Portland cement), cement content, additives, and weather conditions without the need to determine heat generation rate by calorimetry. Then the heat transfer within the hardening cement-based structures is solved with one-dimensional or two-dimensional finite difference method. Although many methods (ACI, 2007; Azenha and Faria, 2008; Ballim, 2004; Bobko et al., 2015; Ge, 2005; Ilc et al., 2009; Kim, 2010; Martinelli et al., 2013; Riding et al., 2006; Saeed et al., 2016; Tahersima and Tikalsky, 2017; Wang, 2013) have been proposed, all of them were developed for Portland cement-based mixtures. It is skeptical if these methods developed for Portland cement-based mixtures can be directly applied to predict temperature profiles in CSA cement-based mixtures since CSA cement is very different from Portland cement. The hydration parameters of CSA cement are not default parameters in previous models. Therefore, there is a research gap to develop a model to predict the temperature profile in hardening CSA cement-based mixtures.

In addition, it is also skeptical if previous methods (ACI, 2007; Azenha and Faria, 2008; Ballim, 2004; Bobko et al., 2015; Ge, 2005; Ilc et al., 2009; Kim, 2010; Martinelli et al., 2013; Riding et al., 2006; Saeed et al., 2016; Tahersima and Tikalsky, 2017; Wang, 2013) can be directly applied to permafrost region applications. When cement-based mixtures are placed and sprayed on frozen ground or permafrost, the heat transfer between hardening cement-based mixtures and surroundings may induce the freezing cement-based mixtures and thawing of the permafrost, these processes accompany with the release or absorption of latent heat that may affect the temperature profiles in cement-based mixtures. Currently, only a few modeling studies (Beya et al., 2019; Liu et al., 2015; Wang et al., 2018) were conducted for permafrost region applications, and these models need further improvement. For example, Beya et al. (2019) developed a

numerical model to predict the temperature profile in Type HE Portland cement-based backfill placed in permafrost regions. In their study, cement hydration heat was omitted, which is inaccurate since cement hydration heat significantly affects the temperature profiles in hardening cement-based mixtures, especially for massive cement-based structures (ACI, 2007; Ballim, 2004). Liu et al. (2015) and Wang et al. (2018) investigated the influence of the hydration heat of Portland cement-based concrete foundation on the thermal profiles of permafrost. However, their studies mainly focused on the temperature profiles in permafrost instead of that in hardening concrete; and the temperature change in the hardening concrete on the heat generation rate of cement was not taken into consideration, which can cause inaccuracy because the temperature profile in the hardening concrete is an important factor affecting cement hydration reaction rate and heat generation rate (ACI, 2010; Choi et al., 2017; Huang et al., 2019, 2020a; Liu et al., 2017). Therefore, these models for permafrost region applications should be improved.

From the above literature review, it can be concluded that no model was developed for predicting the temperature profiles in hardening CSA cement-based mixtures, especially for permafrost region applications. There is a significant research gap to develop a numerical model for understanding the temperature profiles in CSA-based mixtures used in permafrost regions.

To fill this gap, the main objective of this study was to develop a numerical model to understand the temperature profiles in CSA-based mixtures for permafrost region applications. Investigations were performed to understand the influence of curing temperatures, different curing modes (i.e., curing in air and curing in permafrost), and sample sizes on the temperature profiles in hardening CSA-based mixtures. In addition, the temperature profiles in CSA-based mixtures were also compared with those in an OPC-based mixture.

6.2. Methodology

6.2.1. Overview of methodology

Figure 6.1 shows the overview of the methodology for modeling the temperature profiles in CSA cement-based mixtures. To model the temperature profiles, one of the most important steps is to determine the heat generation rate during cement hydration. From the literature (Ballim, 2004; Ilc et al., 2009; Martinelli et al., 2013; Saeed et al., 2016; Tahersima and Tikalsky, 2017; Xu et al., 2010; Xu et al., 2011), there were three commonly used methods for determining the heat generation rate, including adiabatic calorimetry, semi-adiabatic calorimetry, and isothermal calorimetry. Adiabatic or semi-adiabatic calorimetry have obvious disadvantages. First, it is difficult to establish an adiabatic condition since it is impossible to inhibit the heat loss to surroundings (Rilem, 1997); when semi-adiabatic calorimetry is selected, the heat loss to surroundings must be determined (Wadsö, 2003). In addition, using adiabatic or semi-adiabatic calorimetry requires extra effort to determine specific heat capacity and hydration parameters (e.g., activation energy) for calculating heat generation rate (Martinelli et al., 2013). Compared with adiabatic and semi-adiabatic calorimetry, isothermal calorimetry is a better choice for determining heat generation rate since it can directly measure the heat generation rate without the necessity of determining the heat capacity of a sample (Wadsö, 2003), and it can also determine the hydration parameters of cement (Poole et al., 2007). Therefore, similar to previous studies (Tahersima and Tikalsky, 2017; Xu et al., 2010; Xu et al., 2011), the heat generation rate of CSA cement and hydration parameters were determined with isothermal calorimetry. The influence of curing temperatures and the proceeding of hydration on the heat generation rate was calculated based on the Arrhenius equation.

After that, a numerical model based on COMSOL Multiphysics was developed to predict temperature profiles in cement-based mixtures. COMSOL Multiphysics was selected since it is a powerful finite element analysis software that can solve multiple physical governing equations and has a friendly graphical user interface (Hu et al., 2021; Li et al., 2009; Zimmerman, 2006). In COMSOL, the expression of the heat generation rate was input as a function of temperature, hydration parameters, and time. The geometry was built and meshed, and boundary conditions were set to make sure that the results were independent of boundaries and meshes.

To validate the numerical model, Investigation #1 predicted temperature profiles in CSA-based mortars with the same geometries and curing conditions settings as our previous study (Huang et al., 2019), and then the predicted temperature profiles were compared with measured temperature profiles. The model was validated only if the root mean square error (RMSE) between the modeled and measured temperature profiles is smaller than 2 °C, the development of this criterion is illustrated in Section 2.3.5. Investigation #2 was performed to understand the influence of curing temperatures, different curing modes (curing in permafrost and curing in the air) on the temperature profiles in CSA-based mixtures. In Investigation #2, a sand layer with a temperature of 0 °C and -10 °C was used to mimic the influence of permafrost on the CSA cement-based mixtures as did in a previous study (Huang et al., 2019); Investigation #3 was implemented to study the influence of sample sizes on the temperature profiles in CSA-based mixtures. In Investigations #2 and #3, the temperature profiles in CSA-based mixtures were also compared with those in OPC-based mixtures cured at the same conditions.

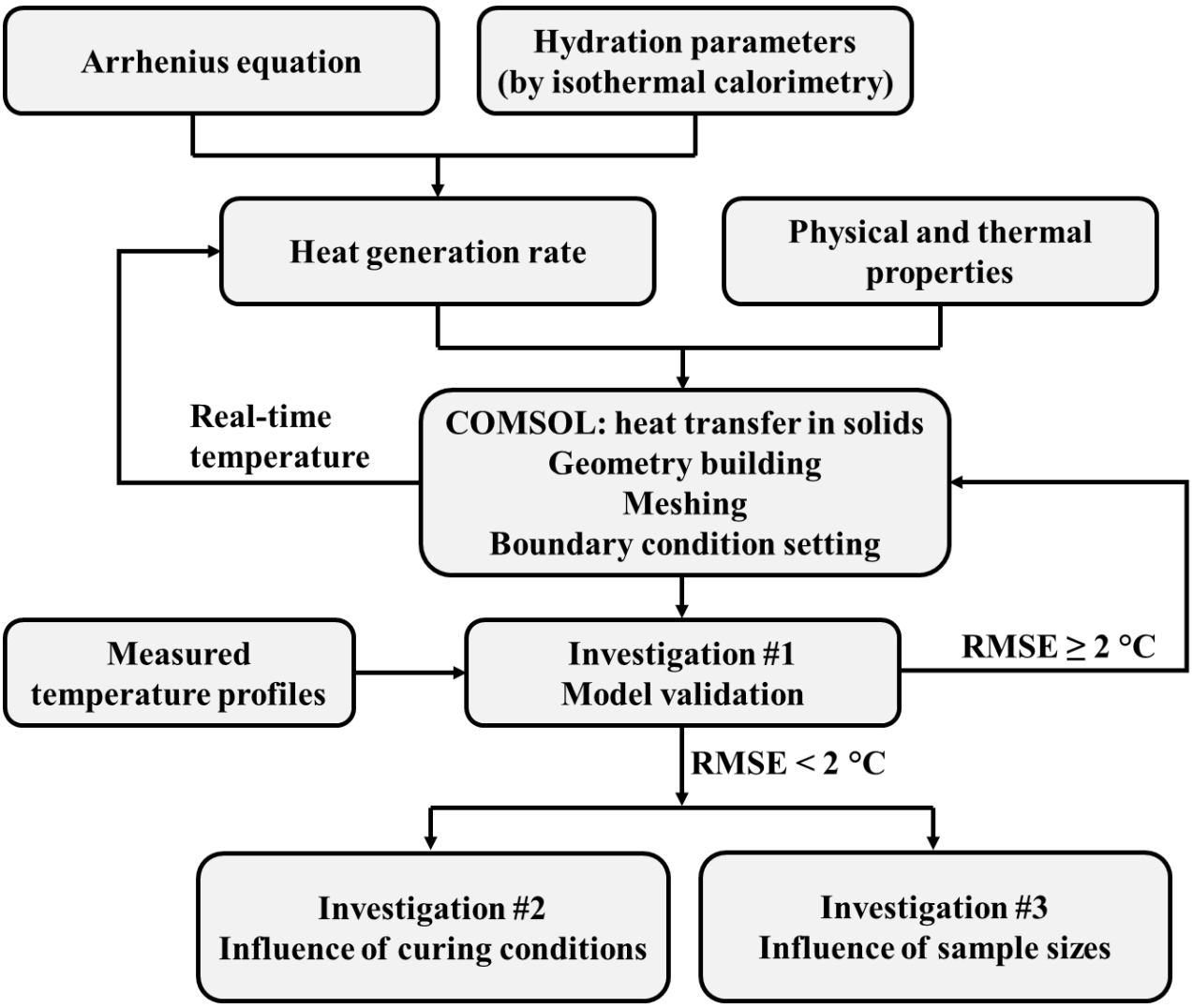

Figure 6.1 A flowchart showing the overview of the methodology.

6.2.2. Heat generation rate prediction

6.2.2.1. Arrhenius equation

Cement hydration is an exothermic reaction (Livesey et al., 1991; Martinelli et al., 2013). To model the temperature development in hardening cement-based mixtures, an important step is to predict the heat generation rate during cement hydration. The heat generation rate can be expressed with the Arrhenius equation (Martinelli et al., 2013), as shown in Equation (6-1).

$$q = A_V e^{-\frac{E_A}{RT}} \tag{6-1}$$

Where A_V is the reference heat generation rate [W/g]; R is the universal gas constant, 8.314 J / mol·K; E_A is the activation energy [J/mol]; T is the temperature [K].

6.2.2.2. Hydration degree and equivalent age

Although the Arrhenius equation can describe the relationship between heat generation rate and temperature, it does not take the amount of available reactant into consideration, which decreases with the processing of hydration reaction. Therefore, hydration degree $\alpha(t)$ is introduced to express the ratio of the amount of reacted cement at time t and the total amount of cement added to the mixture (Xu et al., 2011). As shown in Equation (6-2), hydration degree can be expressed as the ratio of cumulative hydration heat $H(t)$ [J/g] released at time t and total heat Hu [J/g] that can be released when all the cement is reacted since the cumulative hydration heat is proportional to the amount of reacted cement (Martinelli et al., 2013; Xu et al., 2011).

$$\alpha(t) = \frac{H(t)}{Hu} \tag{6-2}$$

At real conditions, the actual hydration degree $\alpha(t)$ in the hardening cement-based mixtures is not likely to be the same as that determined in a lab after hydrated for the same time t [h] since hydration reaction rate is affected by temperatures which vary with the environment temperatures and the proceeding of hydration reaction. Therefore, equivalent age t_e [h] is introduced to correlate the hydration degree $\alpha(t)$ at a real condition with that $\alpha(t_e)$ at a lab condition. As shown in Equation (6-3), equivalent age is defined as the time that is required to achieve the same hydration degree $\alpha(t)$ at a known reference temperature T_r [K] (Xu et al., 2010).

$$\alpha(t) = \alpha(t_e) \tag{6-3}$$

According to the Arrhenius equation, the correlation between t and t_e can be described with Equation (6-4).

$$e^{-\frac{E_A}{RT_r}} \cdot \Delta t_e = e^{-\frac{E_A}{RT}} \cdot \Delta t \tag{6-4}$$

In addition, the hydration degree $\alpha(t_e)$ can determined in a lab at a constant temperature T_r and expressed as an exponential equation with time t_e, as shown in Equation (6-5),

$$\alpha(t_e) = \alpha_{max} \cdot e^{[-(\frac{\tau}{t_e})^{\beta}]} \tag{6-5}$$

in which α_{max} is the maximum hydration degree that can reached, τ [h] is the hydration time parameter, and β is the hydration shape factor (Xu et al., 2010; Xu et al., 2011).

6.2.2.3. Heat generation rate

With the expression of hydration degree $\alpha(t)$, the cumulative hydration heat $H(t)$ at time t can be calculated as shown in Equation (6-6).

$$H(t) = Hu \cdot \alpha(t) \tag{6-6}$$

Then, the heat generation rate $q(t)$ can be obtained by taking the derivative of the hydration heat $H(t)$ using Equation (6-7).

$$q(t) = \frac{dH(t)}{dt} = \frac{dH(t)}{dt_e} \cdot \frac{dte}{dt} \tag{6-7}$$

Consequently, the heat generation rate $q(t)$ is expressed with Equation (6-8) after substituting Equations (6-3), (6-4), (6-5), and (6-6) into Equation (6-7).

$$q(t) = Hu \cdot \alpha_{max} \cdot e^{[-(\frac{\tau}{t_e})^{\beta}]} \cdot \frac{\beta}{t_e} \cdot (\frac{\tau}{t_e}) \cdot e^{-(\frac{E_A}{R})(\frac{1}{T}-\frac{1}{T_r})} \tag{6-8}$$

6.2.2.4. Hydration parameters

In Equation (6-8), there are five unknown hydration parameters, namely E_A, Hu, α_{max}, τ, and β. Among these parameters, activation energy E_A is usually determined by measuring the heat generation rates (q_1 and q_2) during cement hydration at two different constant temperatures (T_1 and T_2) with an isothermal calorimeter (Poole et al., 2007). Then, taking the logarithm of the heat generation rates (q_1 and q_2) gives Equations (6-9) and (6-10) since they can be described with Arrhenius equation.

$$\ln q_1 = lnA_V - \frac{E_A}{RT_1} \tag{6-9}$$

$$\ln q_2 = lnA_V - \frac{E_A}{RT_2} \tag{6-10}$$

From Equations (9) and (10), the activation energy E_A can be calculated as shown in Equation (6-11).

$$E_A = -\ln\left(\frac{q_1}{q_2}\right) \cdot R \cdot (T_1 - T_2) \tag{6-11}$$

The total heat Hu of cement is depended on cement compositions. For Portland cement, the way to estimate the total heat is illustrated as shown in Equation (6-12) (Anton and Kevin, 2005; Poole et al., 2007):

$$Hu = 500\mathrm{P}_{C_3S} + 260\mathrm{P}_{C_2S} + 866\mathrm{P}_{C_3A} + 420\mathrm{P}_{C_4AF} + 624\mathrm{P}_{SO_3} + 1186\mathrm{P}_{free\ Ca} + 850\mathrm{P}_{MgO} \tag{6-12}$$

in which, $\mathrm{P}_{composition}$ is the mass percentage of the corresponding composition in the cement.

It is of note that Equation (6-12) cannot be used to determine the total heat of CSA cement since the amount of heat released from the hydration of ettringite has not been reported in literature.

However, the values of τ and β, and the product of Hu and α_{max} can be determined from isothermal calorimetry results. As shown in Equation (6-13), the cumulative hydration heat $H(t)$ can be presented as a function of the hydration parameters (Hu, α_{max}, τ, and β) after substituting Equation (6-5) to Equation (6-6).

$$H(t_e) = Hu \cdot \alpha_{max} \cdot e^{[-(\frac{\tau}{t_e})^{\beta}]} \quad (6\text{-}13)$$

A least-squares, exponential fit between the measured cumulative heat curve with Equation (6-13) gives the values of τ, β and the product of Hu and α_{max}.

In this study, the hydration parameters for CSA cement are calculated from the isothermal calorimetry results provided by the CTS cement company, USA, while the hydration parameters for OPC are obtained from a previous study by Martinelli et al. (2013), as shown in Table 6.1.

Table 6.1 Hydration parameters of OPC and CSA cement.

Hydration parameters	CSA cement	OPC (Martinelli et al., 2013)
Activation energy E_A [J/mol]	50000	33000
Hydration time parameter τ [Hours]	0.59	9
Hydration shape factor β	0.97	2.1
Product of total heat Hu and maximum hydration degree α_{max} [J/g]	268	231

6.2.3. Numerical model for predicting temperature profiles

6.2.3.1. Governing equation

Equation (6-14) is the governing equation for calculating the temperature profiles in cement mortars (Ballim, 2004):

$$\rho C_p \frac{\partial T}{\partial t} = k\left(\frac{\partial^2 T}{\partial x^2} + \frac{\partial^2 T}{\partial y^2} + \frac{\partial^2 T}{\partial z^2}\right) + q(t) \quad (6\text{-}14)$$

where ρ [kg/m^3] is the density, which is assumed to be the same at frozen and unfrozen conditions. C_p [J/kg/K] is the heat capacity of cement mortars. As shown in Equation (15), the value of heat capacity depends on the fractions (θ_u and θ_f) and heat capacity ($C_{p,u}$ and $C_{p,f}$) of unfrozen and frozen phases, latent heat $L_{f\to u}$, and the rate of phase change against temperature T[K].

$$C_p = \theta_u C_{p,u} + \theta_f C_{p,f} + \frac{1}{2} L_{f\to u} \frac{\partial(\theta_u - \theta_f)}{\partial T} \quad (6\text{-}15)$$

k is the thermal conductivity, its value can be calculated with the factions (θ_u and θ_f) and thermal conductivities (k_u and k_f) of unfrozen and frozen phases, as shown in Equation (6-16).

$$k = \theta_u k_u + \theta_f k_f \quad (6\text{-}16)$$

$$\theta_u + \theta_f = 1 \quad (6\text{-}17)$$

$q(t)$ is the heat generation rate during cement hydration, which is calculated with the analytical model presented above. When modeling the temperature profile in cement mortars cured in sand, the heat transfer in sand is also solved by the same governing equation, where $q(t)$ is zero since there is no heat source in sand. To discretize the governing equation, quadratic shape functions were used since they yield relatively high accuracy in results and low computational cost, which have been widely used in finite element method (Hauptmann et al., 2001; Oden et al., 1998;

Peters et al., 2012). The relevant tolerance was set as 10^{-4} because further reducing tolerance did not increase the accuracy; instead, it extended the computational time.

6.2.3.2. Physical and thermal properties

Table 6.2 lists the physical and thermal properties of CSA-based mortar, OPC-based mortar, and sand, which were used as input parameters in the models. The physical and thermal properties of OPC-based and CSA-based mortars at unfrozen and frozen status were measured in a laboratory or calculated from the data reported in our previous studies (Huang et al., 2020a, 2021; Liu et al., 2011) with the consideration of the influence of water content and freezing. The thermal properties of sand at unfrozen and frozen conditions were obtained from Zhao and Si's study (2019). The latent heat that can be released during the phase change from water to ice is 334 kJ/kg (Legates, 2005). For the sample cured in air without the influence of wind, the heat transfer coefficient between cement mortar and surrounding air was set as 11 $W/m^2/K$ according to the data reported in the literature (Guo et al., 2011b; Lee et al., 2009).

Table 6.2 Physical and thermal properties of CSA-based mortar, OPC-based mortar, and sand

Properties	CSA-based mortar (Huang et al., 2021)		OPC-based mortar (Liu et al., 2011)		Sand (Zhao and Si, 2019)	
	unfrozen	frozen	unfrozen	frozen	unfrozen	frozen
Density [kg/m^3]	2160	2160	2300	2300	1800	1800
Thermal conductivity [W/m/K]	2.0	2.4	2.9	3.4	2.1	2.5
Specific heat capacity [J/kg/K]	1176	914	1263	994	1060	798
Initial water content [%]	12.2		12.2		12.0	
Latent heat of water [kJ/kg] (Legates, 2005)	334					
Heat transfer coefficient [W/m^2/K] (Guo et al., 2011b; Lee et al., 2009)	11					

6.2.3.3. Geometry and boundary conditions

The geometries of models for samples cured in air and sand are presented in Figure 6.2. The dimension parameters of all geometries for different investigations are summarised as shown in Table 6.4. The dimensions of geometry and the boundary conditions were different depending on the purpose of the investigations. Investigation #1 was performed to validate the numerical model. The dimensions of samples, curing conditions, and boundary conditions were set

following the experimental setup for temperature measurement in the laboratory (Huang et al., 2019). In the models, the dimensions of the cylindrical samples were Ø65mm×130mm, which was cured at 20 °C in air, 0 °C and -10 °C in cold sand. The initial temperature of all the samples was set as 20 °C, and the thickness of the sand layer was set as 700 mm following the experimental setup of our previous study (Huang et al., 2019). For samples cured in the sand, the boundary at the out surface of the sand layer was set as a temperature boundary since there was a temperature controller to ensure the temperature in the sand to maintain at around the setting curing temperature in a previous study (Huang et al., 2019). Its temperature was set as the curing temperature.

For the sample cured in air, the heat transfer between cement mortar and the surrounding air is by heat convection, and the heat flux equals to (Lee et al., 2009; Liu et al., 2016):

$$q_h = h_{eff}(T_m - T_a) \tag{6-18}$$

where h_{eff} is the heat transfer coefficient, T_m is the temperature of the surface of cement mortar, and T_a is the air temperature.

Investigation #2 was performed to understand the influence of curing conditions on the temperature profiles in CSA-based mortars and to compare them with those in OPC cement mortars. Models were developed to predict the temperature profiles in CSA-based mortars and OPC-based mortars cured in air and wet sand at 20 °C, 0 °C and -10 °C. The initial temperature of OPC-based and CSA-based mortars was set as 20 °C since ACI 306R-10 (ACI, 2010) suggests increasing the placing temperature to higher than 18 °C when samples with a section size smaller than 300 mm are cured in a temperature range between -1 °C and -18 °C.

Investigation #3 was performed to study the influence of sample size on the temperature profiles in CSA mortars and OPC cement mortars. Models were developed to predict the temperature profiles in CSA-based mortars and OPC-based mortars with four different sizes (i.e., Ø100mm×200mm, Ø150mm×300mm, Ø200mm×400mm, Ø300mm×600mm) cured in wet sand at 0 °C. The initial temperature of cement mortars was set as 20 °C.

In Investigations #2 and #3, the thickness of the sand layer was set as 1000 mm, and the boundary was set as an insulation boundary after an independence test on a CSA cement-based sample with dimensions of Ø300mm×600mm. As shown in Table 6.3, further increasing the thickness of the sand layer from 1000 mm to 2000 mm almost had no influence on the peak temperature in the center of the CSA cement-based sample cured in the sand at 0 °C.

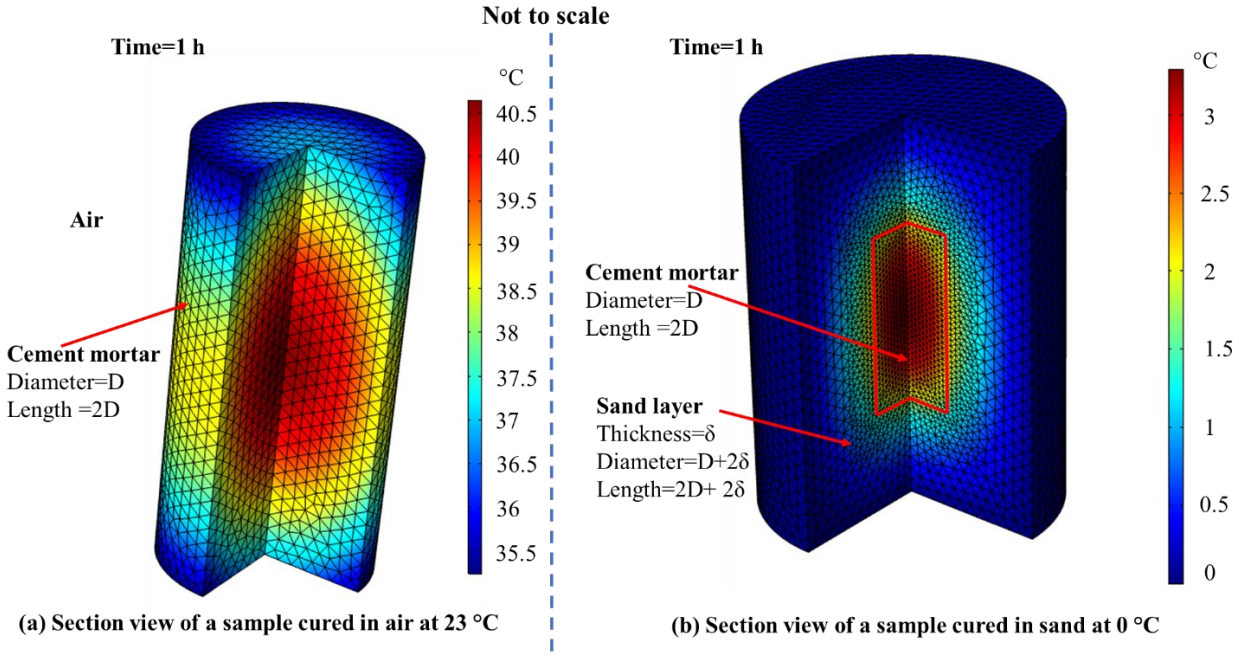

Figure 6.2 The geometries of models for samples cured in (a) air and (b) sand.

Table 6.3 Independence tests for the thickness of the sand layers

Thickness of the sand layer (δ/mm)	Peak temperature (°C)
500	56.6
1000	56.3
2000	56.3

Table 6.4 The dimensions of geometries for different investigations

	Dimensions of cement mortar (D×L)	Curing conditions			
		Curing modes	Curing temperature (T_{Curing})	Thickness of the sand layer (δ)	Cement type
Investigation #1: Model verification	Ø65mm×130mm	Curing in air	20 °C	-	CSA
		Curing in sand	0 °C and -10 °C	70 mm	CSA
Investigation#2: Influence of curing conditions	Ø100mm×200mm	Curing in air	20 °C,	-	CSA and OPC
		Curing in sand	0 °C, and -10 °C	1000 mm	
Investigation #3	Ø100mm×200mm	Curing in sand	0 °C	1000 mm	CSA and

Influence of sample sizes	Ø150mm×300mm Ø200mm×400mm Ø300mm×600mm	OPC

6.2.3.4. Mesh independence tests

The geometries were meshed into free tetrahedra in COMSOL Multiphysics. For each geometry, the influence of mesh size on the results was investigated to ensure that the results are independent of meshing. Table 6.5 presents an example mesh independence test on a CSA-based sample with dimensions of Ø300mm×600mm cured in the sand at 0 °C. As shown in Table 6.5, the peak temperature was 56.3 °C when the mesh sizes of the mortar and sand were 0.0039m-0.091m and 0.0104m-0.143m, respectively. Further refining the mesh size almost had no influence on the peak temperature, while significantly increased the computational time. For example, when the meshes were refined from Mesh #4 to Mesh #6, the peak temperature was still stable at 56.3 °C; however, the computational time extended from 648 s to 4124 s since the number of meshes increased about 6 times. In order to save computational time without compromising the accuracy, the mesh sizes of mortar and sand were selected as 0.0039m-0.091m and 0.0104m-0.143m, respectively.

Table 6.5 Mesh independence test

	Mesh size (minimum-maximum)		Number of elements		Peak temperature	Computational time
	Mortar	Sand	Mortar	Sand	(°C)	(s)
Mesh #1	0.0728m-0.39m	0.0728m-0.39m	382	5017	54.8	37
Mesh #2	0.0468m-0.26m	0.0728m-0.39m	630	5343	55.5	39
Mesh #3	0.0104m-0.143m	0.026m-0.208m	1644	24505	56.2	168
Mesh #4	0.0039m-0.091m	0.0104m-0.143m	3636	70709	56.3	648
Mesh #5	0.00052m-0.052m	0.0039m-0.091m	10421	262180	56.3	1733
Mesh #6	0.0004m-0.03m	0.003m-0.07m	25584	555938	56.3	4124

6.2.3.5. Model validation

(1) Experimental setup

In this study, the developed numerical model was validated by comparing the modeled temperature profiles with those measured in the laboratory and reported in our previous study

(Huang et al., 2019). Figure 6.3 and 4 depict the experimental setup for temperature profile recording in precious study (Huang et al., 2019). Type K thermocouples and HH374 dataloggers were employed to measure and record the temperature profiles in the center of the sample and surroundings (e.g., air and sand). The thermocouples had an accuracy of ±0.1% reading value; the dataloggers recorded temperatures at a time interval of two minutes. Before temperature recording, CSA cement-based samples were mixed and cast into steel molds at a room temperature (20 °C), then thermocouples were inserted into the centers of CSA cement-based samples immediately. After that, the sample cured in air was put in the laboratory with an air temperature of 20 °C; samples cured in sand were embedded in cold sands with temperatures of 0 °C and -10 °C, respectively. The temperature of sands was maintained at the curing temperatures (e.g., 0 °C and -10 °C) through a closed loop control system consisted of a freezer, a temperature controller, and a thermocouple.

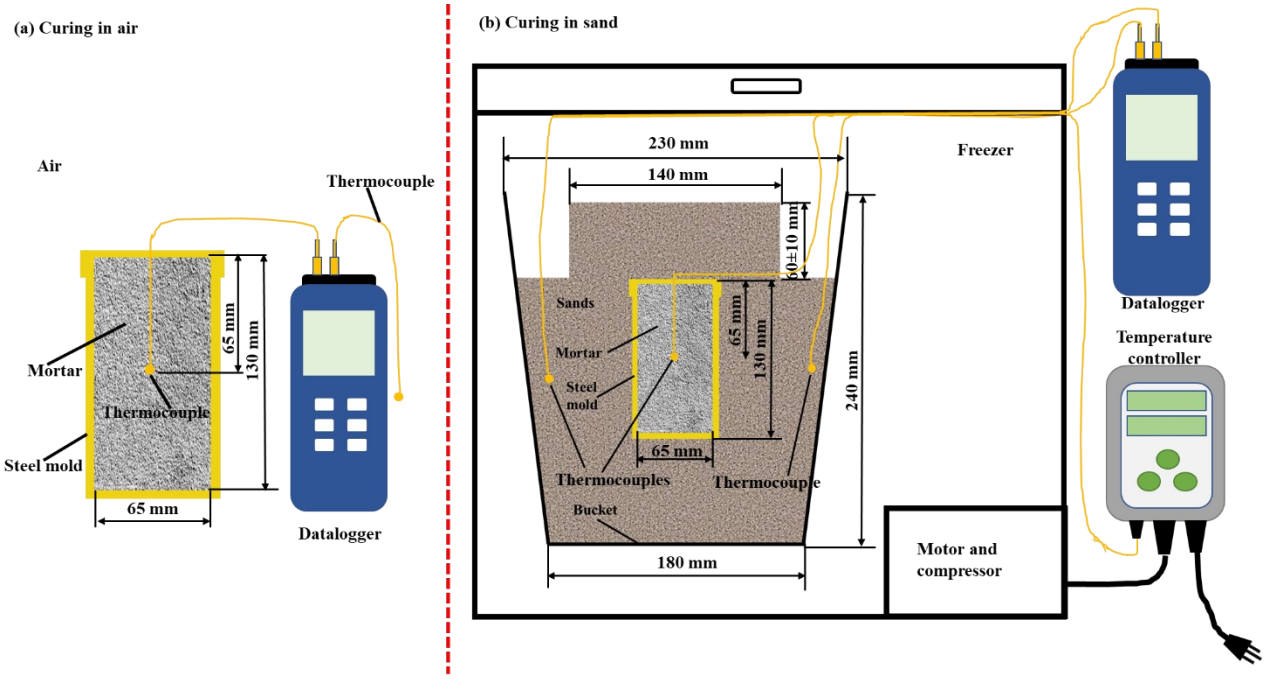

Figure 6.3 Schematics of the experimental setup for temperature profile recording (a) in a sample cured in air; and (b) in a sample cured in sand, modified from the experimental work by Huang et al. (Huang et al., 2019).

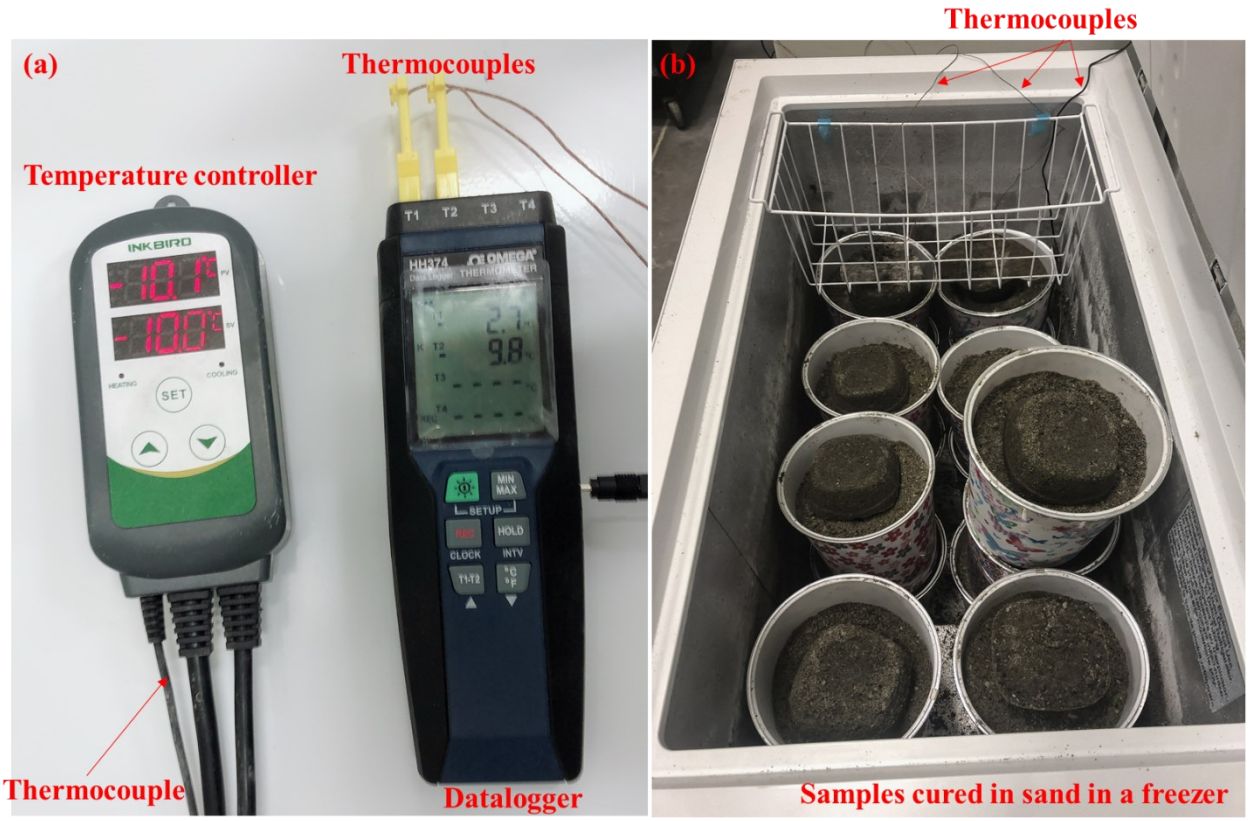

Figure 6.4 Experimental setup for temperature profile recording in the sample cured in sand: (a) Temperature controller and datalogger; (b) samples cured in sand in a freezer.

(2) Model validation criterion

Currently, there is no criterion to decide if the developed model is validated for predicting the temperature profiles in hardening cement-based mixtures, although some models have been developed. Generally, previous researchers (Ballim, 2004; Ilc et al., 2009; Saeed et al., 2016; Tahersima and Tikalsky, 2017; Xu et al., 2010; Xu et al., 2011) plotted the modeled and

measured temperature profiles in a figure; if the modeled temperature file curve was close to the measured one, then they claimed that the model was validated. To establish a criterion to validate the numerical model, the authors grabbed the data from previous studies (Ilc et al., 2009; Tahersima and Tikalsky, 2017; Xu et al., 2011) and calculated the root mean square error (RMSE) between the modeled and measured temperature profiles in these studies with Equation (6-19) (Hu et al., 2020). As shown in Table 6.6, the RMSEs calculated from previous studies were in a range between 1.7 °C to 3.4 °C. Based on these data, the authors in the current study developed a criterion to validate their model that the model is validated if the RMSE is smaller than 2.0 °C.

$$RMSE = \sqrt{\frac{\sum_{i=1}^{n}(T_{modeled} - T_{measured})^2}{n}} \quad (6\text{-}19)$$

Table 6.6 RMSE between the modeled and measured temperature profiles calculated from previous studies (Ilc et al., 2009; Tahersima and Tikalsky, 2017; Xu et al., 2011)

References	Heat generation rate determination method	RMSE (°C)
Tahersima and Tikalsky (2017)	Isothermal calorimetry	2.7
Ilc et al. (2009)	Adiabatic calorimetry	1.7
Xu et al. (2011)	Isothermal calorimetry	3.4
	Semi-adiabatic calorimetry	1.8

6.3. Results and discussion

6.3.1. Model validation

To validate the developed numerical model, a comparison was conducted between the modeled temperature profiles and measured temperature profiles in CSA-based mortar cured at different temperature. As shown in

Figure 6.5, the modeled temperature profiles match well with the measured temperature profiles reported in previous study (Huang et al., 2019). When cured in the air at 20 °C, the modeled temperature in the CSA-based mortar increased sharply and peaked at 44.2 °C, which was 2.8 °C higher than the measured peak temperature (41.4 °C). The modeled peaking time was 40 minutes, being 5 minutes later than the measured peaking time (35 minutes). The RMSE between the modeled and measured temperature profiles was only 1.0 °C. For the samples cured in cold sand at 0 °C and -10 °C, the modeled temperature profiles were also matched very well with the measured temperature profiles. The RMSE was only 1.3 °C for both curing temperatures. All these RMSEs met the criterion (RMSE < 2.0 °C) for validating the model. In conclusion, the numerical model for predicting the temperature profile in hydrating cement mortar was experimentally validated.

It is of note that the temperature in the mortars cured at -10 °C kept constant at about 0 °C for ~2 hours before dropping to -10 °C, which indicated that the influence of latent heat has also been reflected in the model. With the decrease of temperature, water tended to get frozen, this process was accompanied with the release of latent heat (334 kJ/kg of water) (Legates, 2005). The released heat delayed the trend of temperature decreasing until all the water got frozen. As a result, the temperature in the mortars cured at -10 °C kept constant at about 0 °C for ~2 hours before dropping to -10 °C.

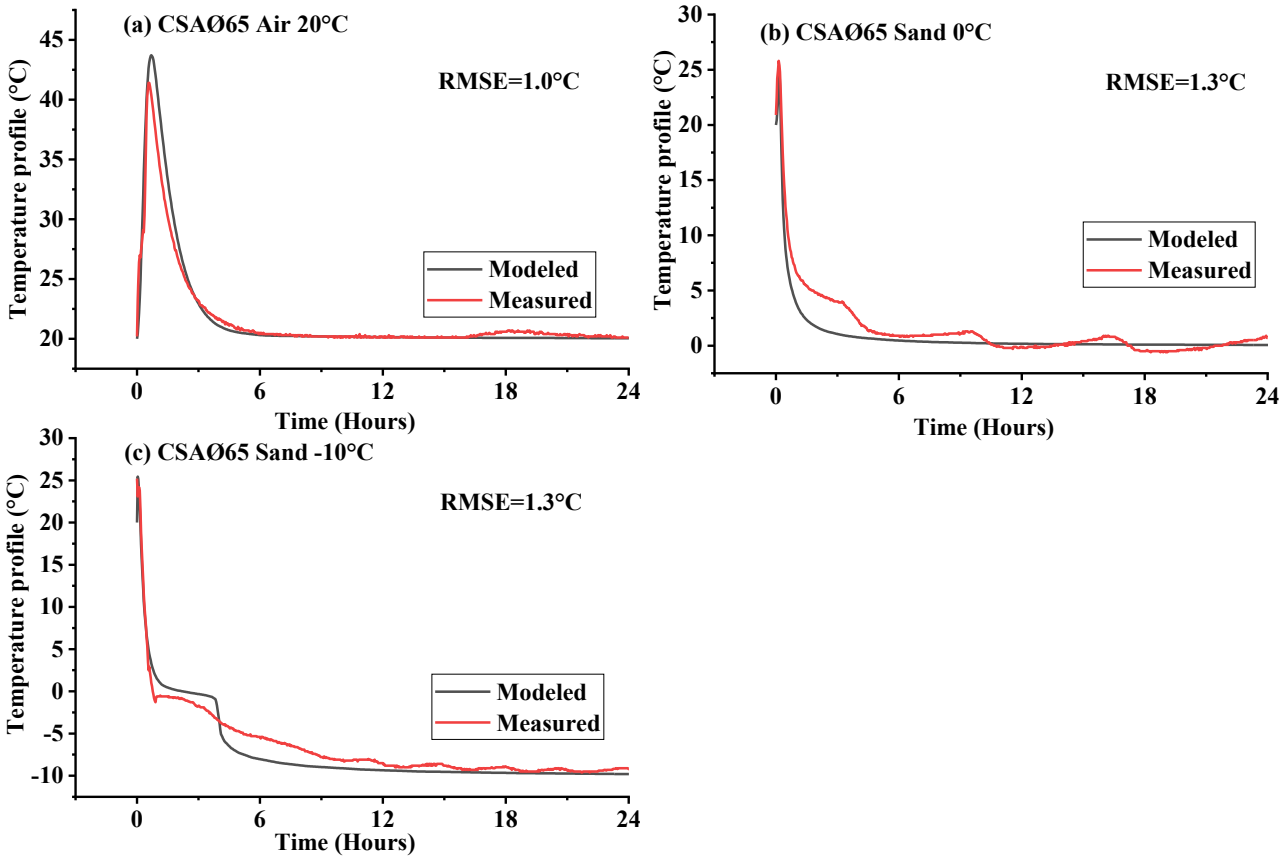

Figure 6.5 Comparison between the modeled and measured temperature profiles in CSA-based mortars cured (a) in air at 20 °C; (b) in sand at 0 °C; and (c) in sand at -10 °C.

6.3.2. Influence of curing conditions on the temperature profiles

Figure 6.6 depicts the influence of curing conditions (i.e., curing temperatures and curing modes) on the temperature profiles in CSA-based mortars and OPC-based mortars. The temperature in CSA-based mortars cured in the air increased sharply to 53.3 °C, 40.2 °C, and 34.1 °C at about 0.6-0.8 hours when the curing temperatures were 20 °C, 0 °C, and -10 °C, respectively. The sharp temperature increase indicates that the hydration reaction of CSA cement at an early age was very intensive even at cold temperatures (i.e., 0 °C, and -10 °C), and the heat generation due to CSA cement hydration was more intensive than the heat loss to the surrounding air through

heat convection. The peak temperature decreased with the decrease of curing temperature, which coincided with the description of the Arrhenius equation (Martinelli et al., 2013) that the hydration reaction rate decreases with the drop in curing temperature. After reaching peaks, temperatures in CSA-based mortars decreased exponentially. This is because the cement hydration got into a deceleration stage during which further hydration was restricted by the availability of unreacted cement, water, and the diffusion of hydration products (Bullard et al., 2011). For OPC-based mortars, the temperature in the sample cured in the air at 20 °C kept constant at 20 for about 5 hours. This is because the hydration reaction of OPC usually experiences an induction period for several hours, during which the hydration reaction is dormant (Bullard et al., 2011; Livesey et al., 1991). After that, the temperature increased and peaked at 26.1 °C at ~10 hours, showing that the hydration reaction of OPC was slower and less intensive than that of CSA cement. At cold temperatures (0 °C and -10 °C), the temperatures in OPC-based mortars cured in the air dropped rapidly to around their curing temperatures, then only a slight increase (< 2.3 °C) can be observed in the OPC-based mortar cured at 0 °C. The temperature profiles in OPC-based mortars indicate that the hydration reaction of OPC was further slowed down at cold temperatures. The difference between temperature profiles in CSA-based and OPC-based mortars shows that CSA cement is more suitable than OPC for concreting in cold temperatures. This is consistent with our previous findings (Huang et al., 2020a) that substituting CSA cement for OPC can achieve faster hydration reaction, more rapid strength development, and prevent early-age frost damage.

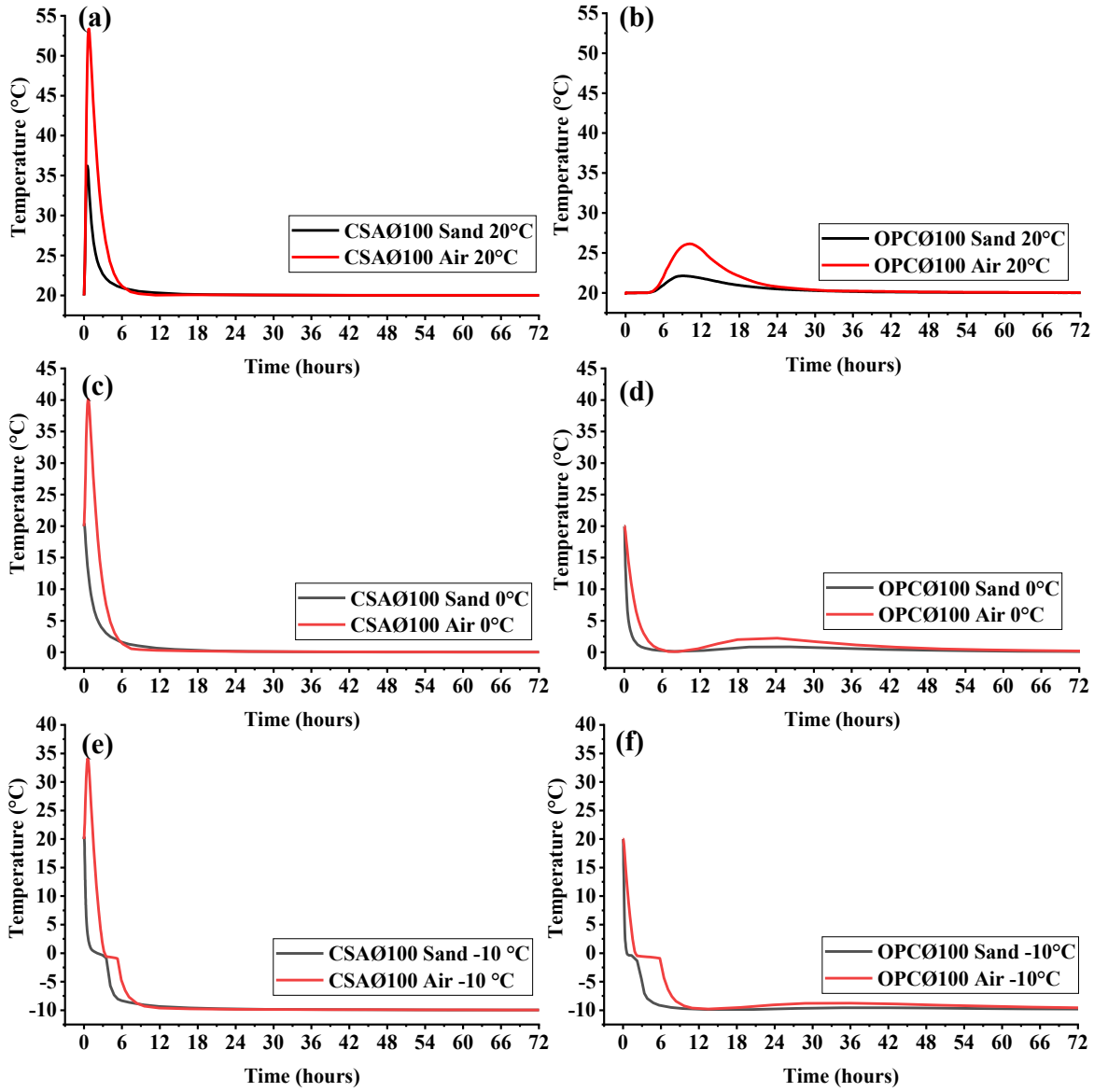

Figure 6.6 Modeled temperature profiles in the center of CSA-based and OPC-based mortars cured at different conditions.

In addition to curing temperatures, curing modes affected the temperature profiles in CSA-based and OPC-based mortars. For OPC-based mortars, the maximum differences caused by curing modes were ~4 °C observed at 10 hours, ~9 °C observed at 0.5 hour and ~13 °C observed at 0.4 hour when OPC-based mortars were cured at 20 °C, 0 °C and -10 °C, respectively. For CSA-

based mortars, the temperature profiles in samples cured in the air were notably higher than that of samples cured in the sand. As shown in Figure 6.6(a), the maximum temperature in the center of CSA-based mortar cured in the sand was 53.3 °C, which was 17.1 °C lower than that of the mortar cured in the air. At cold-curing temperatures, the difference was even higher. For example, the temperature in the CSA-based mortar cured in the air at 0 °C increased sharply to 40.2 °C within 0.7 hour, while the temperature in the same mortar cured in the sand at 0 °C never increased above the initial placing temperature (20 °C); instead, it dropped exponentially to around 0 °C. The maximum temperature difference between CSA-based mortars cured in air and sand was as high as 28 °C at 0.7 hour when cured at 0 °C. The great difference between the temperature profiles was caused by two reasons. First, the heat transfer methods were different; CSA-based mortar cured in sand lost heat to surroundings mainly through heat conduction, while that cured in air dispersed heat to surroundings mainly by natural heat convection (Holman, 2001; Huang et al., 2019). The former one can be more intensive and faster than the latter one at the initial stage. As shown in Figure 6.7(a), the heat flux through the boundaries of CSA cement sample cured in the sand at 0 °C was over 2000 W/m^2 at the first moment, which was considerably higher than that (~220 W/m^2) of sample cured in air. The heat flux from CSA cement sample to the surrounding sand decreased sharply with time; however, it was still higher than the heat flux from CSA cement sample to surrounding air until ~30 minutes. These data show that the heat loss to surroundings was more intensive when the sample was cured in the sand at an initial stage. The intensive heat loss to surroundings caused the sharp decrease in the temperature of CSA-based mortar cured in sand. The decrease in temperature further caused a slower hydration reaction rate and lower heat generation rate in the CSA-based mortar cured in sand. As shown in Figure 6.7(b), the maximum heat generation rate in the CSA-based mortar

cured in sand was 30 mW/g cement, while that for sample cured in air was 77 mW/g cement. The different heat generation rates were the second reason for the difference in the temperature profiles in CSA-based mortars cured in sand and cured in air.

Different curing modes affected the temperature profiles in both CSA-based mortars and OPC-based mortars, especially when cured at cold temperatures. Therefore, the influence of different curing modes (e.g., curing in air and curing in permafrost) should be taken into consideration when conducting research on cement-based mixtures used in cold regions. In the literature, some studies (Brusletto, 2018; Huang et al., 2019; Wang et al., 2020b) investigated the strength development of cement-based mixtures that needed to be attached with or embedded in permafrost or cold ground during their applications; however, samples were usually cured in cold air (Brusletto, 2018; Wang et al., 2020b). This is not the best way to understand the influence of permafrost or cold ground on the strength development of cement-based mixtures since the different curing modes (e.g., curing in air and curing in permafrost) can affect the temperature profiles in hardening cement-based mixtures, consequently affecting the strength development. It would be better to cure samples in cold soil or sand when investigating the performance of cement-based mixtures that are needed to be embedded in or attached with cold or frozen ground, such as concrete piles, concrete pavement, concrete shaft, and shotcrete for rock support in cold regions.

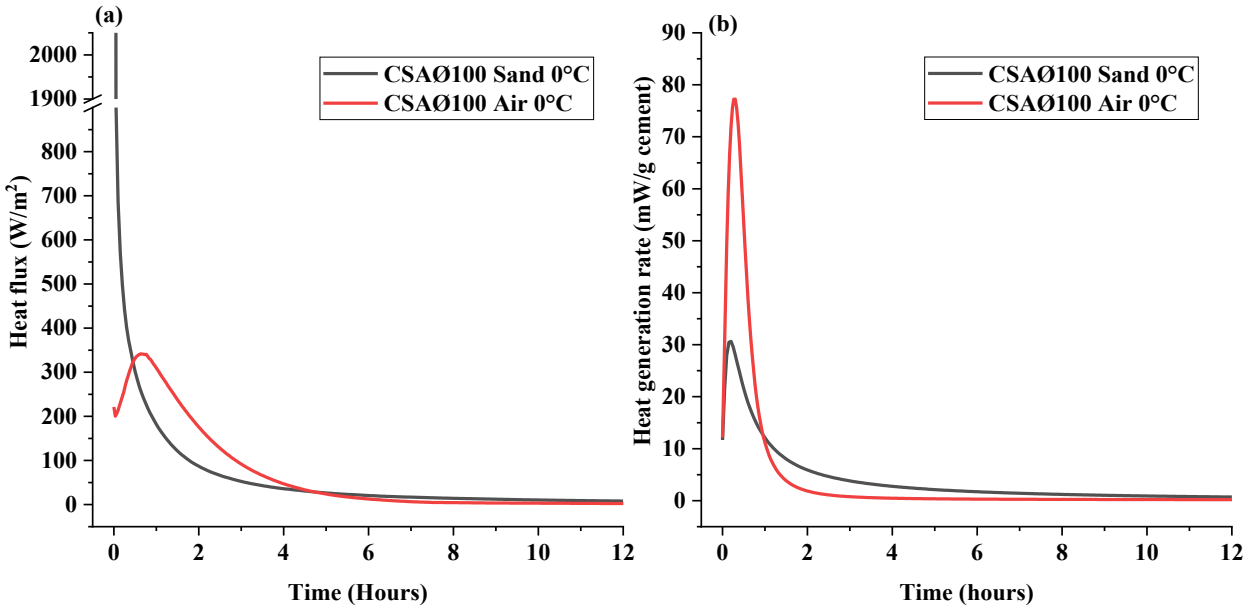

Figure 6.7 Comparison between CSA-based mortars cured in air and cured in sand at 0 °C: (a) the average heat flux through the boundaries; (b) the average heat generation rate in the cylindrical samples.

6.3.3. Influence of sample sizes on the temperature profiles

Figure 6.8 depicts the influence of sample size on the temperature profiles in CSA-based and OPC-based mortars cured in sand at 0 °C. As shown in Figure 6.8 (a), a sharp increase can be observed in the temperature profiles in CSA-based mortars within one hour, except that of the CSA-based sample with a diameter of 100 mm. When the CSA-based sample diameter increased from 100 mm to 150 mm, 200 mm, and 300 mm, the peak temperature in CSA-based samples increased from 20 °C to 26.8 °C, 40 °C, and 56.3 °C, respectively, and the temperature in CSA-based mixture maintained above 5 °C for 2.3 hours, 4.4 hours, 6 hours, and 12.7 hours, respectively. These data indicate that the size of CSA-based sample is an important parameter that affected the hydration and temperature profiles at cold temperatures. CSA-based structures

with a large size may gain a higher strength at cold temperatures since a higher temperature facilitates cement hydration and strength gain (Martinelli et al., 2013). For OPC-based samples, increasing the sample size also decreased the rate of temperature drop at the initial stage and increased the peak temperature at about 20 to 24 hours. For example, the temperature maintained above 5 °C for 0.7 hours in OPC-based sample with a diameter of 100 mm, while it maintained above 5 °C for 6.8 hours in the sample with a diameter of 300 mm. The peak temperature at around 20 to 24 hours increased from 0.9 °C to 7.6 °C when the sample diameter increased from 100 mm to 300 mm. The influence of sample size on the temperature profiles of CSA-based mortars more notable than its influence on OPC-based samples. Therefore, the influence of structure sizes on the hydration, temperature profiles, and strength development of CSA-based structures should be taken into consideration when CSA cement is used in cold temperatures.

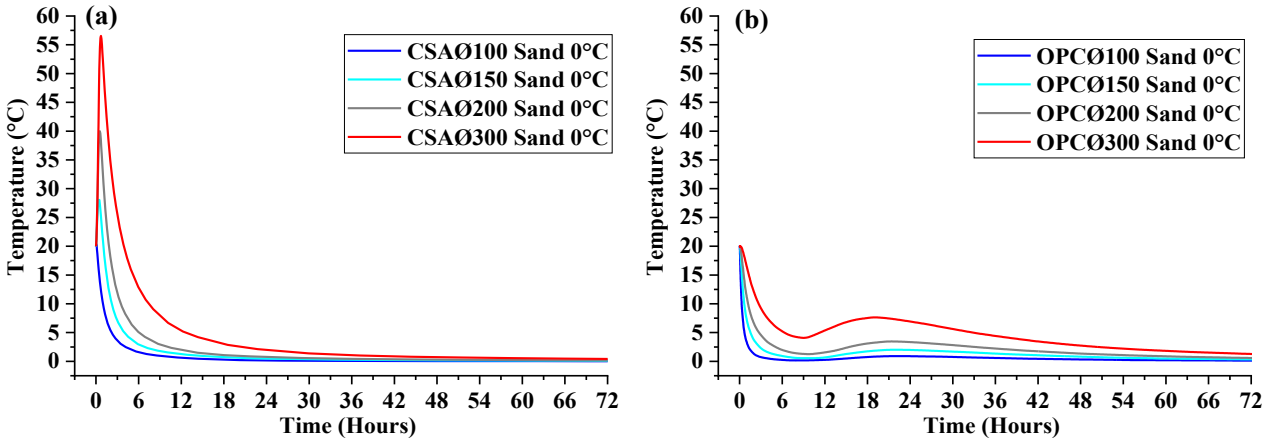

Figure 6.8 The influence of sample sizes on the temperature profiles of (a) CSA-based mortars and (b) OPC-based mortars.

6.3.4. Temperature distribution within samples

Figure 6.9 presents the temperature distribution in CSA-based and OPC-based mortars cured in 0 °C sand at 0.7 hour and 20 hours, respectively. These two time points were selected since the temperatures in the center of the CSA-based and OPC-based mortars reached the maximum values at 0.7 hour and 20 hours, respectively, which help observe the maximum temperature gradient caused by cement hydration heat.

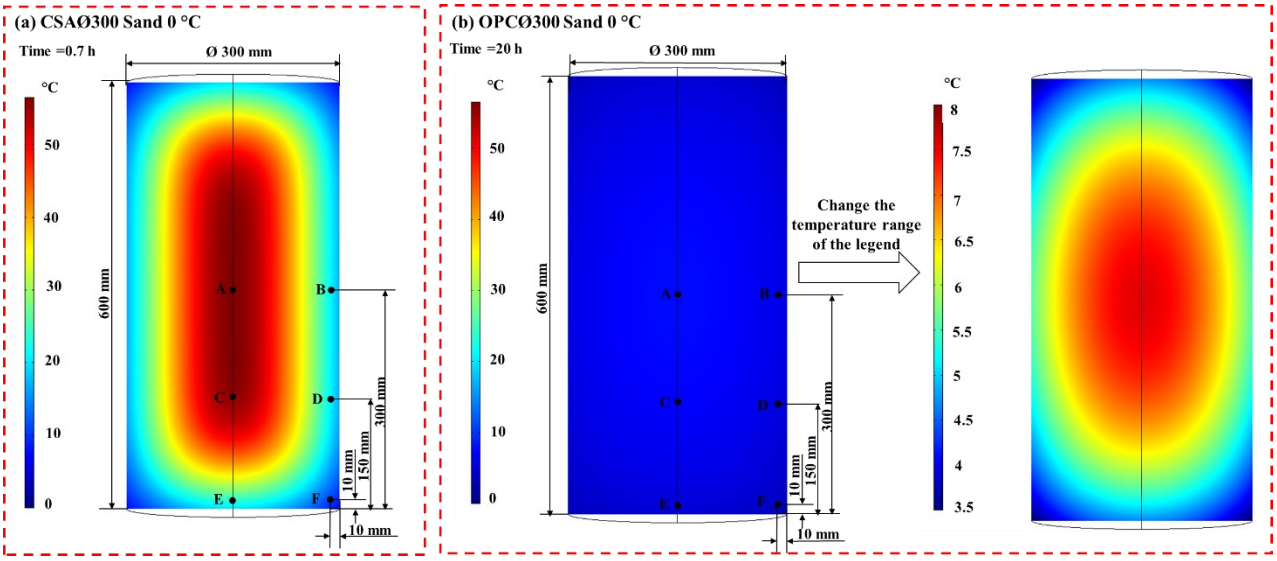

Figure 6.9 Temperature distribution in: (a) CSA-based mortar cured in sand with a temperature of 0 °C at 0.7 hour and (b) OPC-based mortar cured in sand with a temperature of 0 °C at 20 hours.

Figure 6.10 plots the temperature profiles with time at different positions in CSA-based mortar and OPC-based mortar cured in sand at 0 °C. For OPC-based mortar with a diameter of 300 mm, the maximum temperature difference caused by hydration heat within the sample was observed at around 20 hours, which was less than 4 °C. The low temperature difference was observed in OPC-based mortar since the size of the sample was small. In massive concrete (the ratio of

surface area to volume is smaller than 2 (Klemczak and Knoppik-Wróbel, 2011)), a large temperature difference is a problem since it may cause thermal cracks (Harrison, 1981; Huang, 1999; Klemczak and Knoppik-Wróbel, 2011). For example, Klemczak and Knoppik-wróbel (2011) reported that a temperature difference of ~24 °C was observed between the center and top surface of an OPC-based massive concrete with a dimension of 10m×10m×3m cured at 20 °C, and this temperature difference caused thermal cracks in the top surface area and edge area. For CSA-based mortar with a diameter of 300 mm, the maximum temperature was over 55 °C, which was observed at the center (Points A and C) of the sample at ~0.7 hour. At the same time, the temperature at near the boundaries (Points B, D, and E) was around 20 °C, being ~35 °C lower than the temperature in the center. At near the edge (Point F), the temperature was always the lowest, being ~45 °C lower than the temperature at the center of the sample. This data indicates that a large temperature gradient was existing in CSA-based mortar with a small size (Diameter=300mm), and it was significantly higher than the temperature gradient in OPC-based mortar with the same size. A large temperature gradient may cause uneven volume changes, further lead to tensile stress, ultimately induce thermal cracks in CSA-based structure (Harrison, 1981; Huang, 1999; Klemczak and Knoppik-Wróbel, 2011). Therefore, further studies are needed to understand the thermal stress, tensile strength development, and thermal cracks in CSA-based structures even if CSA cement is used for casting small-size structures.

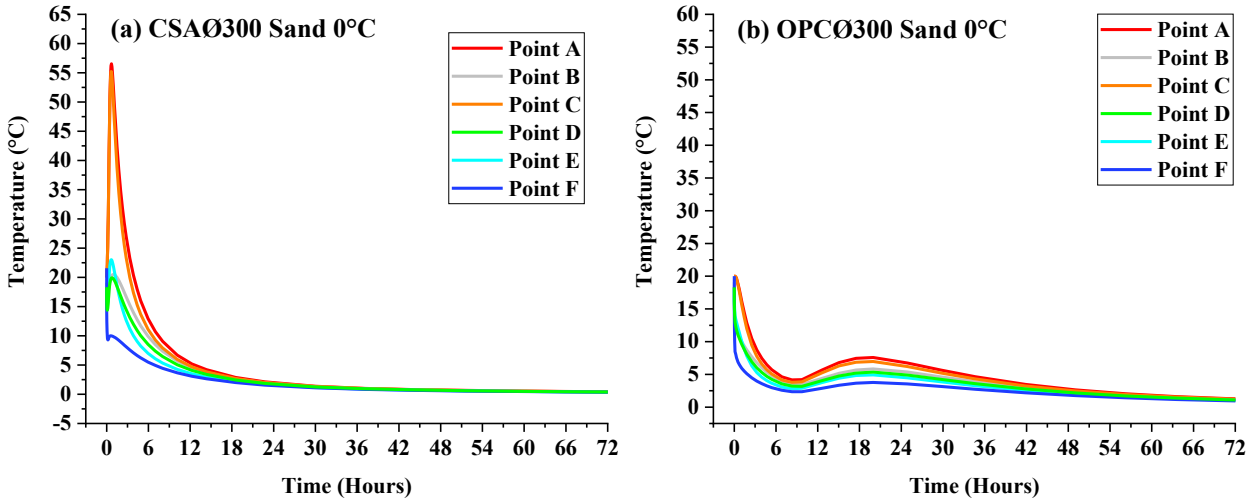

Figure 6.10 Modeled temperature profiles at different positions in: (a) CSA-based mortar cured in sand at 0 °C and (b) OPC-based mortar cured in sand at 0 °C.

6.4. Conclusion

This study developed a numerical model for understanding the temperature profiles in sulfoaluminate (CSA) cement-based mixtures used in permafrost regions (or frozen ground). In the model, CSA cement-based samples were cured in cold sand (0 °C and -10 °C) to mimic the influence of permafrost, and another group was cured in cold air. The influence of curing conditions (curing temperatures and curing modes) and sample sizes were investigated and compared with that on an ordinary Portland cement (OPC)-based mixture. The main concluding remarks are summarised as follows:

(1) A numerical modeling method has been established to model the temperature profiles in hardening CSA cement-based mixtures for permafrost region applications. The root mean square error (RMSE) between the modeled and measured temperature profiles was smaller than 1.3 °C, indicating that the model was validated with experimental results.

(2) The temperature in a CSA-based sample with dimensions of Ø100×200mm increased sharply when cured in the air, even it was at cold temperatures. The temperature increased to 53.3 °C, 40.2 °C, and 34.1 °C at about 0.6-0.8 hours when the curing temperatures were 20 °C, 0 °C, and -10 °C, respectively. However, the temperature in OPC-based never increased over the placing temperature (20 °C) when cured at cold temperatures (0 °C and -10 °C).

(3) The temperature profile in CSA-based samples cured in the sand was notably lower than that of the same mixture cured in air. For example, the maximum temperature difference caused by different curing modes (i.e., curing in air and curing in sand) was 28 °C in the sample with dimensions of Ø100×200mm cured at 0 °C. Based on this, the authors suggest curing samples in cold soil or sand when investigating the performance of cement-based mixtures used in permafrost regions.

(4) The temperature profile in the CSA-based sample was more sensitive to the increase in sample size when compared with OPC-based samples. The maximum temperature in the CSA-based sample cured in sand at 0 °C increased from 20 °C to 56.3 °C when the sample diameter was increased from 100 mm to 300 mm, while the difference caused by the same change in OPC-based samples was only 6.7 °C.

(5) The temperature gradient in CSA-based sample was more significant than that in OPC-based sample. When cured at 0 °C in the sand, the temperature difference can be ~45 °C between the points at the center and near the edge of CSA-based sample with the dimension of Ø300×600mm, while this difference in OPC-based sample was less than 4 °C. Precautions are needed to control the thermal cracks when CSA cement-based mixtures are used in cold temperatures, even if the structure size is small.

Chapter 7. Conclusion and future work

7.1. Conclusions

Overall, this thesis developed calcium sulfoaluminate (CSA) cement mixtures that can achieve fast strength development and has high resistance to early-age frost damage for permafrost region applications. In this study, CSA cement-based mixtures were prepared and cured in cold sands to mimic the influence of permafrost; then experiments and numerical modeling were applied to evaluate and understand the performance of CSA cement-based mixtures cured at permafrost environments. The findings provide a new solution to accelerate strength development and prevent early-age frost damage when cement-based mixtures are applied in permafrost regions.

The main concluding remarks of this thesis are enumerated as follows:

(1) At a normal temperature (23 °C), the hydration of CSA cement is very fast. In anhydrous CSA cement, the ye'elimite and anhydrite contents were 26.3% and 12.8%, respectively. After hydrated for 2 hours, the unreacted contents of ye'elimite and anhydrite decreased to 6.1% and 2.5%, respectively, indicating that most of the ye'elimite and anhydrite were reacted within 2 hours.

(2) The hydration reaction of CSA cement remained fast when cured at cold temperatures (e.g., 0 °C and -10 °C). This can be found in the thermogravimetric analysis (TGA) results. For example, the weight losses of 1-day CSA cement-based samples during the TGA tests were 20.2%, 20.0%, and 20.5% when curing temperatures were 20 °C, 0 °C, and -10 °C, respectively, while those for OPC-based samples were 13.7%, 9.2%, and 7.7%, respectively.

(3) Owing to the fast hydration reaction, CSA cement-based mixtures can achieve rapid strength development at cold temperatures. For example, CSA cement-based samples with the dimension of Ø65×130mm can achieve an unconfined compressive strength (UCS) of 15.5 MPa at 1 day when cured at -10 °C, while that for OPC-based samples was only 1.7 MPa.

(4) CSA cement-based mixtures showed high resistance to early-age frost damage. After re-curing, the CSA cement-based mixture that was exposed to -10 °C at early ages achieved 117% of the UCS of its reference, which was directly cured at 23 °C. The higher strength was attributed to the fact that the re-cured CSA cement-based mixtures had a finer pore structure. However, re-cured OPC-based mixtures only achieved about half of the UCS of their references even if they reached the same hydration degree, showing that OPC-based mixtures experienced severe early-age frost damage.

(5) CSA cement-based thermal insulation materials were developed for permafrost region applications. The 28-day thermal conductivity of CSA cement-based mortars decreased exponentially from 0.97 ± 0.01 W/mK, to 0.57 ± 0.02 W/mK, to 0.29 ± 0.02 W/mK, and to 0.13 ± 0.002 W/mK when the aggregate replacement ratio increased from 0% to 30%, 60%, and 100%. These CSA cement-based mixtures can work as thermal insulation materials for mitigating the heat exchange among permafrost, cement-based mixtures, and air when used for rock support in permafrost regions or reducing the heat loss to the outdoor environment when used as building materials.

(6) A numerical modeling method has been established to model the temperature profiles in hardening CSA cement-based mixtures for permafrost region applications. The root mean square error (RMSE) between the modeled and measured temperature profiles was smaller than 1.3 °C,

indicating that the model can accurately predict the temperature profiles in hardening CSA cement-based mixtures.

(7) The temperature profile in CSA-based samples cured in the sand was notably lower than that of the same mixture cured in air. For example, the maximum temperature difference caused by different curing modes (i.e., curing in air and curing in sand) was 28 °C in the sample with dimensions of Ø100×200mm cured at 0 °C. The results suggest that samples should be cured in cold soil or sand when investigating the performance of cement-based mixtures used in permafrost regions.

(8) The temperature profile in the CSA-based sample was more sensitive to the increase in sample size when compared with OPC-based samples. In addition, the temperature gradient in CSA-based sample was more significant than that in OPC-based sample. When cured at 0 °C in the sand, the temperature difference can be ~45 °C between the points at the center and near the edge of the CSA-based sample with the dimension of Ø300×600mm, while this difference in the OPC-based sample was less than 4 °C. Precautions are needed to control the thermal cracks when CSA cement-based mixtures are used in cold temperatures, even if the structure size is small.

7.2. Key contributions

The findings from this Ph.D. program are significant for the engineering society in permafrost regions. The key contributions of this Ph.D. program are listed as follows:

(1) CSA cement-based mixtures were innovatively developed to achieve immediate support to the targets in permafrost regions; unique experiments were conducted to access the influence of permafrost on the hydration reaction and strength development of CSA cement-based mixtures.

The results show that CSA cement-based mixtures can achieve fast hydration and rapid strength development in permafrost environments. This finding provides a new solution to accelerate the strength development of cement-based mixtures when used in permafrost regions, which will bring enormous safety and economic benefits.

(2) Another significant contribution goes to the evaluation of CSA cement for preventing early-age frost damage. This evaluation has never been done before in the literature. Applying CSA cement at cold temperatures can prevent the early-age frost damage, ensure the quality of the cement-based structures, which is significant for the construction community in the cold regions.

(3) Having filled a knowledge gap, the thermal properties of CSA-based mixtures were measured, and CSA cement-based thermal insulation materials were developed by incorporating expanded perlite. CSA cement-based mixtures can be used for mitigating the heat exchange among permafrost, cement-based mixtures, and air when used for rock support in permafrost regions or reducing the heat loss to the outdoor environment when used as building materials.

(4) For the first time, an accurate numerical model was developed to predict the temperature profiles in hardening CSA cement-based mixtures cured in permafrost environments, which can help understand the hydration reaction and strength development of CSA-based mixtures used in permafrost regions. This numerical model can also guide future practical applications of CSA cement-based mixtures in permafrost regions.

(5) This study created an innovative curing mode (curing in cold sand) to investigate the influence of permafrost on the performance of cement-based mixtures in a laboratory. In addition, a numerical model was used to compare the influence of different curing modes (curing in cold sand and curing in cold air) on the temperature profiles of cement-based mixtures. The

results revealed that samples should be cured in cold soil or sand when investigating the performance of cement-based mixtures used in permafrost regions, especially for CSA cement-based mixtures.

(6) An important suggestion was drawn from numerical modeling: precautions are needed to control the thermal cracks when CSA cement-based mixtures are used in cold temperatures since the temperature gradient in the CSA cement-based mixtures is high even if the structure size is small.

7.3. Limitations and future work

Although this study developed CSA cement-based mixtures that can achieve fast strength development and have high resistance to early-age frost damage when cured in permafrost environments, there are still some limitations in the current study. Further work is needed in the future.

(1) In this Ph.D. program, quantitative X-ray diffraction (QXRD) was only conducted on the CSA cement-based samples cured at a normal temperature (23 °C). The hydration reaction of CSA cement samples cured at cold temperatures was characterized with thermogravimetric analysis, which is a semi-quantitative analysis method. In future studies, a quantitative analysis method should be used to better understand the influence of permafrost environments on the hydration of CSA cement.

(2) In this study, experiments were carried out in a laboratory condition on small size samples (e.g., Ø65×130mm cylindrical samples). The sample size may be very different from the structure size of real applications. Using a small sample may underestimate the rate of hydration reaction and strength development of CSA cement-based mixtures. For example, the results from

numerical modeling show that the temperature profiles in the hardening CSA cement-based mixtures increased with the increase of sample size; a higher temperature can accelerate the hydration reaction and strength development. Therefore, further studies should be carried out to investigate the influence of sample sizes on the strength development of CSA cement-based structures cured in permafrost environments, and field testing is needed to evaluate the performance of CSA cement-based mixture in a real permafrost condition.

(3) Substituting OPC with CSA cement will increase the cost of cement since the price of CSA cement is about 2-4 times of the price of OPC. Blending OPC with CSA cement is a potential solution to reduce the cost of cementing. Therefore, investigations should be conducted to explore the possibility of using OPC-CSA blends to achieve fast strength development and high resistance to early-age frost damage in permafrost regions. Experiments are needed to investigate the hydration reaction, strength development, and resistance to early-age frost damage of OPC-CSA blends-based mixtures cured in permafrost regions.

(4) The results from numerical modeling indicate that the temperature gradient is high even if in CSA cement-based samples with a small size (e.g., Ø300×600mm). Therefore, further studies should be conducted to evaluate the risks of thermal cracking in hardening CSA cement-based mixtures, and measures should be proposed to reduce the risk of thermal cracking without compromising the ability to achieve fast strength development and the resistance to early-frost damage.

(5) The hydration heat can cause a high temperature in hardening CSA cement-based mixtures. When CSA cement-based mixtures are used in permafrost regions, it is worth evaluating the influence of CSA cement hydration heat on the stability of permafrost.

(6) The developed model can predict temperature profiles in hardening CSA cement-based mixtures; however, the prediction of strength development is not included. More work is recommended to understand the correlation among temperature profiles, hydration degree, and strength development; then a model should be developed to predict the strength development of CSA cement-based mixtures used at permafrost regions.

(7) In this study, the durability (the ability to resist weathering action, chemical attack, and abrasion) of CSA cement-based mixtures was not investigated, and research about the durability of CSA cement-based mixtures has rarely been reported in the literature. More investigations are required to understand the durability of CSA cement-based mixtures.

(8) In future studies, different admixtures (e.g., retarders, accelerators, and superplasticizers) for CSA cement should be developed. Studies should be performed to understand their influence on the performance of CSA cement-based mixtures used in permafrost regions.

Bibliography

ACI. (2007). ACI 207.2 R-07, Report on Thermal and Volume Change Effects on Cracking of Mass Concrete American Concrete Institute.

ACI. (2009a). ACI 213R-03, Guide for Structural Lightweight-Aggregate Concrete *ACI Manual of Concrete Practice* (pp. 1-20).

ACI. (2009b). ACI 506.5R-09, Guide for Specifying Underground Shotcrete (pp. 5-52). Farmington Hills, MI, USA: ACI Committee 506.

ACI. (2010). ACI 306R-10, Guide to cold weather concreting (pp. 2-22). Farmington Hills, Michigan, USA.

Administration, U. S. F. H., & McCullough, B. F. (1999). *Fast-track paving: concrete temperature control and traffic opening criteria for bonded concrete overlays*: Citeseer.

Akyurt, M., Zaki, G., & Habeebullah, B. (2002). Freezing phenomena in ice–water systems. *Energy conversion and management, 43*(14), 1773-1789. doi:https://doi.org/10.1016/S0196-8904(01)00129-7

American Concrete Institute. (2005). ACI 506.5R-09, Guide for Specifying Underground Shotcrete (pp. 5-52). Farmington Hills, MI, USA: ACI Committee 506.

Anton, K. S., & Kevin, J. F. (2005). Heat of Hydration Models for Cementitious Materials. *ACI Materials Journal, 102*(1). doi:10.14359/14246

Asadi, I., Shafigh, P., Hassan, Z. F. B. A., & Mahyuddin, N. B. (2018). Thermal conductivity of concrete–A review. *Journal of Building Engineering, 20*, 81-93.

ASTM Interantional. (2015). ASTM C1437-15, Standard Test Method for Flow of Hydraulic Cement Mortar *West Conshohocken, PA, USA*.

ASTM International. (2011). ASTM C39/C39M-18, Standard test method for compressive strength of cylindrical concrete specimens (pp. 1-8).

ASTM International. (2013a). ASTM C191-13, Standard Test Methods for Time of Setting of Hydraulic Cement by Vicat Needle *ASTM International: West Conshohocken, PA, USA*.

ASTM International. (2013b). ASTM C642-13, Standard test method for density, absorption, and voids in hardened concrete *West Conshohocken, PA: ASTM International*.

ASTM International. (2016a). ASTM C90-16a, Standard Specification for Loadbearing Concrete Masonry Units. West Conshohocken, PA: ASTM International.

ASTM International. (2016b). ASTM C192 / C192M-16a, Standard Practice for Making and Curing Concrete Test Specimens in the Laboratory

West Conshohocken, PA.

ASTM international. (2016c). ASTM C597-16, Standard test Method for pulse velocity through concrete. West Conshohochen, PA: ASTM West Conshohocken.

ASTM International. (2017). ASTM C129-17, Standard Specification for Nonloadbearing Concrete Masonry Units. West Conshohocken, PA: ASTM International.

ASTM International. (2018). ASTM C39/C39M-18, Standard test method for compressive strength of cylindrical concrete specimens (pp. 1-8).

ASTM International. (2019). C150/C150M-19, Standard Specification for Portland Cement *American Society for Testing and Materials: West Conshohocken, PA, USA*: ASTM International.

Azenha, M., & Faria, R. (2008). Temperatures and stresses due to cement hydration on the R/C foundation of a wind tower—A case study. *Engineering Structures, 30*(9), 2392-2400.

Ballim, Y. (2004). A numerical model and associated calorimeter for predicting temperature profiles in mass concrete. *Cement and Concrete Composites, 26*(6), 695-703.

Ballou, M. (2013). Rapid-Setting Cement in Shotcrete. *shotcrete magzine,* 46-47.

Barna, L. A., Seman, P. M., & Korhonen, C. J. (2011). Energy-efficient approach to cold-weather concreting. *Journal of Materials in Civil Engineering, 23*(11), 1544-1551.

Bentz, D. P., & Jensen, O. M. (2004). Mitigation strategies for autogenous shrinkage cracking. *Cement & Concrete Composites, 26*(6), 677-685. doi:10.1016/s0958-9465(03)00045-3

Beretka, J., de Vito, B., Santoro, L., Sherman, N., & Valenti, G. L. (1993). Hydraulic behaviour of calcium sulfoaluminate-based cements derived from industrial process wastes. *Cement and Concrete Research, 23*(5), 1205-1214. doi:https://doi.org/10.1016/0008-8846(93)90181-8

Bernhardt, C. J. (1956). Damage Due to Freezing of Fresh Concrete. *Journal Proceedings, 52*(1). doi:10.14359/11616

Bescher, E., & Kim, J. (2019). *Belitic Calcium Sulfoaluminate Cement: History, Chemistry, Performance, and Use in the United States*. Paper presented at the 1st international conference on innovation in low-carbon cement& concrete technology, Londun, United Kingom.

Beya, F. K., Mbonimpa, M., Belem, T., Li, L., Marceau, U., Kalonji, P. K., . . . Ouellet, S. (2019). Mine backfilling in the permafrost, Part I: Numerical prediction of thermal curing conditions within the cemented paste backfill matrix. *Minerals, 9*(3), 165.

Biggar, K. W., Sego, D. C., & Noel, M. M. (1993). Laboratory and field performance of high alumina cement-based grout for piling in permafrost. *Canadian Journal of Civil Engineering, 20*(1), 100-106. doi:10.1139/l93-011

Bissonnette, B. t., Pierre, P., & Pigeon, M. (1999). Influence of key parameters on drying shrinkage of cementitious materials. *Cement and Concrete Research, 29*(10), 1655-1662. doi:https://doi.org/10.1016/S0008-8846(99)00156-8

Bobko, C. P., Zadeh, V. Z., & Seracino, R. (2015). Improved Schmidt Method for Predicting Temperature Development in Mass Concrete. *ACI Materials Journal, 112*(4).

Bogas, J. A., Gomes, M. G., & Gomes, A. (2013). Compressive strength evaluation of structural lightweight concrete by non-destructive ultrasonic pulse velocity method. *Ultrasonics, 53*(5), 962-972. doi:https://doi.org/10.1016/j.ultras.2012.12.012

Boumiz, A., Vernet, C., & Tenoudji, F. C. (1996). Mechanical properties of cement pastes and mortars at early ages: Evolution with time and degree of hydration. *Advanced Cement Based Materials, 3*(3), 94-106. doi:https://doi.org/10.1016/S1065-7355(96)90042-5

Brusletto, T. B. K. (2018). *Sprayed Concrete used as Avalanche Securing of road in the open day during Freezing Conditions*. Paper presented at the 8th International Symposium on Sprayed Concrete – Modern Use of Wet Mix Srayed Concrete for Underground Support, Trondheim, Norway.

Bullard, J. W. (2008). A determination of hydration mechanisms for tricalcium silicate using a kinetic cellular automaton model. *Journal of the American Ceramic Society, 91*(7), 2088-2097. doi: https://doi.org/10.1111/j.1551-2916.2008.02419.x

Bullard, J. W., Jennings, H. M., Livingston, R. A., Nonat, A., Scherer, G. W., Schweitzer, J. S., . . . Thomas, J. J. (2011). Mechanisms of cement hydration. *Cement and Concrete Research, 41*(12), 1208-1223. doi:https://doi.org/10.1016/j.cemconres.2010.09.011

Bullerjahn, F., Zajac, M., Ben Haha, M., & Scrivener, K. L. (2019). Factors influencing the hydration kinetics of ye'elimite; effect of mayenite. *Cement and Concrete Research, 116*, 113-119. doi:https://doi.org/10.1016/j.cemconres.2018.10.026

Burris, L. E., & Kurtis, K. E. (2018). Influence of set retarding admixtures on calcium sulfoaluminate cement hydration and property development. *Cement and Concrete Research, 104*, 105-113. doi:https://doi.org/10.1016/j.cemconres.2017.11.005

Célestin, J. C. H., & Fall, M. (2009). Thermal conductivity of cemented paste backfill material and factors affecting it. *International Journal of Mining, Reclamation and Environment, 23*(4), 274-290. doi:https://doi.org/10.1080/17480930902731943

Chen, P., Jin, Z. Q., & Fan, J. F. (2017). *Static Modulus of Ettringite in Different Environment.* Paper presented at the Key Engineering Materials.

Cheung, J., Jeknavorian, A., Roberts, L., & Silva, D. (2011). Impact of admixtures on the hydration kinetics of Portland cement. *Cement and Concrete Research, 41*(12), 1289-1309. doi:https://doi.org/10.1016/j.cemconres.2011.03.005

Choi, S.-H., Lee, H.-S., Choi, H.-K., Kim, H.-c., Min, T.-B., & Ismail, M. A. (2017). Experimental research on development of heated form incorporating exothermic reaction powder to protect concrete in cold weather. *Construction and Building Materials, 135*, 30-36. doi:http://dx.doi.org/10.1016/j.conbuildmat.2016.12.136

Corr, D. J., Monteiro, P. J., & Bastacky, J. (2003). Observations of ice lens formation and frost heave in young Portland cement paste. *Cement and Concrete Research, 33*(10), 1531-1537.

Cuce, E., Cuce, P. M., Wood, C. J., & Riffat, S. B. (2014). Toward aerogel based thermal superinsulation in buildings: A comprehensive review. *Renewable and Sustainable Energy Reviews, 34*, 273-299. doi:https://doi.org/10.1016/j.rser.2014.03.017

Cuesta, A., Zea-Garcia, J. D., Londono-Zuluaga, D., Angeles, G., Santacruz, I., Vallcorba, O., . . . Aranda, M. A. (2018). Multiscale understanding of tricalcium silicate hydration reactions. *Scientific reports, 8*(1), 8544. doi:https://doi.org/10.1038/s41598-018-26943-y

Çullu, M., & Arslan, M. (2013). The effects of antifreeze use on physical and mechanical properties of concrete produced in cold weather. *Composites Part B: Engineering, 50*, 202-209.

Damidot, D., Bellmann, F., Möser, B., & Sovoidnich, T. (2007). Calculation of the dissolution rate of tricalcium silicate in several electrolyte compositions. *Cement Wapno Beton, 12*(74), 2.

Deboucha, W., Leklou, N., Khelidj, A., & Oudjit, M. N. (2017). Hydration development of mineral additives blended cement using thermogravimetric analysis (TGA): Methodology of calculating the degree of hydration. *Construction and Building Materials, 146*, 687-701. doi:https://doi.org/10.1016/j.conbuildmat.2017.04.132

Demirboğa, R., Karagöl, F., Polat, R., & Kaygusuz, M. A. (2014). The effects of urea on strength gaining of fresh concrete under the cold weather conditions. *Construction and Building Materials, 64*, 114-120. doi:https://doi.org/10.1016/j.conbuildmat.2014.04.008

Dodson, V. H. (2013). *Concrete admixtures*: Springer Science & Business Media.

Gandage, A. S., Rao, V. V., Sivakumar, M., Vasan, A., Venu, M., & Yaswanth, A. (2013). Effect of perlite on thermal conductivity of self compacting concrete. *Procedia-Social and Behavioral Sciences, 104*, 188-197. doi:https://doi.org/10.1016/j.sbspro.2013.11.111

García-Maté, M., Angeles, G., León-Reina, L., Losilla, E. R., Aranda, M. A., & Santacruz, I. (2015). Effect of calcium sulfate source on the hydration of calcium sulfoaluminate eco-

cement. *Cement and Concrete Composites, 55*, 53-61. doi:https://doi.org/10.1016/j.cemconcomp.2014.08.003

García-Maté, M., Londono-Zuluaga, D., De la Torre, A. G., Losilla, E. R., Cabeza, A., Aranda, M. A., & Santacruz, I. (2016). Tailored setting times with high compressive strengths in bassanite calcium sulfoaluminate eco-cements. *Cement and Concrete Composites, 72*, 39-47. doi:https://doi.org/10.1016/j.cemconcomp.2016.05.021

Ge, Z. (2005). Predicting temperature and strength development of the field concrete.

Giraudo, N., Bergdolt, S., Laye, F., Krolla, P., Lahann, J., & Thissen, P. (2018). Dehydration and dehydroxylation of CSH phases synthesized on silicon wafers. *Applied Surface Science, 433*, 589-595. doi:https://doi.org/10.1016/j.apsusc.2017.10.039

Glasser, F. P., Marchand, J., & Samson, E. (2008). Durability of concrete — Degradation phenomena involving detrimental chemical reactions. *Cement and Concrete Research, 38*(2), 226-246. doi:https://doi.org/10.1016/j.cemconres.2007.09.015

Glasser, F. P., & Zhang, L. (2001). High-performance cement matrices based on calcium sulfoaluminate–belite compositions. *Cement and Concrete Research, 31*(12), 1881-1886. doi:https://doi.org/10.1016/S0008-8846(01)00649-4

Gruber, S. (2012). Derivation and analysis of a high-resolution estimate of global permafrost zonation. *The Cryosphere, 6*(1), 221. doi:10.5194/tc-6-221-2012

Guan, Y., Gao, Y., Sun, R., Won, M. C., & Ge, Z. (2017). Experimental study and field application of calcium sulfoaluminate cement for rapid repair of concrete pavements. *Frontiers of Structural and Civil Engineering, 11*(3), 338-345. doi:https://doi.org/10.1007/s11709-017-0411-0

Güneyli, H., Karahan, S., & Güneyli, A. (2017). Water content and temperature effect on ultrasonic pulse velocity of concrete. *Russian Journal of Nondestructive Testing, 53*(2), 159-166.

Guo, C. X., Yang, F. J., Wu, Y. P., Ma, X. N., & Jing, Y. F. (2011a). Influence of concrete hydration heat on the melting and refreezing processes of surrounding rock of tunnels in the permafrost region. *Tiedao Xuebao/Journal of the China Railway Society, 33*(11), 106-110. doi:10.3969/j.issn.1001-8360.2011.11.018

Guo, J. B., Liu, L., & Wang, Q. (2014). Application self-regulating heating cable curing of concrete in winter. *Applied Mechanics and Materials, 638*, 1531-1535. doi:https://doi.org/10.4028/www.scientific.net/AMM.638-640.1531

Guo, L., Guo, L., Zhong, L., & Zhu, Y. (2011b). Thermal conductivity and heat transfer coefficient of concrete. *Journal of Wuhan University of Technology-Mater. Sci. Ed., 26*(4), 791-796. doi:10.1007/s11595-011-0312-3

Gustafsson, S. E. (1991). Transient plane source techniques for thermal conductivity and thermal diffusivity measurements of solid materials. *Review of scientific instruments, 62*(3), 797-804. doi:https://doi.org/10.1063/1.1142087

Gwon, S., Jang, S., & Shin, M. (2018). Combined effects of set retarders and polymer powder on the properties of calcium sulfoaluminate blended cement systems. *Materials, 11*(5), 825. doi:https://doi.org/10.3390/ma11050825

Hanein, T., Galvez-Martos, J.-L., & Bannerman, M. N. (2018). Carbon footprint of calcium sulfoaluminate clinker production. *Journal of Cleaner Production, 172*, 2278-2287. doi:https://doi.org/10.1016/j.jclepro.2017.11.183

Harrison, T. (1981). *Early-age thermal crack control in concrete*.

Hassn, A., Aboufoul, M., Wu, Y., Dawson, A., & Garcia, A. (2016). Effect of air voids content on thermal properties of asphalt mixtures. *Construction and Building Materials, 115*, 327-335. doi:https://doi.org/10.1016/j.conbuildmat.2016.03.106

Hauptmann, R., Doll, S., Harnau, M., & Schweizerhof, K. (2001). Solid-shell'elements with linear and quadratic shape functions at large deformations with nearly incompressible materials. *Computers & Structures, 79*(18), 1671-1685.

Höhlig, B., Schmidt, D., Mechtcherine, V., Hempel, S., Schröfl, C., Trommler, U., & Roland, U. (2015). Effects of dielectric heating of fresh concrete on its microstructure and strength in the hardened state. *Construction and Building Materials, 81*, 24-34. doi:https://doi.org/10.1016/j.conbuildmat.2015.02.004

Holman, J. P. (2001). Heat transfer, eighth SI metric edition. *Mc Gran–Hill Book Company*.

Hu, X., Banks, J., Guo, Y., Huang, G., & Liu, W. V. (2021). Effects of temperature-dependent property variations on the output capacity prediction of a deep coaxial borehole heat exchanger. *Renewable Energy, 165*, 334-349.

Hu, X., Banks, J., Wu, L., & Liu, W. V. (2020). Numerical modeling of a coaxial borehole heat exchanger to exploit geothermal energy from abandoned petroleum wells in Hinton, Alberta. *Renewable Energy, 148*, 1110-1123.

Hu, Y., Li, W., Ma, S., & Shen, X. (2017). Influence of borax and citric acid on the hydration of calcium sulfoaluminate cement. *Chemical Papers, 71*(10), 1909-1919. doi:https://doi.org/10.1007/s11696-017-0185-9

Huang, C.-X. (1999). The three dimensional modelling of thermal cracks in concrete structure. *Materials and Structures, 32*(9), 673-678.

Huang, G., Pudasainee, D., Gupta, R., & Liu, W. V. (2019). Hydration reaction and strength development of calcium sulfoaluminate cement-based mortar cured at cold temperatures. *Construction and Building Materials, 224*, 493-503. doi:https://doi.org/10.1016/j.conbuildmat.2019.07.085

Huang, G., Pudasainee, D., Gupta, R., & Liu, W. V. (2020a). The performance of calcium sulfoaluminate cement for preventing early-age frost damage. *Construction and Building Materials, 254*, 119322. doi:https://doi.org/10.1016/j.conbuildmat.2020.119322

Huang, G., Pudasainee, D., Gupta, R., & Liu, W. V. (2020b). Utilization and performance evaluation of molasses as a retarder and plasticizer for calcium sulfoaluminate cement-based mortar. *Construction and Building Materials, 243*, 118201. doi:https://doi.org/10.1016/j.conbuildmat.2020.118201

Huang, G., Pudasainee, D., Gupta, R., & Liu, W. V. (2021). Thermal properties of calcium sulfoaluminate cement-based mortars incorporated with expanded perlite cured at cold temperatures. *Construction and Building Materials*.

IEA. (2019). *Tracking Buildings*. Retrieved from Paris: https://www.iea.org/reports/tracking-buildings

Ikpong, A. A. (1993). The relationship between the strength and non-destructive parameters of rice husk ash concrete. *Cement and Concrete Research, 23*(2), 387-398. doi:https://doi.org/10.1016/0008-8846(93)90104-H

Ilc, A., Turk, G., Kavčič, F., & Trtnik, G. (2009). New numerical procedure for the prediction of temperature development in early age concrete structures. *Automation in Construction, 18*(6), 849-855.

Ioannidou, K., Kanduč, M., Li, L., Frenkel, D., Dobnikar, J., & Del Gado, E. (2016). The crucial effect of early-stage gelation on the mechanical properties of cement hydrates. *Nature communications, 7*, 12106. doi:DOI: 10.1038/ncomms12106

J.M. Ruiz, S. I. G. Q. X. J. C. D. G. K. C., & Rasmussen, R. O. HIPERPAV III - An Enhanced FHWA Software for Simulating Early-Age Concrete Pavement Behaviors. *ACI Symposium Publication, 266*. doi:10.14359/51663268

Jelle, B. P. (2011). Traditional, state-of-the-art and future thermal building insulation materials and solutions – Properties, requirements and possibilities. *Energy and Buildings, 43*(10), 2549-2563. doi:https://doi.org/10.1016/j.enbuild.2011.05.015

Jennings, H., & Pratt, P. (1979). An experimental argument for the existence of a protective membrane surrounding Portland cement during the induction period. *Cement and Concrete Research, 9*(4), 501-506. doi:https://doi.org/10.1016/0008-8846(79)90048-6

Jeong, Y., Hargis, C. W., Chun, S.-C., & Moon, J. (2018). The effect of water and gypsum content on strätlingite formation in calcium sulfoaluminate-belite cement pastes. *Construction and Building Materials, 166*, 712-722. doi:https://doi.org/10.1016/j.conbuildmat.2018.01.153

Jiang, H., Yi, H., Yilmaz, E., Liu, S., & Qiu, J. (2020). Ultrasonic evaluation of strength properties of cemented paste backfill: Effects of mineral admixture and curing temperature. *Ultrasonics, 100*, 105983. doi:https://doi.org/10.1016/j.ultras.2019.105983

Jones, B. D., Li, S., & Ahuja, V. *Early strength monitoring of shotcrete using thermal imaging*.

Juenger, M. C. G., Winnefeld, F., Provis, J. L., & Ideker, J. H. (2011). Advances in alternative cementitious binders. *Cement and Concrete Research, 41*(12), 1232-1243. doi:https://doi.org/10.1016/j.cemconres.2010.11.012

Karagöl, F., Demirboğa, R., Kaygusuz, M. A., Yadollahi, M. M., & Polat, R. (2013). The influence of calcium nitrate as antifreeze admixture on the compressive strength of concrete exposed to low temperatures. *Cold Regions Science and Technology, 89*, 30-35. doi:10.1016/j.coldregions.2013.02.001

Karagol, F., Demirboga, R., & Khushefati, W. H. (2015). Behavior of fresh and hardened concretes with antifreeze admixtures in deep-freeze low temperatures and exterior winter conditions. *Construction and Building Materials, 76*, 388-395. doi:https://doi.org/10.1016/j.conbuildmat.2014.12.011

Karakoç, M. B., & Demirboga, R. (2010). HSC with expanded perlite aggregate at wet and dry curing conditions. *Journal of materials in civil engineering, 22*(12), 1252-1259. doi:https://doi.org/10.1061/(ASCE)MT.1943-5533.0000134

Ke, G. J., & Zhang, J. (2020). Effects of Retarding Admixture, Superplasticizer and Supplementary Cementitious Material on the Rheology and Mechanical Properties of High Strength Calcium Sulfoaluminate Cement Paste. *Journal of Advanced Concrete Technology, 18*(1), 17-26. doi:10.3151/jact.18.17

Keen, A. (1993). *Zinc mining in permafrost at Polaris*. Paper presented at the World Zinc 93:Proceedings of the Interational Symposium on Zinc., Hobart, Tasmania.

Khan, M. I. (2002). Factors affecting the thermal properties of concrete and applicability of its prediction models. *Building and Environment, 37*(6), 607-614. doi:https://doi.org/10.1016/S0360-1323(01)00061-0

Khokholov, Y. A., & Kurilko, A. (2004). Heat exchange of rock and filling masses in kimberlite mining. *Journal of Mining Science, 40*(1), 31-36.

Kičaitė, A., Pundienė, I., & Skripkiūnas, G. (2017). *The influence of calcium nitrate on setting and hardening rate of Portland cement concrete at different temperatures.* Paper presented at the IOP Conference Series: Materials Science and Engineering.

Kim, H.-C., Min, T.-B., Mun, Y.-B., Kim, J.-Y., Choi, H.-K., & Lee, H.-s. (2016). Effect of high early strength cement and accelerator concentrations on the low-temperature compressive strength of concrete. *Journal of Ceramic Processing Research, 17*(6), 641-647.

Kim, K.-H., Jeon, S.-E., Kim, J.-K., & Yang, S. (2003). An experimental study on thermal conductivity of concrete. *Cement and Concrete Research, 33*(3), 363-371. doi:https://doi.org/10.1016/S0008-8846(02)00965-1

Kim, S. G. (2010). Effect of heat generation from cement hydration on mass concrete placement.

Klemczak, B., & Knoppik-Wróbel, A. (2011). Early age thermal and shrinkage cracks in concrete structures-influence of geometry and dimensions of a structure. *Architecture–Civil Engineering–Environment, 4*(3), 55-70.

Korhonen, C. J., & Cortez, E. R. (1991). Antifreeze admixtures for cold weather concreting. *Concrete International, 13*(3), 38-41.

Kosmatka, S. H., Kerkhoff, B., & Panarese, W. C. (2011). *Design and control of concrete mixtures*: Portland Cement Assoc.

Kramar, S., Žibret, L., Fidanchevska, E., Jovanov, V., Angjusheva, B., & Ducman, V. (2019). Use of fly ash and phosphogypsum for the synthesis of belite-sulfoaluminate clinker. *Materiales de Construcción, 69*(333), 176.

Kumar, R., Prasad, A., Mahure, N., Sharma, P., Gupta, S., & Ratnam, M. (2014). Concreting at Low Ambient Temperatures at Salma Dam Project Afghanistan-A Case Study. *International Journal of Emerging Technology and Advanced Engineering,(IJETAE), 4*(2), 916-920.

Latha, P. K., Darshana, Y., & Venugopal, V. (2015). Role of building material in thermal comfort in tropical climates – A review. *Journal of Building Engineering, 3*, 104-113. doi:https://doi.org/10.1016/j.jobe.2015.06.003

Le Saoût, G., Lothenbach, B., Hori, A., Higuchi, T., & Winnefeld, F. (2013). Hydration of Portland cement with additions of calcium sulfoaluminates. *Cement and Concrete Research, 43*, 81-94. doi:https://doi.org/10.1016/j.cemconres.2012.10.011

Lee, G.-C., Han, M.-C., Baek, D.-H., & Koh, K.-T. (2012). Effect of heat curing methods on the temperature history and strength development of slab concrete for nuclear power plant structures in cold climates. *Nuclear Engineering and Technology, 44*(5), 523-534. doi:https://doi.org/10.5516/NET.09.2011.074

Lee, Y., Choi, M.-S., Yi, S.-T., & Kim, J.-K. (2009). Experimental study on the convective heat transfer coefficient of early-age concrete. *Cement and Concrete Composites, 31*(1), 60-71.

Legates, D. R. (2005). Latent Heat. In J. E. Oliver (Ed.), *Encyclopedia of World Climatology* (pp. 450-451). Dordrecht: Springer Netherlands.

Lencis, U., Udris, A., & Korjakins, A. (2013). Moisture effect on the ultrasonic pulse velocity in concrete cured under normal conditions and at elevated temperature. *Construction Science, 14*(1), 71-78.

Lesage, K., Cizer, Ö., Desmet, B., Vantomme, J., De Schutter, G., & Vandewalle, L. (2015). Plasticising mechanism of sodium gluconate combined with PCE. *Advances in Cement Research, 27*(3), 163-174.

Li, G., Zhang, J., Song, Z., Shi, C., & Zhang, A. (2018). Improvement of workability and early strength of calcium sulphoaluminate cement at various temperature by chemical

admixtures. *Construction and Building Materials, 160*, 427-439. doi:https://doi.org/10.1016/j.conbuildmat.2017.11.076
Li, L., Wang, R., & Zhang, S. (2019). Effect of curing temperature and relative humidity on the hydrates and porosity of calcium sulfoaluminate cement. *Construction and Building Materials, 213*, 627-636. doi:https://doi.org/10.1016/j.conbuildmat.2019.04.044
Li, Q., Ito, K., Wu, Z., Lowry, C. S., & Loheide II, S. P. (2009). COMSOL Multiphysics: A novel approach to ground water modeling. *Groundwater, 47*(4), 480-487.
Li, S., Jones, B., Thorpe, R., & Davis, M. (2016). An investigation into the thermal conductivity of hydrating sprayed concrete. *Construction and Building Materials, 124*, 363-372. doi:https://doi.org/10.1016/j.conbuildmat.2016.07.091
Li, S., Niu, F., Lai, Y., Pei, W., & Yu, W. (2017). Optimal design of thermal insulation layer of a tunnel in permafrost regions based on coupled heat-water simulation. *Applied Thermal Engineering, 110*, 1264-1273.
Liao, Y., Wei, X., & Li, G. (2011). Early hydration of calcium sulfoaluminate cement through electrical resistivity measurement and microstructure investigations. *Construction and Building Materials, 25*(4), 1572-1579. doi:https://doi.org/10.1016/j.conbuildmat.2010.09.042
Liu, F., Liu, L., & Feng, X. (2005). Separation of acetone–butanol–ethanol (ABE) from dilute aqueous solutions by pervaporation. *Separation and Purification Technology, 42*(3), 273-282. doi:https://doi.org/10.1016/j.seppur.2004.08.005
Liu, L., Shen, D., Chen, H., Sun, W., Qian, Z., Zhao, H., & Jiang, J. (2014a). Analysis of damage development in cement paste due to ice nucleation at different temperatures. *Cement and Concrete composites, 53*, 1-9.
Liu, W., Apel, D., & Bindiganavile, V. (2011). Thermal characterisation of a lightweight mortar containing expanded perlite for underground insulation. *International Journal of Mining and Mineral Engineering, 3*(1), 55-71. doi:https://doi.org/10.1504/IJMME.2011.041449
Liu, W., Apel, D., & Bindiganavile, V. (2014b). Thermal properties of lightweight dry-mix shotcrete containing expanded perlite aggregate. *Cement and Concrete Composites, 53*, 44-51. doi:https://doi.org/10.1016/j.cemconcomp.2014.06.003
Liu, W., Apel, D., Bindiganavile, V., & Szymanski, J. (2016). Analytical and numerical modeling for the effects of thermal insulation in underground tunnels. *International journal of mining science and technology, 26*(2), 267-276.
Liu, W., Yu, W., Yi, X., Chen, L., Han, F., & Hu, D. (2015). Thermal regime of frozen soil foundation affected by concrete base of transmission line tower on the Tibetan Plateau. *Applied Thermal Engineering, 75*, 950-957.
Liu, Y., Wang, M., & Wang, W. (2018a). Electric induced curing of graphene/cement-based composites for structural strength formation in deep-freeze low temperature. *Materials & Design, 160*, 783-793. doi:https://doi.org/10.1016/j.matdes.2018.10.008
Liu, Y., Wang, M., & Wang, W. (2018b). Ohmic heating curing of electrically conductive carbon nanofiber/cement-based composites to avoid frost damage under severely low temperature. *Composites Part A: Applied Science and Manufacturing, 115*, 236-246. doi:https://doi.org/10.1016/j.compositesa.2018.10.008
Liu, Z., Sha, A., Hu, L., & Zou, X. (2017). A laboratory study of Portland cement hydration under low temperatures. *Road Materials and Pavement Design, 18*(sup3), 12-22.

Livesey, P., Donnelly, A., & Tomlinson, C. (1991). Measurement of the heat of hydration of cement. *Cement and Concrete Composites, 13*(3), 177-185. doi:https://doi.org/10.1016/0958-9465(91)90018-D

Lo, T. Y., Tang, W. C., & Cui, H. Z. (2007). The effects of aggregate properties on lightweight concrete. *Building and Environment, 42*(8), 3025-3029. doi:https://doi.org/10.1016/j.buildenv.2005.06.031

Lothenbach, B., Winnefeld, F., Alder, C., Wieland, E., & Lunk, P. (2007). Effect of temperature on the pore solution, microstructure and hydration products of Portland cement pastes. *Cement and Concrete Research, 37*(4), 483-491.

Lv, X., Li, J., Lu, C., Liu, Z., Tan, Y., Liu, C., . . . Wang, R. (2020). The Effect of Sodium Gluconate on Pastes' Performance and Hydration Behavior of Ordinary Portland Cement. *Advances in Materials Science and Engineering, 2020*.

Maltese, C., Pistolesi, C., Bravo, A., Cella, F., Cerulli, T., & Salvioni, D. (2007). A case history: Effect of moisture on the setting behaviour of a Portland cement reacting with an alkali-free accelerator. *Cement and Concrete Research, 37*(6), 856-865.

Martín-Sedeño, M. C., Cuberos, A. J., Ángeles, G., Álvarez-Pinazo, G., Ordónez, L. M., Gateshki, M., & Aranda, M. A. (2010). Aluminum-rich belite sulfoaluminate cements: clinkering and early age hydration. *Cement and Concrete Research, 40*(3), 359-369. doi:https://doi.org/10.1016/j.cemconres.2009.11.003

Martinelli, E., Koenders, E. A., & Caggiano, A. (2013). A numerical recipe for modelling hydration and heat flow in hardening concrete. *Cement and Concrete Composites, 40*, 48-58. doi:https://doi.org/10.1016/j.cemconcomp.2013.04.004

Mehta, P., & Monteiro, P. J. (2006). *Concrete: microstructure, properties, and materials* (0071462899). Retrieved from

Meredith, P., Donald, A., & Luke, K. (1995). Pre-induction and induction hydration of tricalcium silicate: an environmental scanning electron microscopy study. *Journal of materials science, 30*(8), 1921-1930.

Mirzanamadi, R., Johansson, P., & Grammatikos, S. A. (2018). Thermal properties of asphalt concrete: A numerical and experimental study. *Construction and Building Materials, 158*, 774-785. doi:https://doi.org/10.1016/j.conbuildmat.2017.10.068

Monteiro, P. (2006). *Concrete: microstructure, properties, and materials*: McGraw-Hill Publishing.

Montgomery, R. (1947). Viscosity and thermal conductivity of air and diffusivity of water vapor in air. *Journal of Meteorology, 4*(6), 193-196. doi:https://doi.org/10.1175/1520-0469(1947)004<0193:VATCOA>2.0.CO;2

Morin, V., Termkhajornkit, P., Huet, B., & Pham, G. (2017). Impact of quantity of anhydrite, water to binder ratio, fineness on kinetics and phase assemblage of belite-ye'elimite-ferrite cement. *Cement and Concrete Research, 99*, 8-17. doi:https://doi.org/10.1016/j.cemconres.2017.04.014

Mydin, M. A. O. (2016). Assessment of thermal conductivity, thermal diffusivity and specific heat capacity of lightweight aggregate foamed concrete. *Jurnal Teknologi, 78*(5). doi:DOI: 10.11113/jt.v78.8374

Natural Resources Canada. (2020). HVAC & Energy Systems. Retrieved from https://www.nrcan.gc.ca/energy/efficiency/data-research-and-insights-energy-efficiency/housing-innovation/hvac-energy-systems/3937

Nguyen, H., Kinnunen, P., Gijbels, K., Carvelli, V., Sreenivasan, H., Kantola, A. M., . . . Illikainen, M. (2019). Ettringite-based binder from ladle slag and gypsum–The effect of citric acid on fresh and hardened state properties. *Cement and Concrete Research, 123*, 105800. doi:https://doi.org/10.1016/j.cemconres.2019.105800

Nmai, C. K. (1998). Cold weather concreting admixtures. *Cement and Concrete Composites, 20*(2), 121-128. doi:https://doi.org/10.1016/S0958-9465(97)00063-2

Oden, J. T., Duarte, C. A. M., & Zienkiewicz, O. C. (1998). A new cloud-based hp finite element method. *Computer Methods in Applied Mechanics and Engineering, 153*(1), 117-126. doi:https://doi.org/10.1016/S0045-7825(97)00039-X

Ohdaira, E., & Masuzawa, N. (2000). Water content and its effect on ultrasound propagation in concrete—the possibility of NDE. *Ultrasonics, 38*(1-8), 546-552.

Oktay, H., Yumrutaş, R., & Akpolat, A. (2015). Mechanical and thermophysical properties of lightweight aggregate concretes. *Construction and Building Materials, 96*, 217-225. doi:https://doi.org/10.1016/j.conbuildmat.2015.08.015

Perez, J.-P. (2007). *The mechanism of action of sodium gluconate on the fluidity and set of Portland cement.* Paper presented at the 12th International Congress on the Chemistry of Cement.

Peters, H., Marburg, S., & Kessissoglou, N. (2012). Structural - acoustic coupling on non - conforming meshes with quadratic shape functions. *International Journal for Numerical Methods in Engineering, 91*(1), 27-38.

Peterson, V. K., Neumann, D. A., & Livingston, R. A. (2005). Hydration of tricalcium and dicalcium silicate mixtures studied using quasielastic neutron scattering. *The Journal of Physical Chemistry B, 109*(30), 14449-14453.

Pietro, L., Bentz, D. P., Lange, D. A., Kovler, K., & Bentur, A. (2004). *Pumice aggregates for internal water curing.* Paper presented at the Int. RILEM Symp. on Concrete Science and Engineering: A Tribute to Arnon Bentur.

Pietro Lura, D. P. B., David A.Lange, Konstantin Kovler, Arnon Bentur. (2004). *Pumice Aggregates for Internal Water Curing*. Paper presented at the International RILEM Symposium, Evanston, Illinois, USA.

Polat, R. (2016). The effect of antifreeze additives on fresh concrete subjected to freezing and thawing cycles. *Cold Regions Science and Technology, 127*, 10-17. doi:https://doi.org/10.1016/j.coldregions.2016.04.008

Poole, J. L., Riding, K. A., Folliard, K. J., Juenger, M. C., & Schindler, A. K. (2007). Methods for calculating activation energy for Portland cement. *ACI Materials Journal, 104*(1), 303-311.

Powers, T. C. (1956). *Resistance of concrete to frost at early ages*. Retrieved from

Provost-Smith, D., Elsayed, M., & Nehdi, M. (2017). Effect of early-age subfreezing temperature on grouted dowel precast concrete wall connections. *Construction and Building Materials, 140*, 385-394.

Qin, L., Gao, X., & Zhang, A. (2018). Potential application of Portland cement-calcium sulfoaluminate cement blends to avoid early age frost damage. *Construction and Building Materials, 190*, 363-372. doi:https://doi.org/10.1016/j.conbuildmat.2018.09.136

Ramadan, M., El-Gamal, S. M. A., & Selim, F. A. (2020). Mechanical properties, radiation mitigation and fire resistance of OPC-recycled glass powder composites containing nanoparticles. *Construction and Building Materials, 251*, 118703. doi:https://doi.org/10.1016/j.conbuildmat.2020.118703

Ran, Y., Li, X., Cheng, G., Zhang, T., Wu, Q., Jin, H., & Jin, R. (2012). Distribution of permafrost in China: an overview of existing permafrost maps. *Permafrost and Periglacial Processes, 23*(4), 322-333. doi:10.1002/ppp.1756

Real, S., Bogas, J. A., Gomes, M. d. G., & Ferrer, B. (2016). Thermal conductivity of structural lightweight aggregate concrete. *Magazine of Concrete Research, 68*(15), 798-808.

Ren, C., Wang, W., Mao, Y., Yuan, X., Song, Z., Sun, J., & Zhao, X. (2017). Comparative life cycle assessment of sulfoaluminate clinker production derived from industrial solid wastes and conventional raw materials. *Journal of Cleaner Production, 167*, 1314-1324. doi:https://doi.org/10.1016/j.jclepro.2017.05.184

Ridi, F., Luciani, P., Fratini, E., & Baglioni, P. (2009). Water confined in cement pastes as a probe of cement microstructure evolution. *The Journal of Physical Chemistry B, 113*(10), 3080-3087.

Riding, K. A. (2007). *Early age concrete thermal stress measurement and modeling.*

Riding, K. A., Poole, J., Folliard, K. J., Juenger, M. C., & Schindler, A. K. (2011). New Model for Estimating Apparent Activation Energy of Cementitious Systems. *ACI Materials Journal, 108*(5).

Riding, K. A., Poole, J. L., Schindler, A. K., Juenger, M. C., & Folliard, K. J. (2006). Evaluation of temperature prediction methods for mass concrete members. *ACI Materials Journal, 103*(5), 357-365.

Rilem, T. (1997). 119-TCE: avoidance of thermal cracking in concrete at early ages. *Materials and Structures, 30*(45), 1-464.

Romanovsky, V., & Osterkamp, T. (1997). Thawing of the active layer on the coastal plain of the Alaskan Arctic. *Permafrost and Periglacial Processes, 8*(1), 1-22. doi:https://doi.org/10.1002/(SICI)1099-1530(199701)8:1<1::AID-PPP243>3.0.CO;2-U

Rosenqvist, M., Fridh, K., & Hassanzadeh, M. (2016). Macroscopic ice lens growth in hardened concrete. *Cement and Concrete Research, 88*, 114-125.

Rossiter, D., Fawell, P., Ilievski, D., & Parkinson, G. (1998). Investigation of the unseeded nucleation of gibbsite, Al (OH) 3, from synthetic bayer liquors. *Journal of crystal growth, 191*(3), 525-536.

Rossiter, D., Ilievski, D., Smith, P., & Parkinson, G. (1996). The mechanism of sodium gluconate poisoning of gibbsite precipitation. *Chemical engineering research & design, 74*(7), 828-834.

Roswurm, J. (2018). Influence of Retarders on Shrinkage and Compressive Strength in Rapid Set Concrete.

Rungchet, A., Chindaprasirt, P., Wansom, S., & Pimraksa, K. (2016). Hydrothermal synthesis of calcium sulfoaluminate–belite cement from industrial waste materials. *Journal of Cleaner Production, 115*, 273-283. doi:https://doi.org/10.1016/j.jclepro.2015.12.068

Rungchet, A., Poon, C. S., Chindaprasirt, P., & Pimraksa, K. (2017). Synthesis of low-temperature calcium sulfoaluminate-belite cements from industrial wastes and their hydration: Comparative studies between lignite fly ash and bottom ash. *Cement and Concrete Composites, 83*, 10-19. doi:https://doi.org/10.1016/j.cemconcomp.2017.06.013

Ryou, J.-S., & Lee, Y.-S. (2012). Properties of early-stage concrete with setting-accelerating tablet in cold weather. *Materials Science and Engineering: A, 532*, 84-90. doi:https://doi.org/10.1016/j.msea.2011.10.066

Ryou, J.-S., & Lee, Y.-S. (2013). Use of tabletting & coating accelerator for the prevention of early-frost of concrete in cold weather. *Cold Regions Science and Technology, 87*, 1-5. doi:https://doi.org/10.1016/j.coldregions.2012.11.005

Saeed, M. K., Rahman, M. K., & Baluch, M. H. (2016). Early age thermal cracking of mass concrete blocks with Portland cement and ground granulated blast-furnace slag. *Magazine of Concrete Research, 68*(13), 647-663.

Salvador, R. P., Cavalaro, S. H. P., Segura, I., Figueiredo, A. D., & Pérez, J. (2016). Early age hydration of cement pastes with alkaline and alkali-free accelerators for sprayed concrete. *Construction and Building Materials, 111*, 386-398. doi:https://doi.org/10.1016/j.conbuildmat.2016.02.101

Schindler, A., Ruiz, J., Rasmussen, R., Chang, G., & Wathne, L. (2004). Concrete pavement temperature prediction and case studies with the FHWA HIPERPAV models. *Cement and Concrete Composites, 26*(5), 463-471.

Sellevold, E. J., & Bjøntegaard, Ø. (2006). Coefficient of thermal expansion of cement paste and concrete: Mechanisms of moisture interaction. *Materials and Structures, 39*(9), 809-815. doi:10.1617/s11527-006-9086-z

Sengul, O., Azizi, S., Karaosmanoglu, F., & Tasdemir, M. A. (2011). Effect of expanded perlite on the mechanical properties and thermal conductivity of lightweight concrete. *Energy and Buildings, 43*(2-3), 671-676. doi:https://doi.org/10.1016/j.enbuild.2010.11.008

Smith, B. J., Roberts, L. R., Funkhouser, G. P., Gupta, V., & Chmelka, B. F. (2012). Reactions and surface interactions of saccharides in cement slurries. *Langmuir, 28*(40), 14202-14217.

Sun, B., Wang, X., Wang, Z., & Gao, Y. (2018). Transient temperature calculation method for deep-water cementing based on hydration kinetics model. *Applied Thermal Engineering, 129*, 1426-1434.

Tahersima, M., & Tikalsky, P. (2017). Finite element modeling of hydration heat in a concrete slab-on-grade floor with limestone blended cement. *Construction and Building Materials, 154*, 44-50. doi:https://doi.org/10.1016/j.conbuildmat.2017.07.176

Tang, S., Zhu, H., Li, Z., Chen, E., & Shao, H. (2015). Hydration stage identification and phase transformation of calcium sulfoaluminate cement at early age. *Construction and Building Materials, 75*, 11-18. doi:https://doi.org/10.1016/j.conbuildmat.2014.11.006

Telesca, A., Marroccoli, M., Pace, M., Tomasulo, M., Valenti, G., & Monteiro, P. (2014). A hydration study of various calcium sulfoaluminate cements. *Cement and Concrete Composites, 53*, 224-232. doi:https://doi.org/10.1016/j.cemconcomp.2014.07.002

Thomas, J. J., Jennings, H. M., & Chen, J. J. (2009). Influence of Nucleation Seeding on the Hydration Mechanisms of Tricalcium Silicate and Cement. *The Journal of Physical Chemistry C, 113*(11), 4327-4334. doi:10.1021/jp809811w

Toby, B. H., & Von Dreele, R. B. (2013). GSAS-II: the genesis of a modern open-source all purpose crystallography software package. *Journal of Applied Crystallography, 46*(2), 544-549.

Toledo, R. D., Ghavami, K., Sanjuan, M. A., & England, G. L. (2005). Free, restrained and drying shrinkage of cement mortar composites reinforced with vegetable fibres. *Cement & Concrete Composites, 27*(5), 537-546. doi:https://doi.org/10.1016/j.cemconcomp.2004.09.005

Topçu, İ. B., & Işıkdağ, B. (2008). Effect of expanded perlite aggregate on the properties of lightweight concrete. *Journal of Materials Processing Technology, 204*(1), 34-38. doi:https://doi.org/10.1016/j.jmatprotec.2007.10.052

Trauchessec, R., Mechling, J.-M., Lecomte, A., Roux, A., & Le Rolland, B. (2015). Hydration of ordinary Portland cement and calcium sulfoaluminate cement blends. *Cement and Concrete Composites, 56*, 106-114. doi:https://doi.org/10.1016/j.cemconcomp.2014.11.005

Uysal, H., Demirboğa, R., Şahin, R., & Gül, R. (2004). The effects of different cement dosages, slumps, and pumice aggregate ratios on the thermal conductivity and density of concrete. *Cement and Concrete Research, 34*(5), 845-848.

Wadsö, L. (2003). An experimental comparison between isothermal calorimetry, semi-adiabatic calorimetry and solution calorimetry for the study of cement hydration. *Nordtest report TR, 522*.

Wang, F., Kong, X., Jiang, L., & Wang, D. (2020a). The acceleration mechanism of nano-C-S-H particles on OPC hydration. *Construction and Building Materials, 249*, 118734. doi:https://doi.org/10.1016/j.conbuildmat.2020.118734

Wang, J. (2010). *Hydration mechanism of cements based on low-CO2 clinkers containing belite, ye'elimite and calcium alumino-ferrite.*

Wang, T., Zhou, G., Chao, D., & Yin, L. (2018). Influence of hydration heat on stochastic thermal regime of frozen soil foundation considering spatial variability of thermal parameters. *Applied Thermal Engineering, 142*, 1-9.

Wang, X.-Y. (2013). Simulation of temperature rises in hardening Portland cement concrete and fly ash blended concrete. *Magazine of Concrete Research, 65*(15), 930-941.

Wang, X., Liu, C., Liu, S., Yan, C., Zhang, J., & Li, H. (2020b). Compressive strength of pile foundation concrete in permafrost environment in China. *Construction and Building Materials, 247*, 118431.

Winnefeld, F., & Barlag, S. (2009a). Calorimetric and thermogravimetric study on the influence of calcium sulfate on the hydration of ye'elimite. *Journal of thermal analysis and calorimetry, 101*(3), 949-957. doi:https://doi.org/10.1007/s10973-009-0582-6

Winnefeld, F., & Barlag, S. (2009b). Influence of calcium sulfate and calcium hydroxide on the hydration of calcium sulfoaluminate clinker. *Zkg Int, 12*, 42-53.

Winnefeld, F., & Lothenbach, B. (2010). Hydration of calcium sulfoaluminate cements — Experimental findings and thermodynamic modelling. *Cement and Concrete Research, 40*(8), 1239-1247. doi:https://doi.org/10.1016/j.cemconres.2009.08.014

Winnefeld, F., Martin, L. H., Müller, C. J., & Lothenbach, B. (2017). Using gypsum to control hydration kinetics of CSA cements. *Construction and Building Materials, 155*, 154-163. doi:https://doi.org/10.1016/j.conbuildmat.2017.07.217

Won, J.-P., Choi, B.-R., & Lee, J.-W. (2012). Experimental and statistical analysis of the alkali–silica reaction of accelerating admixtures in shotcrete. *Construction and Building Materials, 30*, 330-339.

Won, J.-Y., Lee, S.-H., Park, T.-W., & Nam, K.-Y. (2016). Basic applicability of an insulated gang form for concrete building construction in cold weather. *Construction and Building Materials, 125*, 458-464. doi:https://doi.org/10.1016/j.conbuildmat.2016.08.036

Wu, D., Zhang, Y., & Liu, Y. (2016). Mechanical performance and ultrasonic properties of cemented gangue backfill with admixture of fly ash. *Ultrasonics, 64*, 89-96. doi:https://doi.org/10.1016/j.ultras.2015.08.004

Wu, H., Liu, Y., Li, H., Wang, K., & Guo, Y. (2021). Effects of carbonization on gangue–cemented paste backfill properties. *International Journal of Green Energy, 18*(3), 282-296. doi:10.1080/15435075.2020.1854269

Wu, H., Wang, S., & Zhu, D. (2007). Modelling and evaluation of cooling capacity of earth–air–pipe systems. *Energy conversion and management, 48*(5), 1462-1471. doi:https://doi.org/10.1016/j.enconman.2006.12.021

Wu, Y., Wang, J.-Y., Monteiro, P. J. M., & Zhang, M.-H. (2015). Development of ultra-lightweight cement composites with low thermal conductivity and high specific strength for energy efficient buildings. *Construction and Building Materials, 87*, 100-112. doi:https://doi.org/10.1016/j.conbuildmat.2015.04.004

Xu, L., Wu, K., Rößler, C., Wang, P., & Ludwig, H. (2017). Influence of curing temperatures on the hydration of calcium aluminate cement/Portland cement/calcium sulfate blends. *Cement and Concrete Composites, 80*, 298-306. doi:https://doi.org/10.1016/j.cemconcomp.2017.03.016

Xu, Q., Hu, J., Ruiz, J. M., Wang, K., & Ge, Z. (2010). Isothermal calorimetry tests and modeling of cement hydration parameters. *Thermochimica acta, 499*(1-2), 91-99.

Xu, Q., Ruiz, J. M., Hu, J., Wang, K., & Rasmussen, R. O. (2011). Modeling hydration properties and temperature developments of early-age concrete pavement using calorimetry tests. *Thermochimica acta, 512*(1-2), 76-85.

Xu, W., Li, Q., & Liu, B. (2020). Coupled effect of curing temperature and age on compressive behavior, microstructure and ultrasonic properties of cemented tailings backfill. *Construction and Building Materials, 237*, 117738. doi:https://doi.org/10.1016/j.conbuildmat.2019.117738

Yi, S.-T., Pae, S.-W., & Kim, J.-K. (2011). Minimum curing time prediction of early-age concrete to prevent frost damage. *Construction and Building Materials, 25*(3), 1439-1449. doi:https://doi.org/10.1016/j.conbuildmat.2010.09.021

Yu, H., Wu, L., Liu, W. V., & Pourrahimian, Y. (2018). Effects of fibers on expansive shotcrete mixtures consisting of calcium sulfoaluminate cement, ordinary Portland cement, and calcium sulfate. *Journal of Rock Mechanics and Geotechnical Engineering, 10*(2), 212-221. doi:https://doi.org/10.1016/j.jrmge.2017.12.001

Yu, J., Qian, J., Tang, J., Ji, Z., & Fan, Y. (2019). Effect of ettringite seed crystals on the properties of calcium sulphoaluminate cement. *Construction and Building Materials, 207*, 249-257.

Zajac, M., Skocek, J., Bullerjahn, F., & Haha, M. B. (2016). Effect of retarders on the early hydration of calcium-sulpho-aluminate (CSA) type cements. *Cement and Concrete Research, 84*, 62-75. doi:https://doi.org/10.1016/j.cemconres.2016.02.014

Zhang, G., Li, G., & Li, Y. (2016). Effects of superplasticizers and retarders on the fluidity and strength of sulphoaluminate cement. *Construction and Building Materials, 126*, 44-54. doi:https://doi.org/10.1016/j.conbuildmat.2016.09.019

Zhang, J., Qin, L., & Li, Z. (2009). Hydration monitoring of cement-based materials with resistivity and ultrasonic methods. *Materials and Structures, 42*(1), 15-24. doi:10.1617/s11527-008-9363-0

Zhang, J., & Scherer, G. W. (2011). Comparison of methods for arresting hydration of cement. *Cement and Concrete Research, 41*(10), 1024-1036. doi:https://doi.org/10.1016/j.cemconres.2011.06.003

Zhang, X.-f., Li, S.-y., Li, Y.-l., Ge, Y., & Li, H. (2011). Effect of superficial insulation on roller-compacted concrete dams in cold regions. *Advances in Engineering Software, 42*(11), 939-943. doi:https://doi.org/10.1016/j.advengsoft.2011.06.004

Zhang, X., He, Y., Lu, C., & Huang, Z. (2017). Effects of sodium gluconate on early hydration and mortar performance of Portland cement-calcium aluminate cement-anhydrite binder. *Construction and Building Materials, 157*, 1065-1073.

Zhao, D., Qian, X., Gu, X., Jajja, S. A., & Yang, R. (2016). Measurement techniques for thermal conductivity and interfacial thermal conductance of bulk and thin film materials. *Journal of Electronic Packaging, 138*(4). doi:https://doi.org/10.1115/1.4034605

Zhao, Y., & Si, B. (2019). Thermal properties of sandy and peat soils under unfrozen and frozen conditions. *Soil and Tillage Research, 189*, 64-72.

Zhu, B. (2013). *Thermal stresses and temperature control of mass concrete*: Butterworth-Heinemann.

Zimmerman, W. B. (2006). *Multiphysics modeling with finite element methods* (Vol. 18): World Scientific Publishing Company.